# In Pursuit of Specificity: Therapeutic Targeting of HDAC1 in Glioblastoma

by

Costanza Lo Cascio

A Dissertation Presented in Partial Fulfillment
of the Requirements for the Degree
Doctor of Philosophy

Approved April 2022 by the
Graduate Supervisory Committee:

Joshua LaBaer, Chair
Shwetal Mehta
Zaman Mirzadeh
Marco Mangone
Andrew Paek

ARIZONA STATE UNIVERSITY

May 2022

ABSTRACT

Glioblastoma (GBM), the most common and aggressive primary brain tumor affecting adults, is characterized by an aberrant yet druggable epigenetic landscape. The Histone Deacetylases (HDACs), a major family of epigenetic regulators, favor transcriptional repression by mediating chromatin compaction and are frequently overexpressed in human cancers, including GBM. Hence, over the last decade there has been considerable interest in using HDAC inhibitors (HDACi) for the treatment of malignant primary brain tumors. However, to date most HDACi tested in clinical trials have failed to provide significant therapeutic benefit to patients with GBM. This is because current HDACi have poor or unknown pharmacokinetic profiles, lack selectivity towards the different HDAC isoforms, and have narrow therapeutic windows. Isoform selectivity for HDACi is important given that broad inhibition of all HDACs results in widespread toxicity across different organs. Moreover, the functional roles of individual HDAC isoforms in GBM are still not well understood. Here, I demonstrate that HDAC1 expression increases with brain tumor grade and is correlated with decreased survival in GBM. I find that HDAC1 is the essential HDAC isoform in glioma stem cells and its loss is not compensated for by its paralogue HDAC2 or other members of the HDAC family. Loss of HDAC1 alone has profound effects on the glioma stem cell phenotype in a p53-dependent manner and leads to significant suppression of tumor growth *in vivo*. While no HDAC isoform-selective inhibitors are currently available, the second-generation HDACi quisinostat harbors high specificity for HDAC1. I show that quisinostat exhibits potent growth inhibition in multiple patient-derived glioma stem cells. Using a pharmacokinetics-

and pharmacodynamics-driven approach, I demonstrate that quisinostat is a brain-penetrant molecule that reduces tumor burden in flank and orthotopic models of GBM and significantly extends survival both alone and in combination with radiotherapy. The work presented in this thesis thereby unveils the non-redundant functions of HDAC1 in therapy-resistant glioma stem cells and identifies a brain-penetrant HDACi with higher selectivity towards HDAC1 as a potent radiosensitizer in preclinical models of GBM. Together, these results provide a rationale for developing quisinostat as a potential adjuvant therapy for the treatment of GBM.

# DEDICATION

To my parents, Carlo and Alessandra. You have been a constant source of inspiration, guidance, and warmth in every aspect of my life. Your unwavering love, kindness and generosity have supported me every single day. Thank you for everything you have done for me and for always encouraging me to pursue my passions and dreams. Thank you for cultivating my curiosity ever since I was a child and for believing in me every step of the way. I love you more than words will ever be able to describe.

To my brother, Tancredi. Thank you for always encouraging me through good and difficult times. Thank you for always being there for me, picking up my calls in the late hours of the night and for constantly lifting my spirits with your incredible wit and humor. Your creativity, passion and enthusiasm continue to inspire me every day. I look up to you in so many ways and I want the best for you in life.

Despite the very long distance from home, times of uncertainty and the numerous hardships that I have faced in graduate school, the three of you have always been on my mind. I have been showered with your love and affection every day. None of the things I have been able to accomplish during this time would have been possible without you. The work that is presented here is entirely for you.

ACKNOWLEDGMENTS

None of the work presented in this dissertation would have been possible without the help of many people with whom I had the privilege to be and work with over the past five and a half years. I first want to thank my thesis committee members Josh LaBaer, Marco Mangone, Zaman Mirzadeh and Andrew Paek. Thank you for keeping my ideas grounded, focused, and pointed in the right direction. Your probing questions always challenged to think more deeply, and your interest in my work helped me develop confidence in myself and my experiments. I am grateful to all of you for your guidance and commitment to my success during my graduate journey.

I want to thank everyone in the Mehta lab for creating a fun, warm and welcoming environment to do science. Thanks to James McNamara for the countless hours spent in and out of the cell culture room, which led to the generation of a wealth of significant results presented here. Thanks to Connor White, Matt Dufault, Sarah Himes, Zorana Opachich, Leo Elena, and Raymond Hon for their incredible help on a multitude of projects I led throughout graduate school, and for being supportive friends. Thanks to all of you for your advice, helpful academic and personal discussions, and legendary impromptu late night happy hours. Immense thanks also go to Roberto Fiorelli, who taught me everything I know about immunohistochemistry and showed me the beauty of confocal microscopy. I want to thank my dear friends Emily Szeto and Kimberley Meyers for all the wonderful fun times we shared outside the rigors of the lab. Special thanks also go to Marcella Collins and her entire family for their loving support and kindness. You are like a sister to me, and I am so grateful for our friendship.

I want to thank everyone at the Ivy Brain Tumor Center for their collaborative spirit, constant encouragement, and generous feedback. I especially thank Artak Tovmasyan for his support and mentorship, as well as Tigran Margaryan and William Knight for their invaluable expertise and immense contributions to the work presented here. Thanks to Nader Sanai for believing in me and inspiring me to keep my mind set on the big picture when studying a complex and devastating disease like GBM. I am forever grateful for the opportunities you have all given me to grow, learn and succeed.

Special thanks go to Ernesto Luna – my Starboy, colleague, partner in crime throughout so many adventures, and my very best friend. You have been by my side since the beginning of my doctoral training and your unwavering support, love, and patience in and out of the lab over all those years mean the world to me. I wouldn't have been able to do any of this without you. Thank you for everything you have done for me and for all your contributions towards the wonderful work presented in this dissertation.

I am forever indebted to my advisor, Shwetal Mehta. You have been consistently committed both to the success of my research and my happiness as an individual. Thank you for giving me countless opportunities to thrive in your lab, and for your guidance as well as endless patience over the years. Thank you for always challenging me to think more creatively, and for allowing me to pursue my own ideas under your wing. Thank you for trusting me and giving me the honor to be your first graduate student. I will never forget your kindness and generosity when I needed it the most. Thank you for everything.

Finally, I am eternally grateful to the brain tumor patients and their families who contributed to making this dissertation possible. None of the work I present here would have been achievable without their selfless donations, and for that, I thank you.

TABLE OF CONTENTS

LIST OF TABLES

Table Page

LIST OF FIGURES

Figure Page

Figure Page

# CHAPTER 1

# INTRODUCTION

## 1.1 Brain tumors

Tumors of the central nervous system (CNS) constitute a heterogeneous group of tumors arising in the brain, cranial nerves, spinal nerves, spinal cord, and the meninges (Barnholtz-Sloan, Ostrom, and Cote 2018). Tumors of the CNS represent approximately 1% of all newly diagnosed cancers in the United States, and about 2% of all cancer-related deaths (Ostrom et al. 2021). Primary brain tumors can be either benign or malignant and can occur in childhood or adulthood (Barnholtz-Sloan, Ostrom, and Cote 2018). The most common type of malignant primary brain tumors are gliomas, which although rare, are devastating tumors that are challenging to treat. In the sections that will follow, I will provide a summary on adult diffuse gliomas and a comprehensive overview on the biology of glioblastoma, the most aggressive and lethal primary brain tumor (Weller et al. 2021).

### *1.1.1 Classification of adult diffuse gliomas*

Gliomas account for 80% of all malignant primary brain tumors (Ostrom et al. 2021). Gliomas are characterized by high morbidity and mortality due to their location and invasive growth patterns (Chen et al. 2017). The world health organization (WHO) classification of CNS tumors uses a grading system on a scale to 1-4 to indicate different degrees of malignancy. Historically, gliomas were diagnosed based on their histopathology and presumed cell of origin, and were traditionally classified as astrocytic,

oligodendroglial or mixed oligo-astrocytic tumors (Louis, Holland, and Cairncross 2001). Conversely, the current WHO classification combines analysis of both molecular and histopathological features to classify CNS tumors (Louis et al. 2021). Gliomas comprise grade 2, 3 and 4 tumors, with grade 4 tumors being the most malignant (Whitfield and Huse 2022). However, regardless of grade and prognosis, adult diffuse gliomas are highly infiltrative and resistant to therapy, and are considered to be largely incurable (Whitfield and Huse 2022).

Diffuse WHO grade 2 and 3 gliomas are the most common gliomas in young adults and have an inherent tendency to recurrence and malignant progression, and such tumors include IDH-mutant astrocytoma or oligodendroglioma (Weller et al. 2021). As shown in Figure 1.1, these tumors harbor mutations in the *IDH1* or *IDH2* genes and can be distinguished based on the presence or absence of 1p/19q codeletion, inactivating *ARTX* mutations and *TERT* mutations (Weller et al. 2021; Whitfield and Huse 2022). Diffuse grade 4 gliomas are the most aggressive and lethal and can be classified as IDH-wild type (IDH-WT) glioblastoma (GBM) or IDH-mutant astrocytoma. As will be discussed in the following section, IDH-wild type GBM are rapidly proliferating tumors with a very poor prognosis. Along with histopathological features such as microvascular proliferation and/or necrosis, multiple defining molecular features include mutation in the *TERT* promoter, epidermal growth factor receptor (EGFR) amplification, and combined chromosome 7 gain paired with chromosome 10 loss (+7/−10) (Brat et al. 2020). Grade 4 IDH-mutant astrocytoma share histological features with GBM but are characterized by homozygous deletion of *CDKN2A/B* and loss of nuclear *ATRX* (Figure 1.1.)

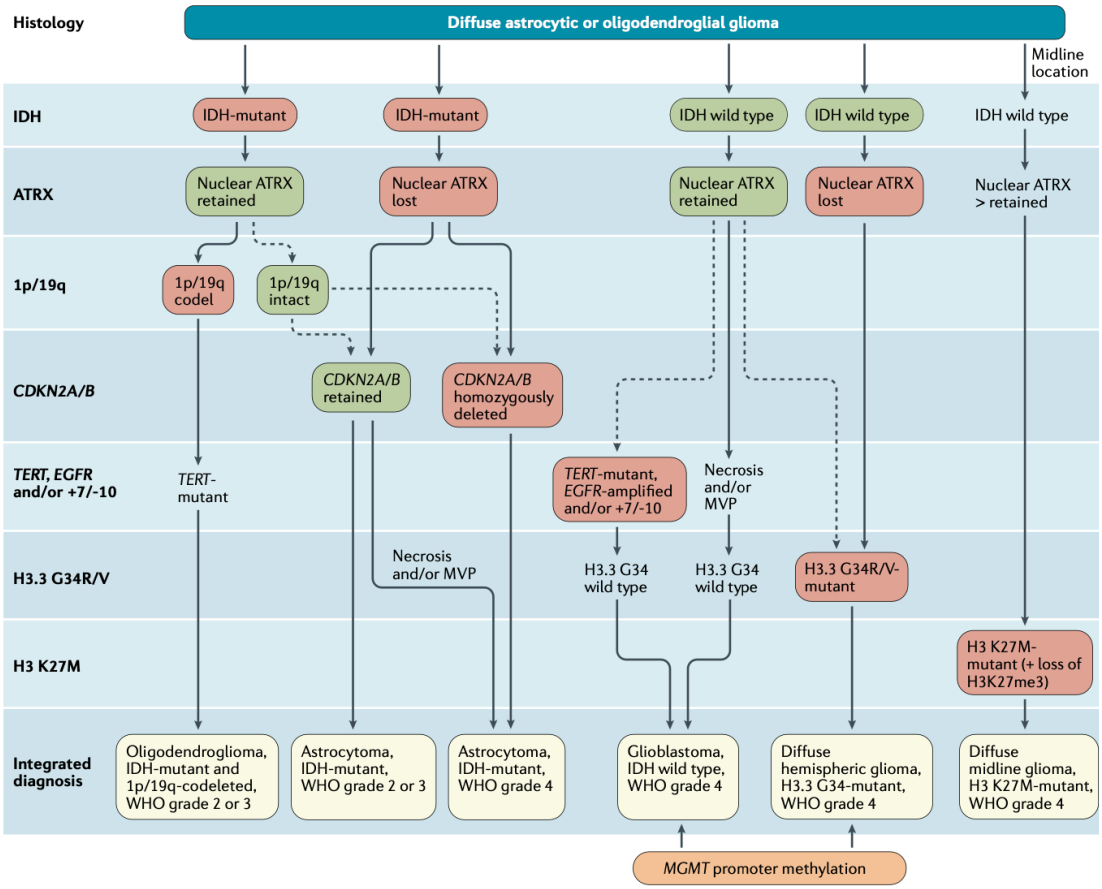


**Figure 1.1. Classification of adult diffuse gliomas.** This diagram illustrates the diagnostic algorithm for the integrated classification of the major diffuse gliomas that occur in adults. Tissue specimens obtained through biopsy sampling in patients with diffuse gliomas are first assessed by immunohistochemistry for the presence of mutant IDH1 (R132H) and loss of nuclear ATRX. If the tumor (in patients older than 55 years) is found in a non-midline location, is negative for mutant IDH1 and retains ARTX expression, it is classified as IDH-wild-type GBM. In all other cases, a lack of IDH1 mutation positivity warrants sequencing of IDH1 and IDH2 to exclude or detect non-canonical mutations in the IDH genes. IDH-wild-type diffuse astrocytic gliomas that lack microvascular proliferation (MVP) or necrosis should be tested for *EGFR* amplification, *TERT* promoter mutation and a gain of chromosome 7, loss of chromosome 10 to confirm molecular characteristics of IDH-wild-type GBM. To identify H3.3 G34-mutant diffuse hemispheric gliomas, which tend to occur in younger patients with IDH-wild-type gliomas, histone H3.3 G34R/V mutations should be assessed by immunohistochemistry or DNA sequencing. Diffuse gliomas that arise in the thalamus, brainstem or spinal cord should be evaluated for histone H3 K27M mutations and loss of nuclear K27-trimethylated histone H3 (H3K27me3) to confirm diagnosis of H3 K27M-mutant diffuse midline gliomas. The molecular alterations characteristic of each tumor type are highlighted in red (deletions, mutations) and green boxes (no mutations or molecular alterations). Taken from:
(Weller et al. 2021)

### *1.1.2 Glioblastoma (GBM)*

Glioblastoma (GBM; WHO grade 4) is the most common primary malignant brain tumor affecting adults, representing approximately 60% of all gliomas, and the average annual incidence of GBM is 3.2 per 100,000 population (Ostrom et al. 2021). Despite aggressive multimodal therapy, the prognosis for patients with GBM is very poor with a median survival of 12-14 months after treatment and this statistic has not changed over the past several decades (Janjua et al. 2021). GBM is considered today as one of the deadliest forms of all cancers, with a 5-year survival rate of less than 6% following diagnosis (Ostrom et al. 2018). The median age at diagnosis is 65 years, but can occur at any age, and incidence of disease is slightly more common in men than in women (Davis 2016). The vast majority (90%) of GBMs arise *de novo*, without a known precursor, and are rereferred to as primary GBM. Secondary GBMs are more rare and develop from WHO grade 2 or 3 gliomas that over time progress into GBM (Ohgaki and Kleihues 2013). Secondary GBMs carry a better prognosis and are more common in younger patients (Tan et al. 2020). As will described in the upcoming sections of this dissertation, GBM is a highly heterogenous, rapidly proliferating tumor that infiltrates into healthy brain tissue. The aggressive nature of this disease can thereby have a devastating impact on the quality of these patients, primarily due to the emergence of debilitating symptoms arising from treatment-related morbidities or tumor growth into functionally intact brain regions that interferes with normal day-to-day activities (Oronsky et al. 2020). Hence, there is an unmet urgent need to develop new effective treatments that improve survival outcomes for patients with GBM.

The clinical presentation of a patient with newly diagnosed GBM varies depending on the size and location of the tumor in the brain (Davis 2016). Common symptoms in patients include increased intracranial pressure, headaches, seizures, as well tumor-induced cognitive deficits such as personality changes, memory loss and loss of executive function (Young et al. 2015). Current diagnosis and classification of gliomas integrates histological grading as well as analyses of molecular markers (Louis et al. 2021; Weller et al. 2021) . At the histological level, GBMs are characterized by high cellularity, pleomorphism, microvascular proliferation, a high mitotic index and pseudopalisading necrosis (Whitfield and Huse 2022). GBMs typically harbor greater rates of epidermal growth factor receptor (*EGFR*) amplification, *TERT* promoter mutations, *PTEN* deletion, no *IDH* mutations, and a +7/–10 cytogenetic signature (gain of chromosome 7 combined with loss of chromosome 10) (Figure 1.1) (Weller et al. 2021). These histological and molecular features are required for a brain tumor to be diagnosed as grade 4 GBM according to the most recent WHO classification of CNS tumors (Louis et al. 2021). More details on common genetic alterations in IDH-WT GBM are reviewed in section 1.1.4.

### *1.1.3 Standard-of-care for GBM*

Treatment of newly diagnosed GBM requires a multidisciplinary approach. The first line of treatment is maximal safe surgical resection of the tumor (Davis 2016). This allows removal of as much tumor tissue as possible, which is then subsequently analyzed through histology and genotyping to allow an accurate diagnosis to be made (Tan et al. 2020). Following recovery from surgery patients undergo a 6-week treatment with

concurrent radiation treatment and temozolomide (TMZ), an oral alkylating agent, followed by adjuvant chemotherapy with TMZ alone for an additional 6 months (Stupp et al. 2005). Prior to 2005, the standard-of-care for GBM consisted of only post-operative radiation therapy (Holland 2000). However, this changed when a pivotal phase III clinical trial demonstrated that the median overall survival of GBM patients treated with radiation plus TMZ (14.6 months) was marginally but significantly higher compared to the median overall survival of patients treated with radiation alone (12.1 months) (Stupp et al. 2005). It was later shown that the cohort receiving radiation plus TMZ contained a higher proportion of long-term survivors compared to radiation-only cohort: 27% versus 10% at two years and 10 versus 2% at five years, respectively (Stupp et al. 2009).

Further analysis of patients who underwent this treatment regimen led to the identification of a strong predictor of patient-related outcomes: the methylation of the *MGMT* gene promoter (Hegi et al. 2005). *MGMT* codes for a DNA repair protein that removes alkyl groups from the O6 position of guanine, an important site of DNA alkylation (Kaina and Christmann 2002; Hegi et al. 2005). As an alkylating agent, TMZ leads to the formation of O6-methylguanine on DNA in glioma cells, which is a cytotoxic lesion that is normally directly repaired by the MGMT enzyme (Mrugala and Chamberlain 2008). If left unrepaired, the O6-methylguanine lesion causes base mispairing, which leads to futile cycles of mismatch repair during DNA replication and ultimately induces apoptosis (Ochs and Kaina 2000; Liu, Markowitz, and Gerson 1996; Karran and Bignami 1992). In approximately 50% of GBM patients, the *MGMT* promoter is methylated and its expression is silenced, thereby rendering glioma cells more sensitive to TMZ-induced DNA damage (Hegi et al. 2005). GBM patients harboring *MGMT*

promoter methylation were found to be associated with more favorable survival outcomes after radiation and TMZ treatment (21.7 months) compared to tumors harboring an unmethylated *MGMT* promoter (14 months) (Hegi et al. 2005). Hence, *MGMT* was identified as a prognostic biomarker that predicts responsiveness to TMZ treatment in GBM patients (Wick et al. 2014).

To date, the standard-of-care for newly diagnosed GBM remains unchanged. While radiation and TMZ treatment improve survival outcomes, GBM patients are still faced with a dismal prognosis and live on average 12-18 months after diagnosis (Fisher and Adamson 2021). Ultimately, almost all GBMs inevitably progress after termination of treatment, resulting in tumor recurrence (Birzu et al. 2020). Treatment options for recurrent GBM are less well defined – there is currently no established standard-of-care for patients with relapsed disease and there is no clinical evidence for any interventions that prolong overall survival. Only one drug has been approved by the FDA for the management of recurrent GBM: bevacizumab. Bevacizumab is a targeted therapeutic antibody that binds to and inhibits the activity of vascular endothelial growth factor (VEGF) to prevent tumor angiogenesis (Cohen et al. 2009). While bevacizumab failed to improve overall survival in patients with recurrent GBM, its administration may be recommended to alleviate adverse symptoms associated with edema and radiation-induced necrosis (Cohen et al. 2009).

Unfortunately, some patients with recurrent GBM may not even be eligible for second-line therapy (Nava et al. 2014). Treatment options after recurrence typically include further surgical resection of the tumor, re-irradiation, approved systemic chemotherapies such bevacizumab, TMZ rechallenge, treatment with other approved

alkylating agents (lomustine, carmustine), experimental drug treatments in clinical trials, or supportive care alone (Omuro and DeAngelis 2013). Another treatment modality which was recently approved by the FDA for the treatment of both primary (2015) and recurrent GBM (2011) are tumor-treating fields (TTFields). TTFields are delivered through a portable device (Optune) applied to a shaved scalp, which emits low-intensity, intermediate-frequency alternating electric fields that disrupt mitosis in tumor cells (Mittal et al. 2018). A phase III clinical trial demonstrated that TTFields used in conjunction TMZ treatment significantly improved overall survival when compared to TMZ alone (20.5 vs. 15.6 months) (Stupp et al. 2015). However, despite its efficacy TTFields are not part of the standard-of-care due to its very expensive cost, inconvenience to patients and marginal survival benefit (Mehta et al. 2017). In summary, despite decades of basic and clinical research there are no novel effective therapies for patients with GBM. While progress has been underwhelming over the past few decades, there are currently a plethora of therapeutic agents or approaches that are under clinical development for the treatment of GBM and other high-grade gliomas, such as immunotherapies, cell/gene therapies and radiosensitizing agents among many others (Jain 2018).

### *1.1.4 Common genetic alternations in GBM*

GBM was the very first cancer type to be systematically studied by The Cancer Genome Atlas Research Network (TCGA) and is considered one of the most well-characterized tumors at the genomic and transcriptomic level. Early karyotype analysis of 54 malignant gliomas reported frequent chromosomal alterations in GBM: gain of

chromosome 7 and loss of chromosome 10 (Bigner et al. 1988), with loss of heterozygosity of 10q being observed in approximately 80% of all GBMs (Fujimoto et al. 1989; Bigner and Vogelstein 1990). Interchromosomal, intrachromosomal (intergenic) and intragenic rearrangements can also be detected in the majority (~70%) of GBM samples (Sturm et al. 2014). The most common intragenic deletion in GBM is an in-frame deletion of exons 2-7 of EGFR, which results in a truncated protein that lacks an extracellular domain and is referred to as EGFRvIII (Moscatello et al. 1996; Gan, Kaye, and Luwor 2009). While this mutant EGFR protein is unable to bind its ligand, it remains constitutively active and has been shown to sustain GBM cell proliferation and tumor growth (Moscatello et al. 1996; An et al. 2018).

With the advent of sequencing technologies, two independent studies identified frequent genetic alterations in GBM which led to the discovery of many of genes that were not known to be altered in GBMs. Through PCR-based sequencing of 22 human GBM tumors, Parsons et al. identified the following genes were commonly altered in GBM: *CDKN2A* (50%); *TP53*, *EGFR* and *PTEN* (30-40%); *NF1*, *CDK4*, *RB1* (12-15%); *PIK3CA* and *PIK3R1* (8-10%) (Parsons et al. 2008). That same year, TCGA reported very similar findings based on integrative analysis of DNA copy number, gene expression and DNA methylation aberrations of over 200 GBM samples (Cancer Genome Atlas Research 2008). These early large-scale sequencing efforts studies were important as they were the first to implicate deregulation of the RB, p53 and RTK/RAS/PI3K pathways in the pathogenesis GBM (Parsons et al. 2008; Cancer Genome Atlas Research 2008). The TCGA expanded the breadth of their analysis to over 500 GBM samples and generated a comprehensive catalog of somatic alterations

associated with GBM through whole-genome, exome, and RNA sequencing as well as copy-number, transcriptomic, epigenomic, and targeted proteomic profiling (Brennan et al. 2013). This large study not only confirmed previously identified genetic aberrations, but also detected additional alterations that included targetable mutations such as *BRAF* and *FGFR1/FGFR2/FGFR3* in a very rare subset of GBMs. Moreover, their analyses found that more than 40% of GBM tumors harbor at least one non-synonymous mutation in genes involved in chromatin remodeling, such as *ATRX*, *CREBBP* and *SMARCA2*, suggesting that chromatin organization may play important roles in GBM pathology (Brennan et al. 2013). While all these studies were instrumental in changing our understanding of the molecular genetics of GBM, such knowledge has not yet translated into novel treatment options for these patients.

## 1.2 Challenges in the treatment of GBM

GBMs have proven very difficult to treat due to their complex biological characteristics and their location in one of the body's most crucial organs – the brain (Aldape et al. 2019). While there are numerous obstacles that have limited progress to improve treatment options for GBM, these can be summarized into three key challenges: the anatomical location of these tumors, unsuccessful drug delivery and extensive intra- and inter-tumoral heterogeneity.

### *1.2.1 Anatomical location*

In various non-CNS malignancies, it is feasible to take very wide surgical margins to remove any residual cancer cells that may be present beyond the edge of the resected

bulk tumor (Wasserberg and Gutman 2008; Kamat et al. 2019; Sambri et al. 2021; Brouwer de Koning et al. 2018). Moreover, some solid tumors can be cured or treated by complete surgical removal of the entire affected organ: mastectomies, colectomies and proctectomies are examples of such radical procedures (Lostumbo, Carbine, and Wallace 2010; Kaiser et al. 2004; Memon et al. 2012). Although maximal surgical resection is the first line of treatment for GBM patients, complete resection of the entire tumor is almost impossible owing to the lack of clear tumor boundaries and widespread infiltration of GBM cells into the surrounding brain tissue (Wilson, Karajannis, and Harter 2014). Extensive resection of these tumors is particularly difficult as they often arise in eloquent areas of the brain that control motor function, memory, speech, and the senses (Davis 2016). Hence, aggressive resection strategies in these regions carry the risk of post-operative neurologic deficits (Davis 2016). While advances in surgical and pre-operative mapping techniques have facilitated the execution of safe resections while minimizing surgical morbidities, neurosurgeons are tasked with the delicate challenge of debulking as much tumor tissue as possible while trying to preserve neurological functions and good quality of life for patients (Tan et al. 2020). Multiple studies have demonstrated that patients who underwent aggressive surgical resections have longer progression-free survival and overall survival outcomes when compared to patients where greater extent of resection was not feasible (Stummer et al. 2006; Sanai and Berger 2008; Lacroix et al. 2001). However, to date surgery is not curative due to the highly invasive nature of GBM. The remaining tumor cells that disseminate into the normal brain parenchyma develop resistance to standard chemoradiation, and as such GBMs almost always universally recur within 6-9 months of treatment (Davis 2016). In over 90% of GBM

patients, tumor recurrence usually occurs within 2 centimeters of the resection cavity of the primary tumor (Hou et al. 2006; Rapp et al. 2017). In the late 1920s, a neurosurgeon attempted treating GBMs by performing hemispherectomies, which are radical procedures wherein an entire brain hemisphere containing the primary tumor site is removed. However, even such drastic measures were shown to be ineffective at preventing tumor recurrence on the contralateral hemisphere, further highlighting the highly aggressive and diffuse nature of GBM (Chaichana and Quinones-Hinojosa 2014). Hence, there is a critical need to develop effective treatments aimed at eradicating infiltrating tumor cells residing in normal brain tissue which cannot be removed through surgery alone.

### *1.2.2 Drug delivery*

In brain tumors, the delivery of therapeutic agents is severely restricted by the presence of the blood-brain-barrier (BBB) – a complex neurovascular structure that is responsible for regulating normal brain homeostasis and protecting neural tissue from exposure to substances in the general circulation (Sweeney et al. 2019). Hence, while the BBB functions as a protective interface between the CNS and systemic circulation, in the context of disease it impedes effective penetration of drugs into the brain (Arvanitis, Ferraro, and Jain 2020). The BBB is comprised endothelial cells, pericytes, astrocytes, microglial and smooth muscle cells (Khaddour, Johanns, and Ansstas 2020). The main component of the BBB is an endothelial cell layer which lines the blood vessels and is held together by restrictive tight junctions (Sweeney et al. 2019). Pericytes and astrocytes provide structural support by regulating the fidelity of these tight junctions and efflux

mechanisms critical to BBB function (Noch, Ramakrishna, and Magge 2018). Together, this dynamic structure forms a complex physical barrier that controls transportation of different molecules (water, ions, immune cells, nutrients) into the CNS. However, it is estimated 98% of small molecules and almost all large molecular weight drugs are incapable of crossing the BBB – only select substances such as small (less than 500 Da) and lipophilic molecules can passively diffuse through this structure (Cardoso, Brites, and Brito 2010). Therefore, the BBB poses several major hurdles for effective drug discovery and delivery in brain tumors.

GBM compromises the structural integrity of the BBB, resulting in enhanced BBB leakage at the tumor core (Ishihara et al. 2008; Wolburg et al. 2003; Noch, Ramakrishna, and Magge 2018). Although this may suggest that drugs may be more permeable at the tumor site, the BBB remains intact at the tumor edge where residual infiltrating tumor cells reside (Shergalis et al. 2018). This results in suboptimal drug concentrations in tumor foci that may be distant form the primary tumor site. In addition to causing BBB dysfunction through anatomical disruption, GBM cells themselves also significantly upregulate the expression of efflux pumps such as P-glycoprotein (P-gp) ATP-binding cassette (ABC) transporters –further limiting the entry of anti-tumorigenic compounds into tumor cells (Calatozzolo et al. 2005; Decleves et al. 2006). As such, inconsistent and insufficient drug delivery to all parts of the tumor are critical factors that contribute to treatment failure and inevitable tumor recurrence. There are currently numerous ongoing research efforts aimed at developing strategies to improve drug delivery for CNS malignancies, which include chemical modification of drugs, efflux transporter inhibition, magnetic resonance-guided focused ultrasound to disrupt the BBB,

and intra-tumoral delivery methods such as convection-enhanced delivery to infuse drugs directly into the tumor bed (Noch, Ramakrishna, and Magge 2018). However, to date these techniques have failed to yield positive results, in part due infusate/drug reflux, technical issues relating to implementation of direct drug delivery methods without compromising normal brain function, and the highly heterogenous nature of GBM (Janjua et al. 2021).

### *1.2.3 Inter- and intra-tumoral heterogeneity*

Inter-tumoral heterogeneity, the differences observed between individual tumors, represents a major barrier in the development of new therapies for GBM. Inter-tumoral heterogeneity in GBM has been studied through molecular profiling analyses, whereby combinations of frequently altered genes were found to stratify individual GBM tumors into molecular subtypes. A gene expression-based molecular classification of GBM by TCGA identified three GBM subtypes based on transcriptional profiling data and detection of dominant driver mutations in bulk tumor specimens (Wang, Hu, et al. 2017; Verhaak et al. 2010). The three subtypes of GBM are referred to as Classical, Proneural and Mesenchymal, and have offered important insights into the genetic regulation of these tumors (Verhaak et al. 2010; Brennan et al. 2013). Most of the analyzed GBMs were found to harbor alterations in common cancer-associated genes (*TP53, NF1, PTEN, CDKs*) and mutations or amplifications in receptor tyrosine kinases (*EGFR, PDGFRa, c-MET*) (Verhaak et al. 2010). The Classical subtype is characterized by *EGFR* amplification, gain of chromosome 10 paired with loss of chromosome 7. Instead, the Proneural subtype features amplification of *PDGFRA* and frequent point mutations in the

*IDH1* and *TP53* genes. Finally, the Mesenchymal subtype was associated with hemizygous deletions of 17q11.2, which contains the gene *NF1*, expression of astrocytic and mesenchymal markers, and marked upregulation of genes related to the TNF and NF-κB pathways (Verhaak et al. 2010). Despite having clearly distinct transcriptional profiles, the clinical prognosis for each GBM subtype remains the same (Verhaak et al. 2010). Only the Proneural subtype has been linked with favorable survival outcome, while the Mesenchymal subtype has been associated with poor survival (Phillips et al. 2006). However, although the TCGA classification attempted to address the challenge of heterogeneity in GBM, so far molecular stratification of these tumors has not led to the development of successful patient-specific therapies.

GBMs display extensive cellular and genetic heterogeneity existing not only between patients, but also within single tumors. Such intra-tumoral heterogeneity is considered one of the key determinants of therapy failure in GBM. Several recent studies have shown that individual GBM tumors display extensive genetic, cellular, and functional intra-tumoral heterogeneity. Perioperative sampling of multiple geographically distinct regions of single GBMs demonstrated that tumor fragments from the same patient may be classified into different subtypes (Sottoriva et al. 2013). Hence, GBMs also exhibit spatial heterogeneity, which undermines past therapeutic efforts considering that previous genomic studies relied on single regional biopsies to subgroup a patient (Sottoriva et al. 2013). These findings were further corroborated by a study that employed single cell RNA-sequencing and found that a single tumor comprised of a heterogenous mixture of cells corresponding to all three GBM subtypes (Patel et al. 2014). Importantly, it was shown that patients harboring a Proneural GBM had decreased

survival if the representation of other subtypes (Classical, Mesenchymal) was also high in the tumor (Patel et al. 2014). Moreover, isolation of single-cell derived GBM subclones revealed that individual cells exhibit different drug resistance profiles (Reinartz et al. 2017). More recently, single-cell transcriptomic profiling of 28 GBM tumors revealed that malignant cells in GBM exist in four main cellular states that recapitulate distinct neural cell types: neural-progenitor-like, oligodendrocyte-progenitor-like, astrocyte-like and mesenchymal-like states (Neftel et al. 2019). Each GBM tumor was found to harbor cells in all 4 states, and the relative frequencies of each state varied by tumor and was found to be influenced by the tumor microenvironment (Neftel et al. 2019). Critically, this study found that a single GBM cells had the potential to generate progeny cells in all four states and exhibited a high degree of plasticity, as cells were found to dynamically transition between different states *in vivo* (Neftel et al. 2019). Together, these studies suggest that the clinical outcome of GBM is influenced by the degree of heterogeneity within the tumor, highlighting the importance of intra-tumoral heterogeneity in promoting therapy evasion.

### 1.3 Glioma stem cells (GSCs)

At the cellular level, functional heterogeneity in GBM can be explained by the presence of rare subpopulations of tumorigenic cancer stem cells, referred to as glioma stem cells (GSCs), that are capable of self- renewal (Singh et al. 2003; Singh et al. 2004; Hemmati et al. 2003). According to the cancer stem cell model, cells within a tumor are organized into a hierarchy wherein cancer stem cells sit at the apex, as they have the ability to self-renew indefinitely and the potential to differentiate into cells of different

lineages (Kreso and Dick 2014). In the context of GBM, GSCs have been found to harbor exclusive tumor-initiating potential and are thought to drive tumor growth and progression after aggressive treatment (Lathia et al. 2015). Seminal studies over the past two decades have shown that human GSCs marked with CD133, a cell surface glycoprotein and a common marker for cancer stem cells, are highly tumorigenic and capable of initiating tumors *in vivo* even when as few as 100 cells are injected intracranially (Singh et al. 2004; Lathia et al. 2015). The potent tumorigenic capacity of GSCs, coupled with ample evidence that these cells are resistant to both chemotherapy and radiotherapy, suggests that these cells contribute to tumor maintenance and thereby recurrence after aggressive treatment in GBM (Figure 1.2) (Bao et al. 2006; Chen et al. 2012; Liu et al. 2006). GSCs harbor a variety of properties that render them resistant to cytotoxic therapies, including hyperactivation of the DNA damage response machinery, increased drug efflux, and residence in poorly vascularized and hypoxic areas (Bao et al. 2006; Hirschmann-Jax et al. 2004; Heddleston et al. 2009)

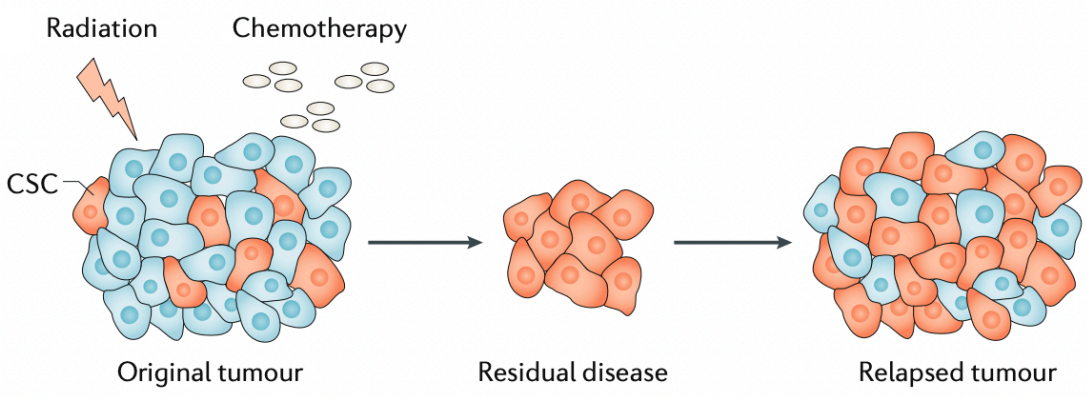


**Figure 1.2 Glioma stem cells drive therapy resistance and tumor recurrence.** Cytotoxic agents such as radiation and chemotherapy are commonly used to treat cancer, which are effective in killing bulk glioma cells (blue cells) but not glioma

stem cells (GSCs) (orange cells). GSCs, which survive treatment, can give rise to a new, more aggressive tumor, leading to recurrence. Taken from: (Lytle, Barber, and Reya 2018).

GSCs are generally defined by a series of functional characteristics that are assessed through a combination of *in vitro* and *in vivo* methods (Figure 1.3). To this day, the golden functional assay for GSC determination remains the ability to initiate tumors that recapitulate the original histopathological features of GBM when transplanted in orthotopically into mice (Lathia et al. 2015). Other required functional characteristics of GSCs include unlimited self-renewal and persistent proliferation (Gimple et al. 2019). GSCs also harbor other properties that, although common, do not functionally define a cancer stem cell. Such examples include their potential to differentiate into different cell lineages, their frequency within a tumor, and the expression of common markers shared with non-malignant stem cells, such as transcription factors (OLIG2, SOX2, NESTIN) and cell surface markers (CD133, CD44, CD15, L1CAM) (Figure 1.3) (Prager et al. 2020; Lathia et al. 2015; Beier et al. 2007).

It is important to note that the term GSC does allude to a tumor cell of origin for GBM, and that functional definitions of GSCs do not suggest that the stem-like state is static. Recent studies have highlighted the striking plasticity that exists between different cellular states within GBM, which allows for dynamic interconversion between GSC and non-GSCs as well as transitions into different phenotypic states (Suva et al. 2014; Neftel et al. 2019). Given their roles in driving therapeutic resistance and tumor recurrence, over the past two decades there has been an explosion in research focused on elucidating the biology and key molecular regulators of GSCs – in the hope that such knowledge may

translate into novel therapies aimed at eradicating GSCs. However, it is now clear that regulation of the GSCs state is extraordinarily complex and maintained by a combination of core intrinsic (genetic, epigenetic, metabolic) and extrinsic (microenvironmental) mechanisms (Lathia et al. 2015; Prager et al. 2020). The following sections of this dissertation will focus on exploring the various epigenetic regulatory mechanisms that contribute to the maintenance of the GSC state and the pathogenesis of GBM.

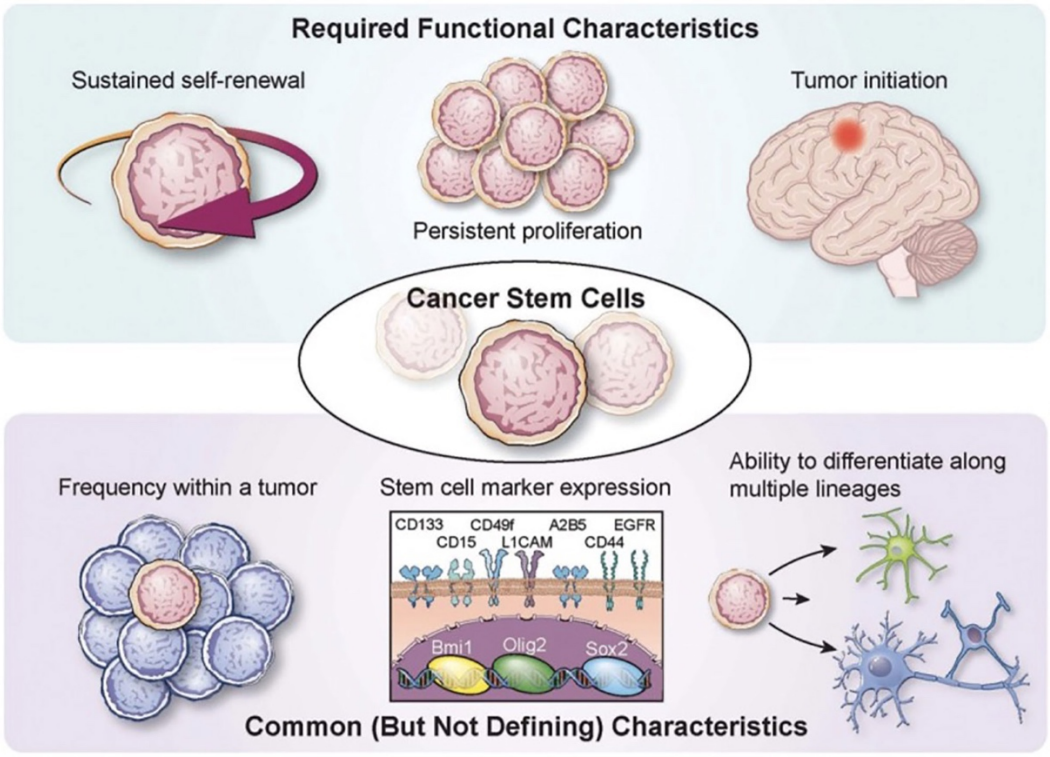


**Figure 1.3 Functional characteristics of glioma stem cells.** GSCs are defined by functional characteristics that include sustained self-renewal, persistent proliferation, and tumor initiation upon secondary transplantation, which is the golden standard functional assay to identify cancer stem cells. GSCs also share features with normal somatic stem cells, including frequency within a tissue (or tumor), stem cell marker expression (examples relevant to GBM are shown), and the ability to differentiate into multiple CNS lineages. Taken from: (Lathia et al. 2015).

## 1.4 Epigenetic dysregulation in GBM

Alongside genetic mutations, aberrant epigenetic alterations have emerged as common hallmarks of many cancers, including GBM (Kondo et al. 2014). As previously mentioned in section 1.1.4, exome sequencing studies of almost 300 GBM tumors revealed approximately 50% of cases have at least one somatic mutation in genes encoding for chromatin-modifying enzymes (Brennan et al. 2013). Such genes included those associated with DNA methylation (*IDH1, IDH2*), histone methylation (*MLL2, MLL3, MLL4, EZH2*) and chromatin remodeling (*ATRX, CREBBP, SMARCA2*) (Brennan et al. 2013). These mutations all contribute to aberrant gene expression programs in GBM due to impaired DNA methylation, histone demethylation and nucleosome positioning (Dawson and Kouzarides 2012). Genome-wide hypomethylation occurs at a high frequency in primary IDH-WT GBMs (~80%), affecting up to an estimated 10 million CpG dinucleotides per tumor cell, resulting in expression of oncogenes and the promotion of genomic instability (Cadieux et al. 2006; Martinez et al. 2009).

Epigenetic mechanisms are also critical for the maintenance of the GSCs phenotype (Valor and Hervas-Corpion 2020). Studies have shown that several processes that regulate the epigenome in GSCs contribute to repression of differentiation programs while supporting stem-like proliferating phenotypes (Stricker et al. 2013; Baronchelli et al. 2013; Bulstrode et al. 2017). Furthermore, GSCs rapidly adapt to diverse microenvironments by modulating their transcriptomes and DNA methylomes (Baysan et al. 2014). The most well-studied epigenetic modulator in GSCs is polycomb repressive complex 2 (PRC2), which is large multimeric complex that plays critical roles in

transcriptional silencing by controlling mono-, di- and tri-methylation of lysine 27 on histone 3 (H3K27) (Kondo et al. 2014). Different components of PRC2, especially its catalytic subunit EZH2, have been implicated in driving the self-renewal, plasticity, therapeutic resistance, and tumorigenic potential of GSCs (Kim, Kim, et al. 2013; Suva et al. 2009; Natsume et al. 2013; Kim, Joshi, et al. 2015). Another important epigenetic modification that is vastly understudied in the context of GBM is histone acetylation, which regulates gene expression by changing the architecture of chromatin. To date, the only form of epigenetic therapy tested in clinical trials for GBM have been drugs that attempt to reverse aberrant histone acetylation programs in these tumors (Chen et al. 2020). However, the exact functional roles and dysregulated activity of the large family of epigenetic modifiers that control histone acetylation in GBM and GSCs remain obscure.

### 1.5 Histone deacetylases (HDACs)

In the nucleus of a eukaryotic cell, the entire genome is compacted into a structure called chromatin. The basic unit of chromatin is called the nucleosome, which is consists of approximately 147 DNA base pairs wrapped around a core histone octamer that includes histones H2A, H2B, H3 and H4 (Luger et al. 1997; Tessarz and Kouzarides 2014). Each nucleosome is 11 nm in diameter, and they are arranged in a beads-on-a-string structure that tightly pack together to form 30 nm supercoiled chromatin fibers, which all together form the chromosome (Figure 1.4) (Olins and Olins 2003). The additional linker histone H1 is not part of the nucleosome itself but is involved in the regulation of higher order chromatin organization (Fyodorov et al. 2018). There are two

main higher order chromatin structures: heterochromatin and euchromatin. Heterochromatin is highly condensed and transcriptionally silent, whereas euchromatin is loosely packed and more accessible to RNA polymerase II and transcriptional regulators (Allfrey, Faulkner, and Mirsky 1964). Hence, dynamic remodeling of chromatin accessibility influences gene expression by making certain genes more or less available for transcription.

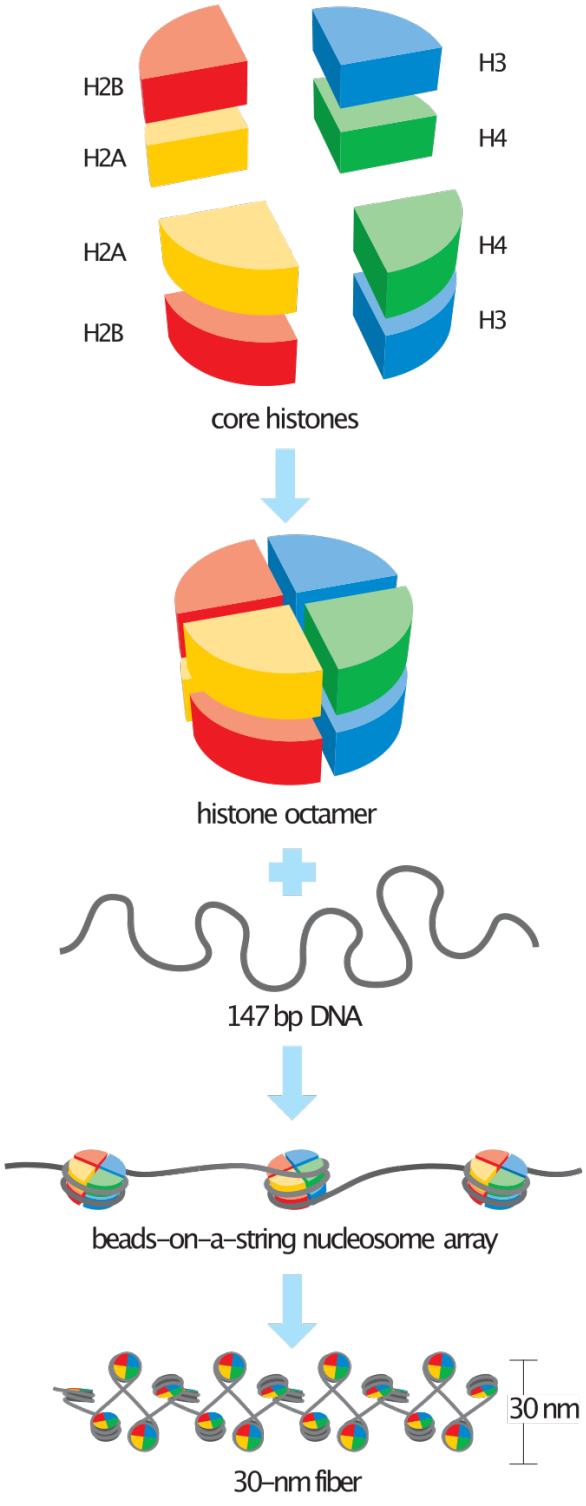


**Figure 1.4 The basic units of chromatin structure**

*1.5.1 Role of histone acetylation in the regulation of eukaryotic gene expression*

The epigenome is comprised of covalent chemical modifications to chromatin, which include DNA methylation and histone post-translational modifications (PTMs). Histone proteins have N-terminal tails that protrude out from the nucleosome core that are subject to various PTMs such as phosphorylation, methylation, and acetylation (Li, Tian, and Zhu 2020). These modifications affect the physical interaction between histones and DNA and play an important role in the modulation of the structure and function of chromatin, and thereby alter gene expression. As illustrated in Figure 1.5, the enzymes responsible for catalyzing these modifications (epigenetic modifiers) can be broadly classified into three categories: writers, readers, and erasers (Taverna et al. 2007; Kutateladze 2011; Zaware and Zhou 2019). Writers are enzymes that establish chemical modifications to DNA or histones. Readers are enzymes with specialized domains that recognize, bind to, and interpret those modifications. Finally, erasers are enzymes that oppose the activity of the writers and catalyze the removal of those chemical modifications. As an example, a common and well-studied form of histone modification is acetylation, which occurs at the ε-amino group of lysine residues in the amino-terminal tail of histones (Strahl and Allis 2000; Jenuwein and Allis 2001). The acetylation of lysine residues on histone tails are added by histone acetyltransferases (HATs; the writers), identified and interpreted by bromodomain-containing proteins (BRD; the readers) which initiate transcriptional programs that result in phenotypic changes, and removed by histone deacetylases (HDACs; the erasers) (Figure 1.5) (Seto and Yoshida 2014). Hence, the establishment and reversal of histone acetylation is a very dynamic

process that is controlled by the balanced activity of two antagonistic families of enzymes – the HATs and HDACs.

Acetylation by HATs neutralizes the positive charge of lysine residues on histone tails, which weakens electrostatic interactions between histones and the negatively charged DNA (Shogren-Knaak et al. 2006). This results in the loosening of tightly coiled heterochromatin, which allows for greater accessibility of chromatin to RNA polymerase II and the transcriptional machinery, leading to increased gene expression (Wang et al. 2009). By contrast, HDAC-mediated deacetylation of histone tail lysine residues restores a compact and transcriptionally repressive chromatin structure (Inoue and Fujimoto 1969; Seto and Yoshida 2014). Considering that histone acetylation is critical for the fine tuning of transcription in eukaryotic cells, it is not surprising that a disrupted equilibrium between the activity of HDACs and HATs has been associated with cancer development (Li and Seto 2016). There is overwhelming evidence that demonstrating that HDACs are aberrantly expressed in various human cancers (Weichert 2009). Abnormal alterations in histone acetylation due to increased HDAC activity can result in decreased expression of tumor suppressor genes and/or enhanced expression of oncogenes (Glozak and Seto 2007). Moreover, unlike the deeply entrenched historical nomenclature suggests, histones are not the sole substrates of HDAC enzymes (Ho, Chan, and Ganesan 2020). HDACs can deacetylate a plethora of non-histone proteins expressed in different cellular compartments that govern numerous important biological processes that promote cancer initiation and progression, such cell cycle regulation, apoptosis, the DNA-damage response, metastasis, angiogenesis, and autophagy (Li and Seto 2016).

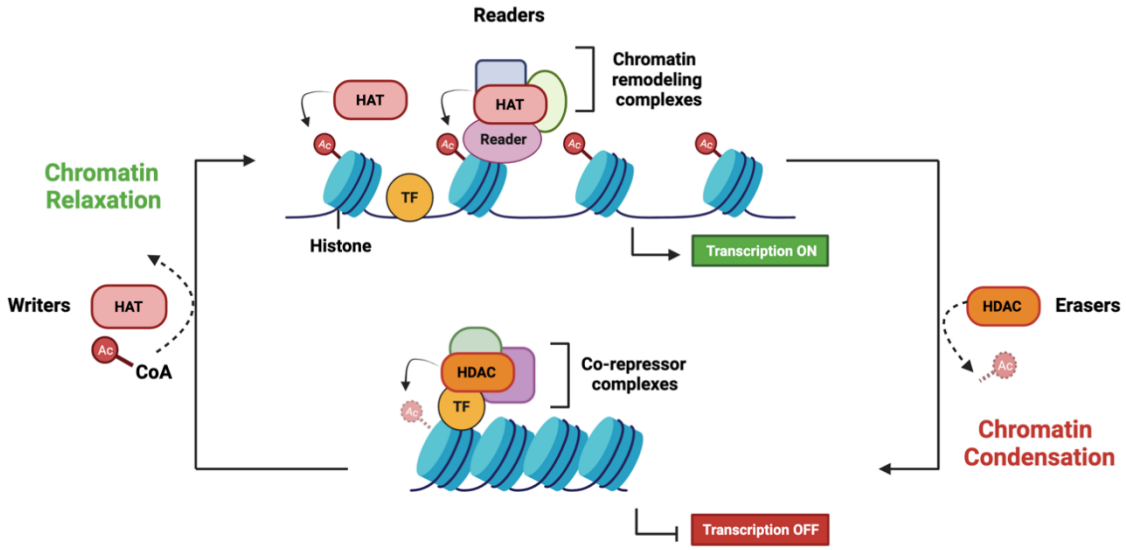


**Figure 1.5 Dynamic regulation of histone tail acetylation by epigenetic modifiers.** Dynamic acetylation of histone tails is critical for the fine-tuning of gene expression. Acetyl groups on lysine residues are transferred by HATs ("writers"), which neutralizes the positively charged amino-terminal tails, preventing the interactions with negatively charged DNA and thus resulting in chromatin relaxation. This relaxed chromatin state allows access to RNA Polymerase II, transcription factors, RNA other transcription co-activators termed 'readers' (e.g. bromodomain proteins) that recognize acetylated lysines on histone tails. This state results in increased gene transcription. HDACs, which act as epigenetic "erasers", oppose the activity of HATs and remove acetyl groups from histone tails, resulting in chromatin compaction and condensation, which represses gene transcription.

### *1.5.2 Classification and function of human HDACs*

There are 18 HDACs that have been identified in human cells, which are grouped into four classes based on their sequence similarities, cellular localization, and homology to yeast HDACs (Seto and Yoshida 2014). However, it should be noted that this classification system is somewhat archaic and masks the functional differences between HDAC isoforms. Within these four groups, HDACs are further divided into two families based on their catalytic mechanisms: the classical histone deacetylase family and the Sirtuin family (SIRTs) (Seto and Yoshida 2014). The classical histone deacetylase family

comprises of the class I proteins (HDAC1, HDAC2, HDAC3 and HDAC8), class II proteins (HDAC4, HDAC5, HDAC6, HDAC7, HDAC9 and HDAC10) and class IV proteins (HDAC11), while the Sirtuins comprise the entirety of the class III proteins (SIRT1-7). Classical HDACs (class I, II and IV) are metalloenzymes that require a zinc ion to hydrolyze the amide bond in acetylated lysines, while the Sirtuins (class III) are nicotinamide adenine dinucleotide ($NAD^+$)-dependent enzymes (Yoshida et al. 2017). Although both families of enzymes perform the same chemical reaction (acyllysine cleavage), the term HDAC usually refers to the zinc-dependent enzymes that are the focus of this dissertation and whose basic domain structures are illustrated in Figure 1.6.

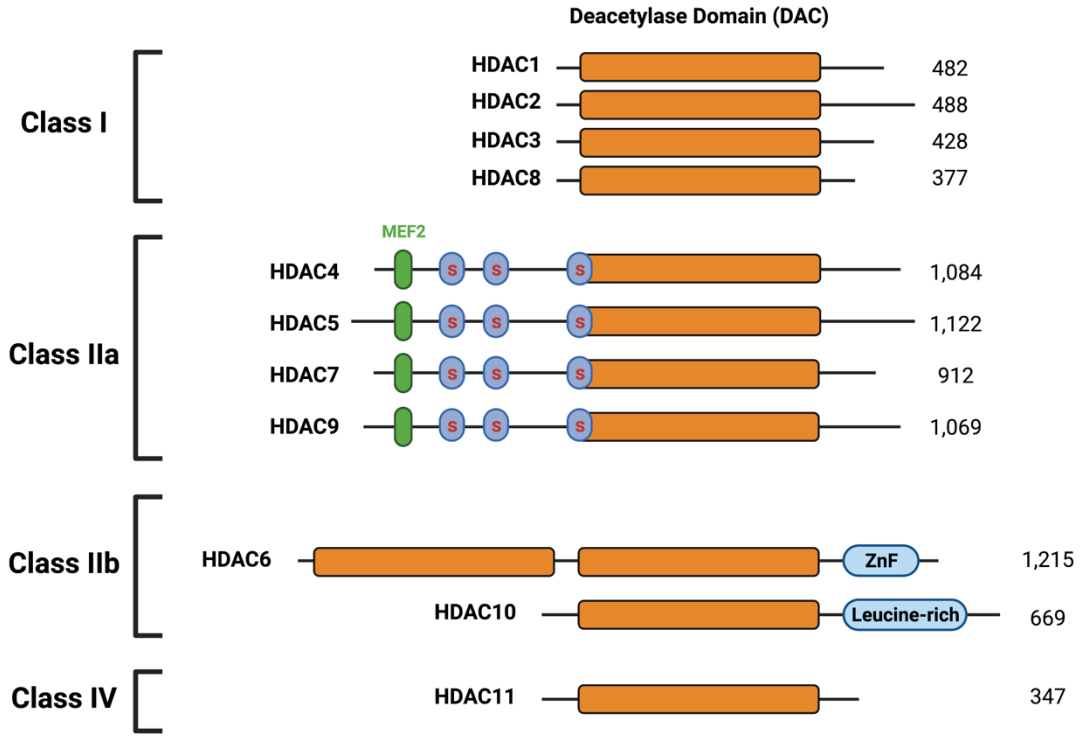


**Figure 1.6 Classification and domain composition of classical human HDACs.** The total number of amino acid residues in each HDAC isoform is shown on the right of

each protein. The catalytic domain of each HDAC is shown as an orange cylinder. Myocyte enhancer factor-2 (MEF2)-binding motifs are depicted as short green cylinders, whereas 14-3-3 binding motifs are depicted as short blue cylinders labeled with “S” (for serine). ZnF, ubiquitin-binding zinc finger. Adapted from: (Park and Kim 2020).

Class I HDACs harbor a highly conserved deacetylase domain and are homologous to the yeast Rpd3 deacetylase (Seto and Yoshida 2014). HDAC1 and HDAC2 are nuclear enzymes that are ubiquitously expressed in human cells and act as major regulators of gene expression (Kelly and Cowley 2013). These two isoforms are bona fide HDACs as they play a major role in regulating histone acetylation and are often recruited in the same transcriptional co-repressor complexes such as Mi-2/nucleosome remodeling deacetylase (NuRD), repressor element-1 silencing transcription corepressor (RCOR1/CoREST), SWI-independent-3A (Sin3A) and mitotic deacetylase complex (MiDAC) (Hassig et al. 1997; Laherty et al. 1997; Ayer 1999; You et al. 2001). As part of these multiprotein complexes, HDAC1 and HDAC2 have been shown to regulate chromatin structure, cell cycle progression and differentiation. HDAC1 and 2 also deacetylate numerous nuclear proteins and transcription factors, such as p53, STAT3, ATM, E2F and CAF1 (Ho, Chan, and Ganesan 2020). HDAC1 and HDAC2 are also highly related – they share 83% amino acid identity and are thought to originate from a gene duplication event (Gregoretti, Lee, and Goodson 2004). While it is established that HDAC1 and HDAC2 share a high degree of functional redundancy, there is increasing evidence that they harbor unique functions that are independent of one another across different developmental stages and tissues (Jurkin et al. 2011; Brunmeir, Lagger, and Seiser 2009; Montgomery et al. 2009; MacDonald and Roskams 2008).

HDAC3 shares 50% homology with HDAC1 and HDAC2 and shuttles in between the nucleus and cytoplasm (Seto and Yoshida 2014). Notably, the stability of HDAC3 is stability is dependent on its association with the nuclear receptor co-repressor (NCoR) and silencing mediator for retinoid or thyroid-hormone receptors (SMRT) complexes (Wen et al. 2000; Emmett and Lazar 2019; Oberoi et al. 2011). HDAC3 is also involved in the deacetylation of histones and non-histone proteins such as the RelA subunit of NF-κB, STAT3 and FOXP3, and has been implicated in the regulation of energy metabolism, neuronal function, and circadian rhythms (Ho, Chan, and Ganesan 2020). Finally, although categorized as a class I enzyme, HDAC8 is fundamentally very distinct from HDAC1-3 (Chakrabarti et al. 2015). Unlike the other class I isoforms, HDAC8 functions independently and does not associate with large chromatin remodeling complexes. Although it remains controversial whether histones are *in vivo* substrates for HDAC8, this isoform has been shown to play important roles in sister chromatid separation, energy homeostasis, microtubule integrity, and muscle contraction (Li et al. 2014; Wilson et al. 2010; Deardorff et al. 2012).

Class II HDACs share sequence homology with the yeast HDAC Hda1 and are further subdivided into two groups: class IIa (HDAC4, HDAC5, HDAC7 and HDAC9) and class IIb (HDAC6 and HDAC10) (Seto and Yoshida 2014). The class IIa isoforms are relatively large in size and harbor a unique N-terminal domain that contains conserved serine residues and binding sites for MEF2 transcription factors (Asfaha et al. 2019). In response to regulatory signals, phosphorylation of the serine residues controls the shuttling of these isoforms between the nucleus and cytoplasm (Yang and Gregoire 2005). Class IIa HDACs have significant weaker deacetylase activity compared to Class I

enzymes, and to date their individual biological functions remain rather obscure (Li, Tian, and Zhu 2020). In fact, whether these isoforms are truly enzymes is debatable due to their poor catalytic activity and are thus commonly referred to as pseudoenzymes. Within the Class IIb subgroup, HDAC6 is a microtubule-associated deacetylase that is predominantly localized in the cytoplasm (Li, Zhang, et al. 2018). As HDAC6 deacetylates α-tubulin and cortactin, it is a key regulator of the cytoskeleton, cell migration and cell morphology (Zhang et al. 2003; Ho, Chan, and Ganesan 2020). HDAC6 is also involved in the misfolded protein response, as deacetylation of Hsp90 is required for its chaperone activity and HDAC6 itself targets misfolded proteins for destruction by aggresomes via its C-terminal ubiquitin-binding zinc finger domain (Kovacs et al. 2005). By contrast, HDAC10 is located both in the nucleus and the cytoplasm and has functions that are completely independent of lysine deacetylation (Ho, Chan, and Ganesan 2020). Interestingly, it was recently found to be a robust polyamine deacetylase, and several studies have demonstrated that HDAC10 is involved in processes such as autophagy, immunoregulation, and DNA repair (Ho, Chan, and Ganesan 2020; Hai et al. 2017).

Finally, HDAC11 is the only member of the class IV group and shares homology to the yeast HDAC, Hos3 (Gao et al. 2002). It is expressed in the nucleus and is the smallest HDAC isoform. Together with HDAC10, HDAC11 is considered the most poorly understood and least characterized isoform in the classical HDAC family. Recent studies have suggested that although HDAC11 has weak deacetylation activity, it may be involved in fatty acid acylation and play important roles in immunomodulation by regulating the expression of cytokines such as IL-10 and IL-1β (Yanginlar and Logie

2018; Shao et al. 2018; Kutil et al. 2018). The key features, cellular localization, and substrates of each HDAC isoform are summarized in Table 1.1.

| isoform | major localization | key features | substrate examples |
|---|---|---|---|
| *In Vitro Acetyl-Lys Peptide Hydrolases* | | | |
| HDAC1, HDAC2 | Nucleus | Exist in vivo as NuRD, Sin3A, CoREST, MiDAC, and MIER complexes | Histones, transcriptional regulators |
| HDAC3 | Nucleus | Complexation with NCoR/SMRT needed for catalysis | Histones, transcriptional regulators |
| HDAC6 | Cytoplasm | Ubiquitin and microtubule binding domains, two catalytic domains | Tubulin, cortactin, Hsp90, Tau |
| *In Vitro Longer Chain Acyl-Lys Peptide Hydrolases* | | | |
| HDAC8 | Nucleus | Moderate AcLys hydrolysis with extended sequence recognition, superior for $C_8$, $C_{12}$, $C_{14}$ acyllysine | Histones, p53, SMC3, longer chain acyllysine residues |
| HDAC11 | Nucleus | Preference for $C_{12}$, $C_{14}$ acyllysine | Longer chain acyllysine residues |
| *In Vitro Ac-polyamine Hydrolase* | | | |
| HDAC10 | Cytoplasm | Narrow substrate channel with glutamate gatekeeper | Acetylpolyamines |
| *In Vitro TrifluoroAc-Lys Peptide Hydrolases* | | | |
| HDAC4, HDAC5, HDAC7. HDAC9 | Nucleus and cytoplasm | Tissue-specific, MEF2 binding domain | None? Recruit substrates for HDAC3 |

**Table 1.1 Key features of the eleven classical human HDAC isoforms.** HDACs are summarized according to substrate preference and localization. Taken from: (Ho, Chan, and Ganesan 2020).

*1.5.3. Roles of HDACs in human cancers*

A hallmark of human cancer is the deregulation of DNA methylation and post-translational histone modifications, in particular histone acetylation, which results in an aberrant epigenetic landscape that promotes tumorigenesis (Ropero and Esteller 2007). Altered expression and function of most classical HDACs has been mechanistically linked to development and pathogenesis of several cancers (Chen et al. 2020). In most malignancies high expression of HDACs, particularly HDAC1, has been associated with advanced disease and poor outcomes in patients (Li and Seto 2016). For example, high expression of class I isoforms HDAC1, 2, and 3 have been linked to poor prognosis in gastric and ovarian cancers (Weichert, Roske, et al. 2008; Weichert, Denkert, et al. 2008), while high expression of HDAC8 was shown to correlate with advanced-stage disease and poor survival outcomes in neuroblastoma (Oehme et al. 2009; Rettig et al. 2015). HDAC activity has also been found to be dysregulated in multiple myeloma, where overexpression HDAC1 was associated with inferior patient outcomes (Mithraprabhu et al. 2014). The mechanisms through which individual HDAC isoforms have been found regulate tumorigenesis are quite diverse. As will be discussed below, HDACs induce a broad range of cellular and molecular effects through hyperacetylation of histone and non-histone proteins, which can result in the repression of tumor suppressor genes or regulation of key the oncogenic cell-signaling pathways though modifications of key molecules involved in the cell cycle, cell death, autophagy, angiogenesis, and the DNA damage response (Figure 1.7) (Li and Seto 2016).

Several HDAC isoforms promote proliferation by transcriptionally repressing cell cycle-related genes involved in the G1/S and G2/M cell-cycle checkpoints. For example, HDAC1 and 2 directly bind to the promoters of the cyclin-dependent inhibitors (CDK) $p21^{WAF1/CIP1}$, $p27^{KIP1}$, and $p57^{KIP2}$ and negatively regulate their expression (Yamaguchi et al. 2010; Zupkovitz et al. 2010). In fact, genetic knockdown of HDAC1 and 2 in tumor cells reverses the promoter hypoacetylation of these genes, resulting in the induction of the expression of CDKs and thereby cell-cycle arrest in the G1 phase (Zupkovitz et al. 2010; Yamaguchi et al. 2010). With respect to G2/M checkpoint, HDAC10 regulates this transition via modulation of cyclin A2 expression (Li, Peng, and Seto 2015). HDAC3 was shown to be a critical regulator of mitosis by modulating Aurora kinase B activity (Li et al. 2006). Numerous studies have demonstrated that drug-mediated HDAC inhibition can arrest the cell cycle at either G1/S or G2/M phase, highlighting that HDACs are important therapeutic targets for blocking abnormal cell growth and proliferation in cancer (Ropero and Esteller 2007).

HDACs have been shown to promote survival of cancer cells by modulating the expression of pro- and anti-apoptotic proteins (Zhang and Zhong 2014). Some HDAC isoforms, such as HDAC1, HDAC2 and HDAC8 promote the expression of anti-apoptotic proteins (Bcl-2, Bcl-xL, Mcl-1) (Kim, Noh, et al. 2013; Kang et al. 2014; Zhang et al. 2006; Li and Seto 2016). Through mechanisms that are not well understood, studies employing HDAC inhibitors across different cancer cell lines demonstrated that inhibition of HDACs cause upregulation of pro-apoptotic Bcl-2 family proteins, such as Bim, Bmf, Bad, Bid, Noxa, Puma and Bax, primary through increased histone H3 or H4 hyperacetylation of their promoters (Matthews, Newbold, and Johnstone 2012;

Wiegmans et al. 2011). In addition to apoptotic factors, HDACs have been implicated in negatively regulating the tumor suppressive functions of p53. HDAC1, which is commonly overexpressed in multiple cancers, is a major regulator of p53 function and activity (Ito et al. 2002). Under stressful cellular conditions or after induction of DNA damage, p53 is normally activated through phosphorylation and acetylation (Tang et al. 2008; Ivanov et al. 2007). Acetylation of p53 at serine residues it essential for p53 stabilization and increased transcriptional activity, which can result in the induction of cell cycle arrest or apoptosis (Reed and Quelle 2014). HDAC1 interacts with p53 *in vitro* and *in vivo* and is directly involved in its deacetylation, causing p53 to be targeted for degradation (Juan et al. 2000; Ito et al. 2002). Hence, aberrant HDAC1 expression and activity play an important role in inhibiting the p53 signaling axis in cancer cells. Moreover, as will be discussed in more detail in Chapter 3, class I and class II HDACs also harbor critical functions in the DNA damage response. HDAC1 and HDAC2 are recruited to DNA double-strand breaks to deacetylate histones H3K56 and H4K16 and facilitate non-homologous end joining DNA repair (Miller et al. 2010). Class I HDAC isoforms also regulate the activity of other proteins involved in the DNA damage response, such as ATR, ATM, BRCA1, and FUS (Thurn et al. 2013; Li et al. 2020). Corroborating these findings, several studies have shown that HDAC inhibition can repress DSB repair and render cancer cells more susceptible to cell death induced by radiation chemotherapeutic agents (Koprinarova, Botev, and Russev 2011; Munshi et al. 2005; Kachhap et al. 2010).

Finally, HDACs have been implicated in promoting metastasis and angiogenesis in some human cancers. The epithelial-to-mesenchymal transition (EMT) is a major

driver of cancer cell invasion and metastasis, and emerging studies have demonstrated that HDACs may play a key role in the regulation of EMT (Wawruszak et al. 2019). For example, in several cancers the EMT transcription factors Zeb and Snail have been shown to recruit HDAC1 and HDAC2 (as part of the mSin3a complex) to the *CHD1* promoter, which results in decreased expression of E-cadherin and thereby promotion of tumor cell invasion and metastasis (Christofori and Semb 1999; Hajra and Fearon 2002; Tong et al. 2012; Aghdassi et al. 2012; von Burstin et al. 2009). Angiogenesis also contributes to tumor growth and metastasis. Angiogenesis is triggered by a hypoxic microenvironment, and the cellular responses to hypoxia are primarily regulated by the transcription factor hypoxia-inducible factor 1α (HIF-1α) (Pugh and Ratcliffe 2003). Several HDAC isoforms have been implicated in the regulation of HIF-1α activity: HDAC1 and HDAC4 block degradation of the protein by directly deacetylating HIF-1α, while HDAC5 and HDAC6 facilitate HIF-1α maturation and stabilization by deacetylating its chaperones, HSP70 and HSP90 (Yoo, Kong, and Lee 2006; Geng et al. 2011; Kong et al. 2006; Chen et al. 2015). Moreover, HDAC4, HDAC5, and HDAC7 enhance the transcriptional activity of HIF-1α by promoting its association with the HAT p300 (Kato, Tamamizu-Kato, and Shibasaki 2004; Seo et al. 2009). In summary, given the multifaceted roles of HDACs in promoting different aspects of tumorigenesis, there has been an increasingly strong interest in developing potent inhibitors that inhibit HDAC activity as promising therapeutics for the treatment of various human cancers.

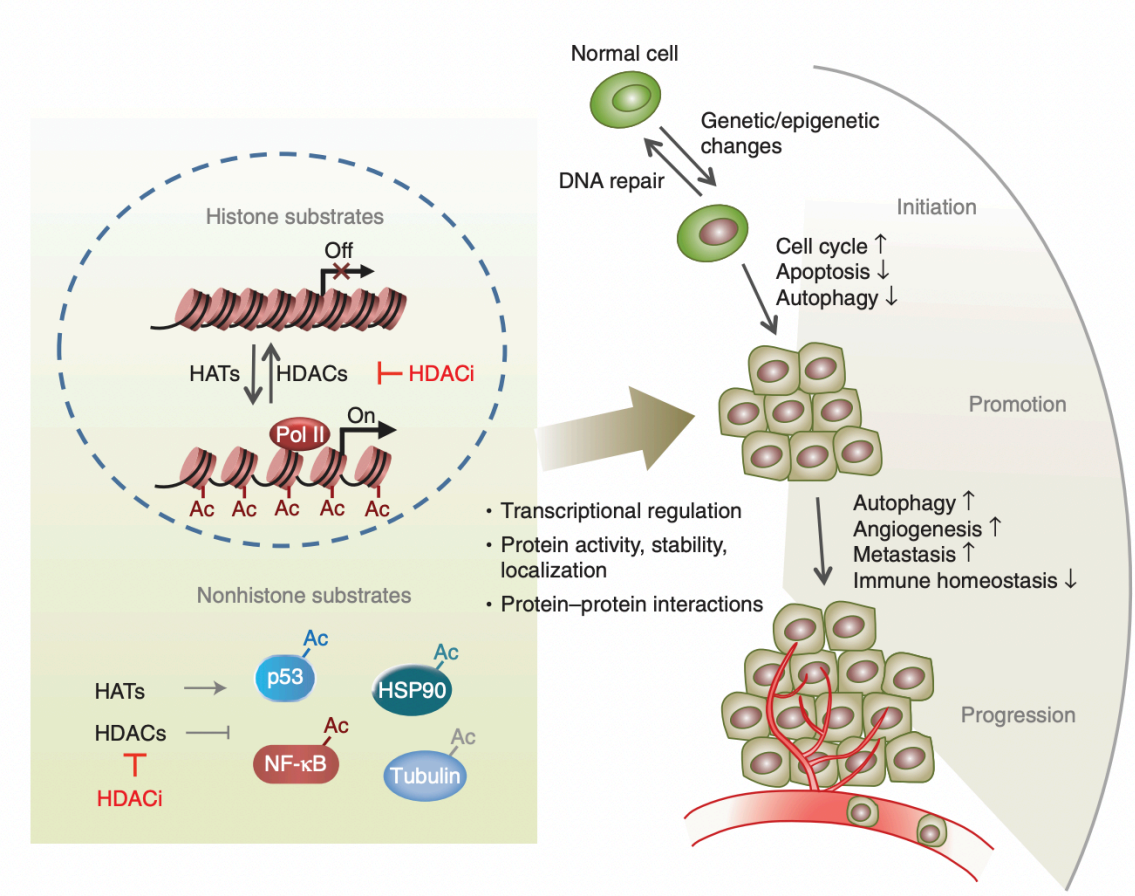


**Figure 1.7 Diverse functions of HDACs in regulating different stages of cancer.** HDACs can regulate multiple aspects of tumorigenesis through different mechanisms. In cancer cells, different HDAC isoforms are frequently overexpressed. The class I HDACs HDAC1 and HDAC2 are expressed in the nucleus and are key regulators of gene expression by regulating histone acetylation. Overexpression of HDAC1 and HDAC2 in cancer cells results in histone hyperacetylation, which contributes to transcriptional silencing of important tumor suppressor genes. In addition to histones, HDACs also have multiple non-histone protein substrates, such as p53, HSP90 and NF-KB. The use of HDAC inhibitors (HDACi) reverses the aberrant activity of HDACs in cancer cells. As seen on the right hand side of the illustration, abnormal HDAC activity promotes initiation, promotion and progression of cancer through dysregulation of multiple biological processes. ↑ denotes processes that are upregulated by HDAC activity, while ↓ denotes processes that are downregulated by HDAC activity. Taken from: (Li and Seto 2016).

### 1.6 HDAC inhibitors (HDACi) as epigenetic therapy for cancer

The identification of HDAC inhibitors (HDACi) preceded the discovery of HDAC enzymes. The first HDACi were identified three decades ago through assessments of their anti-cancer effects in drug screens (Li and Seto 2016). It should be noted that research on HDACi and HDAC biology are intimately linked, as the development of HDACi led to the isolation and identification different HDAC isoforms and have served as valuable tools to dissect the roles of classical HDACs in multiple cell types and diseases models (McClure, Li, and Chou 2018). Importantly, considering established roles of HDAC in promoting tumorigenesis, HDACi have attracted significant attention as a promising class of compounds for the treatment of cancer. HDACi can reverse the aberrant acetylation status of histones and non-histone proteins caused by overexpression of certain HDAC isoforms in in cancer cells (Li and Seto 2016). Through mechanisms that are still not well understood, HDACi have been shown to induce the expression of tumor suppressor proteins, resulting in cell-cycle arrest, apoptosis, autophagy, differentiation, and inhibition of angiogenesis and metastasis (Li, Tian, and Zhu 2020). Furthermore, there is evidence that cancer cells are much more sensitive to HDACi compared to normal non-transformed cells, providing additional value to their therapeutic potential (Ungerstedt et al. 2005; Lee et al. 2010; Gaymes et al. 2006). To date, 4 HDACi have received regulatory approval for the treatment of various malignancies, while many others are currently under clinical development. Vorinostat (SAHA) was the first HDACi to receive approval by the US FDA in 2006 for the treatment of cutaneous T-cell lymphoma (CTCL) (Mann et al. 2007). This was followed by Romidepsin, which was

approved in 2009 to treat both CTCL and peripheral T-cell lymphoma, Belinostat in 2014 for the treatment of peripheral T-cell lymphoma, and Panobinostat in 2015 for the treatment of relapsed multiple myeloma (Frye et al. 2012; McDermott and Jimeno 2014; Richardson et al. 2016). While these inhibitors have been approved as monotherapies, numerous preclinical studies and clinical trials are testing the efficacy of these HDACi in combination with other chemotherapeutic agents or treatment modalities (e.g. radiation) for different malignancies (Jenke et al. 2021).

### *1.6.1 Major classes and general mechanism of action of HDACi*

HDACi have been purified from natural and synthetic sources and can be divided into four major classes based on their chemical structures. These are the hydroxamates, cyclic peptides, benzamides and aliphatic acids (Ho, Chan, and Ganesan 2020). Although they differ structurally, most HDACi belonging to the different classes share a common mechanism of action: they bind to the active site of HDAC enzymes and chelate the zinc ion that is necessary for their catalytic activity (Zhang et al. 2018). As illustrated in Figure 1.8, the pharmacore of most HDACi generally consists of three elements: the zinc-binding group, linker, and cap (Su, Gong, and Liu 2021). HDAC1–11 have a cavity containing a catalytic zinc ion that is connected to the protein–solvent interface by an 11 Å tunnel (Wang et al. 2004). The hydrophobic linker moiety of a HDACi will insert in this tunnel, allowing the zinc-binding group to sequester the zinc ion and thereby negate HDAC activity. The chemical groups that form the cap region varies widely across different HDACi, but this moiety generally interacts with the rim of the enzyme and can

be modified to confer HDACi a greater ability to discriminate between different HDAC enzymes, a concept that is commonly referred to as isoform selectivity (Ho, Chan, and Ganesan 2020).

The hydroxamates (or hydroxamic acids) were the first class of HDACi to be identified and are the most extensively used and well-studied. The first discovered hydroxamate was the natural anti-fungal product trichostatin A (TSA), but its clinical use has been hampered due to its excessive toxicity (Yoshida et al. 1990; Bezecny 2014). Notably, three of the FDA-approved HDACi (vorinostat, belinostat, and panobinostat) are also hydroxamates. These inhibitors are potent and have broad-spectrum activity and have been shown to inhibit the activity of class I, IIb and III HDACs at low nanomolar concentrations (Li and Seto 2016).

Another group of HDACi are the cyclic peptides, of which the FDA-approved drug Romidepsin (FK-288) is the most well-characterized example. Compared to vorinostat and other hydroxamates, romidepsin appears to have a narrow spectrum of HDAC inhibition and thus is considered a more selective HDACi as it only targets class I isoforms (Falkenberg and Johnstone 2014). The benzamide class of HDACi include the drugs Entinostat, Chidamide and Tacedinaline among others, many of which are currently being tested in phase II and III clinical trials for several solid and hematological malignancies (Li and Seto 2016). The amino-benzamide motif present in these HDACi endows these molecules with tight-binding mechanism (slow-on/slow-off), unlike the classic fast-on/fast-off kinetics commonly associated with hydroxamate-based HDACi (Chou, Herman, and Gottesfeld 2008; McClure, Li, and Chou 2018). Similarly to cyclic-peptides like romidepsin, amino-benzamide HDACi harbor higher selectivity towards

class I HDACs. However, in the clinic entinostat was found to harbor a much lower therapeutic index compared to the hydroxamate vorinostat, due to severe off-target toxicity and poor pharmacokinetic properties (Ryan et al. 2005; McClure, Li, and Chou 2018). The least commonly used class of HDACi are the short-chain fatty acids, examples of which include valproic acid (VPA) and phenylbutyrate. This class of molecules can only inhibit HDACs at high millimolar concentrations, and their weak HDAC inhibitory activity is thought to be related to their structure as they have no access to the zinc ion found in the active site of HDACs (Kim and Bae 2011). Hence, while some short-chain fatty acids are currently being tested in clinical trials, they are thought to have limited applications as bona fide HDACi in the clinic compared to other more potent inhibitors (McClure, Li, and Chou 2018).

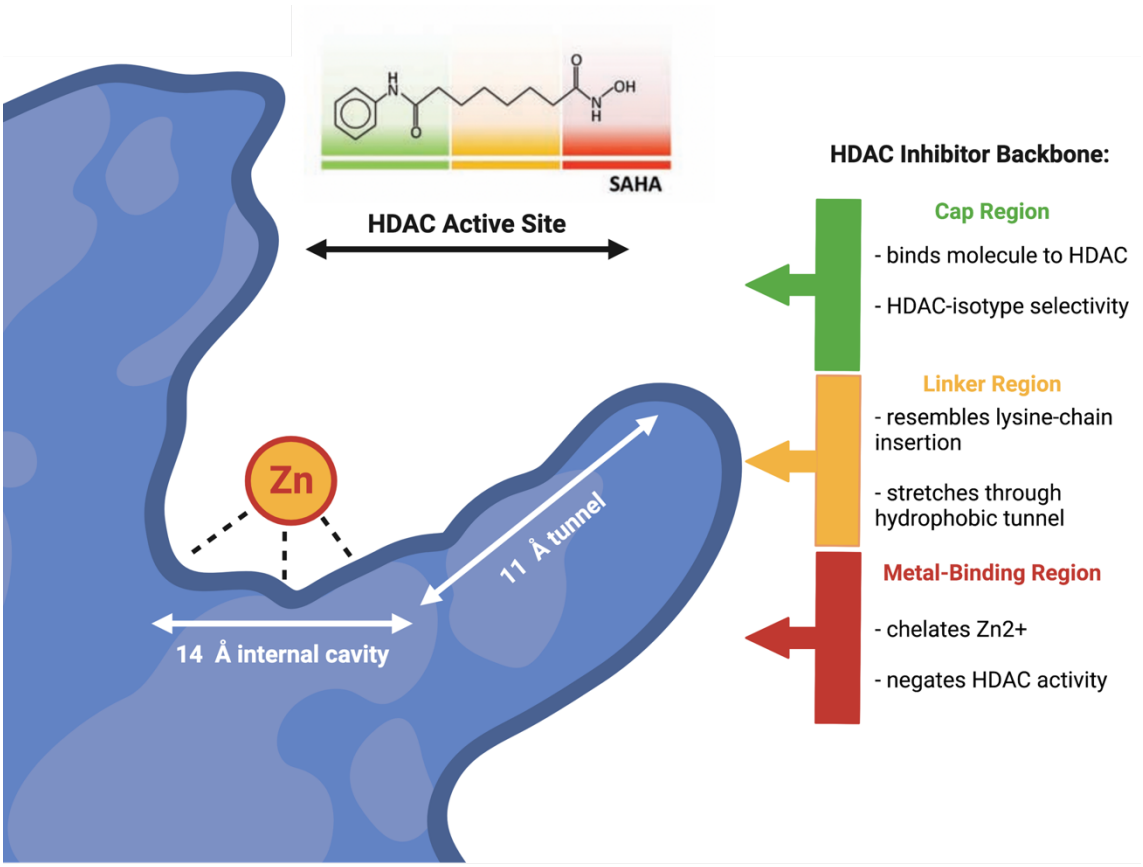


**Figure 1.8 Structural basis of HDAC inhibition.** Diagram of the tunnel and active site of a classical HDAC enzyme. The diagram to the right illustrates the simplified structural components of a typical hydroxamic acid-based HDAC inhibitor. The HDACi pharmacore consists of three groups, and their roles are summarized in the diagram: the cap region, linker region and metal-binding region. These groups are overlayed on top of the chemical structure of Vorinostat (SAHA), a pan-HDACi, for reference. Adapted from: (Hancock et al. 2012).

*1.6.2 Toxicities associated with HDACi and development of isoform-selective inhibitors*

A major limitation hampering the therapeutic potential of currently available HDACi is that they are highly toxic when administered systemically in humans (Li and Seto 2016). Regardless of the structure of HDACi employed, almost all clinical trials have reported very similar adverse events and dose limiting toxicities which often include fatigue, diarrhea, vomiting, anemia, bone marrow toxicity, severe thrombocytopenia, and

cardiac abnormalities (Shah 2019; Subramanian et al. 2010). The widespread toxicities are attributed to the fact that most HDACi are broad-spectrum inhibitors and thereby inhibit the activity of numerous or all HDAC isoforms. While some HDAC isoforms are normally expressed in a tissue-specific manner, class I HDAC1-3 are nuclear isoforms that are ubiquitously expressed and play critical roles in the regulation of gene expression through their ability to modulate histone acetylation (Ho, Chan, and Ganesan 2020). Hence, it is hypothesized the debilitating toxic side effects observed with most HDACi is driven through systemic inhibition of HDAC1-3 which results in severe cytotoxicity in both normal organs and malignant tumors (Ho, Chan, and Ganesan 2020). Moreover, not all HDACs are necessarily equally overexpressed of functionally important within a specific tumor, putting into question the true value and clinical relevance of pan-HDAC inhibition (Su, Gong, and Liu 2021).

Within the field of medicinal chemistry there is evidence that increased target selectivity usually leads to a superior safety profile(Ho, Chan, and Ganesan 2020). Consequently, there has been a strong interest in developing HDACi that can selectively target individual HDAC isoforms, in so doing reducing toxicity by sparing other isoforms that are not involved in pathogenesis of a particular disease. In addition to improving the safety profile for this class of drugs, the development of isoform-selective HDACi may prove important for dissecting the unique biological functions of individual HDAC isoforms across different cell types and disease states. Unfortunately, identification and development of isoform-selective inhibitors has proven to be very challenging because of the high structural homology at the active site of most HDAC enzymes (Li and Seto 2016; Seto and Yoshida 2014). While no pure isoform-selective HDACi currently exist,

new “second-generation” HDACi have been developed over the past decade that harbor enhanced affinity towards certain HDACs over other isoforms, improved pharmacokinetic profiles and prolonged pharmacodynamic responses in tumor tissues (Ho, Chan, and Ganesan 2020). Examples of such HDACi are listed in Table 1.2.

| compd | HDAC isoform, $IC_{50}$ (nM) | | | | | | | | | | |
|---|---|---|---|---|---|---|---|---|---|---|---|
| | 1 | 2 | 3 | 8 | 4 | 5 | 7 | 9 | 6 | 10 | 11 |
| romidepsin (**3**) | 1 | 1 | 1 | >1000 | 647 | >1000 | >1000 | >1000 | 226 | 1 | 0.3 |
| vorinostat (**8**)[a] | 60 | 42 | 36 | 173 | 20 | 36 | 129 | 49 | 29 | 60 | 31 |
| ricolinostat (**11**) | 58 | 48 | 51 | 100 | >1000 | >1000 | >1000 | >1000 | 5 | | >1000 |
| citarinostat (**12**) | 35 | 45 | 46 | 137 | >1000 | >1000 | >1000 | >1000 | 3 | | |
| belinostat (**15**)[a] | 26 | 22 | 19 | 22 | 15 | 25 | 51 | 24 | 10 | 59 | 27 |
| panobinostat (**16**)[a] | 3 | 2 | 2 | 22 | 1 | 1 | 2 | 1 | 1 | 31 | 4 |
| pracinostat (**18**)[a] | 28 | 27 | 19 | 48 | 16 | 21 | 104 | 24 | 247 | 23 | 24 |
| givinostat (**19**) | 133 | 293 | 136 | 837 | >1000 | 532 | 524 | 512 | 312 | 331 | 287 |
| abexinostat (**20**) | 21 | 63 | 148 | 370 | 60 | 48 | 350 | 168 | 12 | 52 | 14 |
| bisthianostat (**22**) | 4 | 13 | 6 | 17 | >1000 | >1000 | >1000 | >1000 | 2 | 2 | 78 |
| quisinostat (**23**) | 0.1 | 0.3 | 5 | 4 | 0.6 | 4 | 119 | 32 | 77 | 0.5 | 0.4 |
| fimepinostat (**25**) | 2 | 5 | 2 | 191 | 409 | 674 | 426 | 554 | 27 | 3 | 5 |

**Table 1.2 HDAC isoform $IC_{50}$ values of clinical candidate and approved hydroxamic acid HDACi.** This table illustrates the biochemical $IC_{50}$ values (in nM concentrations) for each individual classical HDAC isoform obtained using several first and second-generation HDACi. Taken from: (Ho, Chan, and Ganesan 2020)

## 1.7 HDACi for the treatment of GBM

As reviewed previously in section 1.4, GBM is characterized by an aberrant epigenome. However, to date the expression and functions of different HDAC isoforms in GBM are not well characterized and severely understudied (Lee et al. 2017). Despite this, over the past 15 years numerous broad-spectrum HDACi have been studied preclinically in the realm of neuro-oncology, four of which (vorinostat, romidepsin, panobinostat and VPA) have been tested in clinical trials for patients with primary and recurrent GBM (Bezecny 2014). Unfortunately, to date all HDACi have failed to significantly prolong survival in this population of patients. The disappointing clinical results with HDACi can be attributed to inadequate disease modeling at the preclinical level, poor blood-brain barrier penetration, scarce CNS pharmacokinetic profiling and narrow therapeutic windows of pan-HDACi owing to their high toxicity (Bezecny 2014; Sanai 2019; Chen et al. 2020).

### *1.7.1 Preclinical testing of HDACi*

Many studies have been conducted to study the efficacy of numerous pan-HDACi in preclinical models of GBM. These preclinical studies employed human and murine GBM cell lines to examine the therapeutic potential of HDACi *in vitro* and *in vivo*. The most well-studied HDACi are vorinostat, romidepsin, TSA, VPA, phenylbutyrate and tubacin (Lee et al. 2017; Menezes et al. 2019; Was et al. 2019; Diss et al. 2014; Chiao et al. 2013; Wu et al. 2016; Chen et al. 2020). The reported pan-HDACi-mediated cytotoxic effects on human GBM cultures are similar across different studies, irrespective of the class of HDACi used. Multiple *in vitro* analyses conducted in human, mouse and rat

glioma models have shown these pan-HDACi can inhibit cell proliferation and induce apoptosis in a dose-dependent manner. These HDACi upregulate the expression of p21, inducing cell cycle arrest, as well as the expression of pro-apoptotic proteins such as Bad, Bax, Puma and Bim in tandem with increase histone acetylation (Chen et al. 2020; Lee et al. 2017; Bezecny 2014). Through mechanisms that are not entirely clear, there is also evidence that HDACi such vorinostat, VPA and TSA trigger autophagy and promote differentiation into astrocytes (Svechnikova, Almqvist, and Ekstrom 2008; Chiao et al. 2013; Alvarez et al. 2015). Animal modeling studies demonstrated that vorinostat, romidepsin and entinostat could slow the growth of flank and orthotopic xenograft models of GBM and other gliomas, and result in prolonged survival (Sun et al. 2009; Sawa et al. 2004; Eyupoglu, Hahnen, Buslei, et al. 2005). However, it should be noted that for orthotopic tumor models some of these HDACi were administered through direct intracranial diffusions or convection-enhanced delivery, which preclude a true understanding of the brain penetration properties of these drugs (Ugur et al. 2007; Tosi et al. 2020; Sawa et al. 2004). In fact, to date no CNS pharmacokinetic data is available for any HDACi tested in preclinical models of high-grade gliomas – and this is a serious limitation considering that efficient drug delivery is one of the major obstacles hampering successful treatment of brain tumors.

Another noteworthy caveat of these preclinical studies is that they were conducted using serum-grown, immortalized cell lines that do not faithfully recapitulate the intricate biology and extensive heterogeneity of human GBM (Lee et al. 2006). Critically, no studies have addressed how HDACi specifically impact GSC survival *in vitro* and *in vivo*. In summary, our current understanding of the roles of HDACs in GBM has so far been

limited to testing the anti-tumor effects of pan-HDACi such as vorinostat and romidepsin, rather than evaluating the individual functions and importance of different HDAC isoforms in this disease. Identification of which HDAC isoforms contribute to GBM pathogenesis, especially in the context of the GSC phenotype, may provide the rationale for preclinical testing of novel second-generation HDACi that have enhanced isoform-specificity and pharmacokinetic properties in GBM.

### *1.7.2 Clinical testing of HDACi*

Vorinostat was the first HDACi to enter clinical trials for the treatment of primary and recurrent GBM. A phase I/II trial of vorinostat demonstrated that it was safe and well-tolerated in patients when administered with standard TMZ and radiation (NCT00731731); however, it failed to meet its primary efficacy endpoint with no improvement in progression-free survival at 6 months compared to historical controls (Galanis et al. 2018; Galanis et al. 2009). Vorinostat also underwent phase I testing in combination with bevacizumab and irinotecan (a topoisomerase I inhibitor) for recurrent GBM, but this combination was poorly tolerated due to excessive cumulative toxicity (NCT00762255) (Chinnaiyan et al. 2012). Following the FDA-approval of bevacizumab for the treatment of recurrent GBM, vorinostat underwent phase II clinical testing in combination with bevacizumab (NCT01738646) (Ghiaseddin et al. 2018). While this combination was well tolerated, it unfortunately also did not improve progression-free survival at 6 months. Hence, despite some promising results at the preclinical level, to date vorinostat has not yielded any significant therapeutic benefit for GBM patients.

Panobinostat and romidepsin have also been tested in several phase II clinical rials in combination with bevacizumab or radiation treatment (NCT00859222, NCT01324635, NCT00085540) (Lee, Reardon, et al. 2015; Iwamoto et al. 2011). However, these trials also reported that these combination therapies did not significantly improve progression-free survival at 6 months or overall survival in GBM patients. As described earlier, these underwhelming results could in part be attributed due to their poor or unknown CNS pharmacokinetic profiles of most broad-spectrum HDACi and an incomplete understanding of the biological importance of the functionally diverse HDAC isoforms with respect to the pathogenesis and progression of GBM.

By contrast, VPA is the only reported HDACi to provide a significant increase in progression-free survival and overall survival relative to historical control data in a phase II trial (NCT00302159) in combination with the standard-of-care for GBM (Krauze et al. 2015). However, there is a caveat. As will be discussed in more detail in Chapter 3, VPA is anti-epileptic drug with modest HDAC-inhibitory properties, and it is not clear whether the apparent clinical benefits observed with VPA are due to its effects on HDAC activity or due to its ability to potentiate glutamatergic inhibitory neurotransmission.

### 1.8 Overview of the research

Numerous HDACi have been tested in clinical trials for the treatment of GBM and almost unanimously yielded disappointing results. However, the use of these broad-spectrum HDACi preceded our understanding of the functional roles and importance of individual classical HDAC isoforms, particularly within the class I group, in GBM.

Critically, to date there have been no studies aimed at elucidating what isoforms contribute to the maintenance GSC phenotype, the therapy-resistant population of cells that are responsible for GBM recurrence. Hence, understanding which HDAC isoforms are highly expressed in GBM and drive tumor cell growth is crucial to lay the foundation for preclinical and clinical testing of novel HDACi that possess greater isoform-selectivity to treat this devastating disease.

In this dissertation, I will describe work that provides a rationale for selective therapeutic targeting of HDAC1 in GBM. In Chapter 2, I demonstrate that HDAC1, but not its paralogue HDAC2, is the essential class I HDAC that is necessary to sustain proliferation and survival of human GSCs. I show that within the classical HDAC family, HDAC1 expression is positively correlated with increased brain tumor aggressiveness and is more highly expressed in GBM compared to normal brain tissue. Importantly, I found that HDAC1 loss is not compensated for by HDAC2 or other HDACs, revealing that HDAC1 harbors unique non-redundant functions in GSCs. Using cell-based and biochemical assays as well as transcriptomic analyses, I demonstrate that loss of HDAC1 alone significantly attenuates the tumorigenic potential of GSCs. This is the first report that gene silencing of a single class I HDAC isoform is sufficient to provide a survival benefit in patient-derived and mouse models of GBM. Based on these findings, in Chapter 3, I assessed the efficacy, pharmacokinetic properties and translational potential of quisinostat – a second generation HDACi that has very high affinity for HDAC1 over other HDAC isoforms. I show that quisinostat is a brain-penetrant molecule that not only reduces tumor burden *in vivo,* but potently sensitizes tumors to radiation therapy and

significantly extends survival in orthotopic patient-derived xenograft models of GBM. Together, these results provide the foundation for the clinical development of quisinostat in combination with radiation therapy for the treatment of GBM.

# CHAPTER 2

# NON-REDUNDANT, ISOFORM-SPECIFIC ROLES OF HDAC1 IN GLIOMA STEM CELLS

## 2.1 Publication Note

The research reported in this chapter has been published in *JCI Insight* by Costanza Lo Cascio, James McNamara, Ernesto Luna Melendez, Erika M. Lewis, Matthew Dufault, Nader Sanai, Christopher L. Plaisier and Shwetal Mehta. Non-redundant, Isoform-Specific Roles of HDAC1 in Glioma Stem Cells. *JCI Insight* (2021). All co-authors have granted permission for this work to be included in this dissertation.

## 2.2 Introduction

A well-regulated interplay between histone acetylation and deacetylation, mediated by histone acetyltransferases (HATs) and histone deacetylases (HDACs), is essential for the dynamic fine-tuning of gene expression (Allis and Jenuwein 2016). HDACs mediate chromatin compaction, favoring transcriptional repression, and are frequently overexpressed in human cancers, including glioblastoma (GBM) (Haberland, Montgomery, and Olson 2009; Lee, Murphy, et al. 2015). Hence, over the last decade there has been considerable interest in HDAC inhibitors (HDACi) in the field of oncology. However, systemic inhibition of HDACs with pharmacological inhibitors have failed to provide significant therapeutic benefit in clinical trials for primary and recurrent GBM (Galanis et al. 2009; Hooker et al. 2010; Iwamoto et al. 2011; Bezecny 2014; Li

and Seto 2016). HDACi currently in clinical trials have poor brain penetration and a narrow therapeutic window due to their relatively low selectivity for individual HDAC isoforms (Suraweera, O'Byrne, and Richard 2018; Yelton and Ray 2018; Bezecny 2014; Lee, Murphy, et al. 2015; Tosi et al. 2020). Notably, not all HDACs are equally expressed in GBM, and the specific functions of individual HDAC isoforms in these tumors are not well understood (Cancer Genome Atlas Research 2008). Hence, there is a need to dissect the functional importance and requirement for individual HDACs in GBM, especially the therapy-resistant glioma stem cells (GSCs), to provide a rationale for the development of isoform-selective HDACi.

While it is known that HDAC1 and HDAC2 (class-I HDACs) harbor highly specific and non-overlapping roles in the developing brain, it is unclear whether these non-redundant functions are retained in glioma cells (Seto and Yoshida 2014; Haberland, Montgomery, and Olson 2009). Our current knowledge on the role of HDACs in GBM is primarily based on pan-HDACi studies and isoform-specific knockdown or knockout experiments in serum-grown, long-term cultures of GBM cells and not in GSCs (Lee et al. 2006; Li, Chen, et al. 2018; Wang, Bai, et al. 2017; Was et al. 2019; Zhang, Wang, et al. 2016; Menezes et al. 2019; Meyers et al. 2017). Even the Cancer Dependency Map project, which profiled hundreds of cancer cell lines to identify genetic and pharmacological vulnerabilities, utilized traditionally grown glioma cell lines (Meyers et al. 2017). Considering that GBMs frequently hijack normal developmental programs to their advantage and the fact that there is an isoform-specific requirement for HDAC2 over HDAC1 during normal brain development, we questioned whether GSCs maintain similar or divergent isoform-specific requirements for class-I HDAC activity to sustain

tumor growth (Hagelkruys et al. 2014; Jurkin et al. 2011) (Song et al. 2020; Bastola et al. 2020).

In this chapter, we demonstrate that HDAC1 is critical for the proliferative potential of GSCs in a p53-dependent manner. Knockdown of *HDAC1* alone results in significantly prolonged survival in a patient-derived xenograft (PDX) model and a mouse model of human glioma, and the resulting tumors exhibit a more invasive growth pattern. Our data reveal an essential non-redundant role of HDAC1 in GSCs in contrast to its dispensability in normal neural stem cells (Hagelkruys et al. 2014). This molecular selectivity for HDAC1 is evident upon its ablation in hGSCs where its loss is not compensated by upregulation of its paralogue HDAC2 or other HDACs. Furthermore, we observe that ablation of HDAC1 function in GSCs suppresses expression of key glioma stemness markers like SOX2, Nestin and OLIG2. In addition, *HDAC1* silencing stabilizes and acetylates p53, resulting in upregulation of key p53 target genes and induction of programmed cell death. This demonstrates that HDAC1, but not HDAC2, functions as a p53 deacetylase in hGSCs, as previously shown in several normal and tumorigenic cell lines (Luo et al. 2000; Ito et al. 2002; Ni et al. 2020). Our results uncover a previously underappreciated role for HDAC1 in regulating the GSC phenotype and highlight opportunities for the development of isoform-specific HDACi for novel targeted and combinatorial therapies in GBM.

## 2.3 Methods

### *2.3.1 Primary Cell Culture*

Patient-derived glioma stem cell lines (GSCs; GB3, GB82, GB71 and GB84) were established from resected primary GBM tumor tissue at BNI. BT145, BT70, BT187 and BT286 hGSCs were obtained from Dr. Keith Ligon's laboratory at the Dana-Farber Cancer Institute. 211 and 252 hGSCs were obtained from Dr. Harley Kornblum's laboratory at University of California, Los Angeles. All human GSCs were cultured as described previously (Ligon et al. 2007; Mehta et al. 2011). Normal Human Astrocytes were purchased from ThermoFisher Scientific. Human neural progenitor cells (hNPCs) were derived from induced-pluripotent stem cells (iPSCs) from control subjects at the BNI (ihNPCs) (kindly provide by Dr. Rita Sattler's laboratory). ihNPCs, hGSCs and mGSCs, were cultured as spheres on non- tissue culture-treated 10cm plates or as adherent cultures with laminin on tissue culture-treated 10cm plates (ThermoFisher Scientific). ihNPCs and hGSCs were grown in DMEM/F12 media, supplemented with B27 and N2 (Invitrogen, ThermoFisher Scientific) in the presence of 20 ng/ml epidermal growth factor (EGF) and basic fibroblast growth factor (bFGF) (MilliporeSigma). Primary Human Astrocytes (NHA; ScienCell) were grown in Astrocyte Media (5% FBS, Astrocyte Growth Supplement, 1% penn-strep) on Poly-L Lysine coated plates according to manufacturer recommendations.

### *2.3.2 Lentivirus Production*

Lentiviruses were generated in HEK-293FT cells through Polyfect (QIAGEN)-mediated transfection with 4th generation packaging plasmids encoding for HDMH.Hgpm2, TAT,

REV, HDM.G, and lentiviral transfer vector (pGFP-C-shLenti). The *HDAC1*-targeting shRNA lentiviral vectors were obtained from Origene (sh*HDAC1*_A: 5'-GTCCAAAGTAATGGAGATGTTCCAGCCTA-3' and sh*HDAC1*_B: 5'-ATTTGCTGCTCAACTATGGTCTCTACCGA-3'). The *HDAC2*-targeting shRNA lentiviral vector was obtained from Horizon Discovery (sh*HDAC2*: 5'-TCATGAACAGCATCTTCTG-3'). As a negative control we used a non- target shRNA sequence (shNT: 5'-CAACAAGATGAAGAGCACCAA-3'), which does not target any human genes. Retroviruses were generated in HEK-293FT cells by Polyfect- mediated transfection with packaging plasmids encoding VSVG, gag-pol, and a retroviral transfer vector (pWZL) encoding the gene of interest (p53-DN) (Mehta et al. 2011).

### *2.3.3 Cell Viability Assays*

GSCs, hNPCs and NHAs transduced with either shNT or sh*HDAC1* shRNAs at a MOI of 3 were selected with 2 μg/mL puromycin 72 hours post-transduction. Control or *HDAC1*-knockdown GSCs and NPCs were seeded in laminin-coated tissue culture-treated 96-well plates (clear bottom, white plate; Corning) at a density of 1,000-2,000 cells per well (cell line dependent) in GSC media. Transduced NHAs were seeded using their normal growth conditions without laminin (10% FBS in DMEM). Seeded cells were grown for 7 days at which point cell viability was measured and quantified. All cell viability measurements were performed using the *CellTiter-Glo*® Luminescent Cell Viability Assay (Promega) following the manufacturer's instructions. All cell viability results represent the mean of at least 2 biological replicates, each containing three technical replicates.

### *2.3.4 Western Blotting*

Cellular protein from cultured cells were homogenized in RIPA lysis buffer containing protease and phosphatase inhibitors (ThermoFisher Scientific), rotated at 4℃ for 20 minutes and then centrifuged at 15,000 rpm for 10 minutes at 4℃. Protein concentration from whole- cell extracts were determined using the Bradford Protein Assay (ThermoFisher Scientific). Equal amounts of protein (10-40 µg/lane) were loaded onto a 7.5% 10% or 12.5% SDS- PAGE gels and transferred to a polyvinylidene fluoride membrane (PVDF; Millipore-Sigma).

Membranes were blocked with 5% non-fat milk for 1 hour at room temperature and incubated overnight with primary antibody at 4℃; Primary antibodies used in this study were mouse anti-HDAC1 (1:1000; Cell Signaling Technologies, 5356); rabbit anti-HDAC1 (1:1000, Cell Signaling Technologies, 2062), rabbit anti-HDAC2 (1:1000; Cell Signaling Technologies, 2540); mouse anti-HDAC3 (1:1000, Cell Signaling Technologies, 3949), rabbit anti-SOX2 (1:1000; Cell Signaling Technologies, 3579); mouse anti-human Nestin (1:1000; Novus Biologicals, 10C2), rabbit anti-OLIG2 (1:1000, generous gift from the Stiles Lab, Dana-Farber Cancer Institute, Boston), rabbit anti-p21 (1:500; Abcam, ab109520), rabbit anti-EGFR (1:10,000; Abcam, ab52894), mouse anti-STAT3 (1:1000, Cell Signaling Technologies, 9139), rabbit anti-pSTAT3 Tyr705 (1:500, Cell Signaling Technologies, 9145), mouse anti-p53 (1:1000, Cell Signaling Technologies, 2524), rabbit anti-acetyl p53 K382 (1:500, Cell Signaling Technologies, 2570), rabbit anti-acetyl p53 K373 (1:5000, Abcam, 62376), rabbit anti-H3K27ac (2 µg/mL, Abcam, ab4729), rabbit anti-H3K9/14ac (1:1000, Cell Signaling Technologies,

9677), mouse anti- β-actin (1:1000, Bio-Rad, MCA5775GA) and mouse anti-Vinculin (1:10,000, Millipore 05-386). Membranes were probed with fluorophore-conjugated anti-mouse or anti-rabbit secondary antibodies (1:10,000; ThermoFisher Scientific). Western blots were developed using the LI-COR Odyssey CLx imaging system (LI-COR Inc.) and quantitated using the Image Studio Lite software. All Western blots are representative images from a minimum of three biological replicates.

### *2.3.5 Immunocytochemistry*

Cells were grown as adherent cultures on laminin-coated glass coverslips (Thermo Fisher Scientific) in GSC media. 24 hours after plating the cells were transduced with non-target control or HDAC1-targeting shRNAs at a MOI of 3. 72 hours post-transduction, puromycin was added at a concentration of 2μg/mL for 72 hours to select for successfully transduced cells. After selection cells were and fixed with 4% paraformaldehyde (PFA) for 13 minutes at room temperature. Cells were washed with PBS and subsequently permeabilized and blocked with 5% normal goat serum (Sigma Aldrich) and 0.2% Triton X-100 in PBS (blocking solution) for 30 minutes at room temperature. The cells were incubated with primary antibodies overnight at 4°C in blocking solution. Primary antibodies used in this study included rabbit anti-Ki67 (1:1000; Abcam, 15580) and rabbit anti-Cleaved Caspase 3 (1:300; Cell Signaling Technologies, 9661), mouse anti-STAT3 (1:100; Cell Signaling Technologies, 9139). The following day, the cells were washed with PBS three times, incubated with fluorophore-conjugated secondary antibodies at 1:1,000 dilutions (Alexa Fluor 568 goat anti-mouse, Abcam, ab175473; Alexa Fluor 568 goat anti-rabbit, Abcam, ab175471) for 1 hour at room temperature, and

finally washed in PBS three more times. Cells were mounted onto SuperFrost Plus microscope slides using Fluoroshield Mounting Medium containing DAPI (Abcam). Images were acquired using a confocal microscope (Leica Microsystems; TCS SP5) operated with LAS software. The fraction of Ki67- and Cleaved Caspase 3- positive cells were counted from five independent images from each condition. The average and standard deviation were calculated from three biological replicates for all control and *HDAC1*-knockdown (shRNAs A and B) experiments.

### *2.3.6 Real-Time PCR*

Total RNA was extracted from cells by using the PureLink RNA Mini Kit (Ambion) in accordance with the manufacturer's instructions. RNA was quantified on a NanoDrop Spectrophotometer (Tecan), and 1 µg of total RNA was used for cDNA synthesis by using the SuperScript VILO kit (Life Technologies). qPCR was performed using inventoried TaqMan assays for respective target genes and housekeeping control genes (18S) on the QuantStudio 6 Flex Real-Time PCR System (Life Technologies). Fold change in gene expression was analyzed using the delta delta Ct method.

### *2.3.7 Chromatin Immunoprecipitation*

hGSCs with 1% formaldehyde (Sigma) were fixed for 10 min at room temperature. Glycine (125mM) (Fisher Scientific) was added for 5 min at RT to quench formaldehyde. Cells were rinsed with PBS and Protease inhibitors (Pierce, 88266) twice. Cells were pelleted and flash frozen. Cells were sonicated in 50ul of SDS lysis buffer. For each immunoprecipitation, 30µl protein A Dynabeads (Invitrogen) were incubated with 2 µg

of H3K27ac antibody (Abcam) or 1µg of IgG antibody for at least 4 hours at 4°C, and 15µg of sheared chromatin was pre-cleared with 15µl of protein A Dynabeads and incubated at 4°C for 1 hour. The pre-cleared chromatin was subsequently incubated with the antibody-coated beads at 4°C overnight. Beads were washed 6 times with RIPA wash buffer and twice in tris-EDTA. Reverse cross-linking was performed by incubating the beads with 100µl of reverse crosslinking buffer (1% SDS, 0.1M NaCl and 0.1M NaHCO3) overnight at 65°C. The immunoprecipitated DNA was purified using the QIAquick PCR purification kit (QIAGEN) and eluted in ddH2O. Chromatin-immunoprecipitated DNA was analyzed by quantitative PCR using the SYBR Green master mix in a real-time PCR system (Applied Biosciences). The following primers were used(Carro et al. 2010), for the CEBP/β binding site on the *STAT3* promoter: Stat3_1501_f: 5'-CAGGAGGGAGCTGTATCAGG-3' and Stat3_1630_r: 5'-AGGACTTGGGCACAGAAGC-3'.

### *2.3.8 RNA-seq Analysis*

GSCs, hNPCs and NHAs transduced with either shNT or sh*HDAC1* shRNAs at a MOI of 3 were selected with 2 µg/mL puromycin 72 hours post-transduction. 72 hours post-selection, total RNA was extracted from cells using the PureLink RNA Mini Kit (Ambion) in accordance to the manufacturer's instructions. Purified RNA was sent to NovoGene where the RNA was turned into an RNA-seq library using the standard Illumina TruSeq method, and sequenced on an Illumina NextSeq 2500 sequencer. Fastq files were aligned to the genome using STAR (Dobin et al. 2013) and genome build GRCh38 V2.7.1a, counts were be tabulated using htseq-count (Anders, Pyl, and Huber

2015), and DESeq2 (Love, Huber, and Anders 2014) was be used for subsequent differential gene expression analysis. Quality of the sequencing was determined using FastQC, alignment quality was determined by requiring at least 18 million uniquely mapping reads per sample from STAR, and replicate quality was determined through PCA in DESeq2. Differential expression between sh*HDAC1* and shNT were computed in DESeq2 and differentially expressed genes were required to have a log2 fold-change ≥ 1 and Benjamini-Hochberg adjusted p-value ≤ 0.05. Eigengenes for the Neftel et al., 2019 developmental subtypes (Neftel et al. 2019) were computed from the genes in Supplementary Figure 6 using the module Eigengenes function in the WGCNA package in R (Langfelder and Horvath 2008). The data discussed in this publication have been deposited in NCBI's Gene Expression Omnibus (GEO) and are accessible through GEO Series accession number GSE179882 (https://www.ncbi.nlm.nih.gov/geo/query/acc.cgi?acc=GSE179882).

### *2.3.9 Regulatory network inference*

Genes found to be differentially expressed in BT145, GB3, and BT187 cells were independently analyzed for significant enrichment of TF binding sites in the promoters (±5Kbp from the TSS of genes) (Plaisier et al. 2016) using the TF targets python package (https://github.com/cplaisier/TF_targets). Significantly enriched TFs (p-value ≤ 0.05) that were found to be regulators in both BT145 and GB3 but not BT187 were selected for further analyses. The BT145 and GB3 specific TF regulator target genes (with binding sites in their promoters) were tested for functional enrichment with GO BP terms using the enrichr module from the gseapy package on pypi. Significant functional enrichment

was determined by a p-value less than or equal to 0.01. The significantly enriched GO BP terms were then associated with hallmarks of cancer using semantic similarity (Plaisier et al. 2016), (Plaisier, Pan, and Baliga 2012), (Thorsson et al. 2018). Networks were visualized using Cytoscape (Shannon et al. 2003).

### *2.3.10 Live Bioluminescence (IVIS) Imaging*

6 weeks post-implantation, the mice were examined for tumor growth by monitoring bioluminescence every 7 days using the IVIS Xenogen Spectrum platform. D-Luciferin Potassium Salt (Gold Biotechnology) was dissolved in PBS at a final concentration of 15 mg/mL. All mice were weighed each week and were administered D-Luciferin via an intraperitoneal injection (10µl/g). 15 minutes after the injection, the mice were sedated using gaseous isoflurane (Piramal) and placed inside an IVIS Spectrum In Vivo Imaging System (Perkin Elmer) for bioluminescence imaging. The total flux (photons/second) within the region of interest (ROI) was calculated using the Living Image Software 4.5 (Perkin Elmer).

### *2.3.11 Orthotopic Xenograft Studies*

5 to 6-week old *Foxn1*$^{nu}$ nude male mice (The Jackson Laboratory) were used for in vivo orthotopic transplantation of luciferized BT145 (male) cells transduced with either shNT or sh*HDAC1*_A lentivirus. Nude mice were anesthetized using gaseous isoflurane and immobilized on a Leica stereotaxic instrument (cat# 39477001, Leica Microsystems). Following an incision at the midline, a fine hole was drilled 2.5mm lateral to the bregma. Using a 33-guage needle syringe (700 series, Hamilton), 2 µl of dissociated viable cells

(at a density of 50,000 cells/µl) were injected 2 mm deep from the surface of the skull slowly at a constant rate of 1 µl per minute for 2 minutes. The needle was left for 1 additional minute to prevent reflux of the injected cells and was then slowly removed. The incision was closed with surgical staples. All mice were observed daily and were sacrificed upon the onset of severe neurological symptoms and >10% body weight loss. Survival data was plotted and analyzed using GraphPad Prism 8 (GraphPad Software).

### *2.3.12 Immunofluorescence*

Immunofluorescence was performed on free-floating PDX brain tissue sections (40 µm sections). Sections were washed in 0.1 M PB six times, followed (if required) by antigen retrieval in 10mM Citrate Buffer (pH 6.0) at 85°C for 30 minutes on a hot plate. Tissue sections were permeabilized and blocked with 10% goat serum and 0.4% Triton X-100 in 0.1M PB for 2 hours at room temperature. To prevent unspecific staining, sections were further incubated with goat anti-mouse and goat anti-rabbit IgG (Jackson ImmunoResearch Laboratories Inc.; 1:50) in 0.1 M PB, 0.4% Triton X-100 for 30 minutes at room temperature. Sections were then washed three times in 0.1M PB and then incubated in primary antibodies diluted in 2% goat serum and 0.4% Triton X-100 in 0.1M PB overnight at 4°C. Following washes in 0.1M PB, incubation with secondary antibodies (Invitrogen; ThermoFisher Scientific) was performed for two hours at 4°C in 2% goat serum and 0.4% Triton X-100 in 0.1M PB. Nuclear counterstaining was achieved with DAPI (0.5 µg/mL). The following primary antibodies were used in this study: rabbit anti–Ki67 (1:150, Abcam), anti-human mitochondria (1:200, MilliporeSigma, 133-1); mouse anti-OLIG2 (1:400, MilliporeSigma, 211F1.1), rabbit

anti-HDAC1 (1:500, Abcam, 109411), rabbit anti-H3K9/14ac (1:1000, Cell Signaling Technologies, 9677) and rabbit anti-STAT3 (1:500, Cell Signaling Technologies, 9139). Goat anti-mouse and anti-rabbit secondary antibodies were used at 1:1,000 dilutions (Invitrogen; ThermoFisher Scientific). For nuclear counterstaining, DAPI (1:1,000; Sigma-Aldrich) was used. Coverslips were mounted using ProLong Gold Antifade Mountant (ThermoFisher Scientific).

### *2.3.13 Image Acquisition*

Analysis of immunostaining on PDX brain tissue sections was performed on confocal stacks (with a step size of 1.5 μm) acquired with a either a 10x or 20x water-immersion objective on a laser-scanning confocal microscope (Leica Microsystems; TCS SP5) operated with LAS software. The fraction of nuclear STAT3 *in vitro* was quantified using the Intensity Ratio Nuclei Cytoplasm Tool on ImageJ (5-8 images were processed for each experimental condition across four independent experiments). Fluorescent intensity quantifications of STAT3 in PDX tissue were performed on Fiji. Otsu's method was used to threshold engrafted GFP-positive glioma cells and create a selection. The mean gray values of STAT3 pixel intensity within the selected areas were then measured (4 to 5 images were quantified per mouse, with 3 mice total in each experimental group).

### *2.3.14 Statistical Analysis*

Data are presented as the mean ± SEM. If comparing two conditions or cell lines, significance was tested with unpaired two-tailed Student's t-test. Significance of the differences between conditions or cell lines were tested by the two-way ANOVA with

Bonferroni multiple comparison tests using GraphPad Prism 8 (GraphPad software). Survival studies were analyzed using the Kaplan-Meier method with the Mantel-Cox log-rank test (GraphPad software). Statistical significance was defined at * $p < 0.05$, ** $p < 0.01$, *** $p < 0.001$, **** $p < 0.0001$.

### *2.3.15 Study Approval*

The patient samples used for this research were provided by the Biobank Core Facility at St. Joseph's Hospital and Medical Center and Barrow Neurological Institute (BNI). The samples were deidentified and conformed to the Biobank Institutional Review Board's protocol. Animal husbandry was performed in accordance with the guidelines of the St. Joseph's Hospital and Medical Center and Barrow Neurological Institute under the protocol approved by the Institutional Animal Care and Use Committee.

## 2.4 Results

### *2.4.1 HDAC1 expression is correlated with worse survival in GBM*

We evaluated relative mRNA expression levels of *HDAC1* and *HDAC2* across different grades of glioma using the TCGA, CGGA and REMBRANDT databases (Cancer Genome Atlas Research 2008; Madhavan et al. 2009; Zhao et al. 2021). *HDAC1* expression increases with WHO tumor grade and its expression is significantly higher in grade IV (GBM) than in lower-grade gliomas ($p < 0.001$) (Figure 2.1A). In contrast, *HDAC2* is expressed at high levels across all glioma samples (Figure 2.1B). *HDAC1* expression does not differ significantly across the three molecular subgroups of GBM

(Wang, Hu, et al. 2017) (Figure 2.1C), and its expression is higher in GBM compared to normal brain tissue (Figure 2.2A). We also found that the expression of *HDAC1* is inversely correlated with patient survival in three independent datasets that include GBM and low-grade gliomas (Figure 2.1D) (Dali-Youcef et al. 2015). We compared HDAC1 and HDAC2 protein expression in gliomas using the Human Proteome Atlas and found that both are strongly expressed in most gliomas, although HDAC1 expression is higher in GBM than in low-grade gliomas (Uhlen et al. 2015). One caveat with these analyses is that they were conducted on bulk GBM tissue, and thus do not provide information on the functions of these two HDAC paralogues within the GSC population. Hence, given these expression data and the role of HDAC1 as a global repressor of transcription (Seto and Yoshida 2014), we sought to specifically understand its functional impact across multiple patient-derived GBM GSCs (hGSCs).

### *2.4.2 HDAC1 and HDAC2 are abundantly expressed in human GSCs*

We compared the expression of HDAC1 and HDAC2 across eight GSC lines (Figure 2.1E), normal human astrocytes (NHA) and human neural progenitor cells derived from induced pluripotent stem cells from a healthy individual (ihNPC) (Figure 2.1F). HDAC1 and HDAC2 were equally and abundantly expressed in NHAs and GSC lines (Figure 2.1E-F), while HDAC1 levels were lowest in normal ihNPCs (Figure 2.1F). The latter observation is in line with previous reports that demonstrated that HDAC1 and HDAC2 display different lineage-specific or developmental-stage expression patterns – with HDAC2 being more highly expressed than HDAC1 in neural precursors and mature neurons (MacDonald and Roskams 2008; Hagelkruys et al. 2014). Another class I HDAC

that has been previously implicated in GBM biology and whose expression correlates with increased glioma aggressiveness is HDAC3 (Li et al. 2016; McLendon et al. 2008). However, we found that HDAC3 protein levels were very low compared to HDAC1 across multiple primary GSC cell lines (See Figure 2.2B). Hence, our goal was to investigate the significance of high HDAC1 expression in GBM tumors and assess whether GSCs harbor differential dependencies or degrees of functional redundancy with respect to the activity of the two class I HDAC paralogues.

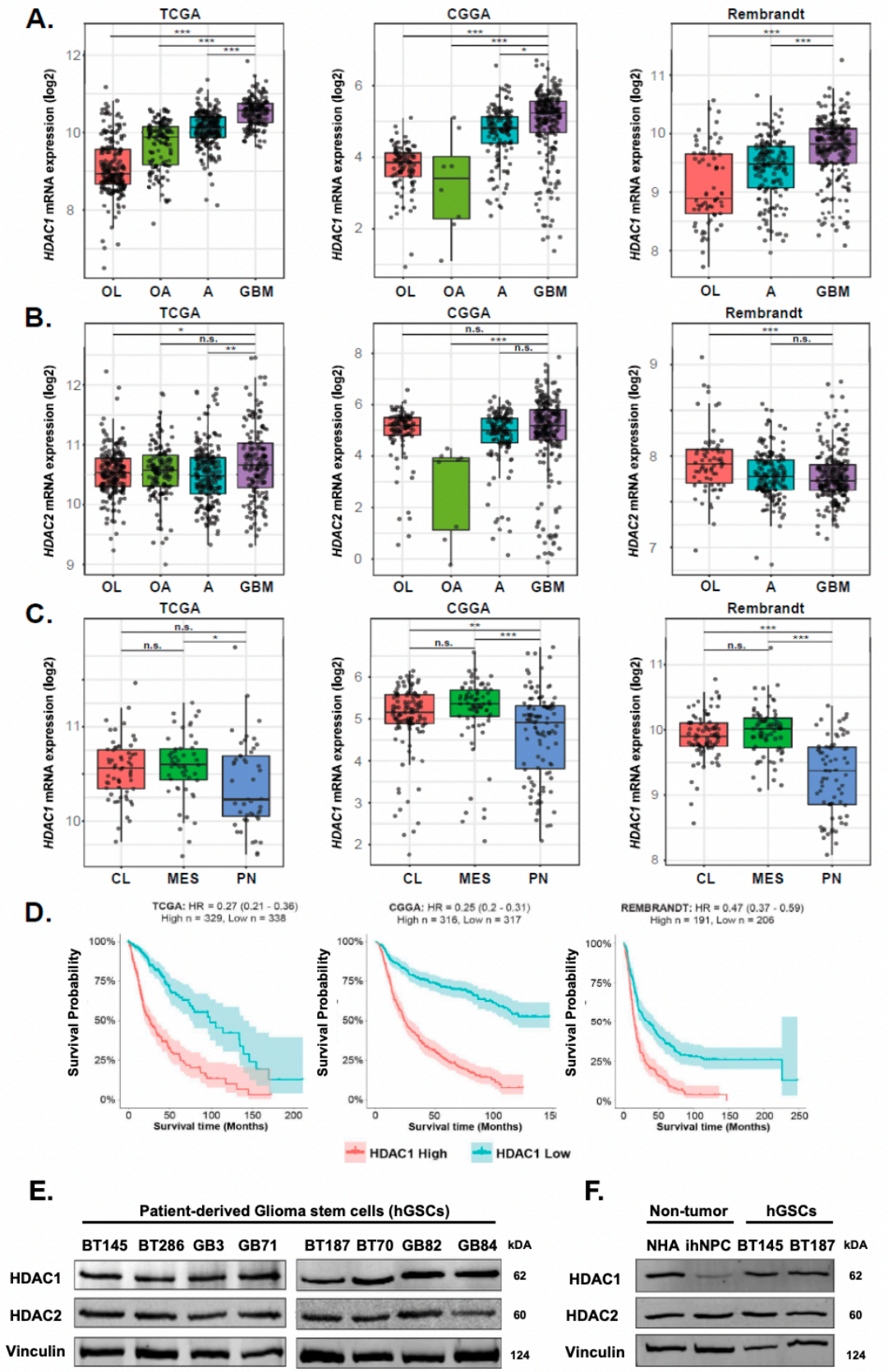
A.
TCGA
CGGA
Rembrandt
HDAC1 mRNA expression (log2)
OL
OA
A
GBM
B.
HDAC2 mRNA expression (log2)
C.
CL
MES
PN
D.
TCGA: HR = 0.27 (0.21 - 0.36)
High n = 329, Low n = 338
CGGA: HR = 0.25 (0.2 - 0.31)
High n = 316, Low n = 317
REMBRANDT: HR = 0.47 (0.37 - 0.59)
High n = 191, Low n = 206
Survival Probability
Survival time (Months)
HDAC1 High
HDAC1 Low
E.
Patient-derived Glioma stem cells (hGSCs)
BT145 BT286 GB3 GB71 BT187 BT70 GB82 GB84 kDA
HDAC1
HDAC2
Vinculin
62
60
124
F.
Non-tumor
hGSCs
NHA ihNPC BT145 BT187 kDA

**Figure 2.1. *HDAC1* Expression Levels in GBM.** (A) *HDAC1* (B) and *HDAC2* expression levels across various grades of gliomas (OL = oligodendroglioma; OA = oligoastrocytoma; A = astrocytoma, GBM = glioblastoma) within the TCGA, CCGA and Rembrandt databases. *HDAC1*, but not *HDAC2*, expression significantly increases with malignancy; Tukey's post-hoc test. (C) *HDAC1* expression levels across the three GBM molecular subtypes (CL = classical; MES = mesenchymal; PN = proneural). (D) Kaplan-Meier analysis stratifying glioma patients with *HDAC1* high and low expression within the TCGA, CCGA and Rembrandt databases; log-rank test. (E) Immunoblot showing basal levels of HDAC1 and HDAC2 in p53-WT hGSCs (BT145, BT286, GB3 AND GB71) and p53-mutant GSCs (BT187, BT70, GB82 and GB84) (n=3). (F) Immunoblot showing basal levels of HDAC1 and HDAC2 in non-tumorigenic normal human astrocytes (NHA) and iPSC-derived human neural progenitor cells (ihNPC) alongside two hGSC lines (n=3). * $p < 0.05$; ** $p < 0.01$; *** $p < 0.001$; n.s., not significant. Taken from: (Lo Cascio et al., 2021).

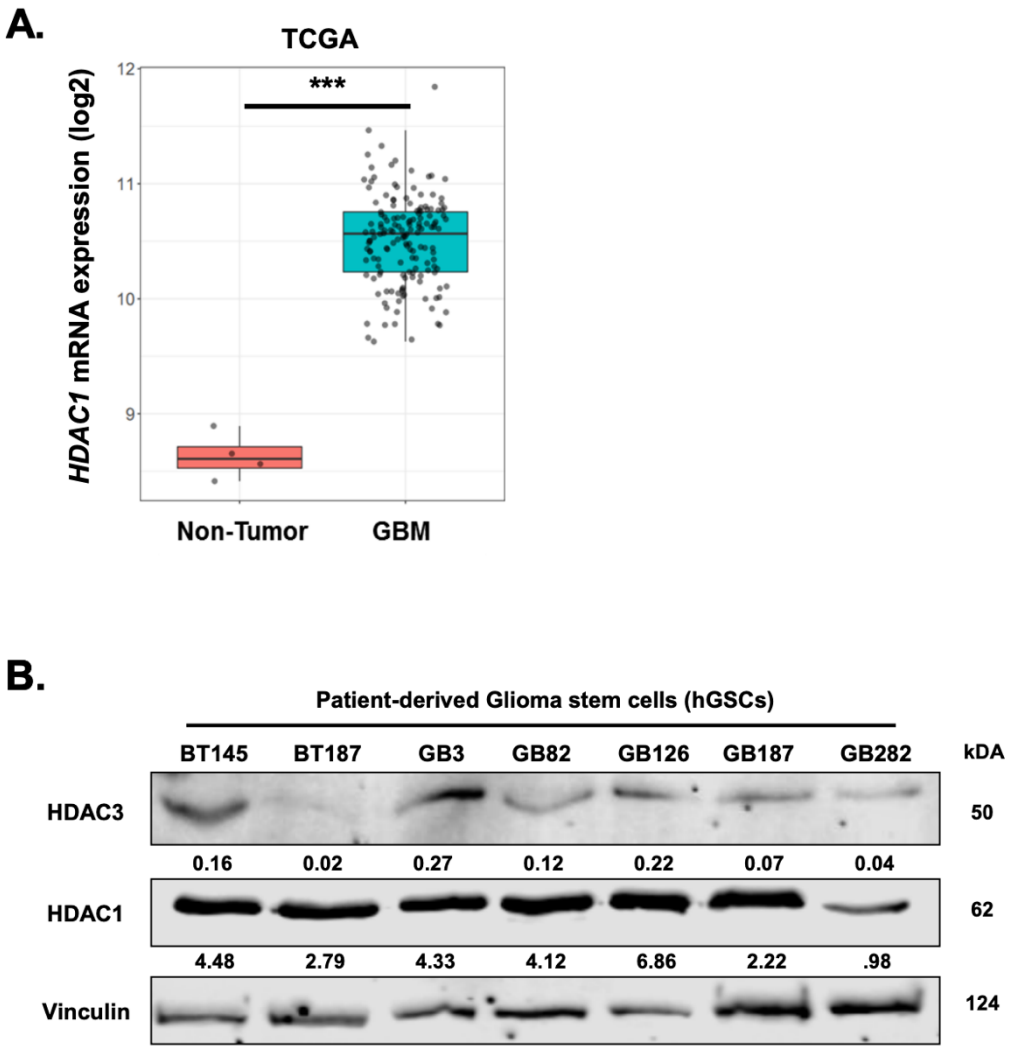


**Figure 2.2 *HDAC1* expression levels in normal brain tissue.** (A) Comparison of HDAC1 expression levels from the TCGA dataset in GBM tissue and normal brain tissue from healthy controls. (B) Immunoblot comparing basal levels of HDAC1 and HDAC3 protein across seven different GSCs lines. Numbers below the bands indicate normalized expression levels of HDAC3 and HDAC1 in each cell line relative to Vinculin. *** $p < 0.001$. Error bars indicate SEM. Taken from: (Lo Cascio et al., 2021).

### *2.4.3 HDAC1 knockdown suppresses viability of GSCs in a p53-dependent manner*

We silenced *HDAC1* expression in four distinct p53 wild-type (p53-WT) hGSC lines (BT145, GB3, BT286, GB71), p53-mutant hGSC lines (BT187, BT70, GB82, GB84), NHAs and ihNPCs using two independent shRNAs targeting *HDAC1* protein-coding regions (sh*HDAC1*_A and sh*HDAC1*_B) (Tables 2.1 and 2.2). Acute knockdown of *HDAC1* resulted in a dramatic reduction in the viability of all four GSC cultures (Figure 2.3A, Figure 2.4A, Figure 2.5A; approximately 85-90% loss in viability compared to controls; $p < 0.0001$). *HDAC1* knockdown had a significant but much more attenuated impact on the survival of p53-mutant GSCs (average 50-55% reduction; Figure 2.3A, Figure 2.4B and Figure 2.5B; $p < 0.001$-$0.0001$). Two IDH-mutant hGSCs harboring p53 mutations were practically unaffected by loss of HDAC1 (HK211, HK252; Figure 2.4E-F, Figure 2.5C). The viability of non-tumorigenic NHAs and ihNPCs were also significantly affected by absence of HDAC1 protein, albeit not to the same extent as p53-WT GSCs (Figure 2.3A, Figure 2.4C and Figure 2.5D).

We assessed the proportion of actively cycling or dying cells after acute *HDAC1* knockdown through immunocytochemistry in both p53-WT and p53-mutant hGSCs (Figures 2.3B-E). We find that in p53-WT cells (BT145), *HDAC1* knockdown led to a significant reduction in the percentage of Ki67-positive cells (>95% decrease; $p < 0.001$) and significant increase in the percentage of cleaved caspase-3-positive cells (average 37% increase; $p < 0.01$) (Figures 2.3B-E). Conversely, *HDAC1* knockdown did not affect proliferation and survival of p53-mutant cells (BT187) compared to non-target controls (Figures 2.3B-E). Hence, reduced proliferation and increased cell death contribute to the decrease in cell viability observed in p53-WT GSCs. To confirm whether the effects of

*HDAC1* knockdown on GSC proliferation are indeed dependent on p53 status, we transduced a p53-WT GSC line (BT145) with a dominant-negative form of *TP53* (p53-DN) (Mehta et al. 2011). As shown in Figure 2.3F, overexpression of p53-DN in BT145 rescued the defect in proliferation observed after *HDAC1* knockdown. Next, to assess the impact of HDAC1 on p53 activation, we examined acetylation status of p53 after HDAC1 knockdown. HDAC1 knockdown resulted in significantly increased acetylation of p53 at lysines 382 and 373 and its stabilization (Figure 2.3G and Figure 2.5E-F). These post-translational modifications have been shown to be important for p53 stabilization, subsequent activation, and transcriptional activity (Ivanov et al. 2007; Ito et al. 2002; Tang et al. 2008). *HDAC1* knockdown did not result in increased transcription of *TP53* or decreased transcription of its negative regulator *MDM2* (Figure 2.5G). These results indicate that HDAC1 regulates p53 acetylation and suppresses its transcriptional functions in p53-WT GSCs, and strongly suggest that p53 status dictates the response of GSCs to acute loss of HDAC1 protein.

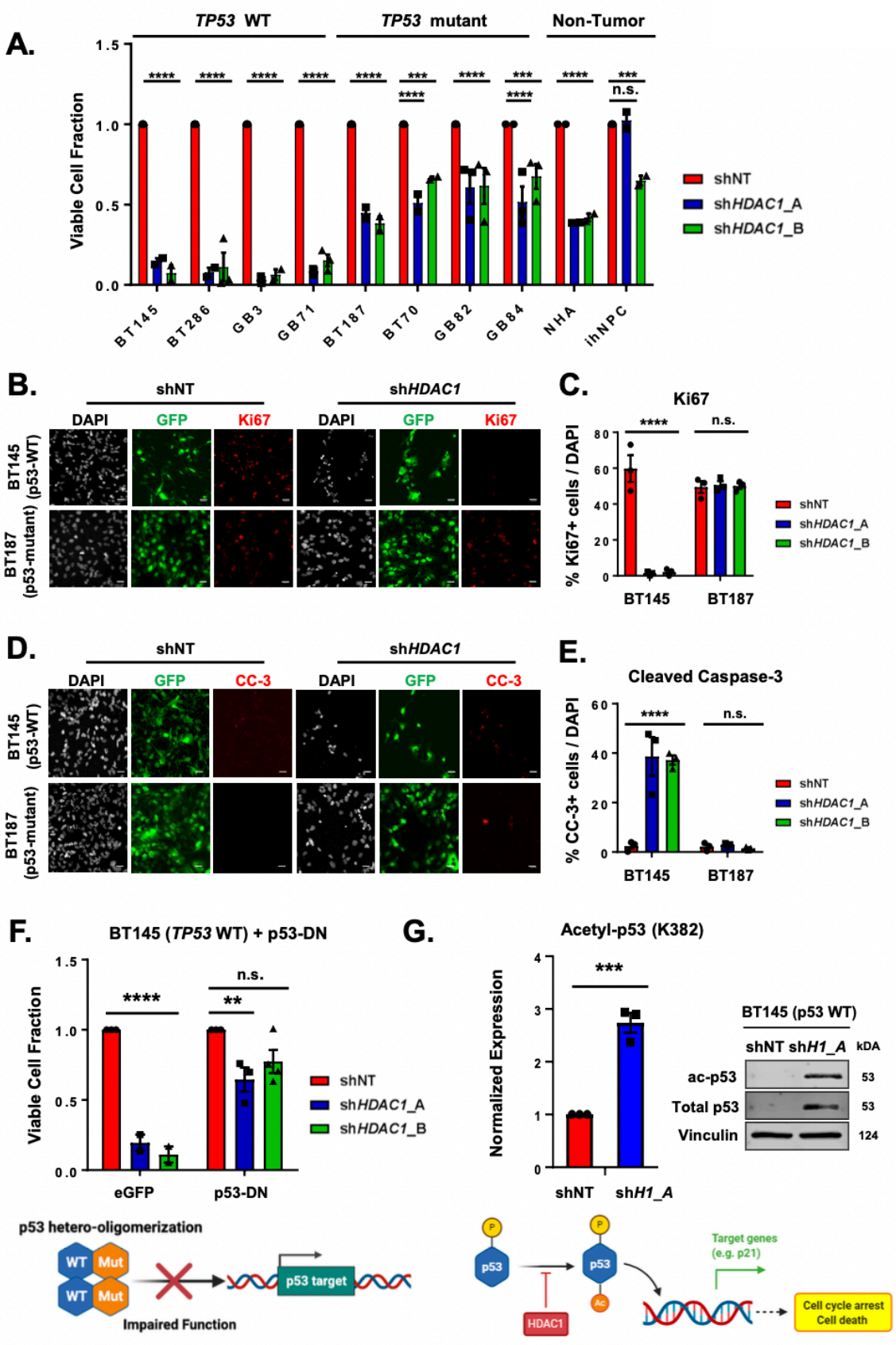
A.
TP53 WT
TP53 mutant
Non-Tumor
Viable Cell Fraction
shNT
shHDAC1_A
shHDAC1_B
BT145
BT286
GB3
GB71
BT187
BT70
GB82
GB84
NHA
ihNPC
n.s.
B.
shNT
shHDAC1
DAPI
GFP
Ki67
BT145 (p53-WT)
BT187 (p53-mutant)
C.
Ki67
% Ki67+ cells / DAPI
D.
CC-3
E.
Cleaved Caspase-3
% CC-3+ cells / DAPI
F.
BT145 (TP53 WT) + p53-DN
eGFP
p53-DN
G.
Acetyl-p53 (K382)
Normalized Expression
shH1_A
BT145 (p53 WT)
kDA
ac-p53
Total p53
Vinculin
p53 hetero-oligomerization
WT
Mut
p53 target
Impaired Function
Target genes
(e.g. p21)
HDAC1
Cell cycle arrest
Cell death

**Figure 2.3. Knockdown of *HDAC1* reduces viability of human glioma stem cells (GSCs) in a p53-dependent manner.** (A) Quantification of the percentage of viable p53-WT and p53-mutant GSCs and two non-tumorigenic cell lines (NHAs, ihNPCs) transduced with sh*HDAC1*_A or sh*HDAC1*_B, compared to control cells transduced with shNT (n=3). (B-C) Immunofluorescence staining (B) and quantification (C) of Ki67-positive GSCs after acute *HDAC1* silencing (n=3). (D-E) Immunofluorescence staining (D) and quantification (E) of cleaved caspase-3-positive cells after acute *HDAC1* silencing (n=3). (F) Quantification of the percentage of viable p53-WT GSCs overexpressing p53-DN or eGFP after *HDAC1* knockdown (n=3). Schematic below illustrates how overexpression of a p53 mutant (p53-DN) affects p53 function. (G) Quantification of immunoblots for total and acetylated p53 (K382) after *HDAC1* silencing (sh*H1*_A = sh*HDAC1*_A) in p53-WT BT145 (n=3). Schematic below illustrates how HDAC1 opposes p53 activation through direct deacetylation. For each cell line, the data are compiled from at least three independent experiments for each shRNA. Error bars indicate SEM. * $p < 0.05$, ** $p < 0.01$, *** $p < 0.001$, **** $p < 0.0001$, n.s., not significant. Magnification, 20x; scale bars, 2 μM. *P* values were determined using the 2-way ANOVA with Tukey's multiple comparisons test or unpaired 2-tailed t-test. Taken from: (Lo Cascio et al., 2021).

| Cell Line | *TP53* Genotype |
|---|---|
| **BT70** | p.A273C |
| **BT187** | DelR283 |
| **GB82** | c.822_825delTTGT |
| **GB84** | p.Cys277 |
| **HK211** | p.N235S / p.Y234C |
| **HK252** | p.P250L |

**Table 2.1 *TP53* mutations in the human GSC line used in the study.**

| Cell Line | Genotype |
|---|---|
| **BT145** | *INK4a/ARF*$^{-/-}$ *; PTENmut/mut ; TP53*$^{+/+}$ |
| **BT286** | *EGFRvIII; TP53*$^{+/+}$ |
| **GB3** | *INK4a/ARF*$^{-/-}$ *; CDK6* gain *; CDK4* amp*; TP53*$^{+/+}$ |
| **GB16** | *INK4a/ARF*$^{-/-}$ *; CDK6* gain *; CDK4* amp*; TP53*$^{+/+}$ |
| **GB71** | *INK4a/ARF*$^{-/-}$ *; EGFR* gain *; CDK6* gain *; PTENmut/mut ; TP53*$^{+/+}$ |
| **BT187** | *PTENmut/mut; P53 mut/mut (*DelR283) |
| **BT70** | *INK4a/ARF*$^{-/-}$ *; PTENmut/mut ; TP53mut/mut (*p.A273C)*; EGFR* amp *; EGFRvIII* |
| **GB82** | *INK4a/ARF*$^{-/-}$*; EGFR* amp *; CDK6* gain; *TP53mut/mut (*c.822_825delTTGT) |
| **GB84** | *INK4a/ARF*$^{-/-}$*; MDM4* loss*; RB1* loss*; PDGFR* loss*; EGFR* amp*; PTEN mut/mut ; CCND2* loss*; CDK4* loss*; MDM1/2* loss *; MDM4* loss *; FOXM1* loss; *; TP53 mut/ mut (*p.Cys277) |
| ***p16/p19*$^{-/-}$*;EGFRvIII*** | *Ink4a/ARF*$^{-/-}$ *; Olig2*$^{+/+}$ *; p53*$^{+/+}$ *;* h*EGFRvIII* |

**Table 2.2 Genotypes of human GSC lines used in the study.**

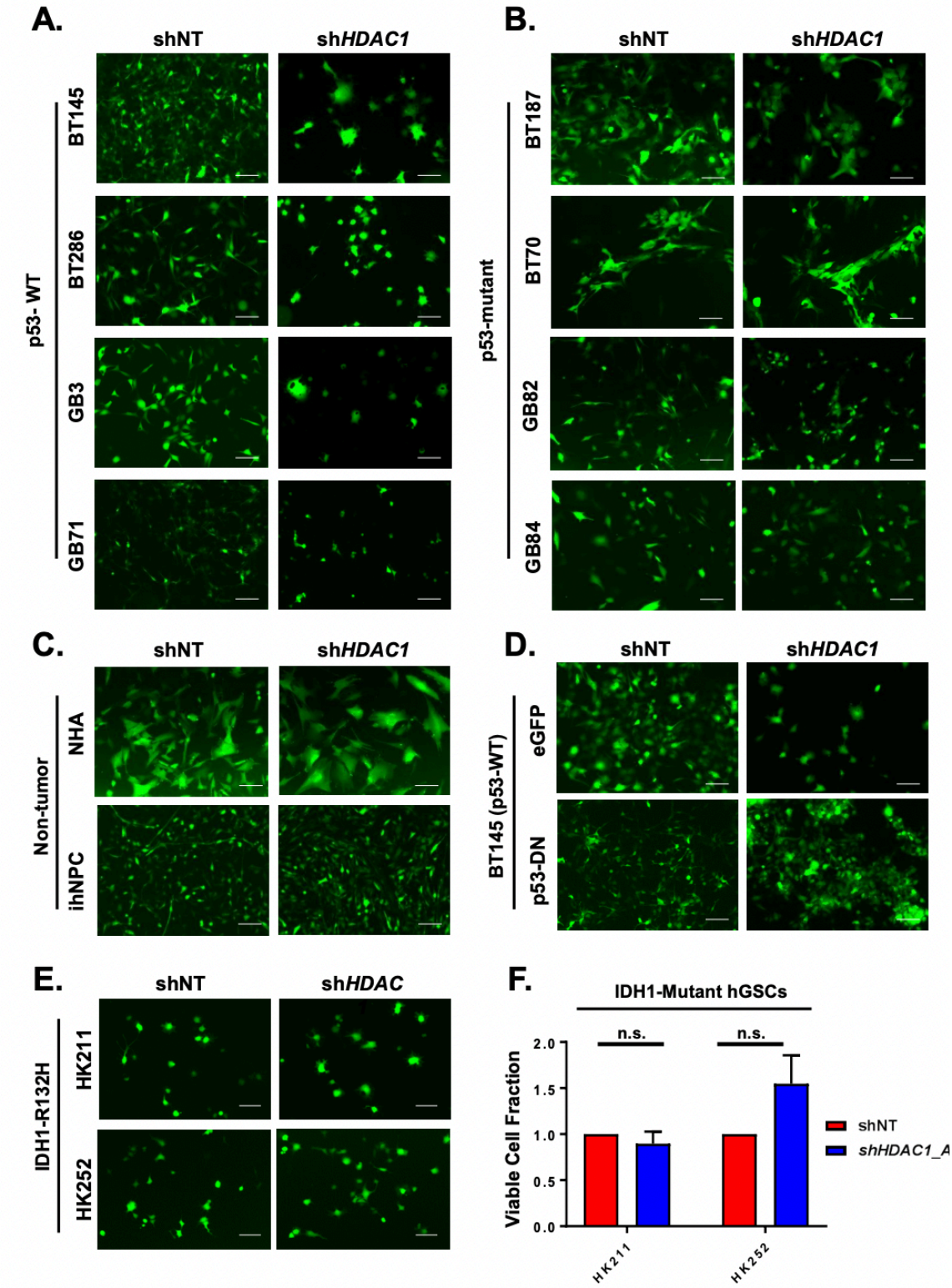
A.
shNT
shHDAC1
p53- WT
BT145
BT286
GB3
GB71
B.
shNT
shHDAC1
p53-mutant
BT187
BT70
GB82
GB84
C.
shNT
shHDAC1
Non-tumor
NHA
iNPC
D.
shNT
shHDAC1
BT145 (p53-WT)
eGFP
p53-DN
E.
shNT
shHDAC
IDH1-R132H
HK211
HK252
F.
IDH1-Mutant hGSCs
n.s.
n.s.
Viable Cell Fraction
2.0
1.5
1.0
0.5
0.0
shNT
shHDAC1_A
HK211
HK252

**Figure 2.4 Morphology of IDH1-WT and IDH-mutant GSCs after knockdown of *HDAC1*.** (A-E) Representative images of control and HDAC1-silenced cells (GFP-positive) in (A) four p53-WT GSCs, (B) four p53-mutant GSCs, (C) non-tumorigenic NHAs and ihNPCs, (D) a p53-WT GSC line (BT145) overexpressing a dominant-negative mutant of p53 (p53-DN) or a control vector (eGFP), and (E) two IDH1-mutant GSCs. (F) Quantification of the viable fraction of IDH1-mutant GSCs after *HDAC1* knockdown compared to control cells transduced with shNT. For each cell line, the data are compiled from at least three independent experiments. Magnification 5x; scale bars, 2 μM; n.s., not significant. Error bars indicate SEM. P values were calculated using unpaired 2-tailed t-test. Taken from: (Lo Cascio et al., 2021).

### *2.4.4 HDAC1 function is non-redundant in hGSCs and is not compensated for by other HDACs*

We sought to determine the global transcriptional consequences of HDAC1 loss and obtain insights into the mechanisms underlying the distinct phenotypes exhibited by GSCs and normal neural cells. We performed RNA-sequencing (RNA-seq) analysis of p53-WT (BT145, GB3) and p53-mutant (BT187) hGSCs as well as NHAs and iNPC cultures after *HDAC1* knockdown. We examined whether ablation of *HDAC1* resulted in compensatory upregulation of any other members of the HDAC family of proteins in hGSCs (Figure 2.6A). In all cell lines, *HDAC2* and *HDAC3* expression levels were modestly but significantly reduced after *HDAC1* knockdown (Figure 2.6A). The only HDACs that were significantly upregulated following *HDAC1* loss were *HDAC9* in NHAs and *HDAC10* and *HDAC11* in BT187 (Figure 2.6A). However, overall our data suggest that unlike the compensation seen in normal neural stem cells (Hagelkruys et al. 2014), *HDAC1* knockdown did not dramatically affect expression of other HDACs in the majority of the cell lines tested.

HDAC1 and HDAC2 are highly homologous and been shown to have individual and overlapping regulatory functions for proliferation and cell survival in other tissues

(Jurkin et al. 2011). To understand whether these paralogues harbor non-redundant functions in hGSCs, we performed knockdown of *HDAC2* in GSCs to see whether silencing its expression would result in a phenotype comparable to that of *HDAC1* knockdown (Figure 2.3A). After *HDAC2* knockdown, HDAC1 protein levels were significantly upregulated (~1.5-2 fold) as a result of *HDAC2* silencing in both p53-WT and p53-mutant GSCs (Figure 2.6B-C). Unlike *HDAC1* knockdown, we found that knockdown of *HDAC2* did not significantly affect the viability of p53-WT and p53-mutant GSCs (Figure 2.6D and Figure 2.7A). Additionally, knockdown of *HDAC2* did not result in increased p53 K382 acetylation, suggesting that p53 activation is a direct result of *HDAC1* silencing (Figure 2.6E). Hence, we demonstrate that HDAC1 harbors unique functional roles in GSCs that cannot be compensated for by HDAC2, and we identify HDAC1 as the essential class I deacetylase for GSC proliferation and survival.

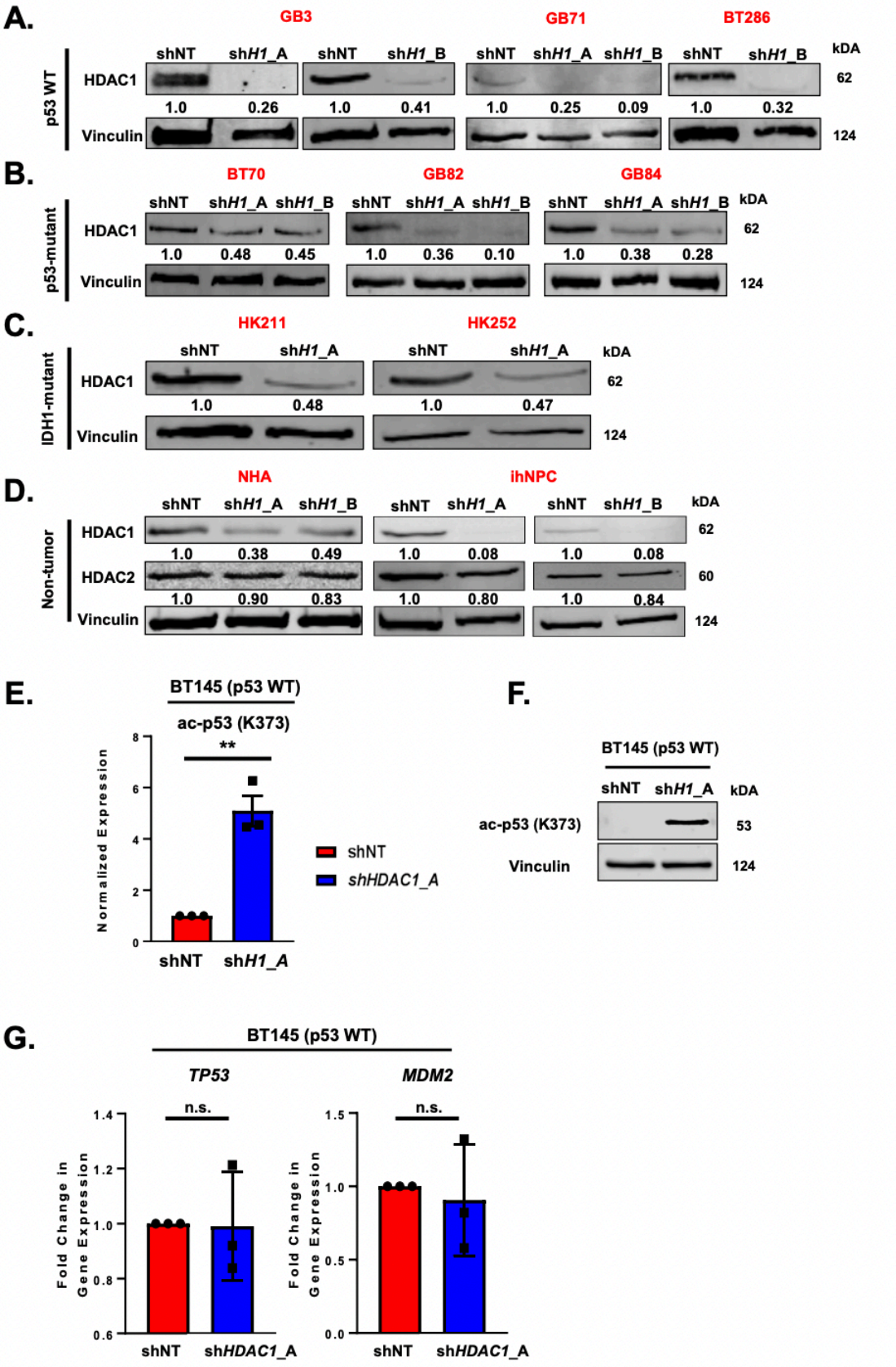
A.
GB3
GB71
BT286
shNT
shH1_A
shH1_B
kDA
p53 WT
HDAC1
62
1.0
0.26
1.0
0.41
1.0
0.25
0.09
1.0
0.32
Vinculin
124
B.
BT70
GB82
GB84
p53-mutant
1.0
0.48
0.45
1.0
0.36
0.10
1.0
0.38
0.28
C.
HK211
HK252
IDH1-mutant
1.0
0.48
1.0
0.47
D.
NHA
ihNPC
Non-tumor
HDAC2
60
1.0
0.38
0.49
1.0
0.08
1.0
0.08
1.0
0.90
0.83
1.0
0.80
1.0
0.84
E.
BT145 (p53 WT)
ac-p53 (K373)
**
Normalized Expression
shHDAC1_A
F.
ac-p53 (K373)
53
G.
TP53
MDM2
n.s.
Fold Change in Gene Expression
shHDAC1_A

**Figure 2.5 Knockdown Efficiency of *HDAC1* in GSCs and relevant putative mechanisms of p53 activation.** (A-D) Immunoblots showing HDAC1 knockdown in (A) p53-WT hGSCs (B) p53-mutant GSCs, (C) IDH1-mutant GSCs and (D) non-tumorigenic NHAs and ihNPCs utilized for all cell viability assays shown in Figure 2. Numbers below the bands indicate normalized expression levels of HDAC1 and HDAC2 in each cell line relative to Vinculin. (E) Quantification of immunoblots for acetylated p53 (K373) after *HDAC1* silencing (shH1_A = shHDAC1_A) in p53-WT BT145 (n=3). (F) Representative immunoblot for p53 K373 acetylation after HDAC1 silencing in p53-WT GSCs (BT145). (G) RT-qPCR shows that TP53 and MDM2 are not differentially expressed in BT145 (p53 WT) GSCs between control (shNT) and HDAC1-silenced cells (sh*HDAC1*_A, n=3). For each cell line, the data are compiled from three independent experiments for each shRNA. ** $p < 0.01$, n.s., not significant. Error bars indicate SEM. P values were calculated using unpaired 2-tailed t-test. Taken from: (Lo Cascio et al., 2021).

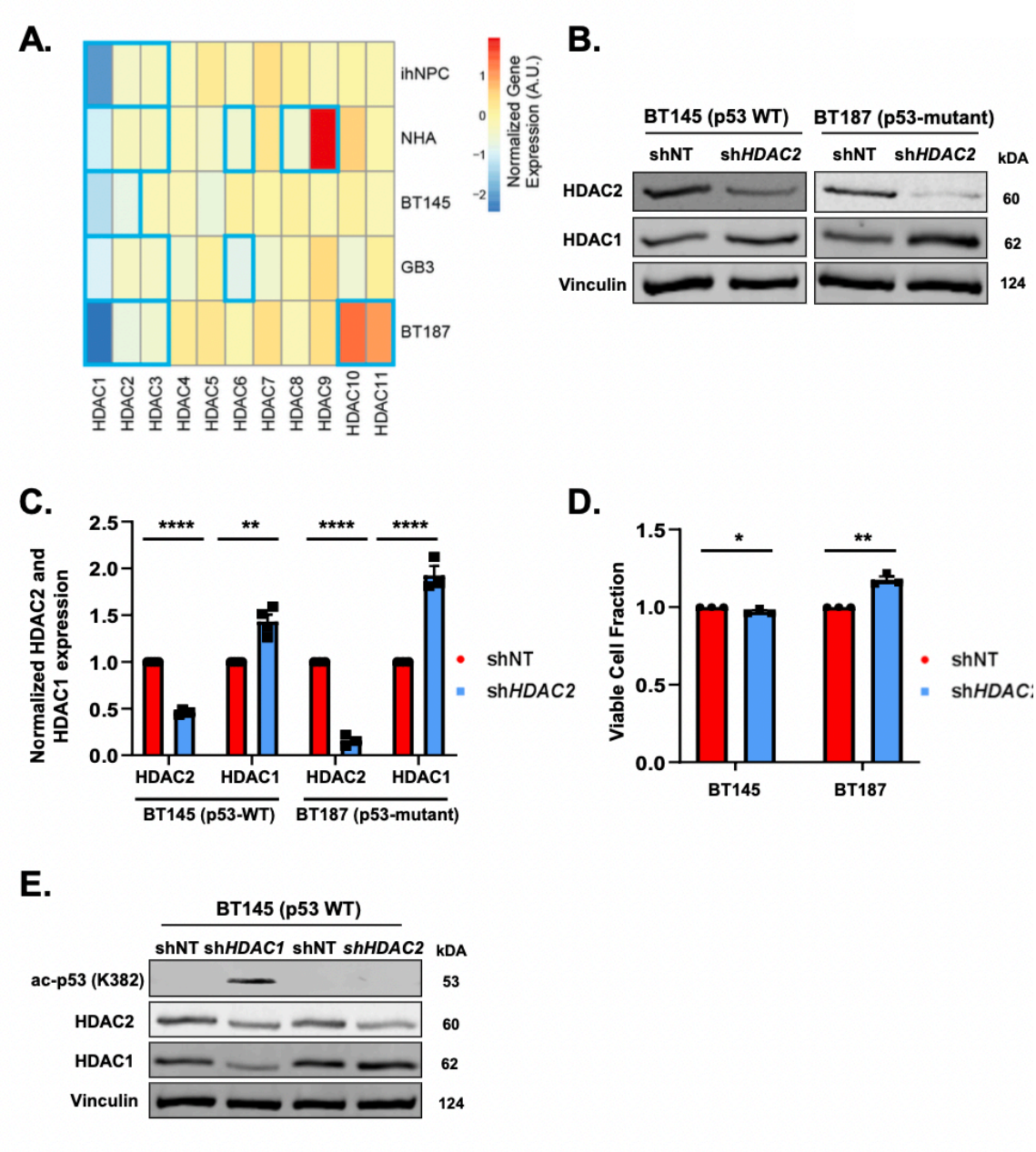


**Figure 2.6. HDAC1 function is non-redundant in GSCs and is not compensated for by its paralogue HDAC2.** (A) Log2 fold change of differential expression for the 11 HDACs (HDAC1–11) after sh*HDAC1* knockdown in two non-tumorigenic (ihNPC and NHA) and three GSC (BT145, GB3, BT187) cell lines. Blue bolded boxes indicate significant differential expression (adjusted *p*-value ≤ 0.05). (B) Representative immunoblot showing protein levels of HDAC1 and HDAC2 after acute *HDAC2* knockdown (sh*HDAC2*) in p53-WT (BT145) and p53-mutant (BT187) GSCs. (C) Quantification of expression HDAC2 and HDAC1 protein (normalized to Vinculin) after *HDAC2* knockdown in BT145 (n=4) and BT187 (n=3). (D) Quantification of the

percentage of viable GSCs (BT145 and BT187) 7 days after *HDAC2* knockdown, relative to shNT controls (n=3). (E) Immunoblot comparing levels of acetylated p53 (K382), HDAC1 and HDAC2 protein after *HDAC1* and *HDAC2* silencing in p53-WT GSC (BT145). For each cell line, the data are compiled from at least three independent experiments for each shRNA. Error bars indicate SEM. * $p < 0.05$, ** $p < 0.01$, **** $p < 0.0001$, n.s., not significant. *P* values were calculated using unpaired 2-tailed t-test. Taken from: (Lo Cascio et al., 2021).

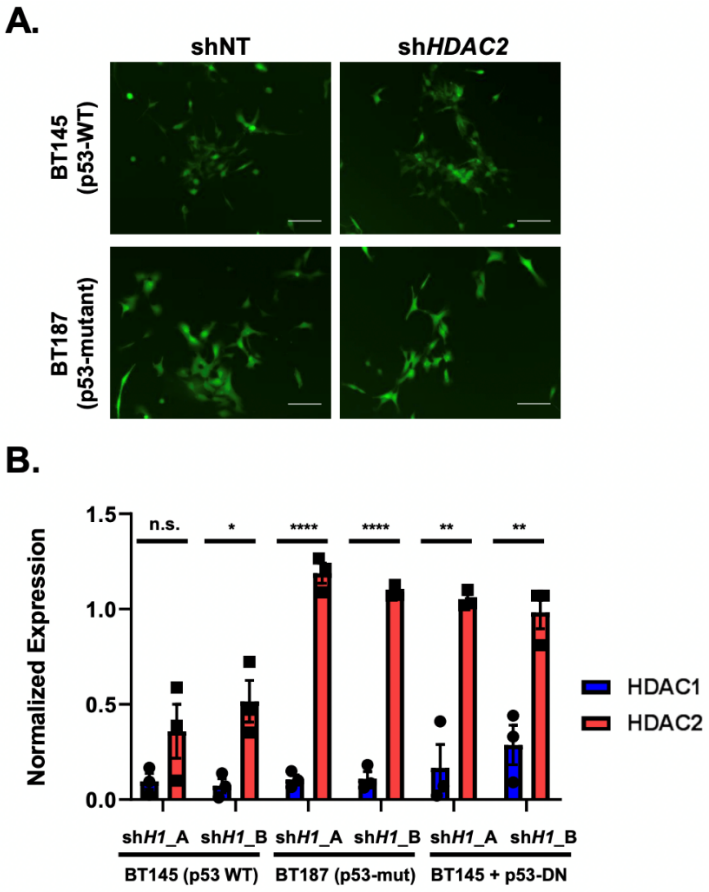


**Figure 2.7 Effects of *HDAC2* knockdown and quantification of the normalized total levels of HDAC1 and HDAC2 proteins in GSCs after *HDAC1* knockdown.** (A) Representative images of control and HDAC2-silenced cells (GFP-positive) in p53-WT (top panel) and p53-mutant (bottom panel) GSCs. (B) Quantification of expression of HDAC1 and HDAC2 protein levels after *HDAC1* knockdown in p53-WT, p53-mutant and p53-WT + p53-DN GSCs (n=3). For each cell line, the data are compiled from at least three independent experiments for each shRNA. Error bars indicate SEM. * $p < 0.05$ , ** $p < 0.01$, **** $p < 0.0001$, n.s., not significant. Magnification 5x; scale bars, 2 μM. P values were calculated using unpaired 2-tailed t-test.

### *2.4.5 HDAC1 knockdown results in increased histone acetylation and reduces expression of key stemness and cell fate factors*

To assess the impact of HDAC1 knockdown on global histone acetylation we analyzed changes in common histone acetylation marks. We first confirmed that knockdown of *HDAC1* in both cell lines led to a dramatic increase in the acetylation of histone H3 at lysines 9, 14 and 27 (H3K9/14 and H3K27). These histone marks are associated with higher activation of gene transcription: H3K9/14ac is highly correlated with active promoters, while the H3K27ac is an active enhancer mark (Figure 2.8A). Loss of HDAC1 in embryonic stem cells affects stem cell proliferation due to increase in cell cycle inhibitor expression (Zupkovitz et al. 2006). We observed marked upregulation of the p21, a direct transcriptional target of p53, in the p53-WT but not p53-mutant cell line (Figure 2.8B-D). We then evaluated changes in the expression of several proteins associated with stem cell identity or cell fate in p53-WT (BT145) and p53-mutant (BT187) GSC lines. Knockdown of *HDAC1* resulted in a significant decrease in the expression of glioma master transcription factors SOX2 and OLIG2, stem cell marker NESTIN and the receptor tyrosine kinase (RTK) epidermal growth factor receptor (EGFR) (Figures 2.8B-D). Overexpression of a p53-domninant negative mutant (p53-DN) in p53-WT cells also resulted in similar expression changes (Figure 2.8B and 2.8E). While HDAC2 protein levels did dramatically decrease in the absence of HDAC1 in p53-WT GSCs (Figure 2.8C), they remain unchanged in p53-mutant cells, p53-WT cells overexpressing a dominant-negative p53 mutant, ihNPCs, and NHAs after HDAC1 knockdown (Figure 2.8D-E; Figure 2.5D; Figure 2.7B). Hence, while HDAC1 expression is upregulated in the absence of HDAC2 protein (Figure 2.6B-C), HDAC2 does not

display any compensatory upregulation after *HDAC1* knockdown in GSCs (Figure 2.8B-E and Figure 2.7B). Together, these data indicate that knockdown of HDAC1 results in a collapse of the stemness-state (irrespective of p53 status) and activation of p53 downstream target genes in surviving p53-WT, but not in p53-mutant, GSCs (Figure 2.8B).

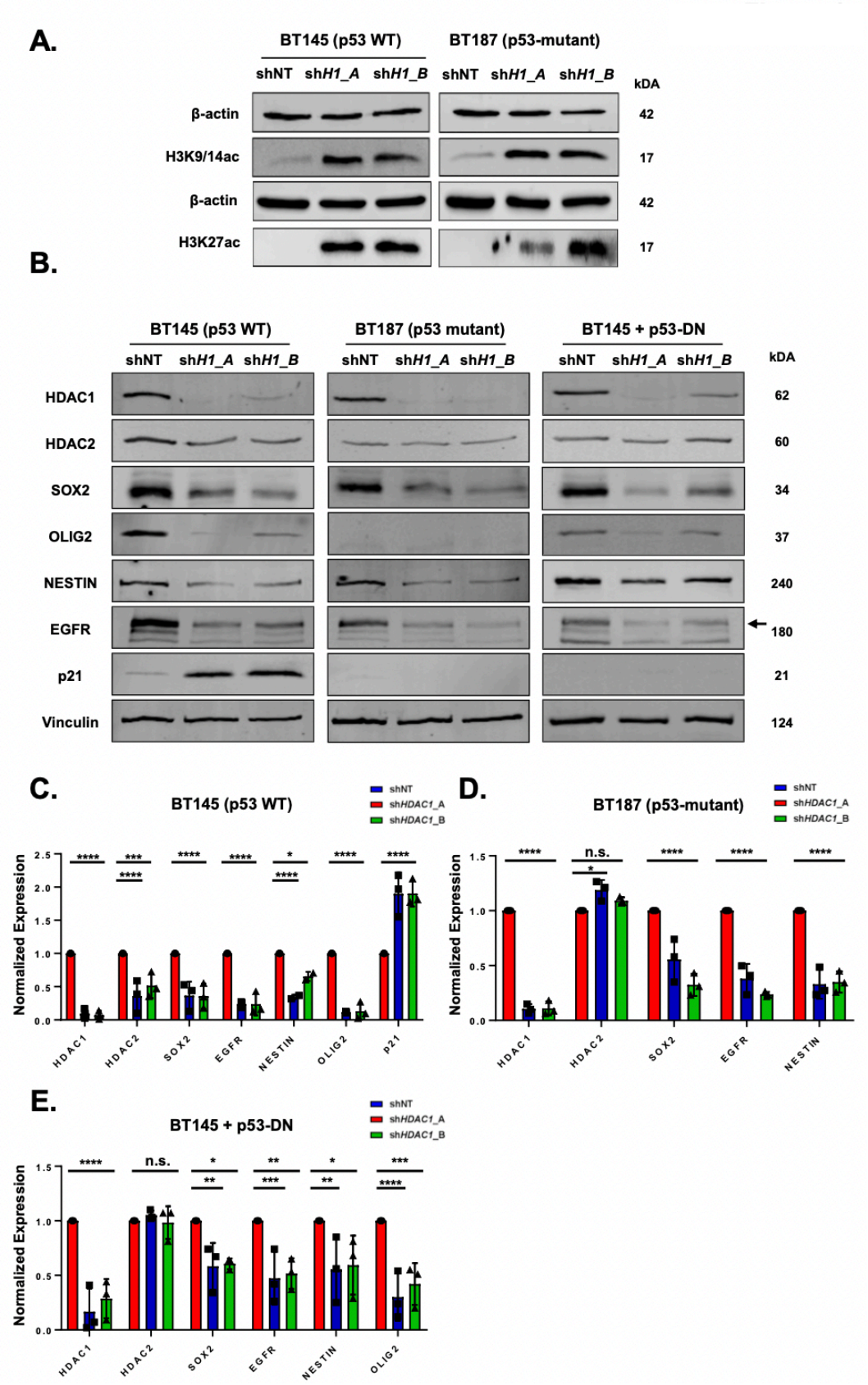
A.
BT145 (p53 WT)
BT187 (p53-mutant)
shNT
shH1_A
shH1_B
kDA
β-actin
H3K9/14ac
β-actin
H3K27ac
42
17
42
17
B.
BT145 (p53 WT)
BT187 (p53 mutant)
BT145 + p53-DN
HDAC1
HDAC2
SOX2
OLIG2
NESTIN
EGFR
p21
Vinculin
62
60
34
37
240
180
21
124
C.
BT145 (p53 WT)
shHDAC1_A
shHDAC1_B
Normalized Expression
HDAC1
HDAC2
SOX2
EGFR
NESTIN
OLIG2
p21
D.
BT187 (p53-mutant)
n.s.
E.
BT145 + p53-DN

**Figure 2.8. *HDAC1* knockdown reduces expression of key stemness and cell fate factors.** (A) Immunoblots showing increase in H3K4/19ac and H3K27ac after *HDAC1* silencing in BT145 and BT187 (sh*H1*_A = sh*HDAC1*_A and sh*H1B* = sh*HDAC1*_B) (n=3). (B) Representative immunoblots of p53-WT (BT145), p53-mutant (BT187) and p53-WT cells overexpressing p53-DN (BT145 + p53-DN) GSCs after acute silencing of *HDAC1* probed for various markers (n=3). (C-E) Quantification of expression of proteins (normalized to Vinculin) after *HDAC1* knockdown from immunoblots using p53-WT (C), p53-mutant (D) and p53-WT cells overexpressing p53-DN (E). For each cell line, the data are compiled from at least three independent experiments for each shRNA. Error bars indicate SEM. * $p < 0.05$, ** $p < 0.01$, *** $p < 0.001$, **** $p < 0.0001$, n.s., not significant. *P* values were determined using the 2-way ANOVA with Tukey's multiple comparisons test. Taken from: (Lo Cascio et al., 2021).

### *2.4.6 HDAC1 knockdown in GSCs significantly attenuates their ability to form tumors and increases survival of tumor-bearing mice*

We next investigated whether loss of HDAC1 affected the tumor-forming potential of p53-WT GSCs. We orthotopically transplanted GSCs (BT145) transduced with a luciferase reporter and either a non-target control shRNA (shNT) and two *HDAC1*-targeting shRNAs in immunocompromised mice. Using bioluminescence imaging, we compared the differences in the tumor growth rate in shNT and sh*HDAC1* tumors at an early time point after GSC engraftment (7 weeks post-injection; Figure 2.9A). *HDAC1* knockdown resulted in a significant lag in tumor growth with both shRNAs, which was maintained throughout the study (Figure 2.9A and Figure 2.10A-B). We confirmed that *HDAC1* silencing was maintained in sh*HDAC1* tumors (Figure 2.10C-D). In line with our *in vitro* phenotypes (Figure 2.8B), we also confirmed that sh*HDAC1* tumors express very low levels of OLIG2 – a master transcription regulator that has previously been shown to be critical for the tumor-propagating potential of p53-WT GSCs (Figure 2.10C) (Mehta et

al. 2011; Suva et al. 2014). Consistent with low HDAC1 expression, the engrafted sh*HDAC1* cells exhibited an increase in H3K9/14 acetylation relative to shNT controls (Figure 2.9B). As shown in Figure 2.9C-D, sh*HDAC1* tumors had a significant reduction in the proportion of proliferating cells compared to the controls. Knockdown of *HDAC1* alone not only delayed tumor growth but resulted in significantly extended overall survival in a PDX model of GBM (BT145; Figure 2.9E) in a murine model of human glioma (Figure 2.9F).

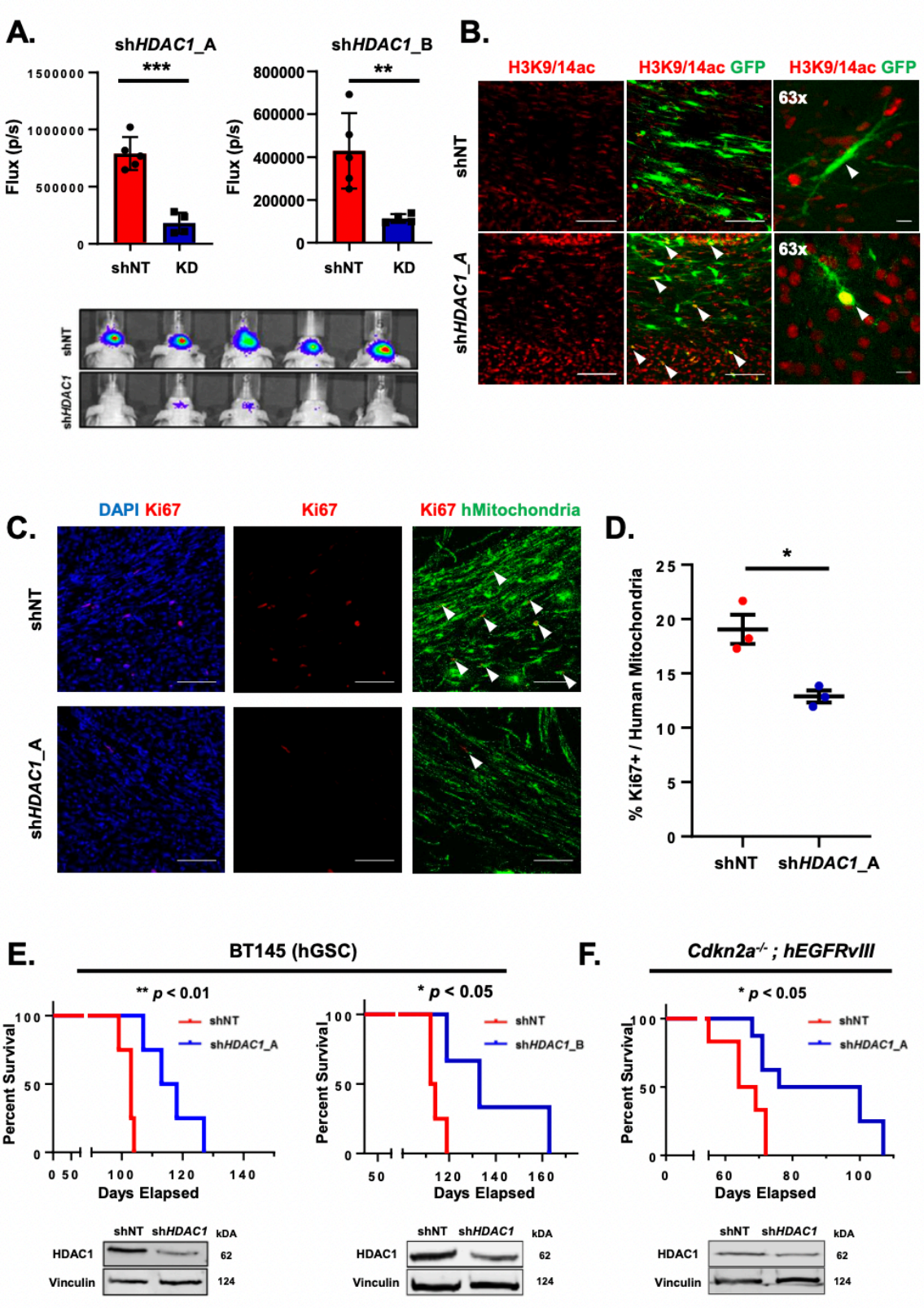
A.
shHDAC1_A
shHDAC1_B
***
**
Flux (p/s)
1500000
1000000
500000
0
800000
600000
400000
200000
shNT
KD
shNT
shHDAC1
B.
H3K9/14ac
H3K9/14ac GFP
H3K9/14ac GFP
63x
63x
shNT
shHDAC1_A
C.
DAPI Ki67
Ki67
Ki67 hMitochondria
shNT
shHDAC1_A
D.
*
% Ki67+ / Human Mitochondria
25
20
15
10
5
0
shNT
shHDAC1_A
E.
BT145 (hGSC)
** p < 0.01
* p < 0.05
Percent Survival
100
50
0
shNT
shHDAC1_A
shHDAC1_B
0 50
100
120
140
160
Days Elapsed
shNT shHDAC1 kDA
HDAC1
Vinculin
62
124
F.
Cdkn2a-/- ; hEGFRvIII
* p < 0.05
0
60
80
100

**Figure 2.9. Knockdown of *HDAC1* significantly extends survival in patient-derived xenograft (PDX) and mouse models of GBM.** (A) Average photon flux (p/s) measured 7 weeks post-injection through bioluminescence imaging of mice implanted with cells expressing control (shNT) and HDAC1 knockdown (*shHDAC1_A and shHDAC1*_B) cells and representative heatmap of bioluminescence intensity between the two groups. (B) Immunostaining for acetylated Histone H3 at lysines 9 and 14 (H3K9/14ac; red) in tumor tissue. Arrowheads indicate GFP-positive cells with H3K9/14a-positive nuclei. (C) Immunostaining for Ki67 (red) and human mitochondria (hMitochondria, green) in shNT and sh*HDAC1* BT145 tumor tissue. Arrowheads indicate double-positive (Ki67+/hMitochondria+) nuclei. (D) Quantification of human Ki67-positive cells in shNT and sh*HDAC1* BT145 tumors (n=3 per cohort). (E) Kaplan-Meier survival analysis of mice implanted intracranially with p53-WT GSCs (BT145) transduced with *HDAC1* shRNA (sh*HDAC1*_A, n=4; sh*HDAC1*_B, n=3) or non-target shRNA (shNT; n=4 in both studies). (F) Kaplan-Meier survival analysis of mice implanted intracranially with murine GSCs (*Cdkn2a* $^{-/-}$*; hEGFRvIII*) transduced with *HDAC1* shRNA (sh*HDAC1*_A, n=5) or non-target shRNA (shNT; n=4). Inset below show immunoblots confirming *HDAC1* knockdown in the implanted GSCs. Error bars indicate SEM. * $p < 0.05$, ** $p < 0.01$, *** $p < 0.001$. Magnification, 20x and 63x; scale bars, 100 μM. *P* values were calculated using unpaired 2-tailed t-test and Kaplan-Meier method with the Mantel-Cox log-rank test. Taken from: (Lo Cascio et al., 2021).

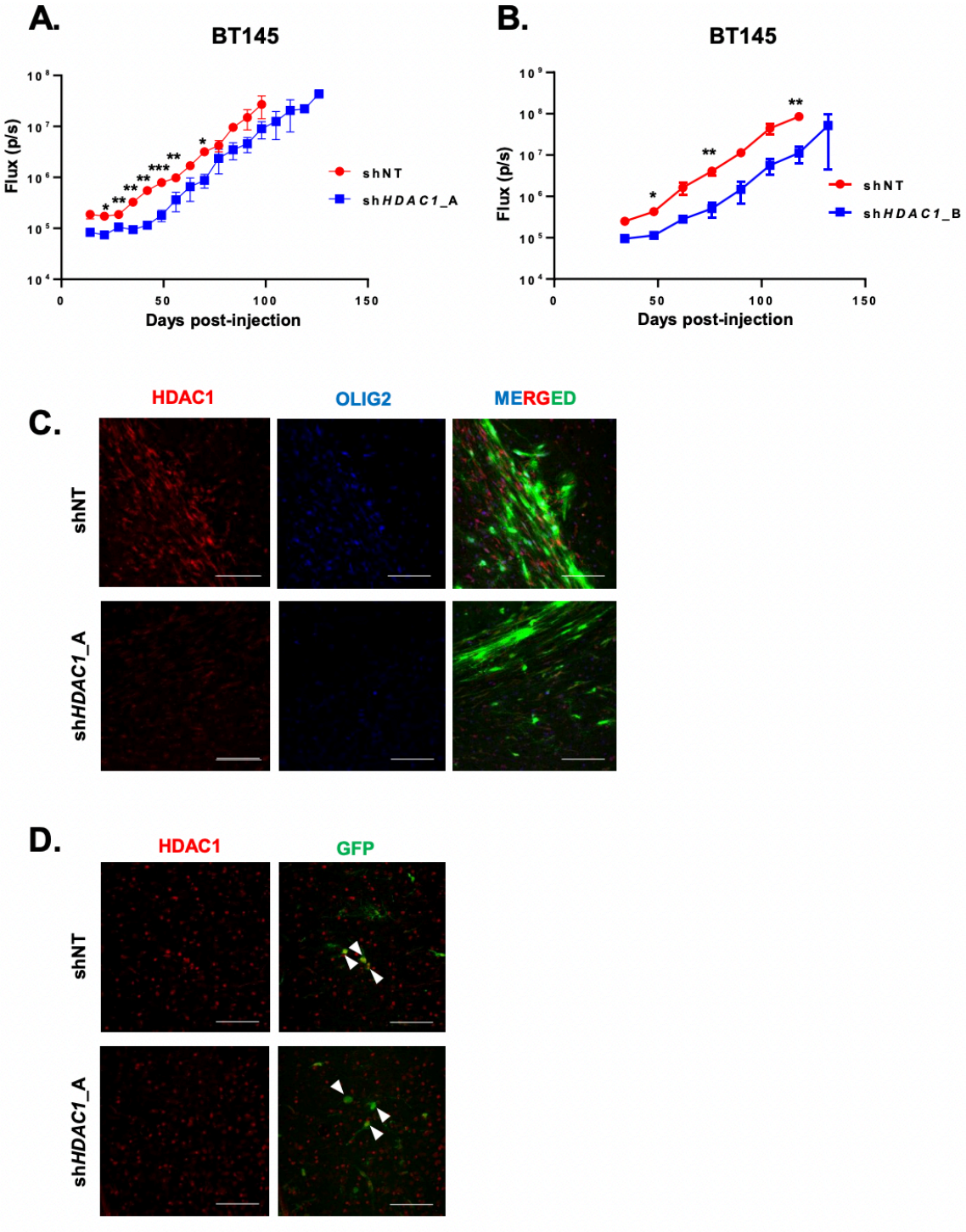


**Figure 2.10. Bioluminescence imaging of shNT and sh*HDAC1* tumors.** (A and B) Average photon flux (p/s) measured through bioluminescence imaging over time of mice with intracranial injections of shNT (n=4 in both experiments) and HDAC1-

targeting shRNAs: sh*HDAC1*_A (n=4) and sh*HDAC1*_B (n=3). (C) Image of HDAC1 (red) and OLIG2 (blue) immunostaining in shNT and sh*HDAC1* BT145 tumor tissue 7 weeks post-injection (tumor core). (D) Image of HDAC1 (red) immunostaining in shNT and shHDAC1 BT145 tumor tissue (GFP) 7 weeks post-injection in the tumor leading edge (invasive front). Error bars indicate SEM. * $p < 0.05$, ** $p < 0.01$, *** $p < 0.001$. Magnification, 20x; scale bars, 100 μM. P values were calculated using unpaired 2-tailed t-test. Taken from: (Lo Cascio et al., 2021).

### *2.4.7 HDAC1 knockdown affects expression of genes involved in apoptosis, the cell cycle, cellular communication, and migration in p53-WT GSCs*

In our RNA-seq analysis, we identified 2,516 differentially upregulated and 3,241 differentially downregulated genes across the 3 GSC lines analyzed (Figure 2.11A). Although p53-WT cell lines had a similar phenotypic response to loss of HDAC1, each cell line appeared to have significantly different responses to HDAC1 knockdown albeit with some overlapping genes, independent of p53 status. This may be partly explained by the distinct genotypes/driver mutations present in each cell line (e.g. p53-WT lines BT145 and GB3 are *EGFR* and *PDGFRA*-driven, respectively), such that *HDAC1* ablation may impart similar phenotypes through regulation of different sets of genes. We performed functional enrichment analyses in p53-WT cells (BT145 and GB3) compared to p53-mutant cells (BT187). Common genes significantly upregulated in p53-WT cell lines were associated with programmed cell death while genes associated with cell cycle and DNA-dependent DNA-replication were significantly downregulated (Figure 6B). These data are consistent with our *in vitro* results following *HDAC1* silencing (Figures 2.3A-E; Figure 2.8B). Interestingly, in p53-WT GSCs we also found significant

enrichment of genes associated with cellular communication, cellular migration, cytokine production, and responses to stress (Figure 2.11C-D).

### *2.4.8 HDAC1 knockdown results in aberrant differentiation and invasion of p53-WT GSCs*

Prolonged treatment with pan-HDAC inhibitors has previously been shown to induce differentiation in GSCs (Chiao et al. 2013). Regulatory network analysis identified 61 transcription factors associated with the regulation of genes upregulated after *HDAC1* knockdown (Figure 2.11D). Interestingly, upregulated genes include neuronal differentiation transcription factors such as *DLX1*and *DLX*6 (Eisenstat et al. 1999; Petryniak et al. 2007; Wang et al. 2010), oligodendrocyte differentiation transcription factors such as *NKX6-2* (Vallstedt, Klos, and Ericson 2005) and *EMX1* (Kessaris et al. 2006), and transcription factors expressed in developing and mature astrocytes such as *NFATC2*, *CEBPB*, *CEBPE*, and *POU3F2* (Zhang, Sloan, et al. 2016).

Considering that knockdown of *HDAC1* led to significant upregulation of expression of transcription factors that promote tissue invasion (Kim et al. 2018; Musa et al. 2017; Xia, Zhang, and Ge 2015) (e.g. *NFATC2*, and *CEBPB*; Figure 2.11D), we questioned whether sh*HDAC1* tumors exhibited a different growth pattern in vivo. While there was a marked difference in tumor burden across the two groups 7 weeks post-implantation, extensive infiltration of GFP-positive sh*HDAC1* tumor cells was seen throughout the brain parenchyma compared to shNT tumor cells – demonstrating that

HDAC1-deficient tumors displayed a more invasive phenotype in vivo (Figure 6E and 6F).

Ablation of *HDAC1* expression did not result in significant shifts between different cellular states described by Neftel et al., (Neftel et al. 2019), although some trends were evident: BT145 cells adopted a more astrocyte-like (AC) state, GB3 cells adopted a more hypoxia-dependent mesenchymal-like (MES2) state, while p53-mutant BT187 cells tended to shift from a hypoxia-independent (MES1) to a hypoxia-dependent mesenchymal-like (MES2) state (Figure 2.12). Our results suggest that *HDAC1* knockdown results in transcriptional changes that not only alter cell survival and death programs but also cell invasion in GSCs in a p53-dependent manner.

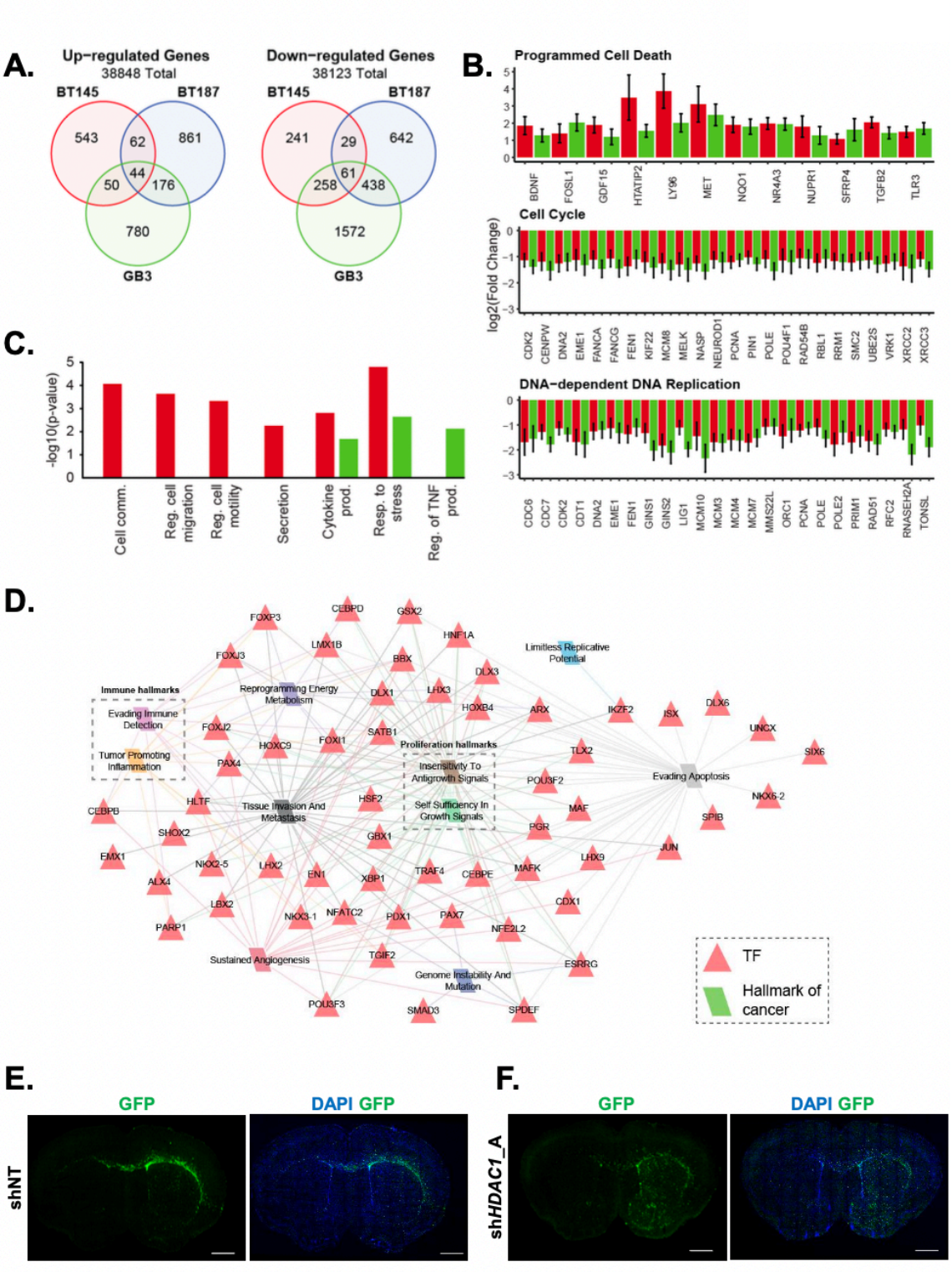
A.
Up−regulated Genes
38848 Total
BT145
BT187
GB3
543
62
861
44
50
176
780
Down−regulated Genes
38123 Total
241
29
642
61
258
438
1572
B.
Programmed Cell Death
BDNF
FOSL1
GDF15
HTATIP2
LY96
MET
NQO1
NR4A3
NUPR1
SFRP4
TGFB2
TLR3
Cell Cycle
log2(Fold Change)
CDK2
CENPW
DNA2
EME1
FANCA
FANCG
FEN1
KIF22
MCM8
MELK
NASP
NEUROD1
PCNA
PIN1
POLE
POU4F1
RAD54B
RBL1
RRM1
SMC2
UBE2S
VRK1
XRCC2
XRCC3
DNA−dependent DNA Replication
CDC6
CDC7
CDK2
CDT1
DNA2
EME1
FEN1
GINS1
GINS2
LIG1
MCM10
MCM3
MCM4
MCM7
MMS22L
ORC1
PCNA
POLE
POLE2
PRIM1
RAD51
RFC2
RNASEH2A
TONSL
C.
-log10(p-value)
Cell comm.
Reg. cell migration
Reg. cell motility
Secretion
Cytokine prod.
Resp. to stress
Reg. of TNF prod.
D.
Immune hallmarks
Evading Immune Detection
Tumor Promoting Inflammation
Reprogramming Energy Metabolism
Tissue Invasion And Metastasis
Proliferation hallmarks
Insensitivity To Antigrowth Signals
Self Sufficiency In Growth Signals
Limitless Replicative Potential
Evading Apoptosis
Sustained Angiogenesis
Genome Instability And Mutation
TF
Hallmark of cancer
E.
GFP
DAPI GFP
shNT
F.
GFP
DAPI GFP
shHDAC1_A

**Figure 2.11. *HDAC1* knockdown upregulates cell migration programs and results in more invasive tumors.** (A) Venn diagram illustrating the overlap between the significantly up-and-down-regulated genes between GSC cell lines after sh*HDAC1* knockdown. (B) Log2 fold change of gene expression after sh*HDAC1* knockdown in p53-WT GSCs BT145 (red) and GB3 (green) GSCs (adjusted $p$-value $\leq 0.05$). (C) Negative-log10 p-value for functional enrichment of relevant GO BP terms for genes with significantly increased gene expression after sh*HDAC1* knock-down in BT145 (red) and/or GB3 (green) tumorigenic cell lines. (D) BT145 and GB3 specific regulatory network for upregulated genes following *HDAC1* knockdown. Red triangles are transcription factor regulators and parallelograms are hallmarks of cancer. Edges indicate association between the target genes of the regulator and a hallmark of cancer, and are colored according to its corresponding hallmark. For each cell line, the data are compiled from three independent experiments. (E-F) Stitched whole-brain images of DAPI (blue) and GFP-positive engrafted tumor cells (green) in (E) shNT and (F) sh*HDAC1* BT145 brain tissue 7 weeks post-engraftment. GFP expression reveals *HDAC1*-deficient tumors are more invasive than control shNT tumors. Magnification, 10x; scale bars, 1 mm. Taken from: (Lo Cascio et al., 2021).

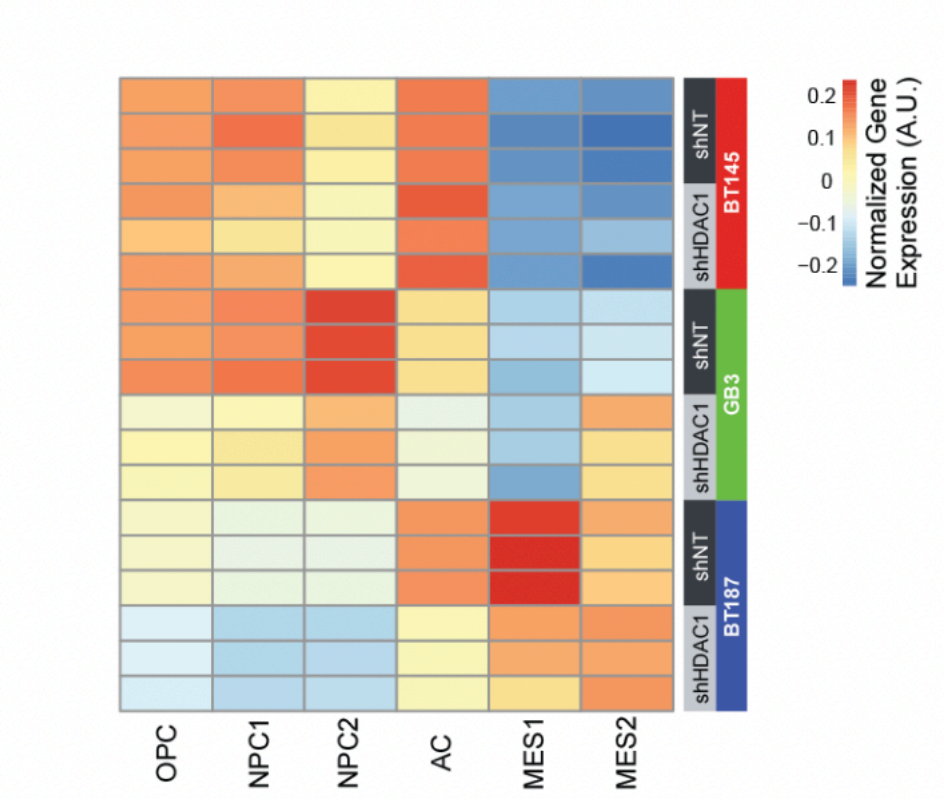


**Figure 2.12. *HDAC1* knockdown does not significantly affect the cellular states of GSCs.** Eigengene expression for the Neftel et al.,25 developmental subtypes across the GSC cell lines after transduction with either shNT or sh*HDAC1*. Developmental subtypes include oligodendrocyte precursor cells (OPC), neural precursor cells (NPC1 & NPC2), astrocyte (AC), mesenchymal (MES1 & MES2). Taken from: (Lo Cascio et al., 2021).

### *2.4.9 Genetic ablation of HDAC1 results in increased STAT3 activity in p53-WT GSCs*

We validated upregulation of genes involved in regulating cancer cell invasion, migration, and survival upon *HDAC1* knockdown using RT-qPCR in p53-WT (BT145) and p53-mutant (BT187) GSCs (Figure 2.13A). We find that expression of *STAT3*, *TGFB2*, *MET*, *ICAM1*, *CSF1*, *ITGB5*, *BDNF*, *NRP1* and *NRG5* were significantly induced after *HDAC1* knockdown almost exclusively in p53-WT but not p53-mutant GSCs (Figure 2.13A). Out of the 9 genes we analysed, 5 have been shown to be direct

targets of or are modulated by p53 (*TGFB2*, *STAT3*, *MET*, *ICAM1*, *CSF1*) (Azzam et al. 2013; Elston and Inman 2012; Gorgoulis et al. 2003; Hwang et al. 2011; Lin, Tang, et al. 2002). Several of these genes (*BDNF*, *TGFB2*, *MET*) are also direct target genes of transcription factors that are upregulated after *HDAC* knockdown in p53-WT GSCs (Figure 2.11D).

We were particularly intrigued to find that *STAT3* – an important oncogenic driver and established master regulator of mesenchymal transformation in GBM (Carro et al. 2010; Bhat et al. 2013)– was significantly induced after *HDAC1* knockdown uniquely in p53-WTGSCs (Figure 2.13A and 2.13B). Moreover, in our transcriptional regulatory network analysis (Figure 2.11D) we found that *CEBPB* – regulator of *STAT3* expression in GBM (Carro et al. 2010) – was significantly upregulated in p53-WT GSCs. Given the intrinsic phenotypic plasticity of glioma cells, we sought to determine whether the STAT3 signaling axis could be a potential compensatory mechanism that is adopted by surviving *HDAC1*-deficientGSCs. Downstream STAT3 enrichment analysis from our RNA-seq datasets revealed that several STAT3 target genes were significantly differentially regulated in p53-WT GSCs (Table 2.3). In addition to increased STAT3 mRNA expression, the phosphorylation of STAT3 at tyrosine 705 (pSTAT3), a transcriptionally active form of the protein, increases significantly following *HDAC1* silencing in p53-WT GSCs (Figure 2.13C). The levels of pSTAT3 are already elevated in p53-mutant GSCs and remain unchanged following *HDAC1* knockdown (Figure 2.13C), and this phenotype could be reproduced when we overexpressed a dominant-negative p53 mutant in p53-WT GSCs (Figure 2.14). Chromatin immunoprecipitation assay confirmed that *HDAC1* knockdown resulted in increased H3K27ac deposition in the C/EBPβ

binding site on the *STAT3* promoter region relative to control p53-WT cells (Figure 2.13D). In agreement with increased STAT3 phosphorylation, we observed increased nuclear localization of STAT3 in p53-WT cells after *HDAC1* knockdown ($p < 0.0001$; Figures 2.13E-F). Furthermore, we also confirmed that STAT3 expression was significantly elevated in sh*HDAC1* p53-WT PDX tumors relative to control tumors ($p < 0.05$; Figures 2.13G-H).

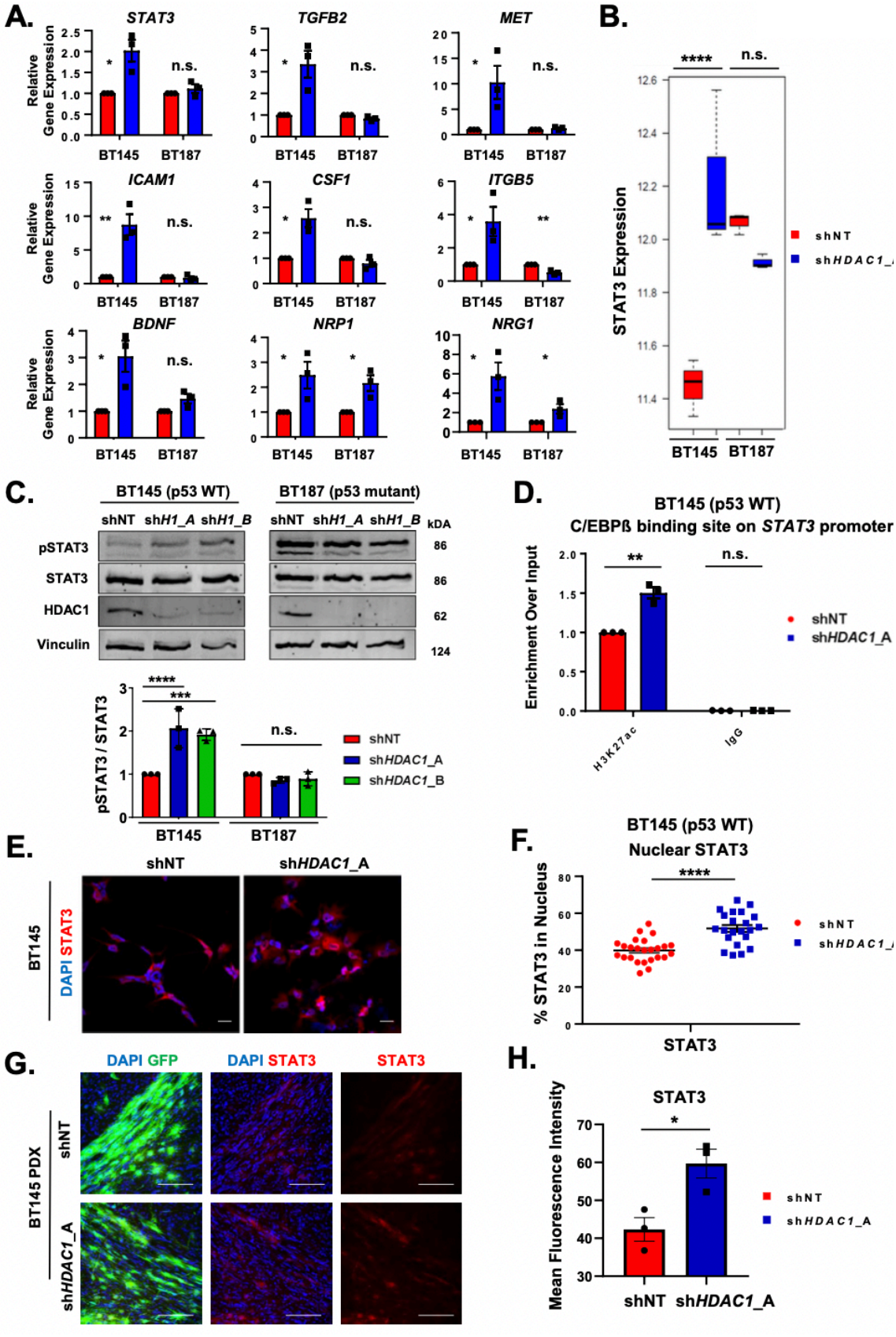
A.
STAT3
TGFB2
MET
ICAM1
CSF1
ITGB5
BDNF
NRP1
NRG1
Relative Gene Expression
BT145
BT187
n.s.
B.
STAT3 Expression
****
n.s.
shNT
shHDAC1_A
C.
BT145 (p53 WT)
BT187 (p53 mutant)
shNT
shH1_A
shH1_B
kDA
pSTAT3
STAT3
HDAC1
Vinculin
86
86
62
124
pSTAT3 / STAT3
shHDAC1_A
shHDAC1_B
D.
BT145 (p53 WT)
C/EBPß binding site on STAT3 promoter
Enrichment Over Input
H3K27ac
IgG
E.
shNT
shHDAC1_A
BT145
DAPI STAT3
F.
BT145 (p53 WT)
Nuclear STAT3
% STAT3 in Nucleus
STAT3
G.
DAPI GFP
DAPI STAT3
STAT3
BT145 PDX
shNT
shHDAC1_A
H.
STAT3
Mean Fluorescence Intensity

**Figure 2.13. *HDAC1* knockdown results in increased STAT3 signaling in p53-WT hGSCs.** (A) RT-qPCR for genes involved in cellular invasion or survival in BT145 (p53 WT) and BT187 (p53 mutant) GSCs (n=3 per target). (B) RNA-seq analysis for *STAT3* expression in BT145 and BT187 after HDAC1 knockdown. (C) Lysates were collected from BT145 and BT187 after acute silencing of *HDAC1* (sh*H1*_A = sh*HDAC1*_A and sh*H1*_B = sh*HDAC1*_B). Immunoblots were probed with antibodies for phosphorylated STAT3 (Tyr705), STAT3, HDAC1 and Vinculin. Bar graph below shows quantification of the normalized ratio of pSTAT3 over total STAT3 protein after *HDAC1* knockdown in BT145 and BT187 GSCs (n=3). (D) Chromatin Immunoprecipitation (ChIP) assay for H3K27ac deposition in the C/EBPβ binding site on the *STAT3* promoter in BT145 (n=3). (E) Immunocytochemistry staining for STAT3 in BT145 after acute *HDAC1* knockdown. (F) Quantification of immunocytochemistry experiments showing significantly increased nuclear localization of STAT3 after HDAC1 knockdown in BT145. Graph shows values from individual experimental values from multiple experiments (n=4) (G) Immunofluorescence staining for STAT3 in BT145 PDX tumor tissue 7 weeks post-engraftment in *HDAC1*-silenced tumors relative to controls. (H) Quantification of mean pixel intensity for STAT3 staining in BT145 shNT and sh*HDAC1* PDX tumors. Graph shows average values from 3 independent animals per experimental condition. Error bars indicate SEM. * $p < 0.05$, ** $p < 0.01$, *** $p < 0.001$, **** $p < 0.0001$, n.s., not significant. For each cell line, the data are compiled from at least three independent experiments. Magnification, 20x; scale bars, 2 μM and 100 μM. *P* values were calculated using unpaired 2-tailed t-test or 2-way ANOVA with Tukey's multiple comparisons test. Taken from: (Lo Cascio et al., 2021).

| Cell Line | P-value | M | N | n | k | k genes |
|---|---|---|---|---|---|---|
| **BT145 up** | **0.002642433** | **27462** | **632** | **81** | **6** | **FAS, HMOX1, MAP3K8, CXCL10, A2M, CSF1** |
| BT145 down | 0.492148388 | 27462 | 558 | 81 | 1 | IL1B |
| **BT187 up** | **0.024730538** | **27462** | **973** | **81** | **6** | **BAK1, HMOX1, IRF1, PIM1, INHBE, PDGFC** |
| **BT187 down** | **0.012796318** | **27462** | **1059** | **81** | **7** | **CD9, CD44, LEPR, IL13RA1, TNFRSF21, CCR1, A2M** |
| **ihNPC up** | **9.05E-08** | **27462** | **939** | **81** | **14** | **TNFRSF12A, FAS, HMOX1, EBI3, TGFB1, IRF1, IL1B, IL6ST, IL15RA, PIM1, CXCL3, CXCL11, JUN, CSF1** |
| ihNPC down | 4.91E-01 | 27462 | 557 | 81 | 1 | TNFRSF21 |
| NHA up | 0.724877191 | 27462 | 859 | 81 | 1 | HMOX1 |
| **NHA down** | **0.000555088** | **27462** | **1152** | **81** | **10** | **CD38, IFNGR1, EBI3, IL18R1, LEPR, IRF1, TNFRSF21, CCR1, CD14, LTB** |
| | | | | | | |
| | | | | | | |
| | | | | | | |
| **M = all genes in genome (from res files)** | | | | | | |
| **N = differentially expressed genes** | | | | | | |
| **n = genes from STAT3 pathway** | | | | | | |
| **k = overlap between n & N** | | | | | | |

**Table 2.3. STAT3 pathway downstream enrichment analysis in BT145, BT187, ihNPCs and NHAs after HDAC1 knockdown.** Downstream targets of the IL6/JAK/STAT3 pathway were examined for differential expression using a hypergeometric distribution model. Bolded cell lines (BT145 upregulated, BT187 upregulated, BT187 downregulated, ihNPC upregulated, NHA downregulated) indicate a significant difference in expression of the group of target genes, suggesting influence from the STAT3 signaling pathway. Taken from: (Lo Cascio et al., 2021).

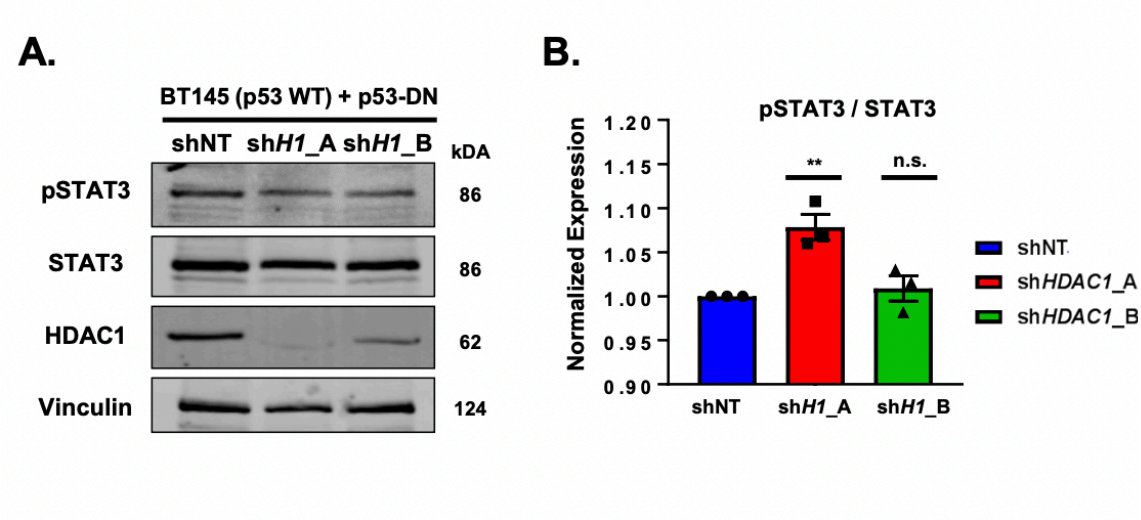


**Figure 2.14. pSTAT3 levels after *HDAC1* knockdown in p53-WT GSCs overexpressing p53-DN** (A) Lysates were collected from BT145 overexpressing p53-DN after acute silencing of HDAC1 with two independent shRNAs (shH1_A = sh*HDAC1*_A and shH1_B = sh*HDAC1*_B) and were immunoblotted with antibodies directed against phosphorylated STAT3 (Tyr705), STAT3, HDAC1 and Vinculin. (B) Quantification of the normalized ratio of pSTAT3 over total STAT3 protein after HDAC1 knockdown from three independent experiments in BT145 overexpressing p53-DN. ** $p < 0.01$, n.s., not significant. Error bars indicate SEM. P values were determined using the 2-way ANOVA with Tukey's multiple comparisons test. Taken from: (Lo Cascio et al., 2021).

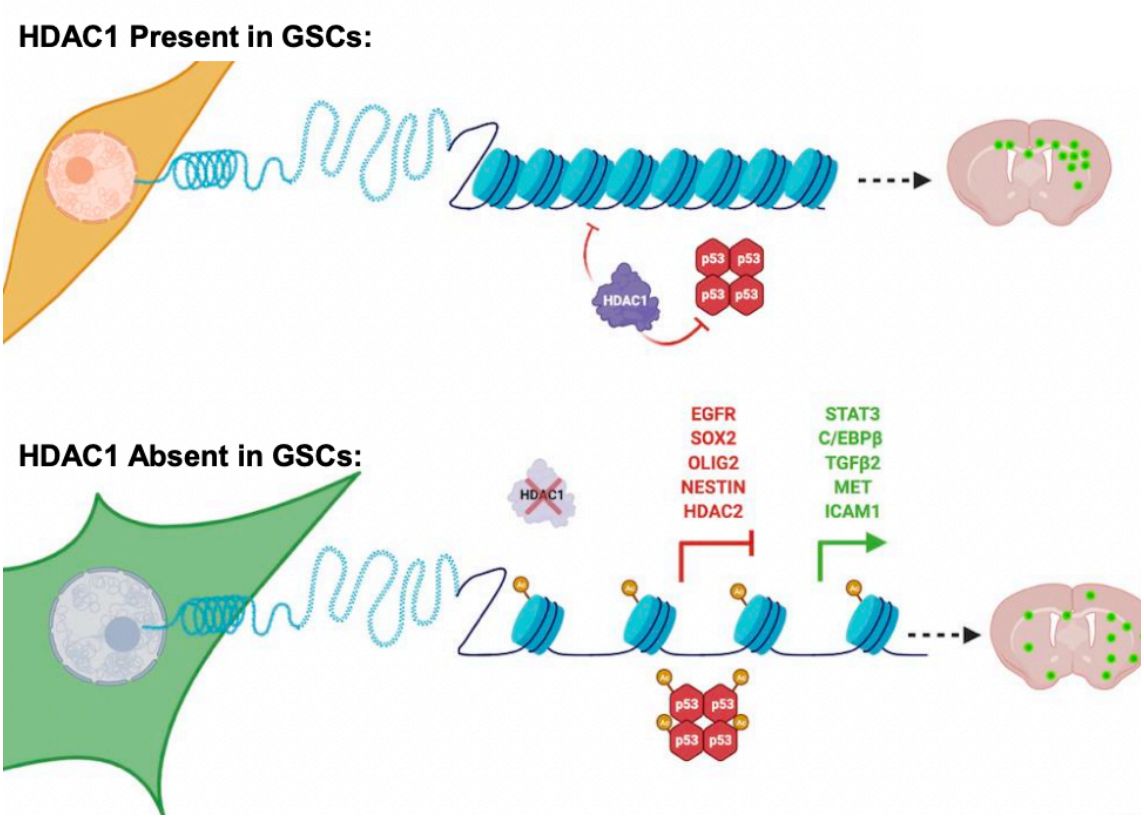


**Figure 2.15. Proposed model: consequences of *HDAC1* silencing in p53-WT hGSCs.** Summary of the cellular and molecular effects of *HDAC1* loss in p53-WT hGSCs. Absence of HDAC1 results in increased histone acetylation and restoration of p53 activation and stability. These changes are accompanied by significant changes in gene expression, wherein genes involved in maintaining stemness are downregulated while genes involved in promoting differentiation, migration and cellular communication are upregulated. *In vitro*, these cells fail to proliferate and die; however, when transplanted *in vivo* these cells form slower growing but more invasive tumors. STAT3 activity, which is known to drive aggressive phenotypes in GBM, is upregulated after HDAC1 loss and may be a potential druggable compensatory pathway that may be targeted in combination with more selective HDAC1 inhibitors. Taken from: (Lo Cascio et al., 2021).

## 2.5 Discussion

Considering the role of HDACs in oncogenesis, there has been an increased interest in testing HDACi for several malignancies, including both adult and pediatric gliomas (Bezecny 2014; Eckschlager et al. 2017). However, almost all HDACi used in clinical trials for primary and recurrent GBM to date were unable to provide significant therapeutic benefit to patients (Lee et al. 2017). These HDACi (e.g. TSA, Vorinostat, SAHA, Panobinostat) are broad-spectrum, have poor pharmacokinetic profiles as well as a narrow therapeutic index (Galanis et al. 2009; Hooker et al. 2010; Iwamoto et al. 2011; Bezecny 2014; Li and Seto 2016). Isoform-specificity for HDACi is important given that not all HDAC enzymes are equally expressed in GBM (Cancer Genome Atlas Research 2008). Most of our knowledge on the presumed roles of HDACs in gliomas is largely based on pre-clinical studies with pan-HDACi, which preclude a true understanding of the requirement and role of individual HDACs in these tumors, especially within the therapy-resistant cancer stem cells (Bastola et al. 2020; Pak et al. 2019; Householder et al. 2018). To this end, we specifically investigated the functional importance of HDAC1 in GSCs, an HDAC isoform whose expression increases with brain tumor grade and is correlated with decreased survival (Cancer Genome Atlas Research 2008; Madhavan et al. 2009) (Figure 2.1). Although several CRISPR-Cas9 screens conducted ohGSCs did not identify HDAC1 as an essential fitness gene governing GSC growth and survival (Toledo et al. 2015; MacLeod et al. 2019), recent studies corroborate our findings that HDAC1 is an attractive therapeutic target for GBM (Bastola et al. 2020; Song et al. 2020). Bastola et al., identified HDAC inhibitors through a large-scale screen of small molecules that demonstrated increased efficacy in targeting glioma cells within the tumor

core versus the invasive edge (Bastola et al. 2020). They also identified HDAC1 as a regulator of CD109 expression, a marker of aggressive mesenchymal GBM cells. Song et al., focused on the role of NFAT2 and demonstrated that NFAT2 binds to the *HDAC1* promoter and regulates its expression to promote mesenchymal transformation of hGSCs (Song et al. 2020). Here, we demonstrate that genetic silencing of *HDAC1* alone attenuates the tumorigenic and stemness potential of GSCs in a p53-dependent manner and significantly extends survival in PDX and mouse models of GBM *in vivo*. Our data provide a rationale for the development of isoform-specific HDAC inhibitors for the treatment of GBM.

Although HDAC1 and HDAC2 have been shown to be functionally redundant in many cellular contexts because of their high sequence homology, several studies have demonstrated this is not the case during early embryogenesis and central nervous system development (Lagger et al. 2002; Dovey, Foster, and Cowley 2010; Hagelkruys et al. 2014). For instance, targeted deletion of *Hdac1* in mice results in embryonic lethality due to severe proliferation and differentiation defects during development (Jamaladdin et al. 2014). On the contrary, in the developing brain, HDAC2 was identified as being both essential and sufficient to ensure normal brain development and survival in the absence of HDAC1 in *Nestin*-Cre transgenic mice (Hagelkruys et al. 2014). Here, we show that HDAC1 is required for the viability and proliferative potential of p53-WT GSCs, while p53-mutant GSCs, normal neural progenitor cells, and astrocytes were significantly but more modestly affected by *HDAC1* silencing (Figure 2.3A). Given that we did not observe increased HDAC2 activity following *HDAC1* knockdown, the severe phenotype exhibited by HDAC1-deficient GSCs reveals that HDAC1 and HDAC2 harbor previously

underappreciated, non-redundant functions in GBM. This is further highlighted by our observation that HDAC2 silencing does not affect the viability of p53-WT and p53-mutant GSCs, and that HDAC1 displays significant compensatory upregulation in these cells when *HDAC2* expression is silenced (Figure 2.6B-C). With respect to the impact of *HDAC1* silencing in normal cells (NHAs, ihNPCs), our results support previous studies that have shown that deletion of *Hdac1* in mature astrocytes does not result in cellular catastrophe, and that HDAC2 is the essential class I deacetylase in neural progenitor cells in absence of its paralogue (Montgomery et al. 2009; Hagelkruys et al. 2014). We do see a significant increase in *HDAC10* and *HDAC11* in p53-mutant GSC lines and *HDAC9* in NHAs, so it is likely that these HDACs may play a compensatory role in astrocytes and p53-mutant lines.

Our findings suggest that HDAC1 function may be dispensable or irrelevant in a context where p53 is mutated in GSCs. Unlike p53-WT GSCs, we did not observe p53-mediated cell growth arrest and apoptosis in p53-mutant cells after acute *HDAC1* silencing (Figure 2.3). Despite this, we found that *HDAC1* knockdown still results in an average 40-30% loss in cell viability in p53-mutant GSCs. This phenomenon might be explained by previous studies that have shown that the presence of functional p53 can dictate the fate of various cancer cell lines in response to HDACi, wherein p53-WT cells preferentially undergo apoptosis while p53-deficient or mutant cells undergo autophagy (Mrakovcic and Frohlich 2018; Mrakovcic, Kleinheinz, and Frohlich 2019). Whether p53 status dictates the induction of autophagy over apoptosis in the absence of specific HDAC isoforms (such as HDAC1) in GSCs remains an important question to be addressed in future studies.

Our results also yield new insights into the previously described molecular mechanism underlying the oppositional relationship between OLIG2 and p53 present in both neural progenitors and malignant glioma (Mehta et al. 2011). Olig2 has been shown to directly repress p21 and oppose p53 functions by suppressing its acetylation (thereby activation) and transcriptional functions (Ligon et al. 2007; Mehta et al. 2011). Here we show that *HDAC1* knockdown in p53-WT GSCs results in downregulation of OLIG2, induction of p21 and increased p53 stabilization and acetylation (Figures 3G and 4B) as previously hypothesized by Meijer et al., (Meijer et al. 2014). Additionally, our observations are consistent with reports demonstrating that deacetylation of p53 is primarily mediated by HDAC1 and not HDAC2 in various non-glioma cell lines (e.g. 293T, 3T3 cells) (Luo et al. 2000; Ito et al. 2002), and is indicative of the reversal of OLIG2-mediated suppression of p53 DNA targeting (Mehta et al. 2011). Acetylation has been shown to be important to promote increased protein stability and transcriptional functions of p53; however, we don't exclude that there are several other possible mechanisms that can affect the regulation of p53 gene expression in the absence of HDAC1 (Ito et al. 2001). Previous studies have shown that certain RNA-binding proteins can control the kinetics of *TP53* mRNA translation (Haronikova et al. 2019). However, since we did not observe increased transcription of *TP53* mRNA in p53-WT GSCs after *HDAC1* knockdown (Figure 2.5G), the observed increase in p53 target gene expression (e.g., p21) might be due to either increased stability of p53 protein and/or transcriptional activity of p53. In addition to acetylation, other post-translational modifications such as phosphorylation and methylation can also promote p53 stability by enhancing

interactions with acetyltransferases and blocking MDM2 association (Reed and Quelle 2014; Chuikov et al. 2004).

Knockdown of *HDAC1* – a single HDAC isoform – is sufficient to prolong survival in vivo (Figure 2.9E-F). Intriguingly, although *HDAC1*-silenced p53-WT hGSCs fail to proliferate and die *in vitro*, these cells can form tumors in immunocompromised mice – albeit at a slower rate compared to controls (Figure 2.9A and Figure 2.10A-B). This strongly suggests that standard GSC *in vitro* culture conditions may lack the appropriate soluble factors and cellular interactions that are required for these cells to thrive in absence of HDAC1 activity or a persister population of cells survives *HDAC1* ablation *in vivo* (Liau et al. 2017). Our transcriptional regulatory network analysis (Figure 2.11D) revealed that HDAC1 silencing in p53-WT GSCs results in the upregulation of multiple transcription factors that are associated with several hallmarks of cancer (e.g. tumor-promoting inflammation, evasion of apoptosis, tissue invasion and metastasis), which promote tumor growth and survival. The observation that sh*HDAC1*-tumors are significantly more invasive at early stages of tumorigenesis thereby prompted us to investigate potential alternative mechanisms that are adopted by these cells to grow in the absence of HDAC1 (Figure 2.11E-F). Indeed, we found that ablation of *HDAC1* expression resulted in marked upregulation of a vast array of genes that have previously been implicated in promoting tumor cell survival, invasion and metastasis in gliomas and other cancers (e.g. *TGFB2*, *ITGB5*, *CSF1*, *NRG1*, *NRP1*, *ICAM1*, *MET*; Figure 2.13A) (Wick, Platten, and Weller 2001; Kesanakurti et al. 2013; Coniglio et al. 2012; Singh et al. 2017; Zhang et al. 2019; Hu et al. 2007; Zhao and Schachner 2013; Eckerich et al. 2007).

We identified STAT3 signaling axis as a promising and druggable compensatory pathway that is upregulated after HDAC1 loss in p53-WT GSCs. STAT3 is an established master regulator of the mesenchymal gene expression signature in GBM, which imparts a highly aggressive, treatment-resistant phenotype that predicts poor clinical outcome (Carro et al. 2010; Masliantsev et al. 2018; Fedele et al. 2019). While we did not observe any evident shift towards the mesenchymal cell state in our cells (Figure 2.12), STAT3 is known to promote tumor survival, proliferation and is a major driver of glioma cell migration and invasion (de la Iglesia, Puram, and Bonni 2009). Moreover, HDAC1 has previously been implicated in regulating STAT3 nucleocytoplasmic partitioning and activity, wherein HDAC1 expression was shown to reduce nuclear accumulation of STAT3 in commonly used cancer and non-tumorigenic cell lines (Ray et al. 2008; Ma et al. 2020; Icardi et al. 2012). Indeed, we observed nuclear translocation of STAT3 in p53-WT GSCs after HDAC1 knockdown (Figure 2.13E).

We found that in p53-mutant cells and p53-WT cells overexpressing a p53 mutant, which were only modestly affected by HDAC1 silencing, pSTAT3 levels were already elevated at baseline and did not change after HDAC1 loss – this is in line with previous studies that have shown that cancer cell lines that harbor p53 mutations or deletions express constitutively active STAT3 (Figure 2.13C and Figure 2.14) (Lin, Tang, et al. 2002; Lin, Jin, et al. 2002; Wormann et al. 2016). These data highlight the importance of the HDAC1-STAT3 signaling axis, which has practical overtones for combination therapy in p53-WT GBMs. As seen in our RNA-seq data, knockdown of *HDAC1* results in distinct changes in every cell line (p53-WT and mutant). Hence, future

studies are required to identify additional genetic markers beyond p53 that predict responsiveness to HDAC1 inhibition. Considering the plastic nature of glioma cells and transitions between cell states (Neftel et al. 2019), relying on molecular subtypes to identify HDACi-responsive tumors might not be a reliable approach.

As seen from clinical trials with class I-specific HDACi such as Romidepsin (Iwamoto et al. 2011), it is unlikely that a monotherapeutic strategy with more isoform-selective HDACi would result in a durable response in patients. Based on our data, we propose that combination therapies with brain-penetrant STAT3 inhibitors is a promising treatment strategy for p53-WT GBM tumors. Although preclinical studies with several HDACi have been shown to suppress growth in murine PDX models (Bastola et al. 2020; Pak et al. 2019) these inhibitors are either toxic at human-equivalent doses and/or have high plasma protein-binding (>96% for AR-42) (Cheng et al. 2016), which will hinder translating these findings to the clinic. A putative brain-available STAT3 inhibitor, WP1066 is currently under clinical trial (NCT01904123). Future combination studies with isoform-specific HDACi and STAT3 inhibitors that incorporate pharmacokinetic and pharmacodynamic (PK/PD) analysis in multiple PDX models will allow translation of these findings to the clinic.

In summary, our data has highlighted an unmet need for isoform-specific HDAC inhibitors in GBM and identified a potential druggable compensatory mechanism that can guide future combination studies.

# CHAPTER 3

# PHARMACOKINETCS AND PHARMACODYNAMICS-BASED EVALUATION OF QUISINOSTAT IN PRECLINICAL MODELS OF GBM

## 3.1 Introduction

HDAC inhibitors (HDACi) are a successful example of epigenetic therapy, with five inhibitors currently FDA-approved for the treatment of different hematological malignancies, and a growing number of agents are currently in different stages of clinical testing for a variety of cancers (Li and Seto 2016). The rationale underlying the use of HDACi as therapeutic agents is that they can reverse the global dysregulation of gene expression present in cancer cells by inducing hyperacetylation of histones and transcription factors (Jenke et al. 2021). Through mechanisms that are not entirely understood, HDACi treatment in transformed cells results in cell cycle arrest, autophagy, differentiation, and/or programmed cell death (Li and Seto 2016). Despite the excitement and promising preclinical results, to date the use of HDACi as either single agents or in combination with other modalities for the treatment of GBM have yielded predominantly disappointing results in the clinic (Chen et al. 2020).

Vorinostat (SAHA) was the first HDACi to be tested in clinical trials for patients with newly diagnosed GBM and it failed to meet its primary efficacy endpoint in a phase I/II clinical trial when combined with standard radiation therapy and temozolomide (NCT00731731) (Galanis et al. 2018). Romidepsin (FK228) and Panobinostat (LBH589) were also found to be ineffective in clinical trials for recurrent GBM (NCT01738646, NCT00859222) (Ghiaseddin et al. 2018; Lee, Reardon, et al. 2015). Although

pharmacological inhibition of HDACs has not led to encouraging results in the realm of adult brain tumors, there are several important considerations to highlight when interpreting such negative clinical data. First, these HDACi have either poor or unknown pharmacokinetic profiles. Hence, a possible reason for the lack of efficacy of HDACi in GBM may be due to poor blood-brain-barrier penetration resulting in subtherapeutic intratumoral drug levels. Moreover, preclinical studies that employed these HDACi in animal models of GBM and other gliomas often resorted to direct intratumoral diffusion or convection-enhanced, rather than systemic, delivery methods to obtain a modest survival benefit. An additional caveat is that these inhibitors are broad-spectrum (pan-HDACi): they non-selectively inhibit the activity of all 11 human HDAC isoforms (Bezecny 2014). Considering that HDACs retain essential functions for cell homeostasis across different tissues, pan-HDACi can be highly toxic to normal organ function – a notable example being the hydroxamic acid Panobinostat (Wood et al. 2018; Ibrahim et al. 2016; Eleutherakis-Papaiakovou et al. 2020). Thus, HDACi-induced toxicities significantly narrow the therapeutic window of these drugs for the treatment of GBM. However, it has been suggested that improved drug target selectivity typically leads to a superior safety profile, and this may hold true for HDACi as well (Ho, Chan, and Ganesan 2020; Su, Gong, and Liu 2021).

Isoform selectivity of HDACi is an important consideration given that not all HDAC enzymes are equally expressed in GBM, and that the specific roles of individual HDAC isoforms in these tumors are not well understood (Cancer Genome Atlas Research 2008). We recently uncovered the functional importance of HDAC1 in GBM, an HDAC isoform whose expression increases with brain tumor grade and is correlated with

decreased survival (Lo Cascio et al. 2021). We found that HDAC1 function is essential for the survival of GSCs, and that its loss is not compensated for by its paralogue HDAC2 or other HDACs. Importantly, we demonstrated that loss of HDAC1 alone significantly prolonged survival *in vivo* – providing a rationale for the development of isoform-selective HDACi for the treatment of GBM (Lo Cascio et al. 2021).

While no HDAC1-selective agents are currently available, quisinostat (JNJ-26481585) is a second-generation HDACi that is highly selective towards class I HDACs, and harbors marked potency towards HDAC1 ($IC_{50}$: 0.1 nM) (Ho, Chan, and Ganesan 2020). Quisinostat has been shown to exhibit potent antitumor activity in preclinical models of different cancers and has been studied in phase I/II clinical trials for ovarian and hematological malignancies (Carol et al. 2014; Arts et al. 2009). Although quisinostat has been tested in several preclinical models of adult and pediatric brain tumors (GL261, SHH medulloblastoma, DIPG), these experiments suggested that quisinostat failed to provide significant treatment benefit as a monotherapy (Householder et al. 2018; Vitanza et al. 2021; Pak et al. 2019). However, these studies did not clearly establish whether quisinostat is a CNS-penetrant molecule, as indicated by lack of direct pharmacokinetic and pharmacodynamic data. Moreover, the effectiveness of quisinostat in orthotopic patient-derived xenograft models of GBM remains unknown. Considering our recent discovery that HDAC1 is the essential class I deacetylase in glioma stem cells, we sought to understand whether quisinostat may be a promising form of epigenetic therapy for the treatment of GBM.

In this chapter, we assessed the pharmacokinetic (PK), pharmacodynamic (PD) and radiation-sensitizing properties of quisinostat in preclinical models of human GBM.

quisinostat exhibited potent growth inhibition in multiple GSC lines, and induced histone hyperacetylation, elevated DNA damage, cell death and cell cycle arrest. We also unveil the PK profile for quisinostat *in vivo* and establish that it is a brain-penetrant molecule. Importantly, we demonstrate that while quisinostat monotherapy had a modest effect on tumor growth, combination treatment with radiation significantly extended survival in an orthotopic GBM model. Together, our results reveal that quisinostat is a potent radiosensitizer, providing a rationale for developing quisinostat as a combination therapy with radiation for the treatment of GBM.

## 3.2 Methods

### *3.2.1 Primary Cell Culture*

Patient-derived glioma stem cell lines (GSCs; GB187, GB239, GB282 and GB71 and GB126) were established from resected primary GBM tumor tissue at BNI. BT145 GSCs were obtained from Dr. Keith Ligon's laboratory at the Dana-Farber Cancer Institute. All human GSCs were cultured as described previously. U87-MG cells (HTB-14) were purchased from the American Type Culture Collection (ATCC). GSCs were cultured as spheres on non-tissue culture-treated 10cm plates or as adherent cultures on laminin on tissue culture-treated 10 cm plates (ThermoFisher Scientific). GSCs were grown in DMEM/F12 media, supplemented with B27, N2 (Invitrogen, ThermoFisher Scientific) 1% penicillin-streptomycin in the presence of 20 ng/ml epidermal growth factor (EGF) and basic fibroblast growth factor (bFGF) (MilliporeSigma). U87-MG cells were grown in DMEM (Corning) supplemented with 10% BCS (Invitrogen, Gibco, Thermo Fisher)

and 1% and 1% penicillin-streptomycin (Gibco) on tissue culture-treated 10 cm plates according to manufacturer recommendations.

### *3.2.2 Cell Viability Assays After Quisinostat Treatment*

GSCs were seeded in laminin-coated tissue culture-treated 96-well plates (clear bottom, white plate; Corning) at a density of 1,000-5,000 cells per well (cell line dependent) in GSC media. U87-MG were seeded using their normal growth conditions without laminin (10% BCS in DMEM). All cells were incubated at 37°C and allowed to adhere overnight. The next day, cells were treated with incremental concentrations of quisinostat (Selleckchem; 0, 10, 25, 50, 100, 250, 500, 1000 nM) diluted in media. Cells treated without quisinostat were treated with DMSO diluted in media. Following treatment with quisinostat, cells were grown for 3-5 days (cell-line dependent) at which point cell viability was measured and quantified. All cell viability measurements were performed using the *CellTiter-Glo*® Luminescent Cell Viability Assay (Promega) following the manufacturer's instructions. All cell viability results represent the mean of at least 2 biological replicates, each containing three technical replicates.

### *3.2.3 Western Blotting*

Cellular protein from cultured cells were homogenized in RIPA lysis buffer containing protease and phosphatase inhibitors (ThermoFisher Scientific), rotated at 4℃ for 20 minutes and then centrifuged at 15,000 rpm for 10 minutes at 4℃. Protein concentration from whole-cell extracts were determined using the Bradford Protein Assay (ThermoFisher Scientific). Equal amounts of protein (10-40 μg/lane) were loaded onto a

10% or 12.5% SDS- PAGE gels and transferred to a polyvinylidene fluoride membrane (PVDF; Millipore-Sigma).

Cellular protein from frozen tissue of non-tumor bearing mouse brains, tumor-bearing mouse brains and flank tumors were homogenized in a pre-chilled glass tissue grinder (VWR) with RIPA lysis buffer containing protease and phosphatase inhibitors (ThermoFisher Scientific). 500uL of RIPA buffer was used for 10 mg of tissue. Once homogenized, the tissue lysates were kept on ice for 30 minutes and vortexed every 10 minutes. The samples were then centrifuged at 15,000 rpm for 10 minutes at 4℃ to collect the protein lysates.

Membranes were blocked with 5% non-fat milk for 1 hour at room temperature and incubated overnight with primary antibody at 4℃; Primary antibodies used in this study were mouse rabbit anti-OLIG2 (1:100,000, generous gift from the Stiles Lab, Dana-Farber Cancer Institute, Boston), rabbit anti-p21 (1:500; Abcam, ab109520), rabbit anti-gamma H2AX (phosphor Ser139; 1:1000, Abcam, ab11174), rabbit anti-H3K27ac (2 µg/mL, Abcam, ab4729), rabbit anti-H3K9/14ac (1:1000, Cell Signaling Technologies, 9677), rabbit anti-pErk1/2 (1:1000, Cell Signaling Technologies, 9101) and mouse anti-β-actin (1:1000, Bio-Rad, MCA5775GA). Membranes were probed with fluorophore-conjugated anti- mouse or anti-rabbit secondary antibodies (1:10,000; ThermoFisher Scientific). Western blots were developed using the LI-COR Odyssey CLx imaging system (LI-COR Inc.) and quantitated using the Image Studio Lite software. All Western blots are representative images from a minimum of three biological replicates.

### *3.2.4 Immunocytochemistry*

Cells were grown as adherent cultures on laminin-coated glass coverslips (Thermo Fisher Scientific) in GSC media. 24 hours after plating the cells were treated with quisinostat or DMSO diluted in GSC media. 72 hours post-treatment, cells were and fixed with 4% paraformaldehyde (PFA) for 13 minutes at room temperature. Cells were washed with PBS and subsequently permeabilized and blocked with 5% normal goat serum (Sigma Aldrich) and 0.2% Triton X-100 in PBS (blocking solution) for 30 minutes at room temperature. The cells were incubated with primary antibodies overnight at 4°C in blocking solution. Primary antibodies used in this study included rabbit anti-Ki67 (1:1000; Abcam, 15580), rabbit anti-Cleaved Caspase 3 (1:400; Cell Signaling Technologies, 9661), rabbit anti-gamma H2AX (phosphor Ser139; 1:1000, Abcam, ab11174), and mouse anti-human Nestin (1:500; Novus Biologicals, 10C2). The following day, the cells were washed with PBS three times, incubated with fluorophore-conjugated secondary antibodies at 1:1,000 dilutions (Alexa Fluor 568 goat anti-mouse, Abcam, ab175473; Alexa Fluor 488 goat anti-rabbit, Abcam, ab150077) for 1 hour at room temperature, and finally washed in PBS three more times. Cells were mounted onto SuperFrost Plus microscope slides using Fluoroshield Mounting Medium containing DAPI (Abcam). Images were acquired using a confocal microscope (Leica Microsystems; TCS SP5) operated with LAS software. The fraction of Ki67- and Cleaved Caspase 3- positive cells were counted from five independent images from each condition. The average and standard deviation were calculated from three biological replicates for all control and Quisinostat-treated experiments.

### *3.2.5 In vitro irradiation studies*

For all *in vitro* radio-sensitization experiments involving treatment with ionizing irradiation (IR) using RS 2000 irradiator (Rad Source), GSCs were plated on laminin-coated tissue culture-treated 96-well plates and incubated at 37°C overnight for 24 hours. The next day the cells were pre-treated with Quisinostat or an equivalent volume of DMSO for one hour and then subsequently irradiated with various doses of IR (cell-line dependent). Cell viability was measured as described above using the *CellTiter-Glo*® assay (Promega) 3-5 days after treatment. For experiments involving protein characterization of IR-treated cells preceded by treatment with Quisinostat, whole-cell lysates were collected 2, 6, 24, 48 and 72 hrs after irradiation. Radiation was delivered using a RS2000 Series Biological Irradiator (Rad Source Technologies).

### *3.2.6 Flank Tumor Implantation*

For flank implantations, the cells were prepared in a 1:1 ratio with 50 uL Matrigel (Corning #356234) and 50 uL of a single cell suspension of U87 (500,000 cells) in a 1 mL syringe fitted with a 26-gauge needle. The mice were anesthetized with isoflurane in a plastic desiccator placed in an externally vented fume hood. The U87-Matrigel cell suspension was then subcutaneously injected into the flank of the mouse on the posterior/lateral aspect of the lower rib cage. The mice were monitored daily and growth of flank tumor area was measured with a digital caliper (ThermoFisher) once a week. Mice were sacrificed once the tumor size grew over 2000 $mm^3$ in size.

### *3.2.7 Orthotopic Xenograft Studies*

7-week old *Foxn1*$^{nu}$ nude male mice (The Jackson Laboratory) were used for *in vivo* orthotopic transplantation of luciferized GB126 (male) cells. Nude mice were anesthetized using gaseous isoflurane and immobilized on a Leica stereotaxic instrument (cat# 39477001, Leica Microsystems). Following an incision at the midline, a fine hole was drilled 2.5mm lateral to the bregma. Using a 33-guage needle syringe (700 series, Hamilton), 2 µl of dissociated viable cells (at a density of 50,000 cells/µl) were injected 2 mm deep from the surface of the skull slowly at a constant rate of 1 µl per minute for 2 minutes. The needle was left for 1 additional minute to prevent reflux of the injected cells and was then slowly removed. The incision was closed with surgical staples. All mice were observed daily and were sacrificed upon the onset of severe neurological symptoms and >10% body weight loss. Survival data was plotted and analyzed using GraphPad Prism 8 (GraphPad Software).

### *3.2.8 Preparation of quisinostat for In Vivo Use*

For *in vivo* preparation, quisinostat was dissolved in 50% PEG-300, 50% sterile water solution for either 5 mg/kg or 10 mg/kg dosing. The suspension was then sonicated for 10 minutes to allow the drug to completely dissolve. Finally, the pH or both the drug and vehicle solutions were adjusted to 7.4 prior to intraperitoneal dosing.

### *3.2.9 Determination of optimal administration route for quisinostat in vivo*

*Foxn1*$^{nu}$ nude male mice (The Jackson Laboratory) were used to determine the drug administration route that would result in best quisinostat bioavailability. Three cohorts of

mice were treated with a single dose of 10 mg/kg quisinostat delivered through either intraperitoneal, subcutaneous or oral gavage routes (3 mice per cohort). Following administration of the single dose, approximately 50 uL of blood was drawn from the tip of the tails at the following timepoints: 0.5, 1, 2, 4, 6, 8 and 24 hours. The collected blood was centrifuged at 3,000 rpm for 10 minutes at 4°C to separate the plasma, which was subsequently flash frozen. At the 24-hour timepoint, following the last blood sample collection, the mice were sacrificed and the whole brains from each mouse were dissected and flash-frozen for subsequent analysis.

### *3.2.10 In vivo irradiation studies*

Intracranial or flank tumor-bearing nude mice were sedated with gaseous isoflurane prior to irradiation. On the first week of treatment, 2 hours after treatment with Quisinostat or vehicle the mice were treated with either 2 or 4 Gy of ionizing radiation (depending on the study) on MWF for a total or either 12 or 6 Gy (3 doses). Ionizing radiation was administered with the RS2000 Series Biological Research Irradiator (Rad Source Technologies).

### *3.2.11 Treatment of flank-implanted mice with Quisinostat and/or radiation*

Mice with implanted flank tumors were allowed to grow until the tumor size reached 100 $mm^3$ volume. Mice were randomized into groups before treatment and underwent treatment on MWF for the entire duration of the experiment until the tumor volumes exceeded 2000 $mm^3$. Treatment groups included vehicle (50% PEG-300), Quisinostat alone (5mg/kg or 10 mg/kg), flank IR treatment with vehicle (2 Gy or 4 Gy), and flank IR

treatment (2 or 4 Gy) with quisinostat (5 mg/kg or 10 mg/kg). For mice receiving IR treatment with or without quisinostat, mice were treated with IR on MWF for a total of 12 or 6 Gy on the first week of treatment. Quisinostat was administered to mice through intraperitoneal injections two hours prior to flank tumor radiation treatment. Upon completion of the radiation regimen, IR-treated mice subsequently received quisinostat or vehicle alone for the rest of the experiment. Tumor growth and treatment response was monitored by manually measuring the tumor area once per week starting at 14 days post-implantation. Upon reaching the 2000 $mm^3$ tumor volume threshold, mice were sacrificed and processed for PD and PK analyses two hours after treatment with a final dose of quisinostat (5 mg/kg or 10 mg/kg).

*3.2.12 Treatment of intracranially-implanted mice with Quisinostat and/or radiation*

Mice with implanted tumors were allowed to grow until the tumor bioluminescence score reached $10^8$ radiance (p/s/cm3/sr). Mice were randomized into groups before treatment. For survival studies, mice underwent treatment on MWF for the entire duration of the experiment until moribund. For mice receiving IR treatment with or without quisinostat, mice were treated with 2 Gy on MWF for a total of 6 Gy on the first week of treatment. Treatment groups included vehicle (50% PEG-3000), quisinostat (10mg/kg) alone, 6 Gy whole brain IR treatment with vehicle and 6 Gy whole brain IR treatment with 10 mg/kg quisinostat. Quisinostat was administered to mice through intraperitoneal injections two hours prior to whole-brain radiation treatment. Upon completion of the radiation regimen, IR-treated mice subsequently received quisinostat or vehicle alone for the rest of the experiment. Tumor growth and treatment response was monitored by IVIS

bioluminescence once per week. For survival studies, mice were sacrificed and processed for PD and PK analyses once moribund two hours after treatment with a final dose of quisinostat (10 mg/kg).

For short-term PK / PD correlation studies, tumor-bearing mice were randomized into groups and underwent a single week of treatment with quisinostat (10mg/kg) on MWF. For mice receiving IR treatment with or without quisinostat, mice were treated with 2 Gy on MWF for a total of 6 Gy. Quisinostat was administered to mice through intraperitoneal injections two hours prior to whole-brain radiation treatment. On the third and last day of treatment, mice were sacrificed and processed for PD and PK analyses 3 hours after administration of quisinostat or vehicle. For PD analyses, the mice were euthanized with isoflurane and the tumors were resected out of the brain and flash-frozen for subsequent analysis through western blotting and RNA-sequencing. Tissue from the hemisphere contralateral to the tumor was also collected as a normal brain / non-tumor reference sample. For PK analyses, the mice were anesthetized with isoflurane and at least 300 µL of blood was drawn from the right atrium of the heart. The blood was collected in tubes containing 1 µL of 0.1 M KOH to prevent XYZ. Blood samples were immediately centrifuged at 3,000 rpm for 10 minutes at 4°C to allow separation of plasma. After collection of the blood the tumor was dissected out of the brain and flash-frozen. Both plasma and erythrocytes were flash-frozen for subsequent analysis.

### *3.2.13 Live Bioluminescence (IVIS) Imaging*

2 weeks post-implantation, the mice were examined for tumor growth by monitoring bioluminescence every 7 days using the IVIS Xenogen Spectrum platform. D-Luciferin Potassium Salt (Gold Biotechnology) was dissolved in PBS at a final concentration of 15 mg/mL. All mice were weighed each week and were administered D-Luciferin via an intraperitoneal injection (10µl/g). 15 minutes after the injection, the mice were sedated using gaseous isoflurane (Piramal) and placed inside an IVIS Spectrum In Vivo Imaging System (Perkin Elmer) for bioluminescence imaging. The total flux (photons/second) within the region of interest (ROI) was calculated using the Living Image Software 4.5 (Perkin Elmer).

### *3.2.14 Immunofluorescence*

Immunofluorescence was performed on free-floating PDX brain tissue sections (40 µm sections). Sections were washed in 0.1 M phosphate buffer (PB) six times, followed (if required) by antigen retrieval in 10mM Citrate Buffer (pH 6.0) at 85°C for 30 minutes on a hot plate. Tissue sections were permeabilized and blocked with 10% goat serum and 0.4% Triton X-100 in 0.1M PB for 2 hours at room temperature. To prevent unspecific staining, sections were further incubated with goat anti-mouse and goat anti-rabbit IgG (Jackson ImmunoResearch Laboratories Inc.; 1:50) in 0.1 M PB, 0.4% Triton X-100 for 30 minutes at room temperature. Sections were then washed three times in 0.1M PB and then incubated in primary antibodies diluted in 2% goat serum and 0.4% Triton X-100 in 0.1M PB overnight at 4°C. Following washes in 0.1M PB, incubation with secondary antibodies (Invitrogen; ThermoFisher Scientific) was performed for two hours at 4°C in

2% goat serum and 0.4% Triton X-100 in 0.1M PB. Nuclear counterstaining was achieved with DAPI (0.5 μg/mL). The following primary antibodies were used in this study: rabbit anti–Ki67 (1:150, Abcam), rabbit anti-cleaved caspase-3 (1:200, MilliporeSigma, 133-1); rabbit anti-HDAC1 (1:500, Abcam, 109411), rabbit anti-H3K9/14ac (1:1000, Cell Signaling Technologies, 9677). Goat anti-mouse and anti-rabbit secondary antibodies were used at 1:1,000 dilutions (Invitrogen; ThermoFisher Scientific). For nuclear counterstaining, DAPI (1:1,000; Sigma-Aldrich) was used. Coverslips were mounted using ProLong Gold Antifade Mountant (ThermoFisher Scientific).

### *3.2.15 Image Acquisition*

Analysis of immunostaining on PDX brain tissue sections or cultured GSCs were performed on confocal stacks (with a step size of 0.5-1.5 μm) acquired with a 20x water-immersion objective on a laser-scanning confocal microscope (Leica Microsystems; TCS SP5) operated with LAS software. All images were processed using the ImageJ software (NIH).

### *3.2.16 Statistical Analysis*

Data are presented as the mean ± SEM. If comparing two conditions or cell lines, significance was tested with unpaired two-tailed Student's t-test. Significance of the differences between conditions or cell lines were tested by the two-way ANOVA with Bonferroni multiple comparison tests using GraphPad Prism 8 (GraphPad software). Survival studies were analyzed using the Kaplan-Meier method with the Mantel-Cox log-

rank test (GraphPad software). Statistical significance was defined at * $p < 0.05$, ** $p < 0.01$, *** $p < 0.001$, **** $p < 0.0001$.

### *3.2.17 Bioanalytical LC-MS/MS Method*

Quisinostat concentrations in specimens were measured using reverse-phase liquid chromatography on the AB SCIEX QTRAP6500+ LC–MS/MS system by operating electrospray in the positive ion mode. For liquid chromatographic separation, gradient elution was performed using a Phenomenex Kinetex F5 100 Å column (100 × 2.1 mm, 2.6 $\mu$m). The initial composition of the mobile phase was composed of 60% phase A (0.1% formic acid in water) and 40% phase B (0.1% formic acid in 1:1 acetonitrile:methanol) with a 0.35 ml/min flow rate. Gradient elution was achieved as follows: organic phase (B) was maintained at 30% from 0 to 0.3 minutes, increased to 95% from 0.3 to 0.8 minutes, maintained at 95% from 0.8 to 2.5 minutes, and lowered to 30% from 2.5 to 2.8 minutes. The total run time was 3.5 minutes. The internal standard used in this study was $D_8$-infigratinib. The retention times for quisinostat and $D_8$-infigratinib were 1.6 and 1.8 minutes, respectively. Mass-to-charge ratio (m/z) transitions were as follows: 395.20 → 144.00 (quisinostat) and 568.08 → 321.00 ($D_8$-infigratinib). LC-MS/MS analysis was performed using Analyst 1.7 Chromatographic Data System (Foster City, CA, USA).

### *3.2.18 Calibration standards and quality control samples*

Stock solutions of quisinostat (1 mM) was prepared in acetonitrile. Stock solutions of $D_8$-infigratinib (250 µM) were prepared in acetonitrile. Working solutions for calibration curve standards and quality controls (QC) were prepared by dilutions with a 40% methanol

mixture. The IS precipitation solution (10 nM) was prepared from the IS stock solutions by dilution with methanol. Calibration standards and batch qualifying QCs were freshly spiked for every batch. For sample analysis in human and mouse matrices, calibration standards were prepared in bulk by spiking appropriate amounts of working solutions into blank human plasma, used as a surrogate matrix due to the instability of quisinostat in mouse plasma. For sample analysis in neural stem cell (NSC) media and cell lysate, calibration standards were prepared in bulk by spiking appropriate amounts of working solutions into NSC media. QC samples were prepared in bulk by spiking appropriate amounts of working solutions into blank mouse plasma or cell media. Preparation of calibration standards and QC samples was performed at 4°C. Final concentrations range of the calibration standards were 1 – 1000 nM in human plasma or NSC media. Three QC levels, namely low (LQC), medium (MQC), and high (HQC), were used during all sample analyses. The concentrations of QC samples in various matrices were 3 nM (LQC), 22 nM (MQC), and 800 nM (HQC). All stock solutions and working solutions were stored at 4°C.

### *3.2.19 Plasma sample preparation*

Frozen plasma samples were thawed at 4°C. An aliquot of 30 µL mouse plasma was transferred into a micro centrifuge tube followed by 30 µL of blank human plasma, and precipitation with 180 µL of IS-containing methanol precipitation solution. The mixture was vortex-mixed for 10 s and centrifuged at 12000 g at 4 °C for 10 min. A 100 µL aliquot of the supernatant was transferred to an autosampler vial and 5 µL was injected into the LC–MS/MS system for analysis.

### *3.2.20 Brain and brain tumor sample preparation*

Normal brain and brain tumor tissue homogenates were prepared by 1:4 (mass/volume) ratio with PBS. Samples were homogenized under 6.00 m/s speed for 40 seconds with three cycles by Bead Ruptor Elite homogenizer (Omni International, USA). Plasma was used as a surrogate matrix for brain/tumor homogenate. Brain homogenate samples from *in vivo* studies were prepared as described for plasma samples. Analyte and IS were extracted by protein precipitation with methanol containing IS. After centrifugation at 12000 rpm for 10 minutes at $4^0$C, 5 µL of supernatant was injected into LC–MS/MS system for analysis.

### *3.2.21 Cell media and lysate sample preparation*

Cell media and lysates were thawed at room temperature. An aliquot of 20 µL of cell media or lysate was transferred into a micro centrifuge tube followed by protein precipitation with 60 µL of IS-containing methanol precipitation solution. The mixture was vortex-mixed for 10 s and centrifuged at 12000 g at 4 °C for 10 min. A 50 µL aliquot of the supernatant was transferred to an autosampler vial and 5 µL was injected into the LC–MS/MS system for analysis.

### *3.2.22 Stability Study in Mouse Plasma, Mouse Brain, Human Plasma, Human Brain, and NSC Media*

The stability of quisinostat was determined in BALB/c mouse plasma, male nude athymic perfused and non-perfused mouse brain homogenate (1:9 w/v of PBS (pH 7.4)), human brain homogenate (1:4 w/v of PBS (pH 7.4)), pooled human plasma, and NSC media.

Quisinostat stock solutions (1mM) were prepared in acetonitrile, subsequently diluted in a 40% methanol mixture, and added to the matrices to make final concentrations of 100 nM or 10 nM. 50 or 30 μL of either plasma or brain homogenate containing quisinostat were aliquoted into 1.5 mL microcentrifuge tubes (Eppendorf) and were incubated at 37°C for 0, 2, 4, 6, 12, or 24 hours ($N$ = 3 at each time point). Both plasma and brain homogenate samples were stored at −80°C until liquid chromatography–tandem mass spectrometry (LC-MS/MS) analysis.

### *3.2.23 Study Approval*

The patient samples used for this research were provided by the Biobank Core Facility at St. Joseph's Hospital and Medical Center and Barrow Neurological Institute (BNI). The samples were de-identified and conformed to the Biobank Institutional Review Board's protocol. Animal husbandry was performed in accordance with the guidelines of the St. Joseph's Hospital and Medical Center and Barrow Neurological Institute under the protocol approved by the Institutional Animal Care and Use Committee.

## 3.3 Results

### *3.3.1 Quisinostat is effective against patient-derived GSCs*

Our laboratory previously discovered that HDAC1 is the indispensable histone deacetylase that is required to sustain the survival and tumorigenic properties of human GSCs, providing a rationale for pharmacological targeting of this epigenetic regulator in GBM (Lo Cascio et al. 2021). While isoform-specific HDACi are not currently available, compounds that harbor enhanced selectivity profiles towards different HDAC isoforms have been identified over the past decades. One such HDACi, which harbors remarkable selectivity towards class I HDACs with a biochemical half maximal inhibitory concentration ($IC_{50}$) of 0.1 nM for HDAC1, is the second-generation hydroxamic acid quisinostat (JNJ-26481585). Quisinostat has demonstrated *in vitro* efficacy across multiple human cell lines derived from aggressive pediatric brain tumors (diffuse intrinsic pontine glioma, sonic hedgehog medulloblastoma) (Vitanza et al. 2021; Pak et al. 2019). However, the potency and efficacy of quisinostat in patient-derived GSCs remain unknown. Considering the disappointing clinical results with pan-HDACi in GBM, we hypothesized that treatment with a brain-penetrant compound that exhibits higher specificity towards class I HDACs would be highly effective in slowing tumor growth in preclinical models of GBM.

To determine the cytotoxic effects of quisinostat, we performed a 72 hr – 5 day dose-titration cell viability assay in 6 patient-derived GSC lines (BT145, GB187, GB239, GB282, GB71, GB126) and one serum-grown human GBM cell line (U87). As GBMs display a high degree of intra-tumoral heterogeneity, we intentionally used primary and

recurrent GSC cultures that harbored distinct genetic mutations or aberrations, growth rates, *MGMT* promoter methylation status and gene expression profiles. We treated these patient-derived cultures with a range of concentrations of quisinostat (10-1000 nM) and observed a potent dose-dependent reduction in GSC cell viability across all cell lines (Figure 3.1 A-B). The cellular $IC_{50}$ for all lines after treatment was in the low nanomolar range (50 – 100 nM), revealing that quisinostat reduced cell viability with much greater potency (< 1 μM) compared to other pan-HDACi (VPA, TSA, vorinostat, entinostat) that have been tested on GBM cells in previous studies (Kim, Shin, and Kim 2004; Van Nifterik et al. 2012; Chinnaiyan et al. 2008; Diss et al. 2014; Pont et al. 2015; Bangert et al. 2011). Statistical significance was observed across all models.

To assess the inhibitory properties of quisinostat on GSC cultures, we used immunofluorescence to measure expression of Ki67, a marker of cell proliferation, and cleaved caspase 3, a marker of apoptosis. We confirmed that treatment with quisinostat at the $IC_{50}$ concentrations induced a significant dose-dependent inhibition in proliferation and an increase in programmed cell death after 72 hours in two different GSC lines (Figure 3.2 C-F). These results thereby indicate that exposure to Quisinostat has a cytotoxic effect on GSC cultures, confirming their vulnerability to more potent and selective pharmacological inhibition of class I HDACs.

### *3.3.2 Quisinostat induces stable global changes in histone hyperacetylation*

We next investigated the cellular effects of quisinostat on histone acetylation dynamics in GSCs. To do this, we treated two independent GSC lines (BT145 and GB126) with increasing concentrations of quisinostat (range: 10-100 nM) and harvested

whole cell protein lysates after a 24-hour period. Immunoblot analysis (Figure 3.1G-J) revealed a significant dose-dependent increase in histone H3 acetylation at lysines 9 and 14 (H3K9/14ac), indicative of target engagement given that histone acetylation is primarily regulated by HDAC1 and HDAC2. We were also able to detect increasing amounts of total histone H3 protein upon treatment with quisinostat, indicative of chromatin loosening and decompaction resulting in greater antibody binding to histone H3. In agreement with the results shown in Figure 3.1C-F, we observed a dose-dependent increase in expression of p21 – tumor suppressor protein and a key negative regulator of the cell cycle (Figure 3.1G-J). These results suggest that Quisinostat induces global changes histone hyperacetylation, increases chromatin accessibility and promotes cell cycle arrest in GSCs.

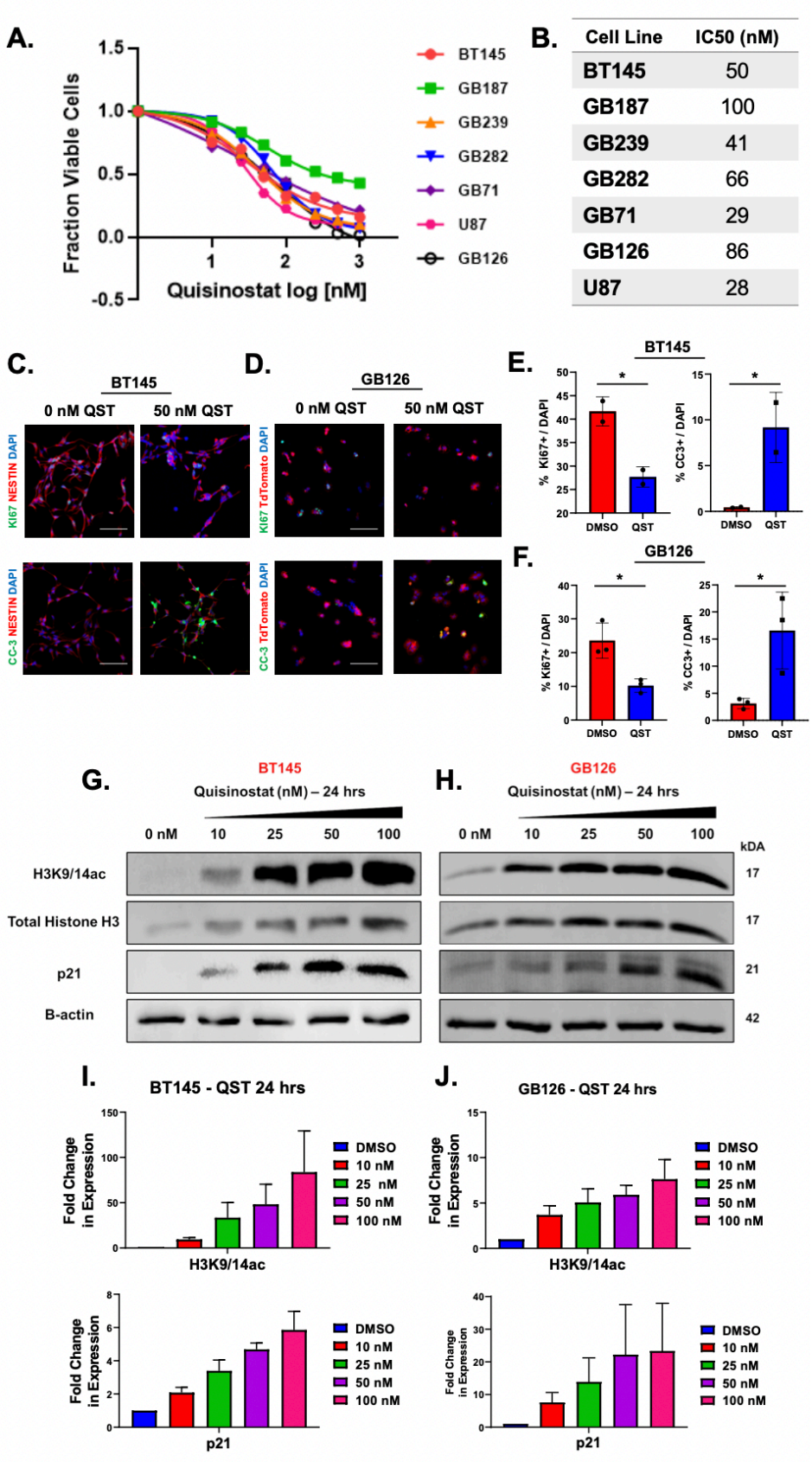


| Cell Line | IC50 (nM) |
|---|---|
| BT145 | 50 |
| GB187 | 100 |
| GB239 | 41 |
| GB282 | 66 |
| GB71 | 29 |
| GB126 | 86 |
| U87 | 28 |

**Figure 3.1 Quisinostat exhibits low nanomolar efficacy against human glioma stem cell cultures.** (A) Dose-response curves with Quisinostat (10-1000 nM). Cell viability was measured across 6 patient-derived GSCs and one serum-grown long-term glioma line (U87) 72 hours after treatment with Quisinostat. (B) Table illustrating the half maximal inhibitory concentration ($IC_{50}$) of quisinostat for each cell line tested. (C-D) Immunofluorescence staining of GSC lines BT145 (C) and GB126 (D) 72 hours after treatment with quisinostat at the $IC_{50}$ concentrations. Control and drug-treated cells were stained for Ki67 and cleaved caspase-3 to assess cell proliferation and cell death respectively. (E-F) Quantification of Ki67-positive and cleaved caspase-3 positive cells in BT145 (E) and GB126 72 hours after treatment with quisinostat (n=3). (G-H) Representative immunoblots showing dose-dependent increase in histone H3 acetylation, total histone H3 and p21 in GSC lines BT145 (G) and GB126 (H) after 24-hour treatment with quisinostat. (I-J) Quantification of normalized H3K9/14ac and p21 protein levels in quisinostat-treated BT145 (I) and GB126 (J) GSCs relative to DMSO-treated cells. QST = quisinostat. Error bars indicate SEM. * $p < 0.05$. Magnification, 20x; scale bars, 2 μM. *P* values were determined using the unpaired 2-tailed t-test.

### *3.3.3 Effects of quisinostat on cellular kinetics of histone acetylation in GSCs*

To characterize the temporal drug-target kinetics of quisinostat, we performed cell washout experiments, wherein the phenotypic consequences of target engagement are analyzed over time after a drug is removed from cell-based system. Cell washout experiments are informative because they allow an assessment on the dynamics, reversibility and stability of drug-mediated HDAC inhibition over time. To investigate this, we treated two different GSC lines at their respective $IC_{50}$ values for quisinostat (50 nM for BT145 and 86 nM for GB126). In the no-drug washout experiments, quisinostat was not removed from the media and protein lysates were harvested at 2, 6, 24 and 72 hours after treatment (left panels of Figures 3.2A-B). Immunoblotting revealed that quisinostat-induced histone H3 hyperacetylation, which increased over a 72-hour period after exposure to the drug (Figures 3.2 A-D). In the washout experiments, the cells were treated quisinostat for 2 hours, after which the media replaced with drug-free media and protein lysates were harvested at 2, 6, 24 and 72 hours after initial removal of the drug

(right panel of Figures 3.2 A-B). Interestingly, the results differed across the two cell lines. In BT145 (Figure 3.2A) the washout experiments demonstrated that quisinostat exhibited target engagement up to 6 hours after removal from the media. Although histone H3 acetylation levels were still significantly higher at 24 hours relative to untreated samples, they returned to baseline levels by 72 hours (Figure 3.2A and 3.2C). By contrast, in GB126 evidence of target engagement was observed to 72 hours after washout of quisinostat from the media. Unlike what we observed in BT145, upon drug washout histone H3 acetylation did not decrease over time and remained stable in the absence of the drug in the media (Figures 3.2B and 3.2D). These contrasting results may be due to differential expression of drug efflux pumps (ABC transporters) , which have been shown to be expressed in GSCs and contribute to drug resistance (Bozzato, Bastiancich, and Preat 2020). These results suggest that quisinostat-induced inhibition of class I HDAC activity is relatively stable and capable of inducing prolonged phenotypic responses in GSCs, even after short-term incubation with the drug.

To further understand the kinetics of drug-target engagement in the washout experiments, we harvested media and BT145 cells at each timepoint with or without removal of quisinostat. At each timepoint, we measured the intracellular levels of the drug as well as its concentrations in the media. We found that intracellular quisinostat levels increased over incubation the period, reaching equilibrium by 10 hours (blue line, Figure 3.2E). Meanwhile, the drug levels decreased in cell media over time, indicating the drug may not be very stable in GSC culture media (orange line, Figure 3.2E). By contrast, in the washout experiments minimal quisinostat levels were measured in cells after removal of the drug at all time points (blue line, Figure 3.2F). The latter finding

correlates with observed pharmacodynamic results observed in BT145, wherein drug washout resulted in the reversal of quisinostat-induced histone H3 hyperacetylation (Figure 3.2F).

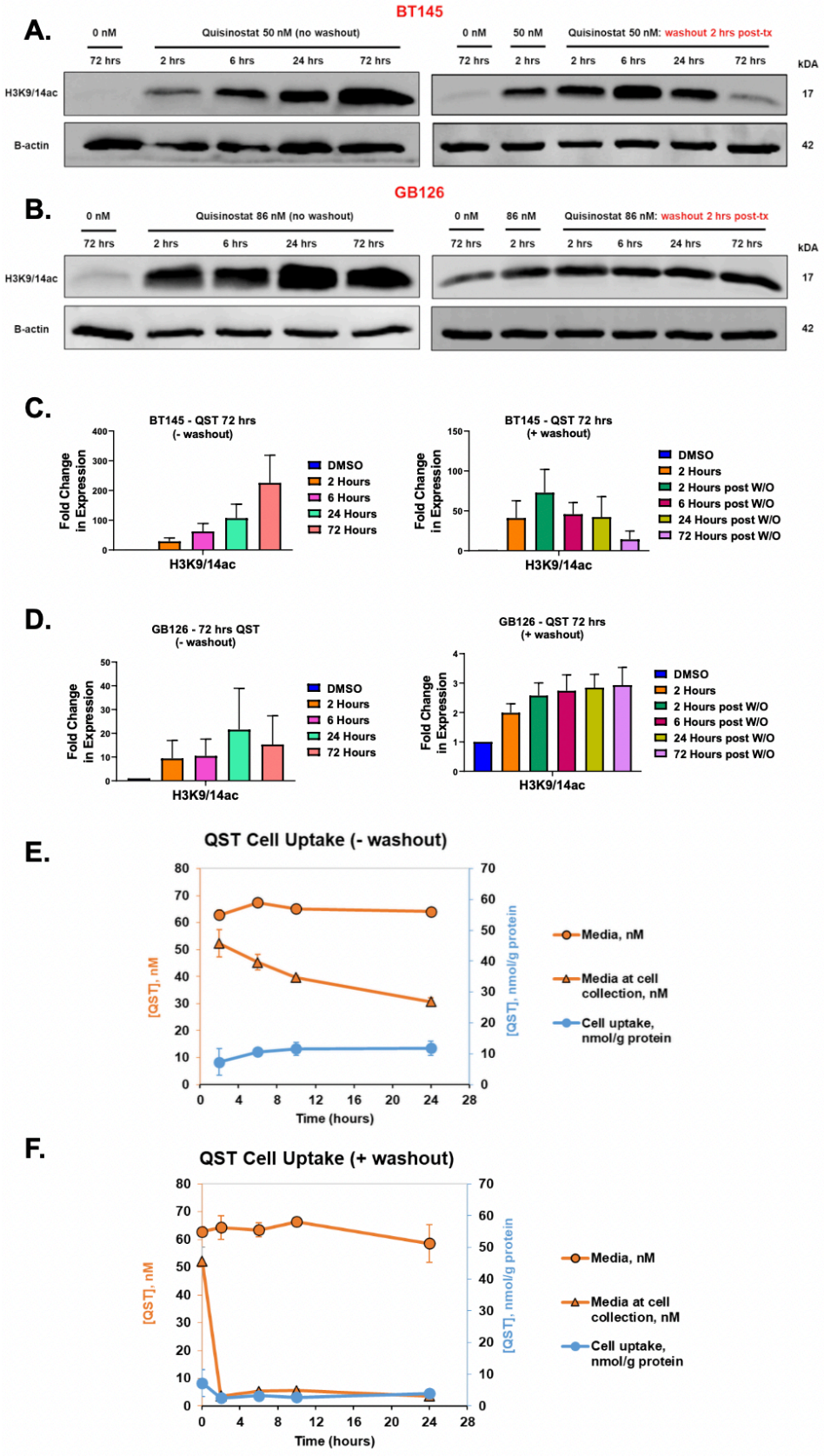
A.
BT145
0 nM
Quisinostat 50 nM (no washout)
0 nM
50 nM
Quisinostat 50 nM: washout 2 hrs post-tx
72 hrs
2 hrs
6 hrs
24 hrs
72 hrs
kDA
H3K9/14ac
17
B-actin
42
B.
GB126
0 nM
Quisinostat 86 nM (no washout)
86 nM
Quisinostat 86 nM: washout 2 hrs post-tx
C.
BT145 - QST 72 hrs (- washout)
BT145 - QST 72 hrs (+ washout)
Fold Change in Expression
H3K9/14ac
DMSO
2 Hours
6 Hours
24 Hours
72 Hours
2 Hours post W/O
6 Hours post W/O
24 Hours post W/O
72 Hours post W/O
D.
GB126 - 72 hrs QST (- washout)
GB126 - QST 72 hrs (+ washout)
E.
QST Cell Uptake (- washout)
[QST], nM
[QST], nmol/g protein
Time (hours)
Media, nM
Media at cell collection, nM
Cell uptake, nmol/g protein
F.
QST Cell Uptake (+ washout)

**Figure 3.2 Target engagement analysis of quisinostat *in vitro*.** (A-B) Representative immunoblot showing evidence of cellular target engagement over time (2-72 hours) after incubation with $IC_{50}$ concentrations of quisinostat in BT145 (A) and GB126 (B). A drug washout time course (right) was performed 2 hours after incubation with Quisinostat in BT145 (A) and GB126 (B) to monitor the levels of histone H3 acetylation after removal of Quisinostat in the media over the course of 72 hours. (C-D) Quantification of the levels of histone H3 acetylation (H3K9/14) after treatment with quisinostat over time, without (left) and with washout (right) of the drug. Protein expression was normalized to DMSO-treated controls. (E) Levels of intracellular quisinostat (nM) without washout of the drug in BT145 24 hours after treatment. (F) Levels of quisinostat (nM/L) in the media (nM) after washout of the drug in the cell line BT145 72 hours after treatment. QST = quisinostat. For each cell line, the data are compiled from at least three independent experiments. Error bars indicate SEM.

### *3.3.4 Quisinostat induces sustained levels of DNA damage*

Previous studies have demonstrated that several HDACi can act as DNA-damaging agents in malignant cells (Munshi et al. 2005; Gaymes et al. 2006; Lee et al. 2010). Although the exact mechanisms underlying this phenomenon remain unclear, there is evidence that HDACi down-regulate the expression of DNA repair proteins or may themselves indirectly induce DNA damage through increased levels of oxidative stress via the generation of reactive oxygen species (Lee et al. 2010; Ruefli et al. 2001; Rosato et al. 2008; Ungerstedt et al. 2005; Robert and Rassool 2012). To test whether quisinostat could induce DNA damage in our cultures, we treated two independent GSC lines with quisinostat at their $IC_{50}$ concentrations and analyzed the levels of variant histone H2AX phosphorylation (γH2AX), an established marker of DNA double-strand breaks (DSB), over the course of 72 hours (Rogakou et al. 1998). Immunoblotting analysis revealed that quisinostat induced the accumulation of γH2AX in both cell lines (left panels, Figures 3.3A-B). In BT145, γH2AX levels were highest at 72 hours post-treatment, while in GB126 γH2AX peaked within 24 hours of treatment but persisted up to 72 hours (Figure

3.3 A-B, C-D). To determine whether the incurred DNA damage persisted after short-term exposure to quisinostat, we performed washout experiments 2 hours after treatment with the drug at the same concentrations (right panels, Figures 3.3A-B). In agreement with the target engagement analysis conducted previously (Figures 3.2A-D), we found that γH2AX levels did not accumulate in BT145 but increased and remained stable over time in GB126 after washout of quisinostat from the cell media. These results suggest that prolonged drug-target engagement is necessary for quisinostat to induce DNA DSBs in GSCs (Figure 3.3 A-B). We additionally employed immunofluorescence staining to confirm the accumulation of γH2AX foci in both cell lines 72 hours after treatment with Quisinostat (Figure 3.3 E-F). Considering that DSBs result in the recruitment of HDAC1 and HDAC2 to sites of DNA damage to stimulate non-homologous end joining (NHEJ), it is likely that quisinostat is not only inducing DNA damage, but also perturbing a major DSB repair pathway through direct inhibition of HDAC1 and HDAC2 activity in GSCs (Miller et al. 2010). To the best of our knowledge, this is the first report that indicates that quisinostat can act as a potent DNA-damaging agent in cancer cells *in vitro*.

### *3.3.5 Quisinostat treatment sensitizes glioma stem cells to ionizing radiation in vitro*

In addition to their use as single-modality anticancer agents, there is preclinical evidence that HDACi may be effective in enhancing radiosensitivity of tumor cells when combined with radiation therapy (Camphausen et al. 2004; Miller et al. 2010; Munshi et al. 2005; Zhang et al. 2009; Groselj et al. 2013). We hypothesized that the accumulation of DNA damage induced by quisinostat in combination with radiation treatment may synergistically reduce GSC viability. To examine this, we treated two cell lines (BT145

and GB126) with increasing nanomolar doses of quisinostat (10-1000 nM) and increasing doses of ionizing radiation (cell-line dependent) (Figure 3.3 G-H). We then analyzed our combinatorial dose-response cell viability data using SynergyFinder, an application that assigns synergy scores using various major reference models (Zheng et al. 2022). Synergy scores greater than 10 indicate the interaction between two treatments is likely synergistic, while a score between 10 and -10 denotes an additive effect. Across both cell lines, combination treatment resulted in greater cytotoxicity compared to independent treatment with quisinostat or radiation. Interestingly, the zero interaction potency (ZIP) model synergy matrix indicated that the greatest synergy was attained when combining the lowest doses of quisinostat (10-25 nM) with the higher doses of ionizing radiation (Figure 3.3 I-J). Together, these data demonstrate that low nanomolar doses of quisinostat can enhance sensitivity of human GBM cells to radiation treatment.

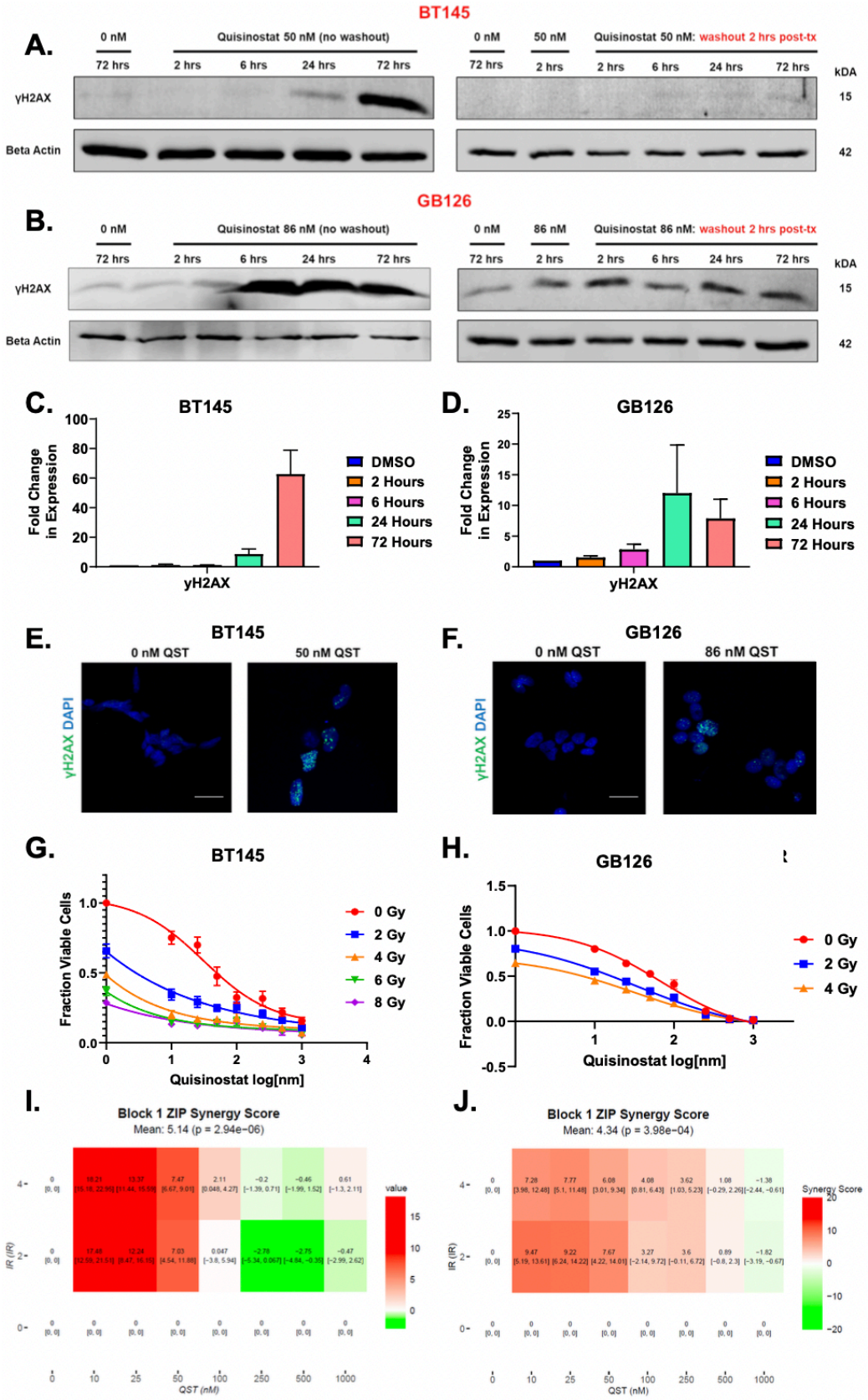
BT145
A.
0 nM
Quisinostat 50 nM (no washout)
0 nM
50 nM
Quisinostat 50 nM: washout 2 hrs post-tx
72 hrs
2 hrs
6 hrs
24 hrs
72 hrs
kDA
γH2AX
Beta Actin
15
42
GB126
B.
0 nM
Quisinostat 86 nM (no washout)
86 nM
Quisinostat 86 nM: washout 2 hrs post-tx
C.
BT145
Fold Change in Expression
yH2AX
DMSO
2 Hours
6 Hours
24 Hours
72 Hours
D.
GB126
E.
0 nM QST
50 nM QST
γH2AX DAPI
F.
86 nM QST
G.
Fraction Viable Cells
Quisinostat log[nm]
0 Gy
2 Gy
4 Gy
6 Gy
8 Gy
H.
I.
Block 1 ZIP Synergy Score
Mean: 5.14 (p = 2.94e−06)
IR (IR)
QST (nM)
value
J.
Mean: 4.34 (p = 3.98e−04)
Synergy Score

**Figure 3.3 Quisinostat synergizes with radiation to sensitize glioma stem cells.** (A-B) Representative immunoblots demonstrating that Quisinostat treatment in (A) BT145 and (B) GB126 results in accumulation of γH2AX over time (left) and with drug washout (right). (C-D) Quantification of γH2AX protein expression levels after quisinostat treatment over time in (C) BT145 and (D) GB126. Protein levels are normalized to DMSO-treated cells. (E-F) Immunofluorescence staining of BT145 (E) and GB126 (F) showing an increase in γH2AX foci 72 hours after treatment with quisinostat but not DMSO-treated cells. (G-H) Dose response curves combining quisinostat and ionizing radiation treatment in BT145 (G) and GB126. (I-J) Matrices illustrating the synergy scores obtained using the zero interaction potency (ZIP) reference model when combining quisinostat with increasing doses of radiation in (I) BT145 and (J) GB126. QST = quisinostat. For each cell line, the data are compiled from at least three independent experiments. Magnification, 63x; scale bars, 2 μM.

### *3.3.6 Determination of optimal route of administration for quisinostat in vivo*

Bioavailability is defined as the fraction of the total drug dose that reaches systemic circulation. Importantly, different administration routes harbor unique capabilities to facilitate a certain drug concentration in plasma for a certain length of time (Price and Patel 2022). Considering that the efficacy of quisinostat in preclinical models of brain tumors remains controversial, we first sought to compare how different routes of administration would impact the rate and extent of bioavailability of quisinostat. We compared three routes of administration to determine which would yield the highest plasma exposure for quisinostat over time. To do this, we treated athymic nude mice with a single dose of quisinostat (10 mg/kg) through either intraperitoneal, subcutaneous or oral delivery and collected blood at 0.5, 1, 2, 4, 6, 8 and 24 hours post-dosing from individual mice for PK analysis. LC/MS analysis revealed that regardless of administration route, quisinostat was practically systemically cleared within 24 hours of dosing (Figure 3.4 A). Intraperitoneal and subcutaneous injections of quisinostat resulted

in significantly higher plasma exposure over time compared to oral delivery (Figure 3.4 B), as oral bioavailability of quisinostat was found to be below 10% in mice.

Our results suggest that drug plasma concentrations through intraperitoneal and subcutaneous dosing were comparable and are therefore the optimal routes of administration to maximize the bioavailability of quisinostat in athymic nude mice.

**A.**

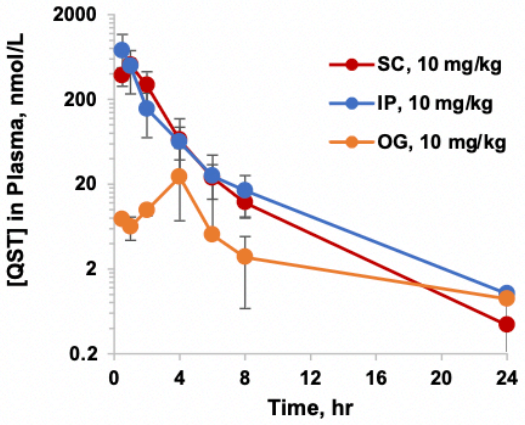


**B.**

| Time, h | Administration Route | | |
|---|---|---|---|
| | SC | IP | OG |
| 0.5 | 379.0 | 752.3 | 7.6 |
| 1 | 509.3 | 492.7 | 6.3 |
| 2 | 293.3 | 153.9 | 9.8 |
| 4 | 66.3 | 62.8 | 24.3 |
| 6 | 23.6 | 24.9 | 5.0 |
| 8 | 12.1 | 16.8 | 2.8 |
| 24 | 0.4 | 1.0 | 0.9 |
| $AUC_{last}$ (h×nM) | 1187.1 | 1202.2 | 106.0 |

**Figure 3.4 Determination of optimal route of administration for quisinostat *in vivo*.** Athymic nude mice were treated with a single dose of quisinostat (10 mg/kg) through either intraperitoneal (IP), subcutaneous (SC) or oral gavage (OG). Blood samples were collected at 0.5, 1, 2, 4, 6, 8 and 24 hours post-dosing and analyzed by LC-MS/MS. (**A**) Plasma concentration-time curved for quisinostat administered through various routes. (**B**) The area under the curve (AUC, h×nM) are calculated for each route to illustrate plasma quisinostat exposure. QST = quisinostat.

### *3.3.7 Pharmacodynamics and pharmacokinetics of quisinostat in an orthotopic patient-derived xenograft model of diffuse GBM*

We next investigated whether long-term treatment with quisinostat would affect tumor growth in a PDX model of GBM. Our aim was to determine whether treatment would result in a significant survival benefit relative to vehicle-treated mice, coupled with PK and PD analyses of quisinostat. To do this, we transplanted a GSC cell line (BT145) that grows diffusely with minimal blood-brain barrier disruption into the brains of immunocompromised mice. Upon exponential growth of the tumor, which was determined through bioluminescence imaging, mice were treated with quisinostat (10 mg/kg) through subcutaneous injection on a Monday-Wednesday-Friday (MWF) schedule. We originally chose to administer the drug subcutaneously rather than intraperitoneally due to its less invasive nature. However, severe ulcers developed at the injection site and dramatic weight loss (10-15%) in most quisinostat-treated mice (Figure 3.5 A) after administration of first two doses subcutaneously. Due to these unexpected adverse events in the early stages of treatment, the delivery route was changed to intraperitoneal injections and halved the dose of quisinostat to 5 mg/kg on the third day of treatment. Administration of quisinostat at this dose lower was relatively well-tolerated (Figure 3.5 A). Individual mice would be given a "drug holiday" on a treatment day if their weight dropped more than 15% in one week, and treatment resumed once the mice recovered their weight. Weekly monitoring of tumor growth through bioluminescence imaging revealed that quisinostat treatment did not reduce tumor burden compared to

vehicle-treated mice, and overall quisinostat failed to significantly prolong survival (Figure 3.5 B-C).

We also performed PK analyses in a cohort of animals that received a total of 10 doses of the drug and determined the total and unbound fraction of drug in the plasma and tumors of quisinostat-treated mice. Blood and brains were harvested 2 hours post-dosing on the $10^{th}$ treatment day. Non-tumor bearing mice treated with quisinostat for the same amount of time served as a baseline reference to understand if the drug accumulated in the tumor cells relative to normal brain tissue. As shown in Figure 3.5 D, the pharmacologically active (unbound) levels of quisinostat in the brains of tumor and non-tumor bearing mice were not significantly different and were lower than the biochemical $IC_{50}$ for HDAC1 (0.1 nM). Immunohistochemical analyses of tumors of quisinostat-treated mice demonstrated that there was no significant increase in the levels of histone H3 acetylation, cell death and no effect on cell proliferation compared to vehicle-treated mice (Figure 3.5 E-I). These PK and PD results suggest that that quisinostat fails to cross the blood-brain-barrier and prolong survival of PDX mice when delivered at a dose of 5 mg/kg in the regimen described above.

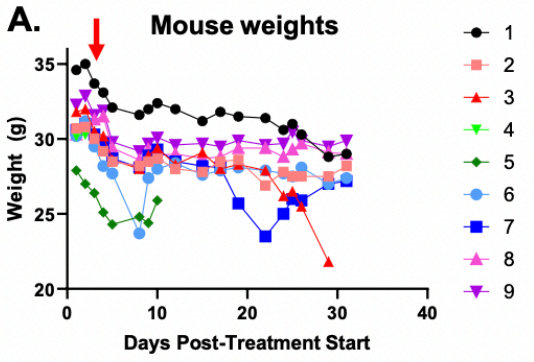


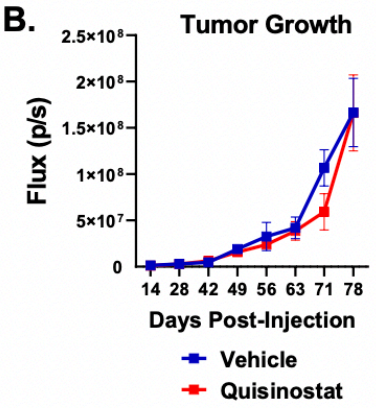


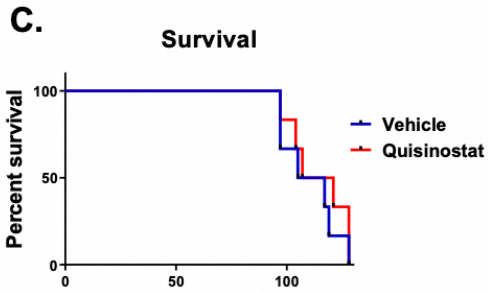


D.

| Matrix | Mouse Type | Quisinostat, nM | |
|---|---|---|---|
| | | Total | Unbound |
| Brain | Normal | 4.68 | 0.033 |
| | Tumor-bearing | 5.175 | 0.036 |
| Plasma | Normal | 62.2 | 12.067 |
| | Tumor-bearing | 97.33 | 18.882 |

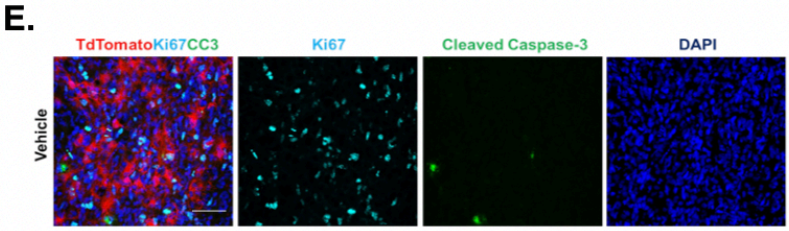


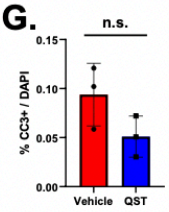


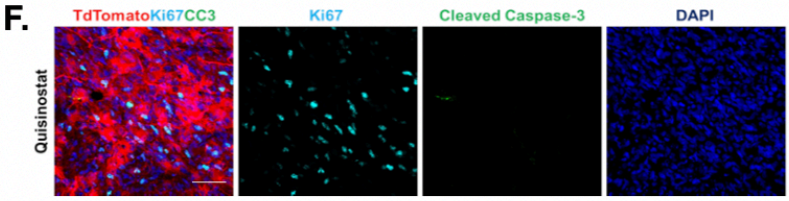


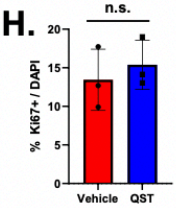


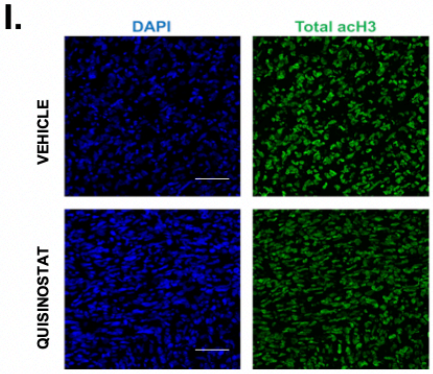

**Figure 3.5 Quisinostat dosed at 5 mg/kg is ineffective at slowing tumor growth in a patient-derived xenograft model of GBM.** (A) Weights of individual mice treated with quisinostat throughout the study. The red arrow indicates the significant drop in weight observed in all mice (n=9) after two doses of 10 mg/kg quisinostat delivered through subcutaneous injection. Dosing was subsequently changed to 5 mg/kg delivered through intraperitoneal injection, which was well tolerated. (B) Average photon flux (p/s) as measured by live bioluminescence imaging of vehicle-treated and quisinostat-treated cohorts over time (n=10 and n=9 respectively). Red arrow indicates start of treatment. (C) Kaplan-Meier survival analysis of vehicle-treated and quisinostat-treated mice. (D) Table showing the total and unbound levels of quisinostat present in plasma and brain of vehicle-treated and quisinostat-treated mice (tumor-bearing and non-tumor bearing). (E-F) Immunostaining for Ki67 (E) and cleaved caspase-3 (F) in BT145 brain tumor tissue in vehicle-treated and quisinostat-treated mice. (G-H) Quantification of human (G) Ki67-positive and (H) cleaved caspase-3-positive cells in control-treated and quisinostat-treated brain tumors (n=3 per cohort). (I) Representative immunostaining for H3K9/14ac in vehicle-treated and quisinostat-treated brain tumor tissue. QST = quisinostat. Error bars indicate SEM. n.s., not significant Magnification, 20x; scale bars, 100 μM. *P* values were calculated using unpaired 2-tailed t-test and Kaplan-Meier method with the Mantel-Cox log-rank test.

### *3.3.8 Quisinostat inhibits tumor growth in a flank model of human GBM*

To evaluate on-tumor efficacy in the absence of the blood-brain-barrier, we treated athymic mice bearing U87-derived flank tumors with quisinostat. Quisinostat was dosed at 5 mg/kg intraperitoneally on a MWF schedule until the average tumor volumes reached 2000 $mm^3$. As shown in Figure 3.6 A, we found that quisinostat did not affect tumor growth compared to the vehicle-treated cohort. However, immunoblot analysis of tumor tissue from individual mice revealed that quisinostat increased histone H3 acetylation. These results suggested that while quisinostat penetrated the flank tumor when dosed at 5 mg/kg, this dose was not cytotoxic and hence not affecting tumor cell proliferation.

In our previous orthotopic study, we had to half the original intended dose (10 mg/kg) of quisinostat due to unexpected toxicity when delivered subcutaneously. However, several studies have shown that athymic mice administered with quisinostat intraperitoneally at 10 mg/kg exhibited acceptable levels of weight loss (less than 10%) (Pak et al. 2019; Vitanza et al. 2021; Torres et al. 2016). Hence, we wanted to examine whether 10 mg/kg quisinostat, in addition to treatment with ionizing radiation, would be effective in slowing tumor growth in the flank model of GBM described above. Tumor-bearing mice receiving radiation were treated with 2 Gy fractions on MWF 2 hours after dosing with either vehicle solution or quisinostat, for a total dose of 6 Gy. Following completion of the radiation treatment, mice continued to receive vehicle or quisinostat until the tumors reached the maximum volume threshold (Figure 3.6B). We found that quisinostat, even when combined with radiation, was well-tolerated throughout the entirety of the treatment study when dosed at 10 mg/kg intraperitoneally MWF (Figure 3.6 C-D). Unlike the 5 mg/kg dosing regimen, we found that 10 mg/kg quisinostat significantly reduced tumor volume compared to vehicle-treated mice (Figure 3.6 B). Combination treatment was more effective in reducing tumor growth than either quisinostat or radiation therapy alone, the average tumor volume being ~ 4.5 fold smaller than tumors from control mice at the end of the study (Figure 3.6 B).

PK analyses of quisinostat- and combination-treated mice demonstrated that average total quisinostat concentrations were more than 10-fold higher in the tumors (~433 nM) than in the plasma samples (~300 nM) (Figure 3.6 E). There was no significant difference in the total levels of quisinostat between monotherapy and combination cohorts (Figure 3.6E). We also confirmed through immunoblotting that

histone H3 acetylation at serines 9, 14, and 27 was significantly increased in mice treated with quisinostat alone or with radiation (Figure 3.6F). Moreover, we observed that all quisinostat-treated tumors exhibited high levels of γH2AX expression – indicative of the presence of double stranded DNA breaks – relative to vehicle-treated controls. These results suggest that 10 mg/kg dosing of quisinostat is effective in reducing tumor burden, induces the intended PD effects and corroborate our previous *in vitro* findings that quisinostat acts as a potent DNA-damaging agent.

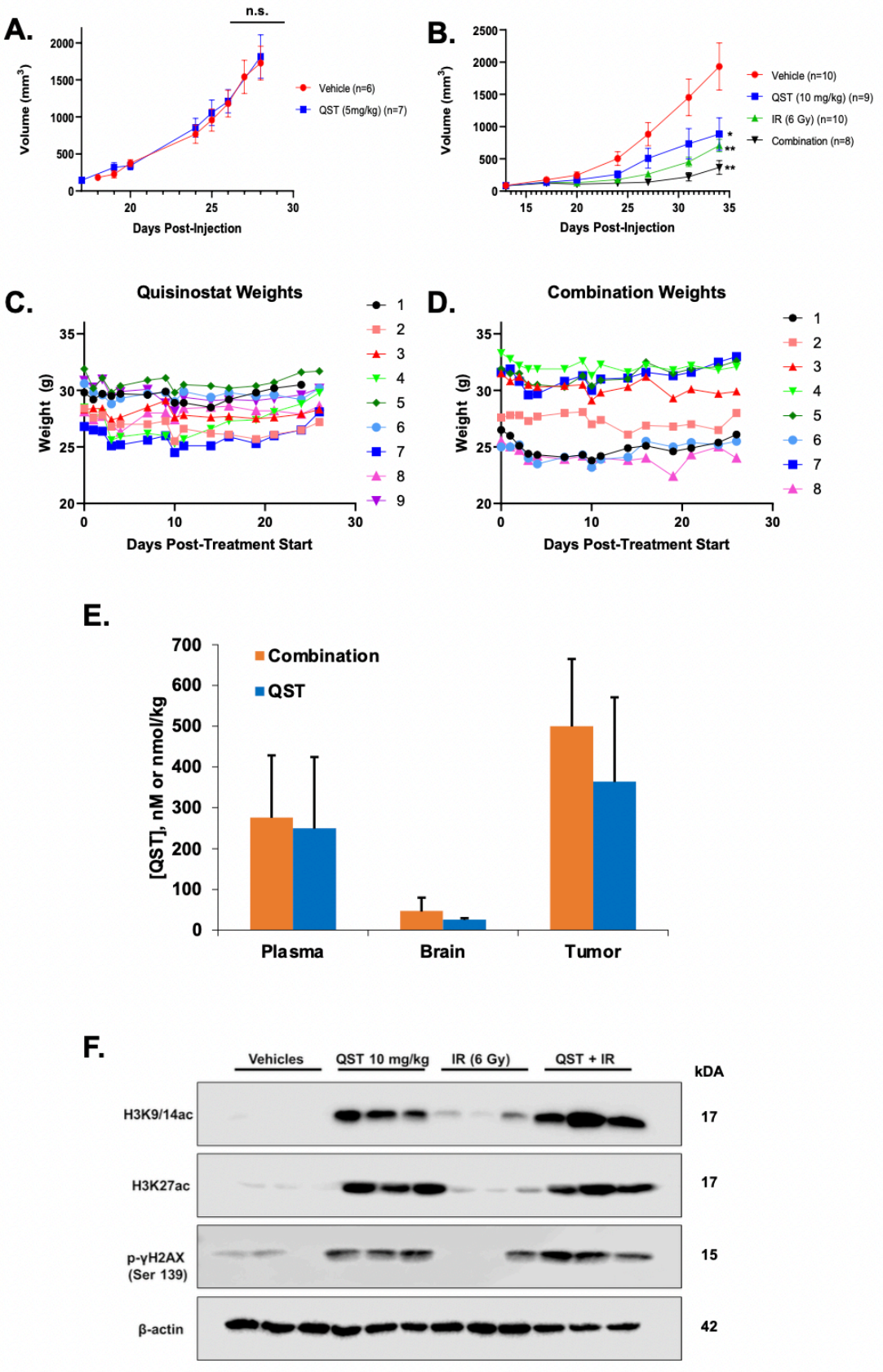
A.
n.s.
Volume (mm3)
Days Post-Injection
Vehicle (n=6)
QST (5mg/kg) (n=7)
B.
Volume (mm3)
Days Post-Injection
Vehicle (n=10)
QST (10 mg/kg) (n=9)
IR (6 Gy) (n=10)
Combination (n=8)
C.
Quisinostat Weights
Weight (g)
Days Post-Treatment Start
D.
Combination Weights
Weight (g)
Days Post-Treatment Start
E.
[QST], nM or nmol/kg
Combination
QST
Plasma
Brain
Tumor
F.
Vehicles
QST 10 mg/kg
IR (6 Gy)
QST + IR
kDA
H3K9/14ac
17
H3K27ac
17
p-γH2AX (Ser 139)
15
β-actin
42

**Figure 3.6 Quisinostat dosed at 10 mg/kg is effective in slowing tumor growth in a flank model of human GBM.** (A) Weekly volume measurements of flank tumors from mice treated with vehicle or 5 mg/kg quisinostat (n=10 in each cohort). (B) Weekly volume measurements of flank tumors from mice treated with vehicle, 10 mg/kg quisinostat, radiation alone (6 Gy) or combination treatment (6 Gy and 10 mg/kg quisinostat) (n=10 in each cohort). (C-D) Weights of individual mice treated with quisinostat (dosed at 10 mg/kg) (C) or combination therapy (D) throughout the entire duration of the study. (E) Total levels of quisinostat in plasma and flank tumors of quisinostat- and combination-treated mice (n=4-5 per cohort). (F) Immunoblotting of protein lysates derived homogenized flank tumors from each cohort (n=3 per group). Membranes were probed for H3K9/14ac, H3K27ac, γH2AX and B-actin. QST = quisinostat. Error bars indicate SEM. * $p < 0.05$, ** $p < 0.01$, n.s., not significant. *P* values were calculated using unpaired 2-tailed t-test.

### *3.3.9 Pharmacokinetics and pharmacodynamics of quisinostat in the normal central nervous system*

Considering that we found that 10 mg/kg dosing of quisinostat dosed was well-tolerated in mice when administered intraperitoneally, we wanted to determine its pharmacokinetic profile in the normal central nervous system (CNS). To do this, we treated a cohort of athymic nude mice with 10 mg/kg quisinostat on a MWF schedule for two weeks. On the last day of treatment, we sacrificed the mice 2 hours after dosing with quisinostat and harvested blood and intact brains (Figure 3.7A). Each brain hemisphere was processed separately to enable us to perform matched PK and PD analyses from the same animal. We found that the average levels of unbound, pharmacologically active quisinostat in the brain (~ 1.7 nM) was over 10 times higher the biochemical $IC_{50}$ for HDAC1 (0.1 nM) (Figure 3.7B). For PD analyses, we exploited the fact that HDACi such as quisinostat can repress the activity of class I HDACs in non-malignant cells in normal tissues. We homogenized entire hemispheres to obtain whole tissue protein lysates from

each mouse and assessed changes histone H3 acetylation levels using immunoblotting. We confirmed that relative to vehicle-treated animals, the levels of H3K9/14 acetylation were significantly increased in the normal brain tissue of six quisinostat-treated mice (Figure 3.7C). Our results therefore reveal that quisinostat is a brain-penetrant HDACi that exhibits clear on-target pharmacodynamic activity in normal CNS cells. We also established a direct correlation between PK and PD modulation *in vivo*, demonstrating that the free unbound levels (~1.7 nM) of quisinostat in the brain can induce substantial histone H3 hyperacetylation.

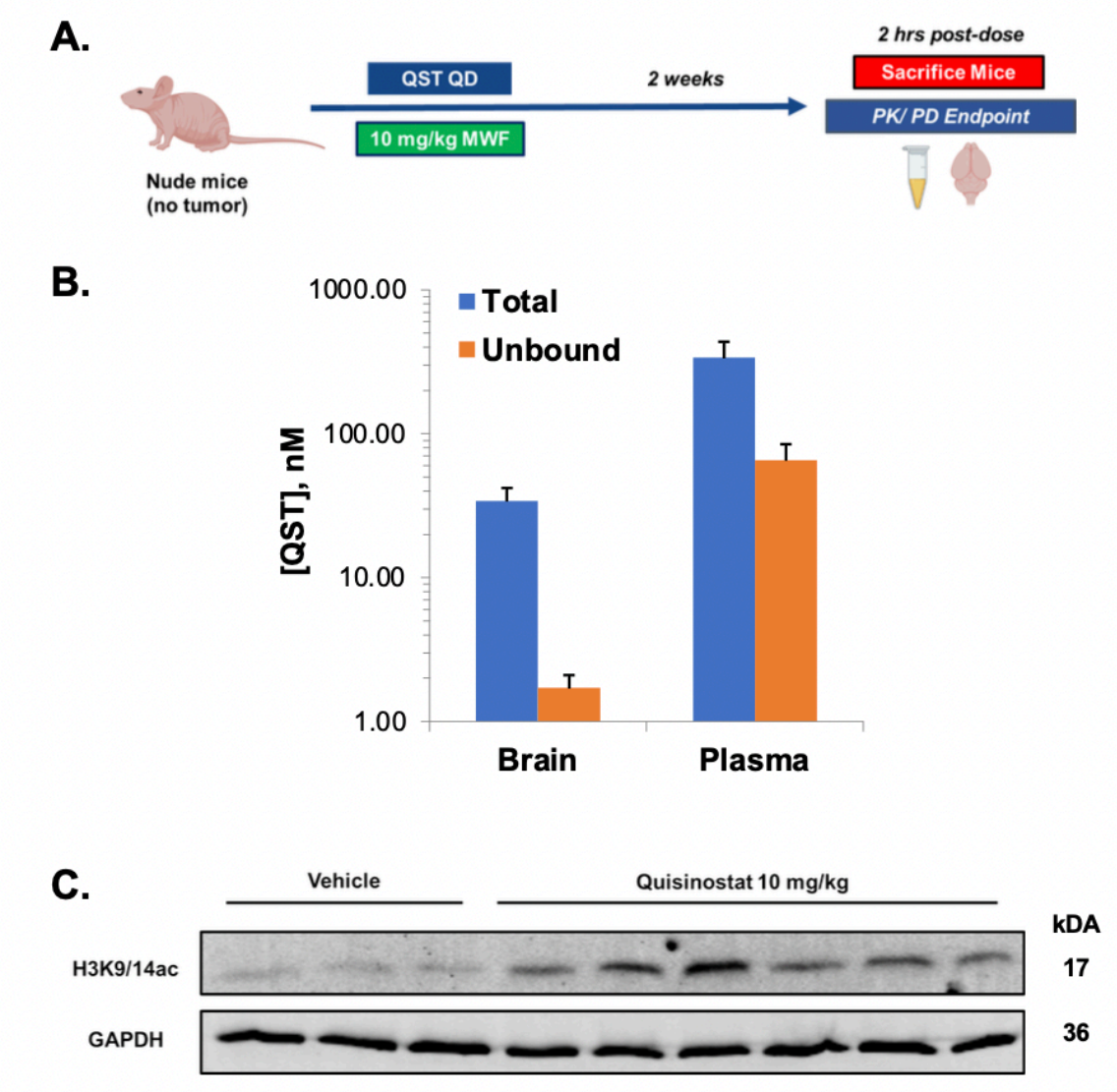


**Figure 3.7 Quisinostat PK-PD correlation study in the normal CNS.** (A) Schematic illustrating the design of the treatment study in non-tumor bearing athymic nude mice. (B) Total (blue) and unbound (orange) levels of quisinostat in normal brain tissue in quisinostat-treated mice (n=6 per cohort). (C) Immunoblotting of protein lysates derived homogenized brains from each cohort (n=3 for vehicle cohort, n=6 for quisinostat cohort). Membranes were probed for H3K9/14ac and B-actin. QST = quisinostat. Error bars indicate SEM.

### *3.3.10 Quisinostat is a potent radio-sensitizer in an orthotopic patient-derived xenograft model of GBM*

We next questioned whether treatment with 10 mg/kg Quisinostat could extend survival when added to radiation in an orthotopic PDX model of GBM. Athymic nude mice implanted with the human GSC line GB126 began treatment once the tumors started growing exponentially. Tumor-bearing mice were treated with quisinostat, dosed at 10 mg/kg, with or without radiation on a MWF schedule. As described previously, ionizing radiation was delivered locally to the brain in 2 Gy fractions 2 hours after being dosed with vehicle solution or quisinostat, for a cumulative delivery of 6 Gy. Following completion of the radiation regimen, mice continued to receive quisinostat at 10 mg/kg on MWF until the end of the study, as determined by large tumor burden and onset of neurological symptoms (Figure 3.8A). Weekly monitoring of tumor growth using bioluminescence imaging demonstrated that monotherapy or combination therapy with quisinostat significantly reduced tumor burden compared to vehicle or radiation-only controls. While quisinostat monotherapy significantly slowed tumor growth, it only resulted in a modest average increase in survival (4 days, $p < 0.01$) relative to vehicle-treated mice (Figure 3.8B). However, combining quisinostat with radiation treatment led to a substantial increase in median survival compared to vehicle and radiation-monotherapy cohorts (37 days and 20 days, respectively, $p < 0.0001$ for both). If the survival benefit resulting from combination therapy were a mere additive effect of the two treatment modalities, the median survival compared to vehicle controls would have been of 21 days instead of 37 days. These data suggest that while quisinostat treatment

alone is not sufficient to produce a therapeutic benefit, combinatorial treatment with fractioned doses of radiation unveils that quisinostat acts a potent radiosensitizer that significantly prolongs survival in an orthotopic PDX model of human GBM.

All the mice in each cohort utilized in the survival study described above were utilized for end-point PK and PD analyses once moribund. Plasma and tumor were harvested 3 hours after dosing with 10 mg/kg quisinostat, allowing for a direct comparison of long-term treatment with the PK/PD data collected from acute (1 week) treatment with quisinostat or combination therapy. As shown in Figure 3.8C, PK analyses revealed that unbound quisinostat accumulated in the tumor (average ~71.4 nM) and peritumoral brain tissue (average ~3.4 nM) over time. There were no significant differences in total or unbound drug concentrations in tumor or brain tissue between the monotherapy or combination therapy cohorts. Immunoblot analysis of resected tumor samples confirmed that quisinostat induced histone H3 hyperacetylation in the bulk tumor compared to the untreated animals, consistent with an *in vivo* on-target effect (Figure 3.8 D). Our results establish that quisinostat is a brain-penetrant drug that accumulates in both normal brain and tumor tissue.

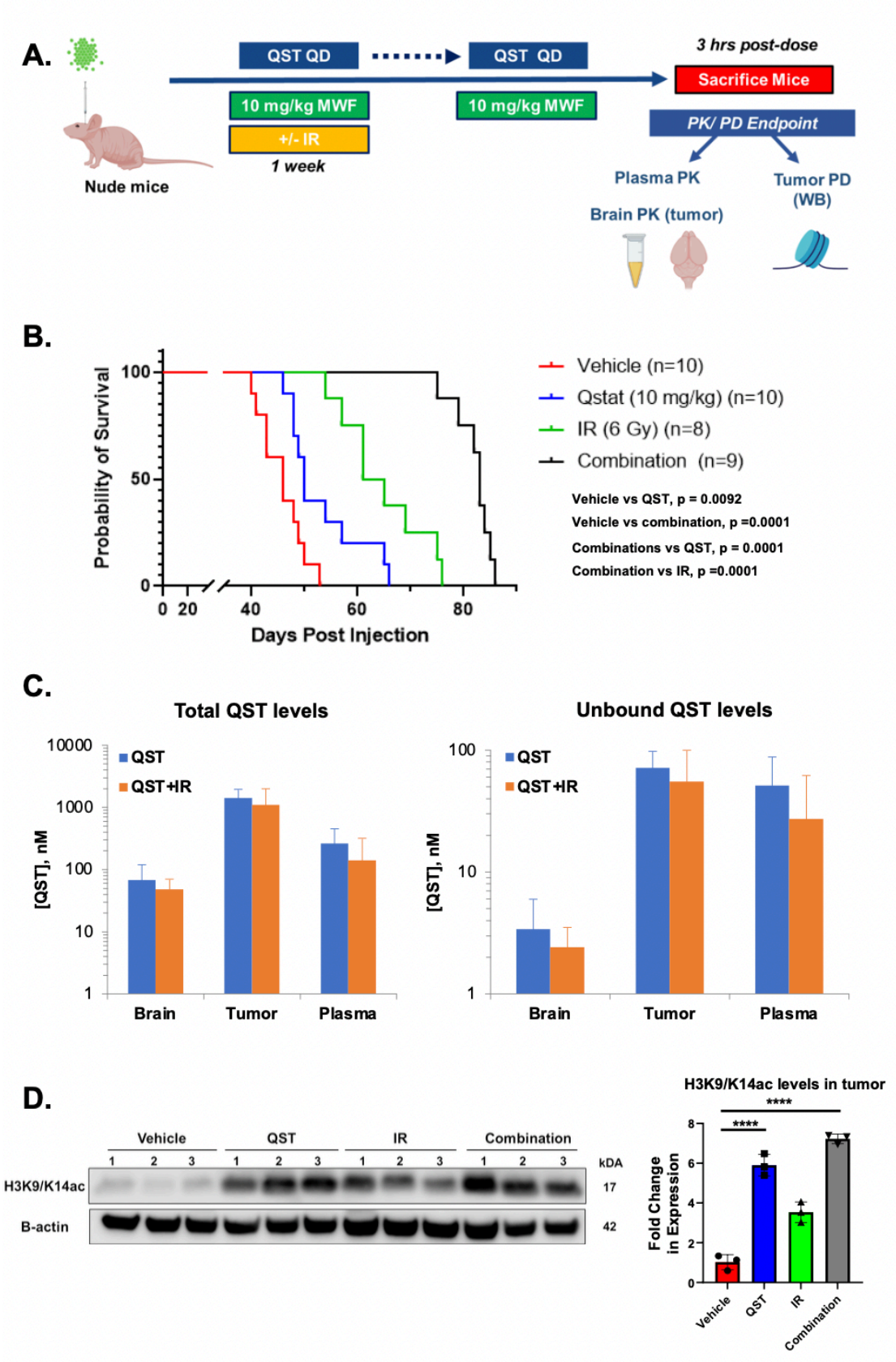
A.
QST QD
QST QD
3 hrs post-dose
Sacrifice Mice
10 mg/kg MWF
10 mg/kg MWF
+/- IR
1 week
PK/ PD Endpoint
Nude mice
Plasma PK
Tumor PD (WB)
Brain PK (tumor)
B.
Probability of Survival
Days Post Injection
Vehicle (n=10)
Qstat (10 mg/kg) (n=10)
IR (6 Gy) (n=8)
Combination (n=9)
Vehicle vs QST, p = 0.0092
Vehicle vs combination, p =0.0001
Combinations vs QST, p = 0.0001
Combination vs IR, p =0.0001
C.
Total QST levels
Unbound QST levels
[QST], nM
QST
QST+IR
Brain
Tumor
Plasma
D.
Vehicle
QST
IR
Combination
H3K9/K14ac
B-actin
kDA
17
42
H3K9/K14ac levels in tumor
Fold Change in Expression
****

**Figure 3.8 Quisinostat functions as a potent radiosensitizer in a patient-derived xenograft model of GBM.** (A) Schematic illustrating the design of the treatment study in an orthotopic PDX model of GBM. (B) Kaplan-Meier survival analysis of vehicle-, quisinostat- (10 mg/kg), radiation- (6 Gy) or combination-treated (6 Gy total radiation and 10 mg/kg quisinostat) mice. (C) Total (left) and unbound (right) levels of quisinostat in tumor tissue and brain tissue contralateral to the tumor in Quisinostat and combination-treated mice (n=4-5 per cohort). (D) Immunoblotting of protein lysates derived homogenized brain tumors from each cohort (n=3-4 per group). Membranes were probed for H3K9/14ac and B-actin. Normalized levels of H3K9/14ac protein in all cohorts are shown to the right. QST = quisinostat. Error bars indicate SEM. * $p <$ 0.05, ** $p < 0.01$, *** $p < 0.001$, n.s., not significant *P* values were calculated using unpaired 2-tailed t-test and Kaplan-Meier method with the Mantel-Cox log-rank test.

### *3.3.11 Inter-species differences in the stability of Quisinostat*

The stability of quisinostat in mouse plasma and brain homogenate was determined to ensure no degradation occurs during the sample preparation and equilibrium dialysis at 37 °C. The drug exhibited significant instability in mouse plasma during a 24-hour incubation time with half-life of ~1 hour (Figure 3.9A). Quisinostat also slowly degraded in mouse brain homogenate (Figure 3.9B). However, the process was significantly inhibited when mice were perfused prior to brain collection. The latter indicates that quisinostat instability in the brain is most likely related to the enzymes present in the mouse plasma. This observation is in correlation with previously published data on instability of hydroxamic acids in rat plasma due to presence of various esterases (Hermant et al. 2017). The degradation of quisinostat can be significantly inhibited if the plasma and brain samples are stored in refrigerator at 4 °C (Figure 3.9C). The sample preparation was therefore performed on ice-cold bath to avoid quisinostat degradation. Interestingly, the drug was completely stable in human plasma and brain homogenate at 37 °C (Figure 3.9 D-E). The stability is probably due to the absence of esterases in human matrixes responsible for degradation of hydroxamic acids. Since we employed

quisinostat for numerous *in vitro* studies, the stability of the molecule was tested also in the cell media used to culture GSCs (see section 3.2 for method details). We demonstrate that ~70% of quisinostat stays intact in the cell media over a 24-hour incubation period at 37 °C (Figure 3.9E). These results are in line with the data obtained in the cellular accumulation experiments shown in Figures 3.2E-F.

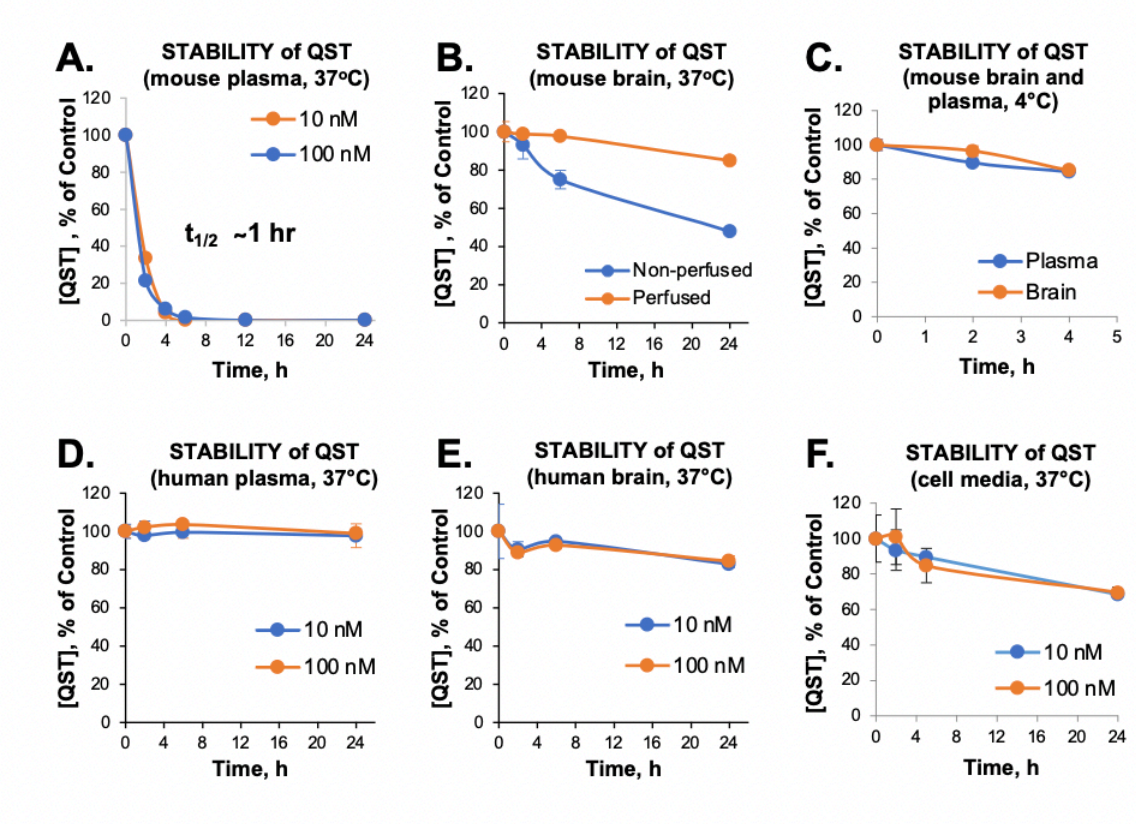


**Figure 3.9 Inter-species differences in the stability of quisinostat in plasma and brain.** (A-C) Stability of quisinostat (10 nM and 100 nM) in mouse plasma (A) and brain (B) homogeneate (1/7 w/v in PBS) was prepared from perfused or non-perfused mouse brains) at 2, 4, 6, 12 and 24 h at 37°C and (C) 4°C. (D-E) Stability of quisinostat (10 nM and 100 nM) in human plasma (D) and brain (E) (homogeneate (1/7 w/v in PBS)) at 2, 6, and 24 h at 37°C. (F) Stability of quisinostat (10 nM and 100 nM) in GSC media at 2, 6, and 24 h at 37°C. Values are the mean of triplicate measurements and error bars represent the SEM from those measurements. QST = quisinostat.

## 3.4 Discussion

Little progress has been made in extending life of adults with GBM over the past four decades. As reviewed in Chapter 1, since the late 1970s the FDA has only approved four drugs and one device for the treatment of high-grade gliomas. These include three alkylating agents (lomustine, carmustine, TMZ), bevacizumab and tumor treating fields (TTfields). Most of these treatments are approved for the treatment of recurrent high-grade gliomas, for which there is no established standard-of-care. Lomustine and carmustine were approved by the FDA for the treatment of GBM in the late 1970s and result in an average overall survival of 11.5-11.75 months (Hochberg et al. 1979; Walker et al. 1978). TMZ is administered with radiation therapy after surgical resection of the tumor and comprises the current standard-of-care, which results in overall survival of approximately 14.6-16.1 months (Stupp et al. 2005). Bevacizumab – a targeted therapeutic antibody against VEGF – is used to alleviate symptomatic edema and radiation necrosis in recurrent GBM but does not improve overall survival (Cohen et al. 2009). TTfields deliver low-intensity, intermediate frequency alternating electric fields that disrupt mitosis in tumor cells (Fisher and Adamson 2021). TTfields were found to significantly improve overall survival in primary and recurrent GBM patients when administered concurrently with TMZ (20.5 months) compared to TMZ alone (15.6 months) (Stupp et al. 2015). Unfortunately, nearly all drugs tested in a phase III trials have failed to show efficacy and improve patient survival over the last several decades. Systemic inhibition of HDACs is the only branch of epigenetic therapy that has been investigated in clinical trials for GBM but has yielded vastly disappointing results

(Bezecny 2014; Lee, Murphy, et al. 2015; Lee et al. 2017). Vorinostat, romidepsin, and panobinostat are the only pan-HDACi that have been tested clinically for GBM as either monotherapies or combination therapies with radiation and/or temozolomide or bevacizumab. All three were found to be ineffective and did not provide a survival benefit when compared to historical control data from previous phase II clinical trials (Galanis et al. 2018; Iwamoto et al. 2011; Lee, Reardon, et al. 2015).

The clinical failure of HDACi for the treatment of GBM can be attributed to the fact that most of these drugs are unable to cross the blood-brain-barrier at significant concentrations, have high toxicity profiles and thereby small therapeutic windows (Tosi et al. 2020; Hooker et al. 2010; Bezecny 2014). Notably, these HDACi advanced to clinical trials with little to no information on their PK and PD properties in preclinical models of aggressive gliomas (Hennika et al. 2017; Wu et al. 2016; Ugur et al. 2007; Eyupoglu, Hahnen, Heckel, et al. 2005).

Several second-generation HDACi have been developed with higher isoform-selectivity with the aim of decreasing toxicity and increasing specificity that warrant preclinical investigation for the treatment of GBM (Ho, Chan, and Ganesan 2020). Considering that it is widely established that individual HDAC enzymes harbor non-redundant, isoform-specific roles in different kinds of cancers, it is hypothesized that HDACi with greater isoform-selectivity may possess a higher therapeutic index and cause less adverse effects (Gryder, Sodji, and Oyelere 2012). As we recently discovered that HDAC1 promotes the tumorigenic properties and survival of glioma stem cells, we questioned whether a brain penetrant HDACi with higher affinity to HDAC1 would be effective in slowing tumor growth *in vivo*. To this end we investigated the translational

potential of quisinostat – a HDACi that is more selective against class I HDACs and exhibits marked potency towards HDAC1 – in preclinical models of GBM.

Here, we demonstrate that quisinostat is highly cytotoxic to human GSC cultures and functions as a potent radiosensitizer in an orthotopic PDX model of GBM. Importantly, we performed brain and tumor tissue-specific pharmacokinetic analyses of total and unbound quisinostat concentrations and demonstrate that it is indeed a brain-penetrant molecule. Our findings are significant considering that the efficacy of quisinostat as a monotherapy for the treatment of malignant brain tumors remains controversial. One study in a mouse model of sonic hedgehog-driven medulloblastoma reported that quisinostat treatment had a statistically significant but modest survival benefit, while studies in a syngeneic model of GBM and a PDX model of diffuse intrinsic pontine glioma (DIPG) reported no therapeutic benefit (Pak et al. 2019; Householder et al. 2018; Vitanza et al. 2021). However, there are several important considerations to highlight when assessing the effectiveness of quisinostat across these previously published studies. First, they all employ different doses of quisinostat – varying from 8 mg/kg to 50 mg/kg – and different drug delivery methods. Second, two of these studies suggested that the failure of quisinostat to prolong survival *in vivo* could be attributed to its inability to cross the blood-brain-barrier, but these claims were made in the absence of direct drug level measurements and lack of evidence of on-target engagement in the brain (Vitanza et al. 2021; Householder et al. 2018). To this end, in our study we utilized an elaborate PK-PD paired analysis approach to establish the brain-penetrant properties of Quisinostat and guide interpretation of the translational potential of this HDACi in GBM. We show that when dosed at 10 mg/kg via intraperitoneal injection, unbound levels of

quisinostat can be detected in normal brain tissue and that this concentration is sufficient to induce significant histone H3 hyperacetylation in brain cells. These results are significant as they reveal, unlike previous speculations, that quisinostat can cross a structurally intact blood-brain-barrier and induce its intended PD effect in normal brain tissue. We also demonstrate that the unbound fraction of quisinostat is significantly higher in the tumor relative to peritumoral brain regions, most likely due to tumor-induced blood-brain-barrier leakage considering we employed a PDX model that grows as a large mass. Notably, we used the same strain of athymic nude mice employed by a previous preclinical study, wherein the authors suggested that quisinostat was not a brain-penetrant drug due to its inability to inhibit growth of orthotopic DIPG tumors (Vitanza et al., 2020). It is possible that the ineffectiveness of quisinostat observed in DIPG models could be due to poor blood-brain-barrier disruption due to the diffuse growth pattern characteristic of these midline tumors, resulting in sub-therapeutic concentrations of free quisinostat required to induce cytotoxicity *in vivo* (Vanan and Eisenstat 2015).

We show that while quisinostat significantly slows growth of intracranial GBM, monotherapy only results in a very modest survival benefit. However, considering that numerous HDACi have been shown to display radiosensitizing properties, we questioned whether quisinostat could enhance radiation-induced cell death in GBM. Indeed, we found that low nanomolar doses of quisinostat robustly synergized with ionizing radiation across multiple glioma cell lines. Importantly, we demonstrate that combinatorial therapy of quisinostat and fractionated radiation resulted in a significant extension of median survival compared to untreated and monotherapy regimens. To the best of our knowledge, this is the first report demonstrating that quisinostat can act as a potent

radiosensitizer *in vitro* and *in vivo* in any preclinical cancer model. Hence, our results have important implications for the management of other malignancies – such as prostate, colon, lung, and esophageal cancer – wherein class I HDACs are frequently overexpressed and where radiation is commonly used as a treatment modality (Robert and Rassool 2012; Schaue and McBride 2015). Furthermore, our results strongly suggest that quisinostat should be re-evaluated as a potential radiosensitizer in preclinical models of DIPG, given that radiation is currently the only treatment option available for children diagnosed with this very aggressive and fatal glioma (Vitanza and Monje 2019). Future directions for this study will include assessing the radiosensitizing properties of quisinostat in multiple orthotopic PDX models of GBM, to ensure our findings can be reproduced in models harboring different genetic aberrations, growth patterns and phenotypes. This is especially critical given the high degree of inter- and intra-tumoral cellular and phenotypic heterogeneity observed in GBM (Neftel et al. 2019; Patel et al. 2014; Tirosh and Suva 2020; Suva and Tirosh 2019; Sottoriva et al. 2013). An important limitation inherent in the use of our PDX models is that they preclude an understanding of how an intact immune system may affect the response to quisinostat when combined with radiation treatment. Brain irradiation is known to induce widespread and chronic neuroinflammation which can compromise blood-brain-barrier integrity, cognition, and cell survival (Makale et al. 2017; Lumniczky, Szatmari, and Safrany 2017; Haddad et al. 2021). Hence, it will be necessary to study the radiosensitizing effects of quisinostat in the context of a brain harboring a fully functioning immune system either in syngeneic mouse models of GBM (e.g. GL261) or patient-derived gliomas stem cells transplanted into humanized mouse models.

We found that quisinostat treatment resulted in elevated levels of DNA double stranded breaks (DSBs) in glioma stem cells, both *in vitro* and *in vivo*. It is well established that other hydroxamic acid-based HDACi (TSA, vorinostat, panobinostat, belinostat) can induce DNA damage and negatively regulate the different pathways of DNA damage response (DDR) (Petruccelli et al. 2011; Pettazzoni et al. 2011; Kim, Lee, et al. 2015; Zhang et al. 2007; Robert and Rassool 2012). While the precise mechanisms through which HDACi directly induce DNA damage and synergize with radiation remain unclear, several hypotheses have been proposed to explain the basis of these phenomena. With respect to the direct induction of DNA damage, previous studies have shown that HDACi can lead to the accumulation of ROS which can result in oxidized DNA base lesions (Ruefli et al. 2001; Rosato et al. 2008; Ungerstedt et al. 2005). If left unrepaired, the oxidative stress-induced single strand DNA breaks can be converted to DSB during DNA replication (Caldecott 2007; Lee and Pervaiz 2011). Moreover, HDACi can downregulate the expression of DDR proteins such as EXO1, FEN1 and XPA, which are involved in the base excision repair (BER) and nucleotide excision repair (NER), both of which are necessary for repair of oxidative DNA damage (Lindahl and Wood 1999; Rosato et al. 2008; Hansen and Kelley 2000). Numerous studies have shown that treatment with HDACi across various cancer cell lines also results in the transcriptional downregulation of genes involved in homologous recombination and non-homologous end-joining (*Ku70*, *Ku86*, *DNA-PKcs*, *RAD51*, *BRCA1* and *BRCA2*), which are critical for DSB repair (Rosato et al. 2008; Lee et al. 2010; Robert and Rassool 2012). These data suggest that HDACi-induced ROS generation and dampening of the DDR may contribute to the accumulation of DSBs.

Another proposed mechanism for DNA damage is through histone hyperacetylation from HDACi treatment resulting in drastic structural changes in chromatin, exposing large portions of DNA to radiation or other chemotherapeutic agents (Khan and La Thangue 2012; Bakkenist and Kastan 2003). Hence, it is hypothesized that combination treatment of HDACi and radiation synergize by inducing excessive DNA damage and subsequent apoptosis (Camphausen et al. 2004; Karagiannis and El-Osta 2006). It is also worth noting that both HDAC1 and HDAC2 have been shown to harbor important roles in the DDR by promoting DSB repair. One seminal study demonstrated that HDAC1 and HDAC2 localize to DSB sites and induce local chromatin condensation through deacetylation of histone marks H3K56 and H4K16, repressing transcription and preventing transcription from interfering with DNA repair processes (Miller et al. 2010). Depletion of both HDAC1 and HDAC2 rendered cancer cells hypersensitive to ionizing radiation and resulted in diminished DSB repair capacity, particularly by non-homologous end-joining (Miller et al. 2010). Hence, we speculate that the radio-sensitizing effects of quisinostat in glioma stem cells may be partly driven through potent inhibition of HDAC1 and HDAC2, against which quisinostat exhibits the highest isoform selectivity ($IC_{50}$: 0.1 nM and 0.3 nM, respectively) (Ho, Chan, and Ganesan 2020).

Future and ongoing studies entail understanding how quisinostat treatment, alone and in combination with radiation, affects the DDR pathways in GBM. We will analyze brain tumor tissue samples derived from mice that underwent acute or long-term treatment with quisinostat (described in section 3.3.10 and 3.3.11) with RNA-sequencing. These experiments will help us elucidate whether DDR proteins or specific DDR pathways are being downregulated following quisinostat treatment and identify potential

compensatory mechanisms that may promote the emergence of therapeutic resistance over time. Furthermore, it will be interesting to assess how quisinostat affects DNA repair dynamics in non-malignant neural cells compared to glioma stem cells, considering there is evidence that normal somatic cells repair HDACi-induced DNA damage much more efficiently compared to transformed cells (Lee et al. 2010; Ungerstedt et al. 2005).

Quisinostat is currently being tested in phase I and II clinical trials for lung, ovarian and breast cancer, and is well-tolerated at a maximum-tolerated dose of 12 mg/kg given three times weekly. It should be noted that quisinostat harbors superior clinical tolerability compared to panobinostat, another HDACi currently in trials for aggressive gliomas. Data from phase I trials found that while hematologic toxicities (grade 1 and 2) were rare in patients treated with quisinostat (< 5%), while such toxicities were fare more common and severe (grade 3 and 4) during treatment with panobinostat (Venugopal et al. 2013; Wood et al. 2018; Ibrahim et al. 2016; Zaja et al. 2018). While the tolerability of quisinostat in combination with other agents in humans remains unexplored, our preclinical data support that combinatorial treatment with fractionated radiation is well tolerated in mice.

A crucial experimental finding in our study was the identification that quisinostat is highly unstable in mouse plasma, with a short half-life of approximately 30 minutes. Conversely, quisinostat was highly stable in human plasma – revealing that quisinostat exhibits distinct stability profiles across different species. Importantly, a similar trend was also observed in the mouse brain, wherein quisinostat was found to be much less stable compared to human brain. A recent study reported that hydroxamic acids such quisinostat are common substrates of a family of esterases (carboxylesterases) that are

abundantly present in rodent plasma, but absent in human plasma (Hermant et al. 2017). Our results therefore highlight a large discrepancy in the metabolic stability between rodent and human species. This is an important consideration for translating preclinical studies to the clinic as such differences may hinder the development of promising drug candidates at the preclinical level. Our data and method development will thereby be a valuable resource and note of caution for future preclinical studies employing quisinostat or similar drugs with species-specific stability, as the drug is undetectable in mouse plasma over two hours post-dosing.

The identification of drugs that can enhance the effects of radiation treatment is an intense area of research within the field of neuro-oncology. Nevertheless, while the use of radiosensitizers represents a promising strategy in GBM, the development of these novel agents has been underwhelming (Degorre et al. 2021). Here, we provide the first report that a hydroxamic-based HDACi can act as a radiosensitizer in GSCs and PDX models of GBM. However, it is worth noting that the short-chain fatty acid-based HDACi valproic acid (VPA) was also shown to harbor radiosensitizing effects in gliomas. VPA is an anti-convulsant drug with HDAC-inhibitory properties that is widely used for the treatment of epilepsy and has also been studied across multiple preclinical and clinical studies for the treatment of GBM (Romoli et al. 2019; Chinnaiyan et al. 2008; Camphausen et al. 2005; Krauze et al. 2015; Kerkhof et al. 2013; Van Nifterik et al. 2012). Through mechanisms that remain unclear, VPA was shown to sensitize glioma cells to radiation treatment *in vitro* and *in vivo* (Chinnaiyan et al. 2008; Camphausen et al. 2005). It should be noted that VPA's inhibitory activity against HDAC enzymes is very weak and is only evident at high micromolar or millimolar concentrations *in vitro*, and as such caution should be used

when referring to VPA as a bone-fide HDACi (Bondarev et al. 2021; Berendsen et al. 2019). A phase II clinical trial found that when VPA was added to the standard-of-care, patients a median overall survival of 29.6 months, which represented an improvement over historical control data (Krauze et al. 2015). Despite these promising outcomes, the use of VPA as a radiosensitizer remains controversial. A pooled analysis of multiple clinical trials found that administration of VPA with radiation and TMZ failed to prolong survival (Happold et al. 2016). A recent study also demonstrated that VPA does not result in increased histone acetylation in tumor tissue from GBM patients treated with clinical doses of VPA prior to surgery (Berendsen et al. 2019). However, these analyses are hard to interpret due to lack of information on the administered doses of VPA. While the exact mechanism of action of VPA are largely unknown, it is thought to exert its broad spectrum of biological effects primarily through the enhancement of γ-aminobutyric acid (GABA) synthesis and release, resulting in the potentiation of GABA-ergic inhibitory neurotransmission in the brain (Loscher 1993; Bondarev et al. 2021). In future studies, it will be interesting to compare the radiosensitizing properties of VPA and quisinostat across different preclinical models of GBM and understand whether quisinostat outperforms the therapeutic benefit obtained with VPA treatment *in vivo*.

In conclusion, we demonstrate that quisinostat is a brain penetrant HDACi with potent radiosensitizing properties in preclinical models of GBM. Future investigation is required to dissect the molecular consequences of quisinostat treatment and its synergistic relationship with radiation-induced DNA damage in GSCs. Overall, our results provide a rationale for developing quisinostat as a potential combination therapy with radiation for the treatment of GBM.

# CHAPTER 4

# CONCLUSION

GBM is the most common and aggressive form of primary brain cancer affecting adults. It is a devastating disease with a poor prognosis, as the median survival after initial diagnosis is less than year without treatment. The current standard-of-care, which comprises of surgical resection followed by concurrent administration of radiation and TMZ, has remained unchanged over almost two decades with modest improvement in patient survival. Despite numerous clinical trials and GBM representing one of the most comprehensively characterized cancer types at the genomic and transcriptomic level, no chemotherapeutic drug apart from TMZ has been found to be effective in prolonging patient survival. As reviewed in Chapter 1, the highly infiltrative nature of GBM, high degree of inter- and intra-tumoral heterogeneity and protection conferred by the blood brain barrier are challenges that have hindered progress in developing new effective treatments for this population of patients. The discovery that malignant brain tumors harbor rare pools of self-renewing, tumorigenic GSCs transformed our understanding of GBM biology (Singh et al. 2003; Singh et al. 2004; Hemmati et al. 2003). As GSCs have been shown to contribute to tumor progression, therapeutic resistance and tumor recurrence, there has been a significant interest to develop targeted therapies aimed at eliminating this subpopulation of cells in GBM over the past decade (Lathia et al. 2015).

It is well-established that epigenetic mechanisms play an important role in the maintenance of the GSC phenotype, and various epigenetic regulators have been found to sustain an aberrant chromatin landscape in GSCs. Well-studied examples include members of the polycomb repressive complexes 1 and 2 (PRC1 and PRC2), such as the

H3K27 methylase EZH2 (the catalytic subunit of PRC2) and the PRC1 ring finger protein BMI1, both of which have been shown to promote the self-renewal and tumor-propagating potential of GSCs (Suva et al. 2009; Stazi et al. 2019; Abdouh et al. 2009; Godlewski et al. 2008). Additionally, EZH2 was shown to inhibit GSC differentiation by recruiting the DNA methyltransferase DNMT1 to PRC2 target gene promoters (Lee et al. 2008). Other important epigenetic regulators in GBM include the bromodomain and extraterminal (BET) protein family (BRD2, BRD4) that are overexpressed in GBM and were found to promote GSC proliferation (Pastori et al. 2014). Moreover, some HDAC isoforms are known to be overexpressed in GBM, although their functional roles in GSCs remain unclear (Lee et al. 2017). It is worth noting that although these epigenetic mechanisms and the GSC epigenome are well-characterized, all this knowledge has not translated into successful epigenetic therapies for patients with GBM.

The only form of epigenetic therapy tested in clinical trials for GBM have been HDACi that have been approved for the treatment of other cancers, such as 170omidepsin for cutaneous T-cell lymphoma and 170omidepsin170t for refractory multiple myeloma (Bezecny 2014). However, these drugs unanimously failed to provide significant therapeutic benefit for GBM patients (Galanis et al. 2018; Iwamoto et al. 2011; Lee, Reardon, et al. 2015). The HDACi employed in these trials are broad-spectrum drugs that target all HDAC isoforms, but it is unknown whether all HDAC isoforms are equally important for the progression of GBM. Considering that systemic pharmacological inhibition of all HDACs leads to widespread toxicity in patients, significant emphasis has been placed on developing HDACi with higher isoform selectivity profiles with the aim of improving efficacy while minimizing toxic side effects. The most common toxicities

exhibited in patients treated with the pan-HDACi 171omidepsin, 171omidepsin, 171omidepsin171t, 171omidepsin were severe diarrhea, nausea, fatigue, vomiting, anorexia, and life-threatening grade 3 or 4 hematological toxicities (Li and Seto 2016; Munster et al. 2009; Bruserud et al. 2007). Hence, discovering which individual HDACs are relevant and necessary to drive GBM pathogenesis – especially in GSCs – may provide a rationale for the development of isoform-selective inhibitors for GBM treatment. In this dissertation, I sought to understand the unique isoform-specific roles of HDAC1 in GSCs, as this class I HDAC is highly overexpressed in GBM compared to normal brain tissue.

The current classification of the HDAC family of enzymes (classes I-IV) is largely based on structural similarity and cellular localization but masks the functional diversity of each HDAC isoform (de Ruijter et al. 2003). The 11 human HDACs are frequently overexpressed in many different cancers, but the isoform-specific roles and unique functions of each HDAC in the context of different malignancies remain poorly characterized (Weichert 2009). This is particularly true for HDAC1 and HDAC2, which are ubiquitously expressed in the nucleus and act as bona fide histone deacetylases (Ho, Chan, and Ganesan 2020). HDAC1 and HDAC2 share 80% sequence homology, are often found in the same chromatin remodeling complexes, and have been shown to exhibit compensatory functions when one isoform is absent as demonstrated through genetic silencing or knockout experiments across different cell types and tissues (Jurkin et al. 2011). However, this traditional view of the relationship between the two HDAC sister proteins is rapidly changing. There is now ample evidence that while HDAC1 and HDAC2 indeed have overlapping regulatory functions, they also harbor numerous

distinct and non-redundant functions across different cell types, tissues, developmental stages, and cancers (Jurkin et al. 2011; Dovey, Foster, and Cowley 2010; Hagelkruys et al. 2014; MacDonald and Roskams 2008; Lagger et al. 2002).

As discussed in Chapter 2, a previous study demonstrated that HDAC2 is the essential HDAC in neural stem cells in the developing murine brain (Hagelkruys et al. 2014). The presence of a single *Hdac2* allele in the absence of *Hdac1* was necessary and sufficient to control the fate of neural progenitor cells to ensure normal brain development. However, a single allele of *Hdac1* in the absence of *Hdac2* resulted in the accumulation of DNA damage, apoptosis, and an embryonic lethal phenotype (Hagelkruys et al. 2014). Interestingly, Hdac1 and Hdac2 exhibit exceptional cell type-specific expression patterns in the adult murine brain: HDAC1 is primarily expressed in astrocytes, while HDAC2 is more highly expressed in mature neurons (Hagelkruys et al. 2014; MacDonald and Roskams 2008). Considering that GBMs arise in the brain and that there are robust similarities between gliomagenesis and processes underlying normal CNS development, we questioned whether HDAC1 and HDAC2 exhibited similar or divergent functions in GBM.

In Chapter 2 of this dissertation, we demonstrated that HDAC1, but not HDAC2, is important for the proliferation and survival of GSCs across a panel of patient-derived cell lines (n=8). This is in stark contrast to what has been reported in the normal developing CNS and highlights how the non-overlapping functions of HDAC1 and HDAC2 can change across different cellular contexts. We were particularly interested in understanding the requirement for HDAC1 and HDAC2 in GSCs since this population of cells is hypothesized to drive treatment resistance and recurrence in GBM. We found that

high HDAC1 expression was positively correlated with increasing WHO brain tumor grade and associated with poor survival outcomes in GBM patients. Interestingly, we showed that genetic ablation of HDAC1 negatively impacted the proliferative capacity and survival of GSCs in a p53-dependent manner, and that p53 transcriptional activity was restored in p53-WT GSCs. On the contrary, knockdown of HDAC2 had no significant effect on GSC survival and I also found that loss of *HDAC1* expression was not compensated for by increased expression of other HDACs. Importantly, we demonstrated that lack of HDAC1 expression in GSCs significantly slowed tumor growth *in vivo*. These results are noteworthy as they are the first report revealing that the absence of a single HDAC isoform can result in a significant extension of survival in orthotopic PDX and mouse models of GBM. A potential limitation of our study is that in all our experiments we primarily employed treatment naïve GSCs derived from primary GBMs. In future studies, it will be interesting and necessary to understand whether GSCs derived from recurrent GBMs display a similar vulnerability in loss of HDAC1 function, as recurrent tumors are typically more aggressive and phenotypically or genetically distinct from primary GBMs (Wang et al. 2016; Wang, Hu, et al. 2017). Given the extensive genetic heterogeneity present in GBM, will also be important to assess the effects of HDAC1 loss across a larger panel of GSCs to determine how the observed dependency on HDAC1 may differ in the presence of distinct driver mutations.

Intriguingly, although p53-WT GSCs died *in vitro*, these cells could still form tumors in immunocompromised mice – albeit at a slower rate compared to controls. This strongly suggests that the normal brain milieu is a growth-permissive environment for HDAC1-deficient GSCs, whereas standard *in vitro* culture conditions lack the appropriate

soluble factors that are required for these cells to survive and proliferate in the absence of HDAC1 activity. An unexpected finding was the observation that tumors where HDAC1 was silenced exhibited a more invasive growth pattern relative to control tumors, a result that highlights the intrinsic phenotypic plasticity of GSCs in response to stress or perturbations. Indeed, RNA-sequencing analysis confirmed that loss of HDAC1 expression in GSCs resulted in the upregulation of genes involved in cellular invasion and migration. However, it is likely that these transcriptional changes not only alter the phenotype of the GSCs themselves but may also affect how GSCs influence or interact with the tumor microenvironment. We demonstrated that *HDAC1* knockdown induced high levels of pSTAT3 in GSCs, which is known to upregulate the production of various immunosuppressive cytokines that recruit and shape the function of resident microglia and astrocytes which in turn can influence glioma growth and invasion (Hambardzumyan, Gutmann, and Kettenmann 2016; Wu et al. 2010; Henrik Heiland et al. 2019). We therefore hypothesize that high pSTAT3 activity in *HDAC1*-silenced GSCs may result in increased microglia activation and peritumoral astrocyte reactivity *in vivo*. While not the direct focus of my research, it is becoming increasingly clear that a tumor-promoting microenvironment results from a complex crosstalk between tumor cells/GSCs, microglia and reactive astrocytes (Lathia et al. 2015; Prager et al. 2020). Activated microglia have an established role in glioma maintenance and progression, and produce several anti-inflammatory cytokines (TGFβ, IL-6, IL-10, ARG1) that promote proliferation, survival, and migration of GSCs (Hambardzumyan, Gutmann, and Kettenmann 2016). While these dynamic interactions are still not well understood, dissecting how the activity and functions of HDAC1 and other HDACs influence or

remodel the tumor microenvironment in GBM will be an important avenue for future research. Additionally, it will be necessary to study these interactions in syngeneic or humanized mouse models of GBM, both of which are more physiologically relevant models as they harbor a fully functioning immune system.

We additionally identified that the STAT3 signaling axis is a compensatory pathway that is upregulated after loss of HDAC1 activity to promote survival of GSCs. Hence, we postulate that a combinatorial therapy comprising of more selective HDAC1 and STAT3 inhibitors may be a promising therapeutic strategy that should be validated in preclinical models of GBM. However, while the efficacy of numerous small molecules targeting STAT3 have been tested across multiple models of GBM *in vitro* and *in vivo*, the extent to which these drugs effectively penetrate the blood brain barrier remains unclear (Jensen et al. 2017; Haftchenary et al. 2013; Mukthavaram et al. 2015; Li et al. 2019; Stechishin et al. 2013). Hence, it will be necessary to examine the permeability of multiple STAT3 inhibitors *in vivo* to identify the most promising drug to target this major signaling axis in GBM in combination with HDACi.

Here, we present the first report demonstrating that loss of a single HDAC isoform can have profound effects on the GSC phenotype without any evident compensation from its paralogue HDAC2 or other isoforms. These data raise many important questions with respect to the non-redundant roles of other HDAC isoforms in GBM as well as in other aggressive gliomas such as DIPG or pediatric GBM, where histone H3 mutations are major epigenetic drivers of disease progression (Wu et al. 2012; Schwartzentruber et al. 2012). While HDAC1 and HDAC2 are key regulators of gene expression through direct deacetylation of histones and transcription factors, the other

remaining 9 HDACs span a wide variety of functions that remain completely unexplored in the context of GSC biology (Ho, Chan, and Ganesan 2020). It is worth highlighting that HDAC3, HDAC6, HDAC7 and HDAC8 also exhibit increased expression in GBM tissue relative to normal brain, while HDAC4, HDAC5, HDAC10 and HDAC11 are downregulated (Cancer Genome Atlas Research 2008). In non-transformed cells, these HDACs are involved in the regulation of the cytoskeleton, cell death, protein misfolding, cell mobility, autophagy, immunoregulation and DNA repair (Li and Seto 2016). Not all HDACs are equal – as such, characterization of the unique roles of each isoform in GBM, and how those differ compared to their functions in normal CNS cells, has the potential to transform our understanding of the biological relevance of HDACs in malignant brain tumors.

Interest in pursuing pharmacological targeting of HDACs for the treatment of GBM dramatically diminished when panobinostat, romidepsin and vorinostat unanimously failed to prolong survival of patients when combined with either the standard-of-care or as monotherapies in phase I/II clinical trials (Galanis et al. 2018; Lee, Reardon, et al. 2015; Iwamoto et al. 2011). As discussed in Chapter 3, it should be noted that the use of pan-HDACi in the clinic preceded our understanding of which HDAC isoforms are functionally important or relevant for the progression of GBM. These pan-HDACi have broad specificity and target all HDAC proteins, and it is thought that the lack of isoform-selectivity results in serious systemic toxicity which narrows the therapeutic window of these drugs (Peng et al. 2020). Moreover, the preclinical studies that provided the basis for testing these HDACi in GBM demonstrated very modest evidence of efficacy without supporting information on drug penetration into intact brain

– all of which are valuable data necessary for effective clinical translation (Ugur et al. 2007; Hennika et al. 2017; Wu et al. 2016). In Chapter 2, we show that HDAC1 plays a critical role in therapy-resistant GSCs and that genetic ablation of HDAC1 extends survival of PDX and mouse models of GBM, providing a rationale for isoform-specific targeting of HDAC1 as an adjuvant treatment in GBM. While HDAC1-selective inhibitors are not available, the second-generation HDACi quisinostat is more selective towards class I HDACs and harbors remarkable sub-nanomolar affinity for HDAC1 ($IC_{50}$: 0.1 nM) (Arts et al. 2009). In Chapter 3, we performed a comprehensive PK-PD correlation analysis for quisinostat in preclinical *in vitro* and *in vivo* models of GBM, a study that is first in its kind for any HDACi studied in the field of neuro-oncology.

We found that quisinostat is a potent HDACi that can sensitize patient-derived GSC cultures to radiation treatment at low nanomolar concentrations. We also establish that quisinostat is a blood-brain-barrier permeable molecule and characterize the full PK profile of quisinostat, which will serve as a valuable resource for future studies that will study this drug in other aggressive adult or pediatric brain tumor models. Importantly, quisinostat was found to reduce tumor growth in flank and orthotopic PDX models of GBM and significantly extends survival when administered in combination with radiation therapy. Together, these results provide a rationale for developing quisinostat as a potential adjuvant therapy with radiation for GBM treatment. Our study also emphasizes the importance of implementing a PK-PD guided approach when evaluating or developing new drugs for GBM. While PK analyses are now commonly performed in preclinical trials for a variety of different brain tumors, these studies typically only measure the total brain-to-plasma concentration (Kp) ratio as a measure of drug-brain

penetration (Sachamitr et al. 2021; Verreault et al. 2016; Kizilbash et al. 2021). However, the value of this ratio is rather limited and may lead to erroneous conclusions as it does not consider the protein- or lipid-binding fraction of drug in the plasma and the brain (Gonzalez, Schmidt, and Derendorf 2013). To this end, we employed an equilibrium dialysis method combined with LC-MS/MS analysis to measure the unbound, or "free", brain-to-plasma concentrations (Kp, uu) which represents the pharmacologically active fraction of a drug. Hence, measurement of both total and unbound drug concentrations in plasma and brain tissues are necessary to establish accurate PK-PD correlations and to understand whether therapeutically relevant concentrations of the drug are present in a brain tumor.

To date, no hydroxamic acid-based HDACi has been shown to harbor radiosensitizing properties in preclinical models of GBM. However, it remains unclear whether these inhibitors failed to provide any therapeutic benefit due to inadequate brain penetration and/or insufficient on-target modulation. Considering there are other several second-generation HDACi (abexinostat, bisthianostat, fimepinostat) that have high selectivity for HDAC1 but whose therapeutic potential in preclinical models of GBM remain unexplored, future PK-PD studies will be necessary to determine whether any of these inhibitors harbor better efficacy or radiosensitizing properties than Quisinostat (Ho, Chan, and Ganesan 2020). Finally, it should be noted while the high sequence homology of HDAC1 and HDAC2 is a major obstacle in the development of an inhibitor that precisely discriminates between the two isoforms, there is preliminary evidence that some non-hydroxamate *ortho*-aminoanilide HDACi may achieve enhanced kinetic selectivity against the two sister proteins (Methot et al. 2008; Methot et al. 2014). If such an

inhibitor is ever discovered, preclinical characterization and validation in a preclinical setting should be warranted for any malignancy where HDAC1 has been shown to contribute to disease pathogenesis.

Preclinical models are an essential and necessary component of drug discovery for cancer; however, they can pose several limitations with respect to drug development for CNS tumors. While PDX models are often employed as brain tumor patient "avatars" to predict drug responses, there are important caveats. As discussed in Chapter 3, establishment of PDXs requires the use of immunocompromised animals, which preclude an understanding of the role of the immune system in response to a particular treatment. PDX models also incompletely recapitulate the extensive heterogeneity that is present in a human GBM, as they are derived from a small fragment of tissue that is biopsied from a single region of the tumor during surgery. Moreover, and perhaps most importantly, there are critical species-specific physiological differences between human and murine cells that must be taken into consideration when translating research findings observed in PDX models. Examples include differences in the structure of the blood-brain-barrier, drug metabolism and the tumor microenvironment – all of which can affect the interpretation of data obtained from preclinical studies (Liu et al. 2021). This was evident in our own study, where we found that quisinostat was very unstable in murine plasma and brain but stable in the human counterparts. We hypothesized that these differences in stability could be attributed to a family of esterases that rapidly metabolize hydroxamates which are absent in human plasma but highly expressed in mouse plasma (Hermant et al. 2017). This observation raises a critical question: if quisinostat is highly stable in human plasma, would the levels of free drug present in a human brain, specifically within a brain tumor,

be higher than what we were able to measure in a PDX model? If so, would higher intra-tumoral concentrations of quisinostat result in greater therapeutic benefit when the drug is administered either as a monotherapy or in combination with radiation therapy? It is challenging to infer these outcomes and how a drug will perform in humans based on preclinical modeling studies alone.

Given the dismal prognosis of GBM patients, ever-increasing costs of drug discovery, continuous clinical failures and longstanding challenges in CNS drug delivery, the way in which clinical trials are designed and implemented for this population of patients is rapidly changing. This is most evident by the widespread adoption of the "phase 0" clinical trial paradigm, which has taken a strong foothold in the field of neuro-oncology (Vogelbaum et al. 2020; Sanai 2019). The scope of a phase 0 clinical trial, which was first introduced in 2004 by the FDA, is to accelerate the early-phase development of new or repurposed drugs that penetrate the tumor and modulate their intended molecular target(s) (Kinders et al. 2007). In the realm of neuro-oncology, the Phase 0 mechanism takes advantage of the fact that virtually all GBM patients require surgical resection of the tumor (Sanai 2019). An example of a typical phase 0 clinical trial design for brain tumors is illustrated in Figure 4.1. In the days preceding surgery, patients are given safe, pharmacologically active, but subtherapeutic doses of an experimental drug. During surgery, the tumor, blood, and cerebrospinal fluid are collected for PK and PD analyses to determine evidence of positive CNS penetration of the drug and target modulation. If responses to PD and PK are positive, patients are qualified to receive treatment with therapeutic doses of the drug and enroll in a phase II clinical trial (Sanai 2019). Considering quisinostat is an HDACi that has passed phase I

clinical trials in several cancers and was found to be well-tolerated in humans, it qualifies for phase 0 testing in GBM patients (Venugopal et al. 2013). This approach would enable the characterization of the PK-PD relationship of quisinostat in humans and fast-track development of quisinostat as an adjuvant to radiation therapy in phase II trials for GBM if the results from a phase 0 are positive. It is worth noting that there is a strong interest in developing effective and potent radiosensitizers for GBM treatment, as radiation therapy remains the most effective treatment modality for all GBM patients (Degorre et al. 2021). There is a particular incentive in developing radiosensitizers for GBM patients that harbor unmethylated *MGMT*, as this population of patients does not respond to TMZ treatment (Hegi et al. 2005). It should be noted that the PDX model we employed for preclinical testing of Quisinostat was derived from a patient with recurrent GBM that harbored an unmethylated *MGMT* promoter. Considering that quisinostat was successful in radiosensitizing a recurrent, TMZ-unresponsive tumor in our study, we believe that quisinostat would be well-suited for clinical testing in patients with *MGMT*-unmethylated primary or recurrent GBM wherein TMZ does not confer any added survival benefit.

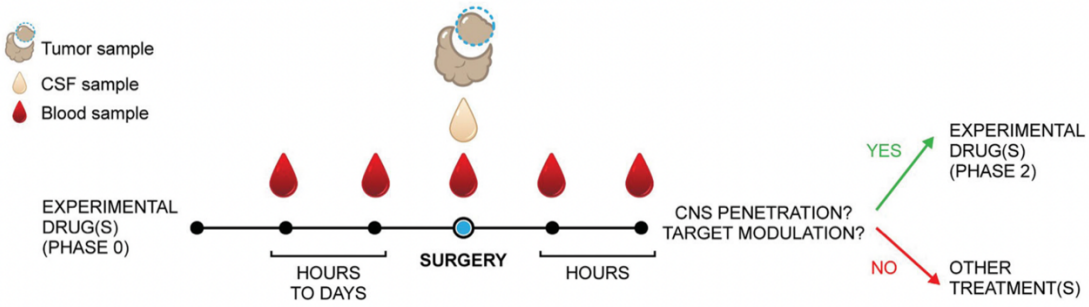


**Figure 4.1 Sample Phase 0/2 clinical trial study design for brain tumors.** Patients undergo an initial phase 0 study by taking safe but sub-therapeutic doses of an experimental drug, with PK and PD endpoints assessed within 7-10 days of surgery. Positive PK and PD responses would qualify individual patients for subsequent therapeutic dosing as part of the phase 2 study component. Taken from: (Sanai 2019).

In conclusion, the work that I presented here describes the isoform-specific functions of HDAC1 in therapy-resistant GSCs and elucidates a novel therapeutic strategy to target this major epigenetic regulator in GBM. I discovered that quisinostat, a HDACi that exhibits high selectivity against HDAC1, is highly cytotoxic against GSCs *in vitro* and is an effective DNA-damaging agent that potently synergizes with radiation treatment *in vitro* and *in vivo*. Together, these data identify a critical role for HDAC1 in GSC biology and provide a rationale for clinical development of quisinostat as a radiosensitizer for the treatment of GBM.

REFERENCES

Abdouh, M., S. Facchino, W. Chatoo, V. Balasingam, J. Ferreira, and G. Bernier. 2009. "BMI1 sustains human glioblastoma multiforme stem cell renewal." *J Neurosci* 29 (28):8884-96. doi: 10.1523/JNEUROSCI.0968-09.2009.

Aghdassi, A., M. Sendler, A. Guenther, J. Mayerle, C. O. Behn, C. D. Heidecke, H. Friess, M. Buchler, M. Evert, M. M. Lerch, and F. U. Weiss. 2012. "Recruitment of histone deacetylases HDAC1 and HDAC2 by the transcriptional repressor ZEB1 downregulates E-cadherin expression in pancreatic cancer." *Gut* 61 (3):439-48. doi: 10.1136/gutjnl-2011-300060.

Aldape, K., K. M. Brindle, L. Chesler, R. Chopra, A. Gajjar, M. R. Gilbert, N. Gottardo, D. H. Gutmann, D. Hargrave, E. C. Holland, D. T. W. Jones, J. A. Joyce, P. Kearns, M. W. Kieran, I. K. Mellinghoff, M. Merchant, S. M. Pfister, S. M. Pollard, V. Ramaswamy, J. N. Rich, G. W. Robinson, D. H. Rowitch, J. H. Sampson, M. D. Taylor, P. Workman, and R. J. Gilbertson. 2019. "Challenges to curing primary brain tumours." *Nat Rev Clin Oncol* 16 (8):509-520. doi: 10.1038/s41571-019-0177-5.

Allfrey, V. G., R. Faulkner, and A. E. Mirsky. 1964. "Acetylation and Methylation of Histones and Their Possible Role in the Regulation of Rna Synthesis." *Proc Natl Acad Sci U S A* 51:786-94. doi: 10.1073/pnas.51.5.786.

Allis, C. D., and T. Jenuwein. 2016. "The molecular hallmarks of epigenetic control." *Nat Rev Genet* 17 (8):487-500. doi: 10.1038/nrg.2016.59.

Alvarez, A. A., M. Field, S. Bushnev, M. S. Longo, and K. Sugaya. 2015. "The effects of histone deacetylase inhibitors on glioblastoma-derived stem cells." *J Mol Neurosci* 55 (1):7-20. doi: 10.1007/s12031-014-0329-0.

An, Z., O. Aksoy, T. Zheng, Q. W. Fan, and W. A. Weiss. 2018. "Epidermal growth factor receptor and EGFRvIII in glioblastoma: signaling pathways and targeted therapies." *Oncogene* 37 (12):1561-1575. doi: 10.1038/s41388-017-0045-7.

Anders, S., P. T. Pyl, and W. Huber. 2015. "HTSeq--a Python framework to work with high-throughput sequencing data." *Bioinformatics* 31 (2):166-9. doi: 10.1093/bioinformatics/btu638.

Arts, J., P. King, A. Marien, W. Floren, A. Belien, L. Janssen, I. Pilatte, B. Roux, L. Decrane, R. Gilissen, I. Hickson, V. Vreys, E. Cox, K. Bol, W. Talloen, I. Goris, L. Andries, M. Du Jardin, M. Janicot, M. Page, K. van Emelen, and P. Angibaud. 2009. "JNJ-26481585, a novel "second-generation" oral histone deacetylase inhibitor, shows broad-spectrum preclinical antitumoral activity." *Clin Cancer Res* 15 (22):6841-51. doi: 10.1158/1078-0432.CCR-09-0547.

Arvanitis, C. D., G. B. Ferraro, and R. K. Jain. 2020. "The blood-brain barrier and blood-tumour barrier in brain tumours and metastases." *Nat Rev Cancer* 20 (1):26-41. doi: 10.1038/s41568-019-0205-x.

Asfaha, Y., C. Schrenk, L. A. Alves Avelar, A. Hamacher, M. Pflieger, M. U. Kassack, and T. Kurz. 2019. "Recent advances in class IIa histone deacetylases research." *Bioorg Med Chem* 27 (22):115087. doi: 10.1016/j.bmc.2019.115087.

Ayer, D. E. 1999. "Histone deacetylases: transcriptional repression with SINers and NuRDs." *Trends Cell Biol* 9 (5):193-8. doi: 10.1016/s0962-8924(99)01536-6.

Azzam, G., X. Wang, D. Bell, and M. E. Murphy. 2013. "CSF1 is a novel p53 target gene whose protein product functions in a feed-forward manner to suppress apoptosis and enhance p53-mediated growth arrest." *PLoS One* 8 (9):e74297. doi: 10.1371/journal.pone.0074297.

Bakkenist, C. J., and M. B. Kastan. 2003. "DNA damage activates ATM through intermolecular autophosphorylation and dimer dissociation." *Nature* 421 (6922):499-506. doi: 10.1038/nature01368.

Bangert, A., S. Hacker, S. Cristofanon, K. M. Debatin, and S. Fulda. 2011. "Chemosensitization of glioblastoma cells by the histone deacetylase inhibitor MS275." *Anticancer Drugs* 22 (6):494-9. doi: 10.1097/CAD.0b013e32834631e0.

Bao, S., Q. Wu, R. E. McLendon, Y. Hao, Q. Shi, A. B. Hjelmeland, M. W. Dewhirst, D. D. Bigner, and J. N. Rich. 2006. "Glioma stem cells promote radioresistance by preferential activation of the DNA damage response." *Nature* 444 (7120):756-60. doi: 10.1038/nature05236.

Barnholtz-Sloan, J. S., Q. T. Ostrom, and D. Cote. 2018. "Epidemiology of Brain Tumors." *Neurol Clin* 36 (3):395-419. doi: 10.1016/j.ncl.2018.04.001.

Baronchelli, S., A. Bentivegna, S. Redaelli, G. Riva, V. Butta, L. Paoletta, G. Isimbaldi, M. Miozzo, S. Tabano, A. Daga, D. Marubbi, M. Cattaneo, I. Biunno, and L. Dalpra. 2013. "Delineating the cytogenomic and epigenomic landscapes of glioma stem cell lines." *PLoS One* 8 (2):e57462. doi: 10.1371/journal.pone.0057462.

Bastola, S., M. S. Pavlyukov, D. Yamashita, S. Ghosh, H. Cho, N. Kagaya, Z. Zhang, M. Minata, Y. Lee, H. Sadahiro, S. Yamaguchi, S. Komarova, E. Yang, J. Markert, L. B. Nabors, K. Bhat, J. Lee, Q. Chen, D. K. Crossman, K. Shin-Ya, D. H. Nam, and I. Nakano. 2020. "Glioma-initiating cells at tumor edge gain signals from tumor core cells to promote their malignancy." *Nat Commun* 11 (1):4660. doi: 10.1038/s41467-020-18189-y.

Baysan, M., K. Woolard, S. Bozdag, G. Riddick, S. Kotliarova, M. C. Cam, G. I. Belova, S. Ahn, W. Zhang, H. Song, J. Walling, H. Stevenson, P. Meltzer, and H. A. Fine. 2014. "Micro-environment causes reversible changes in DNA methylation and

mRNA expression profiles in patient-derived glioma stem cells." *PLoS One* 9 (4):e94045. doi: 10.1371/journal.pone.0094045.

Beier, D., P. Hau, M. Proescholdt, A. Lohmeier, J. Wischhusen, P. J. Oefner, L. Aigner, A. Brawanski, U. Bogdahn, and C. P. Beier. 2007. "CD133(+) and CD133(-) glioblastoma-derived cancer stem cells show differential growth characteristics and molecular profiles." *Cancer Res* 67 (9):4010-5. doi: 10.1158/0008-5472.CAN-06-4180.

Berendsen, S., E. Frijlink, J. Kroonen, W. G. M. Spliet, W. van Hecke, T. Seute, T. J. Snijders, and P. A. Robe. 2019. "Effects of valproic acid on histone deacetylase inhibition in vitro and in glioblastoma patient samples." *Neurooncol Adv* 1 (1):vdz025. doi: 10.1093/noajnl/vdz025.

Bezecny, P. 2014. "Histone deacetylase inhibitors in glioblastoma: pre-clinical and clinical experience." *Med Oncol* 31 (6):985. doi: 10.1007/s12032-014-0985-5.

Bhat, K. P. L., V. Balasubramaniyan, B. Vaillant, R. Ezhilarasan, K. Hummelink, F. Hollingsworth, K. Wani, L. Heathcock, J. D. James, L. D. Goodman, S. Conroy, L. Long, N. Lelic, S. Wang, J. Gumin, D. Raj, Y. Kodama, A. Raghunathan, A. Olar, K. Joshi, C. E. Pelloski, A. Heimberger, S. H. Kim, D. P. Cahill, G. Rao, W. F. A. Den Dunnen, Hwgm Boddeke, H. S. Phillips, I. Nakano, F. F. Lang, H. Colman, E. P. Sulman, and K. Aldape. 2013. "Mesenchymal differentiation mediated by NF-kappaB promotes radiation resistance in glioblastoma." *Cancer Cell* 24 (3):331-46. doi: 10.1016/j.ccr.2013.08.001.

Bigner, S. H., J. Mark, P. C. Burger, M. S. Mahaley, Jr., D. E. Bullard, L. H. Muhlbaier, and D. D. Bigner. 1988. "Specific chromosomal abnormalities in malignant human gliomas." *Cancer Res* 48 (2):405-11.

Bigner, S. H., and B. Vogelstein. 1990. "Cytogenetics and molecular genetics of malignant gliomas and medulloblastoma." *Brain Pathol* 1 (1):12-8. doi: 10.1111/j.1750-3639.1990.tb00633.x.

Birzu, C., P. French, M. Caccese, G. Cerretti, A. Idbaih, V. Zagonel, and G. Lombardi. 2020. "Recurrent Glioblastoma: From Molecular Landscape to New Treatment Perspectives." *Cancers (Basel)* 13 (1). doi: 10.3390/cancers13010047.

Bondarev, A. D., M. M. Attwood, J. Jonsson, V. N. Chubarev, V. V. Tarasov, and H. B. Schioth. 2021. "Recent developments of HDAC inhibitors: Emerging indications and novel molecules." *Br J Clin Pharmacol* 87 (12):4577-4597. doi: 10.1111/bcp.14889.

Bozzato, E., C. Bastiancich, and V. Preat. 2020. "Nanomedicine: A Useful Tool against Glioma Stem Cells." *Cancers (Basel)* 13 (1). doi: 10.3390/cancers13010009.

Brat, D. J., K. Aldape, H. Colman, D. Figrarella-Branger, G. N. Fuller, C. Giannini, E. C. Holland, R. B. Jenkins, B. Kleinschmidt-DeMasters, T. Komori, J. M. Kros, D. N. Louis, C. McLean, A. Perry, G. Reifenberger, C. Sarkar, R. Stupp, M. J. van den Bent, A. von Deimling, and M. Weller. 2020. "cIMPACT-NOW update 5: recommended grading criteria and terminologies for IDH-mutant astrocytomas." *Acta Neuropathol* 139 (3):603-608. doi: 10.1007/s00401-020-02127-9.

Brennan, C. W., R. G. Verhaak, A. McKenna, B. Campos, H. Noushmehr, S. R. Salama, S. Zheng, D. Chakravarty, J. Z. Sanborn, S. H. Berman, R. Beroukhim, B. Bernard, C. J. Wu, G. Genovese, I. Shmulevich, J. Barnholtz-Sloan, L. Zou, R. Vegesna, S. A. Shukla, G. Ciriello, W. K. Yung, W. Zhang, C. Sougnez, T. Mikkelsen, K. Aldape, D. D. Bigner, E. G. Van Meir, M. Prados, A. Sloan, K. L. Black, J. Eschbacher, G. Finocchiaro, W. Friedman, D. W. Andrews, A. Guha, M. Iacocca, B. P. O'Neill, G. Foltz, J. Myers, D. J. Weisenberger, R. Penny, R. Kucherlapati, C. M. Perou, D. N. Hayes, R. Gibbs, M. Marra, G. B. Mills, E. Lander, P. Spellman, R. Wilson, C. Sander, J. Weinstein, M. Meyerson, S. Gabriel, P. W. Laird, D. Haussler, G. Getz, L. Chin, and Tcga Research Network. 2013. "The somatic genomic landscape of glioblastoma." *Cell* 155 (2):462-77. doi: 10.1016/j.cell.2013.09.034.

Brouwer de Koning, S. G., Mtfd Vrancken Peeters, K. Jozwiak, P. A. Bhairosing, and T. J. M. Ruers. 2018. "Tumor Resection Margin Definitions in Breast-Conserving Surgery: Systematic Review and Meta-analysis of the Current Literature." *Clin Breast Cancer* 18 (4):e595-e600. doi: 10.1016/j.clbc.2018.04.004.

Brunmeir, R., S. Lagger, and C. Seiser. 2009. "Histone deacetylase HDAC1/HDAC2-controlled embryonic development and cell differentiation." *Int J Dev Biol* 53 (2-3):275-89. doi: 10.1387/ijdb.082649rb.

Bruserud, O., C. Stapnes, E. Ersvaer, B. T. Gjertsen, and A. Ryningen. 2007. "Histone deacetylase inhibitors in cancer treatment: a review of the clinical toxicity and the modulation of gene expression in cancer cell." *Curr Pharm Biotechnol* 8 (6):388-400. doi: 10.2174/138920107783018417.

Bulstrode, H., E. Johnstone, M. A. Marques-Torrejon, K. M. Ferguson, R. B. Bressan, C. Blin, V. Grant, S. Gogolok, E. Gangoso, S. Gagrica, C. Ender, V. Fotaki, D. Sproul, P. Bertone, and S. M. Pollard. 2017. "Elevated FOXG1 and SOX2 in glioblastoma enforces neural stem cell identity through transcriptional control of cell cycle and epigenetic regulators." *Genes Dev* 31 (8):757-773. doi: 10.1101/gad.293027.116.

Cadieux, B., T. T. Ching, S. R. VandenBerg, and J. F. Costello. 2006. "Genome-wide hypomethylation in human glioblastomas associated with specific copy number alteration, methylenetetrahydrofolate reductase allele status, and increased proliferation." *Cancer Res* 66 (17):8469-76. doi: 10.1158/0008-5472.CAN-06-1547.

Calatozzolo, C., M. Gelati, E. Ciusani, F. L. Sciacca, B. Pollo, L. Cajola, C. Marras, A. Silvani, L. Vitellaro-Zuccarello, D. Croci, A. Boiardi, and A. Salmaggi. 2005. "Expression of drug resistance proteins Pgp, MRP1, MRP3, MRP5 and GST-pi in human glioma." *J Neurooncol* 74 (2):113-21. doi: 10.1007/s11060-004-6152-7.

Caldecott, K. W. 2007. "Mammalian single-strand break repair: mechanisms and links with chromatin." *DNA Repair (Amst)* 6 (4):443-53. doi: 10.1016/j.dnarep.2006.10.006.

Camphausen, K., W. Burgan, M. Cerra, K. A. Oswald, J. B. Trepel, M. J. Lee, and P. J. Tofilon. 2004. "Enhanced radiation-induced cell killing and prolongation of gammaH2AX foci expression by the histone deacetylase inhibitor MS-275." *Cancer Res* 64 (1):316-21. doi: 10.1158/0008-5472.can-03-2630.

Camphausen, K., D. Cerna, T. Scott, M. Sproull, W. E. Burgan, M. A. Cerra, H. Fine, and P. J. Tofilon. 2005. "Enhancement of in vitro and in vivo tumor cell radiosensitivity by valproic acid." *Int J Cancer* 114 (3):380-6. doi: 10.1002/ijc.20774.

Cancer Genome Atlas Research, Network. 2008. "Comprehensive genomic characterization defines human glioblastoma genes and core pathways." *Nature* 455 (7216):1061-8. doi: 10.1038/nature07385.

Cardoso, F. L., D. Brites, and M. A. Brito. 2010. "Looking at the blood-brain barrier: molecular anatomy and possible investigation approaches." *Brain Res Rev* 64 (2):328-63. doi: 10.1016/j.brainresrev.2010.05.003.

Carol, H., R. Gorlick, E. A. Kolb, C. L. Morton, D. M. Manesh, S. T. Keir, C. P. Reynolds, M. H. Kang, J. M. Maris, A. Wozniak, I. Hickson, D. Lyalin, R. T. Kurmasheva, P. J. Houghton, M. A. Smith, and R. Lock. 2014. "Initial testing (stage 1) of the histone deacetylase inhibitor, quisinostat (JNJ-26481585), by the Pediatric Preclinical Testing Program." *Pediatr Blood Cancer* 61 (2):245-52. doi: 10.1002/pbc.24724.

Carro, M. S., W. K. Lim, M. J. Alvarez, R. J. Bollo, X. Zhao, E. Y. Snyder, E. P. Sulman, S. L. Anne, F. Doetsch, H. Colman, A. Lasorella, K. Aldape, A. Califano, and A. Iavarone. 2010. "The transcriptional network for mesenchymal transformation of brain tumours." *Nature* 463 (7279):318-25. doi: 10.1038/nature08712.

Chaichana, K. L., and A. Quinones-Hinojosa. 2014. "The need to continually redefine the goals of surgery for glioblastoma." *Neuro Oncol* 16 (4):611-2. doi: 10.1093/neuonc/not326.

Chakrabarti, A., I. Oehme, O. Witt, G. Oliveira, W. Sippl, C. Romier, R. J. Pierce, and M. Jung. 2015. "HDAC8: a multifaceted target for therapeutic interventions." *Trends Pharmacol Sci* 36 (7):481-92. doi: 10.1016/j.tips.2015.04.013.

Chen, J., Y. Li, T. S. Yu, R. M. McKay, D. K. Burns, S. G. Kernie, and L. F. Parada. 2012. "A restricted cell population propagates glioblastoma growth after chemotherapy." *Nature* 488 (7412):522-6. doi: 10.1038/nature11287.

Chen, R., M. Smith-Cohn, A. L. Cohen, and H. Colman. 2017. "Glioma Subclassifications and Their Clinical Significance." *Neurotherapeutics* 14 (2):284-297. doi: 10.1007/s13311-017-0519-x.

Chen, R., M. Zhang, Y. Zhou, W. Guo, M. Yi, Z. Zhang, Y. Ding, and Y. Wang. 2020. "The application of histone deacetylases inhibitors in glioblastoma." *J Exp Clin Cancer Res* 39 (1):138. doi: 10.1186/s13046-020-01643-6.

Chen, S., C. Yin, T. Lao, D. Liang, D. He, C. Wang, and N. Sang. 2015. "AMPK-HDAC5 pathway facilitates nuclear accumulation of HIF-1alpha and functional activation of HIF-1 by deacetylating Hsp70 in the cytosol." *Cell Cycle* 14 (15):2520-36. doi: 10.1080/15384101.2015.1055426.

Cheng, H., Z. Xie, W. P. Jones, X. T. Wei, Z. Liu, D. Wang, S. K. Kulp, J. Wang, C. C. Coss, C. S. Chen, G. Marcucci, R. Garzon, J. M. Covey, M. A. Phelps, and K. K. Chan. 2016. "Preclinical Pharmacokinetics Study of R- and S-Enantiomers of the Histone Deacetylase Inhibitor, AR-42 (NSC 731438), in Rodents." *AAPS J* 18 (3):737-45. doi: 10.1208/s12248-016-9876-3.

Chiao, M. T., W. Y. Cheng, Y. C. Yang, C. C. Shen, and J. L. Ko. 2013. "Suberoylanilide hydroxamic acid (SAHA) causes tumor growth slowdown and triggers autophagy in glioblastoma stem cells." *Autophagy* 9 (10):1509-26. doi: 10.4161/auto.25664.

Chinnaiyan, P., D. Cerna, W. E. Burgan, K. Beam, E. S. Williams, K. Camphausen, and P. J. Tofilon. 2008. "Postradiation sensitization of the histone deacetylase inhibitor valproic acid." *Clin Cancer Res* 14 (17):5410-5. doi: 10.1158/1078-0432.CCR-08-0643.

Chinnaiyan, P., S. Chowdhary, L. Potthast, A. Prabhu, Y. Y. Tsai, B. Sarcar, S. Kahali, S. Brem, H. M. Yu, A. Rojiani, R. Murtagh, and E. Pan. 2012. "Phase I trial of vorinostat combined with bevacizumab and CPT-11 in recurrent glioblastoma." *Neuro Oncol* 14 (1):93-100. doi: 10.1093/neuonc/nor187.

Chou, C. J., D. Herman, and J. M. Gottesfeld. 2008. "Pimelic diphenylamide 106 is a slow, tight-binding inhibitor of class I histone deacetylases." *J Biol Chem* 283 (51):35402-9. doi: 10.1074/jbc.M807045200.

Christofori, G., and H. Semb. 1999. "The role of the cell-adhesion molecule E-cadherin as a tumour-suppressor gene." *Trends Biochem Sci* 24 (2):73-6. doi: 10.1016/s0968-0004(98)01343-7.

Chuikov, S., J. K. Kurash, J. R. Wilson, B. Xiao, N. Justin, G. S. Ivanov, K. McKinney, P. Tempst, C. Prives, S. J. Gamblin, N. A. Barlev, and D. Reinberg. 2004.

"Regulation of p53 activity through lysine methylation." *Nature* 432 (7015):353-60. doi: 10.1038/nature03117.

Cohen, M. H., Y. L. Shen, P. Keegan, and R. Pazdur. 2009. "FDA drug approval summary: bevacizumab (Avastin) as treatment of recurrent glioblastoma multiforme." *Oncologist* 14 (11):1131-8. doi: 10.1634/theoncologist.2009-0121.

Coniglio, S. J., E. Eugenin, K. Dobrenis, E. R. Stanley, B. L. West, M. H. Symons, and J. E. Segall. 2012. "Microglial stimulation of glioblastoma invasion involves epidermal growth factor receptor (EGFR) and colony stimulating factor 1 receptor (CSF-1R) signaling." *Mol Med* 18:519-27. doi: 10.2119/molmed.2011.00217.

Dali-Youcef, N., S. Froelich, F. M. Moussallieh, S. Chibbaro, G. Noel, I. J. Namer, S. Heikkinen, and J. Auwerx. 2015. "Gene expression mapping of histone deacetylases and co-factors, and correlation with survival time and 1H-HRMAS metabolomic profile in human gliomas." *Sci Rep* 5:9087. doi: 10.1038/srep09087.

Davis, M. E. 2016. "Glioblastoma: Overview of Disease and Treatment." *Clin J Oncol Nurs* 20 (5 Suppl):S2-8. doi: 10.1188/16.CJON.S1.2-8.

Dawson, M. A., and T. Kouzarides. 2012. "Cancer epigenetics: from mechanism to therapy." *Cell* 150 (1):12-27. doi: 10.1016/j.cell.2012.06.013.

de la Iglesia, N., S. V. Puram, and A. Bonni. 2009. "STAT3 regulation of glioblastoma pathogenesis." *Curr Mol Med* 9 (5):580-90. doi: 10.2174/156652409788488739.

de Ruijter, A. J., A. H. van Gennip, H. N. Caron, S. Kemp, and A. B. van Kuilenburg. 2003. "Histone deacetylases (HDACs): characterization of the classical HDAC family." *Biochem J* 370 (Pt 3):737-49. doi: 10.1042/BJ20021321.

Deardorff, M. A., M. Bando, R. Nakato, E. Watrin, T. Itoh, M. Minamino, K. Saitoh, M. Komata, Y. Katou, D. Clark, K. E. Cole, E. De Baere, C. Decroos, N. Di Donato, S. Ernst, L. J. Francey, Y. Gyftodimou, K. Hirashima, M. Hullings, Y. Ishikawa, C. Jaulin, M. Kaur, T. Kiyono, P. M. Lombardi, L. Magnaghi-Jaulin, G. R. Mortier, N. Nozaki, M. B. Petersen, H. Seimiya, V. M. Siu, Y. Suzuki, K. Takagaki, J. J. Wilde, P. J. Willems, C. Prigent, G. Gillessen-Kaesbach, D. W. Christianson, F. J. Kaiser, L. G. Jackson, T. Hirota, I. D. Krantz, and K. Shirahige. 2012. "HDAC8 mutations in Cornelia de Lange syndrome affect the cohesin acetylation cycle." *Nature* 489 (7415):313-7. doi: 10.1038/nature11316.

Decleves, X., A. Amiel, J. Y. Delattre, and J. M. Scherrmann. 2006. "Role of ABC transporters in the chemoresistance of human gliomas." *Curr Cancer Drug Targets* 6 (5):433-45. doi: 10.2174/156800906777723930.

Degorre, C., P. Tofilon, K. Camphausen, and P. Mathen. 2021. "Bench to bedside radiosensitizer development strategy for newly diagnosed glioblastoma." *Radiat Oncol* 16 (1):191. doi: 10.1186/s13014-021-01918-y.

Diss, E., N. Nalabothula, D. Nguyen, E. Chang, Y. Kwok, and F. Carrier. 2014. "Vorinostat(SAHA) Promotes Hyper-Radiosensitivity in Wild Type p53 Human Glioblastoma Cells." *J Clin Oncol Res* 2 (1).

Dobin, A., C. A. Davis, F. Schlesinger, J. Drenkow, C. Zaleski, S. Jha, P. Batut, M. Chaisson, and T. R. Gingeras. 2013. "STAR: ultrafast universal RNA-seq aligner." *Bioinformatics* 29 (1):15-21. doi: 10.1093/bioinformatics/bts635.

Dovey, O. M., C. T. Foster, and S. M. Cowley. 2010. "Histone deacetylase 1 (HDAC1), but not HDAC2, controls embryonic stem cell differentiation." *Proc Natl Acad Sci U S A* 107 (18):8242-7. doi: 10.1073/pnas.1000478107.

Eckerich, C., S. Zapf, R. Fillbrandt, S. Loges, M. Westphal, and K. Lamszus. 2007. "Hypoxia can induce c-Met expression in glioma cells and enhance SF/HGF-induced cell migration." *Int J Cancer* 121 (2):276-83. doi: 10.1002/ijc.22679.

Eckschlager, T., J. Plch, M. Stiborova, and J. Hrabeta. 2017. "Histone Deacetylase Inhibitors as Anticancer Drugs." *Int J Mol Sci* 18 (7). doi: 10.3390/ijms18071414.

Eisenstat, D. D., J. K. Liu, M. Mione, W. Zhong, G. Yu, S. A. Anderson, I. Ghattas, L. Puelles, and J. L. Rubenstein. 1999. "DLX-1, DLX-2, and DLX-5 expression define distinct stages of basal forebrain differentiation." *J Comp Neurol* 414 (2):217-37. doi: 10.1002/(sici)1096-9861(19991115)414:2<217::aid-cne6>3.0.co;2-i.

Eleutherakis-Papaiakovou, E., N. Kanellias, E. Kastritis, M. Gavriatopoulou, E. Terpos, and M. A. Dimopoulos. 2020. "Efficacy of Panobinostat for the Treatment of Multiple Myeloma." *J Oncol* 2020:7131802. doi: 10.1155/2020/7131802.

Elston, R., and G. J. Inman. 2012. "Crosstalk between p53 and TGF-beta Signalling." *J Signal Transduct* 2012:294097. doi: 10.1155/2012/294097.

Emmett, M. J., and M. A. Lazar. 2019. "Integrative regulation of physiology by histone deacetylase 3." *Nat Rev Mol Cell Biol* 20 (2):102-115. doi: 10.1038/s41580-018-0076-0.

Eyupoglu, I. Y., E. Hahnen, R. Buslei, F. A. Siebzehnrubl, N. E. Savaskan, M. Luders, C. Trankle, W. Wick, M. Weller, R. Fahlbusch, and I. Blumcke. 2005. "Suberoylanilide hydroxamic acid (SAHA) has potent anti-glioma properties in vitro, ex vivo and in vivo." *J Neurochem* 93 (4):992-9. doi: 10.1111/j.1471-4159.2005.03098.x.

Eyupoglu, I. Y., E. Hahnen, A. Heckel, F. A. Siebzehnrubl, R. Buslei, R. Fahlbusch, and I. Blumcke. 2005. "Malignant glioma-induced neuronal cell death in an organotypic glioma invasion model. Technical note." *J Neurosurg* 102 (4):738-44. doi: 10.3171/jns.2005.102.4.0738.

Falkenberg, K. J., and R. W. Johnstone. 2014. "Histone deacetylases and their inhibitors in cancer, neurological diseases and immune disorders." *Nat Rev Drug Discov* 13 (9):673-91. doi: 10.1038/nrd4360.

Fedele, M., L. Cerchia, S. Pegoraro, R. Sgarra, and G. Manfioletti. 2019. "Proneural-Mesenchymal Transition: Phenotypic Plasticity to Acquire Multitherapy Resistance in Glioblastoma." *Int J Mol Sci* 20 (11). doi: 10.3390/ijms20112746.

Fisher, J. P., and D. C. Adamson. 2021. "Current FDA-Approved Therapies for High-Grade Malignant Gliomas." *Biomedicines* 9 (3). doi: 10.3390/biomedicines9030324.

Frye, R., M. Myers, K. C. Axelrod, E. A. Ness, R. L. Piekarz, S. E. Bates, and S. Booher. 2012. "Romidepsin: a new drug for the treatment of cutaneous T-cell lymphoma." *Clin J Oncol Nurs* 16 (2):195-204. doi: 10.1188/12.CJON.195-204.

Fujimoto, M., D. W. Fults, G. A. Thomas, Y. Nakamura, M. P. Heilbrun, R. White, J. L. Story, S. L. Naylor, K. S. Kagan-Hallet, and P. J. Sheridan. 1989. "Loss of heterozygosity on chromosome 10 in human glioblastoma multiforme." *Genomics* 4 (2):210-4. doi: 10.1016/0888-7543(89)90302-9.

Fyodorov, D. V., B. R. Zhou, A. I. Skoultchi, and Y. Bai. 2018. "Emerging roles of linker histones in regulating chromatin structure and function." *Nat Rev Mol Cell Biol* 19 (3):192-206. doi: 10.1038/nrm.2017.94.

Galanis, E., S. K. Anderson, C. R. Miller, J. N. Sarkaria, K. Jaeckle, J. C. Buckner, K. L. Ligon, K. V. Ballman, D. F. Moore, Jr., M. Nebozhyn, A. Loboda, D. Schiff, M. S. Ahluwalia, E. Q. Lee, E. R. Gerstner, G. J. Lesser, M. Prados, S. A. Grossman, J. Cerhan, C. Giannini, P. Y. Wen, Oncology Alliance for Clinical Trials in, and Abtc. 2018. "Phase I/II trial of vorinostat combined with temozolomide and radiation therapy for newly diagnosed glioblastoma: results of Alliance N0874/ABTC 02." *Neuro Oncol* 20 (4):546-556. doi: 10.1093/neuonc/nox161.

Galanis, E., K. A. Jaeckle, M. J. Maurer, J. M. Reid, M. M. Ames, J. S. Hardwick, J. F. Reilly, A. Loboda, M. Nebozhyn, V. R. Fantin, V. M. Richon, B. Scheithauer, C. Giannini, P. J. Flynn, D. F. Moore, Jr., J. Zwiebel, and J. C. Buckner. 2009. "Phase II trial of vorinostat in recurrent glioblastoma multiforme: a north central cancer treatment group study." *J Clin Oncol* 27 (12):2052-8. doi: 10.1200/JCO.2008.19.0694.

Gan, H. K., A. H. Kaye, and R. B. Luwor. 2009. "The EGFRvIII variant in glioblastoma multiforme." *J Clin Neurosci* 16 (6):748-54. doi: 10.1016/j.jocn.2008.12.005.

Gao, L., M. A. Cueto, F. Asselbergs, and P. Atadja. 2002. "Cloning and functional characterization of HDAC11, a novel member of the human histone deacetylase family." *J Biol Chem* 277 (28):25748-55. doi: 10.1074/jbc.M111871200.

Gaymes, T. J., R. A. Padua, M. Pla, S. Orr, N. Omidvar, C. Chomienne, G. J. Mufti, and F. V. Rassool. 2006. "Histone deacetylase inhibitors (HDI) cause DNA damage in leukemia cells: a mechanism for leukemia-specific HDI-dependent apoptosis?" *Mol Cancer Res* 4 (8):563-73. doi: 10.1158/1541-7786.MCR-06-0111.

Geng, H., C. T. Harvey, J. Pittsenbarger, Q. Liu, T. M. Beer, C. Xue, and D. Z. Qian. 2011. "HDAC4 protein regulates HIF1alpha protein lysine acetylation and cancer cell response to hypoxia." *J Biol Chem* 286 (44):38095-38102. doi: 10.1074/jbc.M111.257055.

Ghiaseddin, A., D. Reardon, W. Massey, A. Mannerino, E. S. Lipp, J. E. Herndon, 2nd, F. McSherry, A. Desjardins, D. Randazzo, H. S. Friedman, and K. B. Peters. 2018. "Phase II Study of Bevacizumab and Vorinostat for Patients with Recurrent World Health Organization Grade 4 Malignant Glioma." *Oncologist* 23 (2):157-e21. doi: 10.1634/theoncologist.2017-0501.

Gimple, R. C., S. Bhargava, D. Dixit, and J. N. Rich. 2019. "Glioblastoma stem cells: lessons from the tumor hierarchy in a lethal cancer." *Genes Dev* 33 (11-12):591-609. doi: 10.1101/gad.324301.119.

Glozak, M. A., and E. Seto. 2007. "Histone deacetylases and cancer." *Oncogene* 26 (37):5420-32. doi: 10.1038/sj.onc.1210610.

Godlewski, J., M. O. Nowicki, A. Bronisz, S. Williams, A. Otsuki, G. Nuovo, A. Raychaudhury, H. B. Newton, E. A. Chiocca, and S. Lawler. 2008. "Targeting of the Bmi-1 oncogene/stem cell renewal factor by microRNA-128 inhibits glioma proliferation and self-renewal." *Cancer Res* 68 (22):9125-30. doi: 10.1158/0008-5472.CAN-08-2629.

Gonzalez, D., S. Schmidt, and H. Derendorf. 2013. "Importance of relating efficacy measures to unbound drug concentrations for anti-infective agents." *Clin Microbiol Rev* 26 (2):274-88. doi: 10.1128/CMR.00092-12.

Gorgoulis, V. G., P. Zacharatos, A. Kotsinas, D. Kletsas, G. Mariatos, V. Zoumpourlis, K. M. Ryan, C. Kittas, and A. G. Papavassiliou. 2003. "p53 activates ICAM-1 (CD54) expression in an NF-kappaB-independent manner." *EMBO J* 22 (7):1567-78. doi: 10.1093/emboj/cdg157.

Gregoretti, I. V., Y. M. Lee, and H. V. Goodson. 2004. "Molecular evolution of the histone deacetylase family: functional implications of phylogenetic analysis." *J Mol Biol* 338 (1):17-31. doi: 10.1016/j.jmb.2004.02.006.

Groselj, B., N. L. Sharma, F. C. Hamdy, M. Kerr, and A. E. Kiltie. 2013. "Histone deacetylase inhibitors as radiosensitisers: effects on DNA damage signalling and repair." *Br J Cancer* 108 (4):748-54. doi: 10.1038/bjc.2013.21.

Gryder, B. E., Q. H. Sodji, and A. K. Oyelere. 2012. "Targeted cancer therapy: giving histone deacetylase inhibitors all they need to succeed." *Future Med Chem* 4 (4):505-24. doi: 10.4155/fmc.12.3.

Haberland, M., R. L. Montgomery, and E. N. Olson. 2009. "The many roles of histone deacetylases in development and physiology: implications for disease and therapy." *Nat Rev Genet* 10 (1):32-42. doi: 10.1038/nrg2485.

Haddad, A. F., J. S. Young, D. Amara, M. S. Berger, D. R. Raleigh, M. K. Aghi, and N. A. Butowski. 2021. "Mouse models of glioblastoma for the evaluation of novel therapeutic strategies." *Neurooncol Adv* 3 (1):vdab100. doi: 10.1093/noajnl/vdab100.

Haftchenary, S., H. A. Luchman, A. O. Jouk, A. J. Veloso, B. D. Page, X. R. Cheng, S. S. Dawson, N. Grinshtein, V. M. Shahani, K. Kerman, D. R. Kaplan, C. Griffin, A. M. Aman, R. Al-Awar, S. Weiss, and P. T. Gunning. 2013. "Potent Targeting of the STAT3 Protein in Brain Cancer Stem Cells: A Promising Route for Treating Glioblastoma." *ACS Med Chem Lett* 4 (11):1102-7. doi: 10.1021/ml4003138.

Hagelkruys, A., S. Lagger, J. Krahmer, A. Leopoldi, M. Artaker, O. Pusch, J. Zezula, S. Weissmann, Y. Xie, C. Schofer, M. Schlederer, G. Brosch, P. Matthias, J. Selfridge, H. Lassmann, J. A. Knoblich, and C. Seiser. 2014. "A single allele of Hdac2 but not Hdac1 is sufficient for normal mouse brain development in the absence of its paralog." *Development* 141 (3):604-616. doi: 10.1242/dev.100487.

Hai, Y., S. A. Shinsky, N. J. Porter, and D. W. Christianson. 2017. "Histone deacetylase 10 structure and molecular function as a polyamine deacetylase." *Nat Commun* 8:15368. doi: 10.1038/ncomms15368.

Hajra, K. M., and E. R. Fearon. 2002. "Cadherin and catenin alterations in human cancer." *Genes Chromosomes Cancer* 34 (3):255-68. doi: 10.1002/gcc.10083.

Hambardzumyan, D., D. H. Gutmann, and H. Kettenmann. 2016. "The role of microglia and macrophages in glioma maintenance and progression." *Nat Neurosci* 19 (1):20-7. doi: 10.1038/nn.4185.

Hancock, W. W., T. Akimova, U. H. Beier, Y. Liu, and L. Wang. 2012. "HDAC inhibitor therapy in autoimmunity and transplantation." *Ann Rheum Dis* 71 Suppl 2:i46-54. doi: 10.1136/annrheumdis-2011-200593.

Hansen, W. K., and M. R. Kelley. 2000. "Review of mammalian DNA repair and translational implications." *J Pharmacol Exp Ther* 295 (1):1-9.

Happold, C., T. Gorlia, O. Chinot, M. R. Gilbert, L. B. Nabors, W. Wick, S. L. Pugh, M. Hegi, T. Cloughesy, P. Roth, D. A. Reardon, J. R. Perry, M. P. Mehta, R. Stupp, and M. Weller. 2016. "Does Valproic Acid or Levetiracetam Improve Survival in Glioblastoma? A Pooled Analysis of Prospective Clinical Trials in Newly Diagnosed Glioblastoma." *J Clin Oncol* 34 (7):731-9. doi: 10.1200/JCO.2015.63.6563.

Haronikova, L., V. Olivares-Illana, L. Wang, K. Karakostis, S. Chen, and R. Fahraeus. 2019. "The p53 mRNA: an integral part of the cellular stress response." *Nucleic Acids Res* 47 (7):3257-3271. doi: 10.1093/nar/gkz124.

Hassig, C. A., T. C. Fleischer, A. N. Billin, S. L. Schreiber, and D. E. Ayer. 1997. "Histone deacetylase activity is required for full transcriptional repression by mSin3A." *Cell* 89 (3):341-7. doi: 10.1016/s0092-8674(00)80214-7.

Heddleston, J. M., Z. Li, R. E. McLendon, A. B. Hjelmeland, and J. N. Rich. 2009. "The hypoxic microenvironment maintains glioblastoma stem cells and promotes reprogramming towards a cancer stem cell phenotype." *Cell Cycle* 8 (20):3274-84. doi: 10.4161/cc.8.20.9701.

Hegi, M. E., A. C. Diserens, T. Gorlia, M. F. Hamou, N. de Tribolet, M. Weller, J. M. Kros, J. A. Hainfellner, W. Mason, L. Mariani, J. E. Bromberg, P. Hau, R. O. Mirimanoff, J. G. Cairncross, R. C. Janzer, and R. Stupp. 2005. "MGMT gene silencing and benefit from temozolomide in glioblastoma." *N Engl J Med* 352 (10):997-1003. doi: 10.1056/NEJMoa043331.

Hemmati, H. D., I. Nakano, J. A. Lazareff, M. Masterman-Smith, D. H. Geschwind, M. Bronner-Fraser, and H. I. Kornblum. 2003. "Cancerous stem cells can arise from pediatric brain tumors." *Proc Natl Acad Sci U S A* 100 (25):15178-83. doi: 10.1073/pnas.2036535100.

Hennika, T., G. Hu, N. G. Olaciregui, K. L. Barton, A. Ehteda, A. Chitranjan, C. Chang, A. J. Gifford, M. Tsoli, D. S. Ziegler, A. M. Carcaboso, and O. J. Becher. 2017. "Pre-Clinical Study of Panobinostat in Xenograft and Genetically Engineered Murine Diffuse Intrinsic Pontine Glioma Models." *PLoS One* 12 (1):e0169485. doi: 10.1371/journal.pone.0169485.

Henrik Heiland, D., V. M. Ravi, S. P. Behringer, J. H. Frenking, J. Wurm, K. Joseph, N. W. C. Garrelfs, J. Strahle, S. Heynckes, J. Grauvogel, P. Franco, I. Mader, M. Schneider, A. L. Potthoff, D. Delev, U. G. Hofmann, C. Fung, J. Beck, R. Sankowski, M. Prinz, and O. Schnell. 2019. "Tumor-associated reactive astrocytes aid the evolution of immunosuppressive environment in glioblastoma." *Nat Commun* 10 (1):2541. doi: 10.1038/s41467-019-10493-6.

Hermant, P., D. Bosc, C. Piveteau, R. Gealageas, B. Lam, C. Ronco, M. Roignant, H. Tolojanahary, L. Jean, P. Y. Renard, M. Lemdani, M. Bourotte, A. Herledan, C. Bedart, A. Biela, F. Leroux, B. Deprez, and R. Deprez-Poulain. 2017.

"Controlling Plasma Stability of Hydroxamic Acids: A MedChem Toolbox." *J Med Chem* 60 (21):9067-9089. doi: 10.1021/acs.jmedchem.7b01444.

Hirschmann-Jax, C., A. E. Foster, G. G. Wulf, J. G. Nuchtern, T. W. Jax, U. Gobel, M. A. Goodell, and M. K. Brenner. 2004. "A distinct "side population" of cells with high drug efflux capacity in human tumor cells." *Proc Natl Acad Sci U S A* 101 (39):14228-33. doi: 10.1073/pnas.0400067101.

Ho, T. C. S., A. H. Y. Chan, and A. Ganesan. 2020. "Thirty Years of HDAC Inhibitors: 2020 Insight and Hindsight." *J Med Chem* 63 (21):12460-12484. doi: 10.1021/acs.jmedchem.0c00830.

Hochberg, F. H., R. Linggood, L. Wolfson, W. H. Baker, and P. Kornblith. 1979. "Quality and duration of survival in glioblastoma multiforme. Combined surgical, radiation, and lomustine therapy." *JAMA* 241 (10):1016-8.

Holland, E. C. 2000. "Glioblastoma multiforme: the terminator." *Proc Natl Acad Sci U S A* 97 (12):6242-4. doi: 10.1073/pnas.97.12.6242.

Hooker, J. M., S. W. Kim, D. Alexoff, Y. Xu, C. Shea, A. Reid, N. Volkow, and J. S. Fowler. 2010. "Histone deacetylase inhibitor, MS-275, exhibits poor brain penetration: PK studies of [C]MS-275 using Positron Emission Tomography." *ACS Chem Neurosci* 1 (1):65-73. doi: 10.1021/cn9000268.

Hou, L. C., A. Veeravagu, A. R. Hsu, and V. C. Tse. 2006. "Recurrent glioblastoma multiforme: a review of natural history and management options." *Neurosurg Focus* 20 (4):E5. doi: 10.3171/foc.2006.20.4.2.

Householder, K. T., D. M. DiPerna, E. P. Chung, A. R. Luning, D. T. Nguyen, S. E. Stabenfeldt, S. Mehta, and R. W. Sirianni. 2018. "pH driven precipitation of quisinostat onto PLA-PEG nanoparticles enables treatment of intracranial glioblastoma." *Colloids Surf B Biointerfaces* 166:37-44. doi: 10.1016/j.colsurfb.2018.02.048.

Hu, B., P. Guo, I. Bar-Joseph, Y. Imanishi, M. J. Jarzynka, O. Bogler, T. Mikkelsen, T. Hirose, R. Nishikawa, and S. Y. Cheng. 2007. "Neuropilin-1 promotes human glioma progression through potentiating the activity of the HGF/SF autocrine pathway." *Oncogene* 26 (38):5577-86. doi: 10.1038/sj.onc.1210348.

Hwang, C. I., A. Matoso, D. C. Corney, A. Flesken-Nikitin, S. Korner, W. Wang, C. Boccaccio, S. S. Thorgeirsson, P. M. Comoglio, H. Hermeking, and A. Y. Nikitin. 2011. "Wild-type p53 controls cell motility and invasion by dual regulation of MET expression." *Proc Natl Acad Sci U S A* 108 (34):14240-5. doi: 10.1073/pnas.1017536108.

Ibrahim, N., E. I. Buchbinder, S. R. Granter, S. J. Rodig, A. Giobbie-Hurder, C. Becerra, A. Tsiaras, E. Gjini, D. E. Fisher, and F. S. Hodi. 2016. "A phase I trial of

panobinostat (LBH589) in patients with metastatic melanoma." *Cancer Med* 5 (11):3041-3050. doi: 10.1002/cam4.862.

Icardi, L., R. Mori, V. Gesellchen, S. Eyckerman, L. De Cauwer, J. Verhelst, K. Vercauteren, X. Saelens, P. Meuleman, G. Leroux-Roels, K. De Bosscher, M. Boutros, and J. Tavernier. 2012. "The Sin3a repressor complex is a master regulator of STAT transcriptional activity." *Proc Natl Acad Sci U S A* 109 (30):12058-63. doi: 10.1073/pnas.1206458109.

Inoue, A., and D. Fujimoto. 1969. "Enzymatic deacetylation of histone." *Biochem Biophys Res Commun* 36 (1):146-50. doi: 10.1016/0006-291x(69)90661-5.

Ishihara, H., H. Kubota, R. L. Lindberg, D. Leppert, S. M. Gloor, M. Errede, D. Virgintino, A. Fontana, Y. Yonekawa, and K. Frei. 2008. "Endothelial cell barrier impairment induced by glioblastomas and transforming growth factor beta2 involves matrix metalloproteinases and tight junction proteins." *J Neuropathol Exp Neurol* 67 (5):435-48. doi: 10.1097/NEN.0b013e31816fd622.

Ito, A., Y. Kawaguchi, C. H. Lai, J. J. Kovacs, Y. Higashimoto, E. Appella, and T. P. Yao. 2002. "MDM2-HDAC1-mediated deacetylation of p53 is required for its degradation." *EMBO J* 21 (22):6236-45. doi: 10.1093/emboj/cdf616.

Ito, A., C. H. Lai, X. Zhao, S. Saito, M. H. Hamilton, E. Appella, and T. P. Yao. 2001. "p300/CBP-mediated p53 acetylation is commonly induced by p53-activating agents and inhibited by MDM2." *EMBO J* 20 (6):1331-40. doi: 10.1093/emboj/20.6.1331.

Ivanov, G. S., T. Ivanova, J. Kurash, A. Ivanov, S. Chuikov, F. Gizatullin, E. M. Herrera-Medina, F. Rauscher, 3rd, D. Reinberg, and N. A. Barlev. 2007. "Methylation-acetylation interplay activates p53 in response to DNA damage." *Mol Cell Biol* 27 (19):6756-69. doi: 10.1128/MCB.00460-07.

Iwamoto, F. M., K. R. Lamborn, J. G. Kuhn, P. Y. Wen, W. K. Yung, M. R. Gilbert, S. M. Chang, F. S. Lieberman, M. D. Prados, and H. A. Fine. 2011. "A phase I/II trial of the histone deacetylase inhibitor romidepsin for adults with recurrent malignant glioma: North American Brain Tumor Consortium Study 03-03." *Neuro Oncol* 13 (5):509-16. doi: 10.1093/neuonc/nor017.

Jain, K. K. 2018. "A Critical Overview of Targeted Therapies for Glioblastoma." *Front Oncol* 8:419. doi: 10.3389/fonc.2018.00419.

Jamaladdin, S., R. D. Kelly, L. O'Regan, O. M. Dovey, G. E. Hodson, C. J. Millard, N. Portolano, A. M. Fry, J. W. Schwabe, and S. M. Cowley. 2014. "Histone deacetylase (HDAC) 1 and 2 are essential for accurate cell division and the pluripotency of embryonic stem cells." *Proc Natl Acad Sci U S A* 111 (27):9840-5. doi: 10.1073/pnas.1321330111.

Janjua, T. I., P. Rewatkar, A. Ahmed-Cox, I. Saeed, F. M. Mansfeld, R. Kulshreshtha, T. Kumeria, D. S. Ziegler, M. Kavallaris, R. Mazzieri, and A. Popat. 2021. "Frontiers in the treatment of glioblastoma: Past, present and emerging." *Adv Drug Deliv Rev* 171:108-138. doi: 10.1016/j.addr.2021.01.012.

Jenke, R., N. Ressing, F. K. Hansen, A. Aigner, and T. Buch. 2021. "Anticancer Therapy with HDAC Inhibitors: Mechanism-Based Combination Strategies and Future Perspectives." *Cancers (Basel)* 13 (4). doi: 10.3390/cancers13040634.

Jensen, K. V., O. Cseh, A. Aman, S. Weiss, and H. A. Luchman. 2017. "The JAK2/STAT3 inhibitor pacritinib effectively inhibits patient-derived GBM brain tumor initiating cells in vitro and when used in combination with temozolomide increases survival in an orthotopic xenograft model." *PLoS One* 12 (12):e0189670. doi: 10.1371/journal.pone.0189670.

Jenuwein, T., and C. D. Allis. 2001. "Translating the histone code." *Science* 293 (5532):1074-80. doi: 10.1126/science.1063127.

Juan, L. J., W. J. Shia, M. H. Chen, W. M. Yang, E. Seto, Y. S. Lin, and C. W. Wu. 2000. "Histone deacetylases specifically down-regulate p53-dependent gene activation." *J Biol Chem* 275 (27):20436-43. doi: 10.1074/jbc.M000202200.

Jurkin, J., G. Zupkovitz, S. Lagger, R. Grausenburger, A. Hagelkruys, L. Kenner, and C. Seiser. 2011. "Distinct and redundant functions of histone deacetylases HDAC1 and HDAC2 in proliferation and tumorigenesis." *Cell Cycle* 10 (3):406-12. doi: 10.4161/cc.10.3.14712.

Kachhap, S. K., N. Rosmus, S. J. Collis, M. S. Kortenhorst, M. D. Wissing, M. Hedayati, S. Shabbeer, J. Mendonca, J. Deangelis, L. Marchionni, J. Lin, N. Hoti, J. W. Nortier, T. L. DeWeese, H. Hammers, and M. A. Carducci. 2010. "Downregulation of homologous recombination DNA repair genes by HDAC inhibition in prostate cancer is mediated through the E2F1 transcription factor." *PLoS One* 5 (6):e11208. doi: 10.1371/journal.pone.0011208.

Kaina, B., and M. Christmann. 2002. "DNA repair in resistance to alkylating anticancer drugs." *Int J Clin Pharmacol Ther* 40 (8):354-67. doi: 10.5414/cpp40354.

Kaiser, A. M., J. C. Kang, L. S. Chan, P. Vukasin, and R. W. Beart, Jr. 2004. "Laparoscopic-assisted vs. open colectomy for colon cancer: a prospective randomized trial." *J Laparoendosc Adv Surg Tech A* 14 (6):329-34. doi: 10.1089/lap.2004.14.329.

Kamat, M., B. D. Rai, R. S. Puranik, and U. V. Datar. 2019. "A comprehensive review of surgical margin in oral squamous cell carcinoma highlighting the significance of tumor-free surgical margins." *J Cancer Res Ther* 15 (3):449-454. doi: 10.4103/jcrt.JCRT_273_17.

Kang, Y., H. Nian, P. Rajendran, E. Kim, W. M. Dashwood, J. T. Pinto, L. A. Boardman, S. N. Thibodeau, P. J. Limburg, C. V. Lohr, W. H. Bisson, D. E. Williams, E. Ho, and R. H. Dashwood. 2014. "HDAC8 and STAT3 repress BMF gene activity in colon cancer cells." *Cell Death Dis* 5:e1476. doi: 10.1038/cddis.2014.422.

Karagiannis, T. C., and A. El-Osta. 2006. "Modulation of cellular radiation responses by histone deacetylase inhibitors." *Oncogene* 25 (28):3885-93. doi: 10.1038/sj.onc.1209417.

Karran, P., and M. Bignami. 1992. "Self-destruction and tolerance in resistance of mammalian cells to alkylation damage." *Nucleic Acids Res* 20 (12):2933-40. doi: 10.1093/nar/20.12.2933.

Kato, H., S. Tamamizu-Kato, and F. Shibasaki. 2004. "Histone deacetylase 7 associates with hypoxia-inducible factor 1alpha and increases transcriptional activity." *J Biol Chem* 279 (40):41966-74. doi: 10.1074/jbc.M406320200.

Kelly, R. D., and S. M. Cowley. 2013. "The physiological roles of histone deacetylase (HDAC) 1 and 2: complex co-stars with multiple leading parts." *Biochem Soc Trans* 41 (3):741-9. doi: 10.1042/BST20130010.

Kerkhof, M., J. C. Dielemans, M. S. van Breemen, H. Zwinkels, R. Walchenbach, M. J. Taphoorn, and C. J. Vecht. 2013. "Effect of valproic acid on seizure control and on survival in patients with glioblastoma multiforme." *Neuro Oncol* 15 (7):961-7. doi: 10.1093/neuonc/not057.

Kesanakurti, D., C. Chetty, D. Rajasekhar Maddirela, M. Gujrati, and J. S. Rao. 2013. "Essential role of cooperative NF-kappaB and Stat3 recruitment to ICAM-1 intronic consensus elements in the regulation of radiation-induced invasion and migration in glioma." *Oncogene* 32 (43):5144-55. doi: 10.1038/onc.2012.546.

Kessaris, N., M. Fogarty, P. Iannarelli, M. Grist, M. Wegner, and W. D. Richardson. 2006. "Competing waves of oligodendrocytes in the forebrain and postnatal elimination of an embryonic lineage." *Nat Neurosci* 9 (2):173-9. doi: 10.1038/nn1620.

Khaddour, K., T. M. Johanns, and G. Ansstas. 2020. "The Landscape of Novel Therapeutics and Challenges in Glioblastoma Multiforme: Contemporary State and Future Directions." *Pharmaceuticals (Basel)* 13 (11). doi: 10.3390/ph13110389.

Khan, O., and N. B. La Thangue. 2012. "HDAC inhibitors in cancer biology: emerging mechanisms and clinical applications." *Immunol Cell Biol* 90 (1):85-94. doi: 10.1038/icb.2011.100.

Kim, E., M. Kim, D. H. Woo, Y. Shin, J. Shin, N. Chang, Y. T. Oh, H. Kim, J. Rheey, I. Nakano, C. Lee, K. M. Joo, J. N. Rich, D. H. Nam, and J. Lee. 2013.

"Phosphorylation of EZH2 activates STAT3 signaling via STAT3 methylation and promotes tumorigenicity of glioblastoma stem-like cells." *Cancer Cell* 23 (6):839-52. doi: 10.1016/j.ccr.2013.04.008.

Kim, G. C., H. K. Kwon, C. G. Lee, R. Verma, D. Rudra, T. Kim, K. Kang, J. H. Nam, Y. Kim, and S. H. Im. 2018. "Upregulation of Ets1 expression by NFATc2 and NFKB1/RELA promotes breast cancer cell invasiveness." *Oncogenesis* 7 (11):91. doi: 10.1038/s41389-018-0101-3.

Kim, H. J., and S. C. Bae. 2011. "Histone deacetylase inhibitors: molecular mechanisms of action and clinical trials as anti-cancer drugs." *Am J Transl Res* 3 (2):166-79.

Kim, J. H., J. H. Shin, and I. H. Kim. 2004. "Susceptibility and radiosensitization of human glioblastoma cells to trichostatin A, a histone deacetylase inhibitor." *Int J Radiat Oncol Biol Phys* 59 (4):1174-80. doi: 10.1016/j.ijrobp.2004.03.001.

Kim, J. K., J. H. Noh, J. W. Eun, K. H. Jung, H. J. Bae, Q. Shen, M. G. Kim, Y. G. Chang, S. J. Kim, W. S. Park, J. Y. Lee, J. Borlak, and S. W. Nam. 2013. "Targeted inactivation of HDAC2 restores p16INK4a activity and exerts antitumor effects on human gastric cancer." *Mol Cancer Res* 11 (1):62-73. doi: 10.1158/1541-7786.MCR-12-0332.

Kim, M. J., J. S. Lee, S. E. Park, H. J. Yi, I. G. Jeong, J. S. Kang, J. Yun, J. Y. Lee, S. Ro, J. S. Lee, E. K. Choi, J. J. Hwang, and C. S. Kim. 2015. "Combination treatment of renal cell carcinoma with belinostat and 5-fluorouracil: a role for oxidative stress induced DNA damage and HSP90 regulated thymidine synthase." *J Urol* 193 (5):1660-8. doi: 10.1016/j.juro.2014.11.091.

Kim, S. H., K. Joshi, R. Ezhilarasan, T. R. Myers, J. Siu, C. Gu, M. Nakano-Okuno, D. Taylor, M. Minata, E. P. Sulman, J. Lee, K. P. Bhat, A. E. Salcini, and I. Nakano. 2015. "EZH2 protects glioma stem cells from radiation-induced cell death in a MELK/FOXM1-dependent manner." *Stem Cell Reports* 4 (2):226-38. doi: 10.1016/j.stemcr.2014.12.006.

Kinders, R., R. E. Parchment, J. Ji, S. Kummar, A. J. Murgo, M. Gutierrez, J. Collins, L. Rubinstein, O. Pickeral, S. M. Steinberg, S. Yang, M. Hollingshead, A. Chen, L. Helman, R. Wiltrout, M. Simpson, J. E. Tomaszewski, and J. H. Doroshow. 2007. "Phase 0 clinical trials in cancer drug development: from FDA guidance to clinical practice." *Mol Interv* 7 (6):325-34. doi: 10.1124/mi.7.6.9.

Kizilbash, S. H., S. K. Gupta, K. E. Parrish, J. K. Laramy, M. Kim, G. Gampa, B. L. Carlson, K. K. Bakken, A. C. Mladek, M. A. Schroeder, P. A. Decker, W. F. Elmquist, and J. N. Sarkaria. 2021. "In Vivo Efficacy of Tesevatinib in EGFR-Amplified Patient-Derived Xenograft Glioblastoma Models May Be Limited by Tissue Binding and Compensatory Signaling." *Mol Cancer Ther* 20 (6):1009-1018. doi: 10.1158/1535-7163.MCT-20-0640.

Kondo, Y., K. Katsushima, F. Ohka, A. Natsume, and K. Shinjo. 2014. "Epigenetic dysregulation in glioma." *Cancer Sci* 105 (4):363-9. doi: 10.1111/cas.12379.

Kong, X., Z. Lin, D. Liang, D. Fath, N. Sang, and J. Caro. 2006. "Histone deacetylase inhibitors induce VHL and ubiquitin-independent proteasomal degradation of hypoxia-inducible factor 1alpha." *Mol Cell Biol* 26 (6):2019-28. doi: 10.1128/MCB.26.6.2019-2028.2006.

Koprinarova, M., P. Botev, and G. Russev. 2011. "Histone deacetylase inhibitor sodium butyrate enhances cellular radiosensitivity by inhibiting both DNA nonhomologous end joining and homologous recombination." *DNA Repair (Amst)* 10 (9):970-7. doi: 10.1016/j.dnarep.2011.07.003.

Kovacs, J. J., P. J. Murphy, S. Gaillard, X. Zhao, J. T. Wu, C. V. Nicchitta, M. Yoshida, D. O. Toft, W. B. Pratt, and T. P. Yao. 2005. "HDAC6 regulates Hsp90 acetylation and chaperone-dependent activation of glucocorticoid receptor." *Mol Cell* 18 (5):601-7. doi: 10.1016/j.molcel.2005.04.021.

Krauze, A. V., S. D. Myrehaug, M. G. Chang, D. J. Holdford, S. Smith, J. Shih, P. J. Tofilon, H. A. Fine, and K. Camphausen. 2015. "A Phase 2 Study of Concurrent Radiation Therapy, Temozolomide, and the Histone Deacetylase Inhibitor Valproic Acid for Patients With Glioblastoma." *Int J Radiat Oncol Biol Phys* 92 (5):986-992. doi: 10.1016/j.ijrobp.2015.04.038.

Kreso, A., and J. E. Dick. 2014. "Evolution of the cancer stem cell model." *Cell Stem Cell* 14 (3):275-91. doi: 10.1016/j.stem.2014.02.006.

Kutateladze, T. G. 2011. "SnapShot: Histone readers." *Cell* 146 (5):842-842 e1. doi: 10.1016/j.cell.2011.08.022.

Kutil, Z., Z. Novakova, M. Meleshin, J. Mikesova, M. Schutkowski, and C. Barinka. 2018. "Histone Deacetylase 11 Is a Fatty-Acid Deacylase." *ACS Chem Biol* 13 (3):685-693. doi: 10.1021/acschembio.7b00942.

Lacroix, M., D. Abi-Said, D. R. Fourney, Z. L. Gokaslan, W. Shi, F. DeMonte, F. F. Lang, I. E. McCutcheon, S. J. Hassenbusch, E. Holland, K. Hess, C. Michael, D. Miller, and R. Sawaya. 2001. "A multivariate analysis of 416 patients with glioblastoma multiforme: prognosis, extent of resection, and survival." *J Neurosurg* 95 (2):190-8. doi: 10.3171/jns.2001.95.2.0190.

Lagger, G., D. O'Carroll, M. Rembold, H. Khier, J. Tischler, G. Weitzer, B. Schuettengruber, C. Hauser, R. Brunmeir, T. Jenuwein, and C. Seiser. 2002. "Essential function of histone deacetylase 1 in proliferation control and CDK inhibitor repression." *EMBO J* 21 (11):2672-81. doi: 10.1093/emboj/21.11.2672.

Laherty, C. D., W. M. Yang, J. M. Sun, J. R. Davie, E. Seto, and R. N. Eisenman. 1997. "Histone deacetylases associated with the mSin3 corepressor mediate mad

transcriptional repression." *Cell* 89 (3):349-56. doi: 10.1016/s0092-8674(00)80215-9.

Langfelder, P., and S. Horvath. 2008. "WGCNA: an R package for weighted correlation network analysis." *BMC Bioinformatics* 9:559. doi: 10.1186/1471-2105-9-559.

Lathia, J. D., S. C. Mack, E. E. Mulkearns-Hubert, C. L. Valentim, and J. N. Rich. 2015. "Cancer stem cells in glioblastoma." *Genes Dev* 29 (12):1203-17. doi: 10.1101/gad.261982.115.

Lee, D. H., H. W. Ryu, H. R. Won, and S. H. Kwon. 2017. "Advances in epigenetic glioblastoma therapy." *Oncotarget* 8 (11):18577-18589. doi: 10.18632/oncotarget.14612.

Lee, E. Q., D. A. Reardon, D. Schiff, J. Drappatz, A. Muzikansky, S. A. Grimm, A. D. Norden, L. Nayak, R. Beroukhim, M. L. Rinne, A. S. Chi, T. T. Batchelor, K. Hempfling, C. McCluskey, K. H. Smith, S. C. Gaffey, B. Wrigley, K. L. Ligon, J. J. Raizer, and P. Y. Wen. 2015. "Phase II study of panobinostat in combination with bevacizumab for recurrent glioblastoma and anaplastic glioma." *Neuro Oncol* 17 (6):862-7. doi: 10.1093/neuonc/nou350.

Lee, J. H., M. L. Choy, L. Ngo, S. S. Foster, and P. A. Marks. 2010. "Histone deacetylase inhibitor induces DNA damage, which normal but not transformed cells can repair." *Proc Natl Acad Sci U S A* 107 (33):14639-44. doi: 10.1073/pnas.1008522107.

Lee, J., S. Kotliarova, Y. Kotliarov, A. Li, Q. Su, N. M. Donin, S. Pastorino, B. W. Purow, N. Christopher, W. Zhang, J. K. Park, and H. A. Fine. 2006. "Tumor stem cells derived from glioblastomas cultured in bFGF and EGF more closely mirror the phenotype and genotype of primary tumors than do serum-cultured cell lines." *Cancer Cell* 9 (5):391-403. doi: 10.1016/j.ccr.2006.03.030.

Lee, J., M. J. Son, K. Woolard, N. M. Donin, A. Li, C. H. Cheng, S. Kotliarova, Y. Kotliarov, J. Walling, S. Ahn, M. Kim, M. Totonchy, T. Cusack, C. Ene, H. Ma, Q. Su, J. C. Zenklusen, W. Zhang, D. Maric, and H. A. Fine. 2008. "Epigenetic-mediated dysfunction of the bone morphogenetic protein pathway inhibits differentiation of glioblastoma-initiating cells." *Cancer Cell* 13 (1):69-80. doi: 10.1016/j.ccr.2007.12.005.

Lee, P., B. Murphy, R. Miller, V. Menon, N. L. Banik, P. Giglio, S. M. Lindhorst, A. K. Varma, W. A. Vandergrift, 3rd, S. J. Patel, and A. Das. 2015. "Mechanisms and clinical significance of histone deacetylase inhibitors: epigenetic glioblastoma therapy." *Anticancer Res* 35 (2):615-25.

Lee, S. F., and S. Pervaiz. 2011. "Assessment of oxidative stress-induced DNA damage by immunoflourescent analysis of 8-oxodG." *Methods Cell Biol* 103:99-113. doi: 10.1016/B978-0-12-385493-3.00005-X.

Li, G., Y. Tian, and W. G. Zhu. 2020. "The Roles of Histone Deacetylases and Their Inhibitors in Cancer Therapy." *Front Cell Dev Biol* 8:576946. doi: 10.3389/fcell.2020.576946.

Li, J., S. Chen, R. A. Cleary, R. Wang, O. J. Gannon, E. Seto, and D. D. Tang. 2014. "Histone deacetylase 8 regulates cortactin deacetylation and contraction in smooth muscle tissues." *Am J Physiol Cell Physiol* 307 (3):C288-95. doi: 10.1152/ajpcell.00102.2014.

Li, S., X. Chen, L. Mao, K. R. Zahid, J. Wen, L. Zhang, M. Zhang, J. Duan, J. Duan, X. Yin, Y. Wang, L. Zhao, X. Tang, X. Wang, and G. Xu. 2018. "Histone deacetylase 1 promotes glioblastoma cell proliferation and invasion via activation of PI3K/AKT and MEK/ERK signaling pathways." *Brain Res* 1692:154-162. doi: 10.1016/j.brainres.2018.05.023.

Li, S., B. Shi, X. Liu, and H. X. An. 2020. "Acetylation and Deacetylation of DNA Repair Proteins in Cancers." *Front Oncol* 10:573502. doi: 10.3389/fonc.2020.573502.

Li, T., C. Zhang, S. Hassan, X. Liu, F. Song, K. Chen, W. Zhang, and J. Yang. 2018. "Histone deacetylase 6 in cancer." *J Hematol Oncol* 11 (1):111. doi: 10.1186/s13045-018-0654-9.

Li, Y., G. D. Kao, B. A. Garcia, J. Shabanowitz, D. F. Hunt, J. Qin, C. Phelan, and M. A. Lazar. 2006. "A novel histone deacetylase pathway regulates mitosis by modulating Aurora B kinase activity." *Genes Dev* 20 (18):2566-79. doi: 10.1101/gad.1455006.

Li, Y., L. Peng, and E. Seto. 2015. "Histone Deacetylase 10 Regulates the Cell Cycle G2/M Phase Transition via a Novel Let-7-HMGA2-Cyclin A2 Pathway." *Mol Cell Biol* 35 (20):3547-65. doi: 10.1128/MCB.00400-15.

Li, Y., and E. Seto. 2016. "HDACs and HDAC Inhibitors in Cancer Development and Therapy." *Cold Spring Harb Perspect Med* 6 (10). doi: 10.1101/cshperspect.a026831.

Li, Z. Y., Q. Z. Li, L. Chen, B. D. Chen, B. Wang, X. J. Zhang, and W. P. Li. 2016. "Histone Deacetylase Inhibitor RGFP109 Overcomes Temozolomide Resistance by Blocking NF-kappaB-Dependent Transcription in Glioblastoma Cell Lines." *Neurochem Res* 41 (12):3192-3205. doi: 10.1007/s11064-016-2043-5.

Li, Z., T. Zhu, Y. Xu, C. Wu, J. Chen, Y. Ren, L. Kong, S. Sun, W. Guo, Y. Wang, C. Jing, J. Dong, J. Zhou, L. Zhang, Q. Shen, and X. Zhou. 2019. "A novel STAT3 inhibitor, HJC0152, exerts potent antitumor activity in glioblastoma." *Am J Cancer Res* 9 (4):699-713.

Liau, B. B., C. Sievers, L. K. Donohue, S. M. Gillespie, W. A. Flavahan, T. E. Miller, A. S. Venteicher, C. H. Hebert, C. D. Carey, S. J. Rodig, S. J. Shareef, F. J. Najm, P. van Galen, H. Wakimoto, D. P. Cahill, J. N. Rich, J. C. Aster, M. L. Suva, A. P. Patel, and B. E. Bernstein. 2017. "Adaptive Chromatin Remodeling Drives Glioblastoma Stem Cell Plasticity and Drug Tolerance." *Cell Stem Cell* 20 (2):233-246 e7. doi: 10.1016/j.stem.2016.11.003.

Ligon, K. L., E. Huillard, S. Mehta, S. Kesari, H. Liu, J. A. Alberta, R. M. Bachoo, M. Kane, D. N. Louis, R. A. Depinho, D. J. Anderson, C. D. Stiles, and D. H. Rowitch. 2007. "Olig2-regulated lineage-restricted pathway controls replication competence in neural stem cells and malignant glioma." *Neuron* 53 (4):503-17. doi: 10.1016/j.neuron.2007.01.009.

Lin, J., X. Jin, K. Rothman, H. J. Lin, H. Tang, and W. Burke. 2002. "Modulation of signal transducer and activator of transcription 3 activities by p53 tumor suppressor in breast cancer cells." *Cancer Res* 62 (2):376-80.

Lin, J., H. Tang, X. Jin, G. Jia, and J. T. Hsieh. 2002. "p53 regulates Stat3 phosphorylation and DNA binding activity in human prostate cancer cells expressing constitutively active Stat3." *Oncogene* 21 (19):3082-8. doi: 10.1038/sj.onc.1205426.

Lindahl, T., and R. D. Wood. 1999. "Quality control by DNA repair." *Science* 286 (5446):1897-905. doi: 10.1126/science.286.5446.1897.

Liu, G., X. Yuan, Z. Zeng, P. Tunici, H. Ng, I. R. Abdulkadir, L. Lu, D. Irvin, K. L. Black, and J. S. Yu. 2006. "Analysis of gene expression and chemoresistance of CD133+ cancer stem cells in glioblastoma." *Mol Cancer* 5:67. doi: 10.1186/1476-4598-5-67.

Liu, L., S. Markowitz, and S. L. Gerson. 1996. "Mismatch repair mutations override alkyltransferase in conferring resistance to temozolomide but not to 1,3-bis(2-chloroethyl)nitrosourea." *Cancer Res* 56 (23):5375-9.

Liu, P., S. Griffiths, D. Veljanoski, P. Vaughn-Beaucaire, V. Speirs, and A. Bruning-Richardson. 2021. "Preclinical models of glioblastoma: limitations of current models and the promise of new developments." *Expert Rev Mol Med* 23:e20. doi: 10.1017/erm.2021.20.

Lo Cascio, C., J. B. McNamara, E. L. Melendez, E. M. Lewis, M. E. Dufault, N. Sanai, C. L. Plaisier, and S. Mehta. 2021. "Nonredundant, isoform-specific roles of HDAC1 in glioma stem cells." *JCI Insight* 6 (17). doi: 10.1172/jci.insight.149232.

Loscher, W. 1993. "In vivo administration of valproate reduces the nerve terminal (synaptosomal) activity of GABA aminotransferase in discrete brain areas of rats." *Neurosci Lett* 160 (2):177-80. doi: 10.1016/0304-3940(93)90407-c.

Lostumbo, L., N. E. Carbine, and J. Wallace. 2010. "Prophylactic mastectomy for the prevention of breast cancer." *Cochrane Database Syst Rev* (11):CD002748. doi: 10.1002/14651858.CD002748.pub3.

Louis, D. N., E. C. Holland, and J. G. Cairncross. 2001. "Glioma classification: a molecular reappraisal." *Am J Pathol* 159 (3):779-86. doi: 10.1016/S0002-9440(10)61750-6.

Louis, D. N., A. Perry, P. Wesseling, D. J. Brat, I. A. Cree, D. Figarella-Branger, C. Hawkins, H. K. Ng, S. M. Pfister, G. Reifenberger, R. Soffietti, A. von Deimling, and D. W. Ellison. 2021. "The 2021 WHO Classification of Tumors of the Central Nervous System: a summary." *Neuro Oncol* 23 (8):1231-1251. doi: 10.1093/neuonc/noab106.

Love, M. I., W. Huber, and S. Anders. 2014. "Moderated estimation of fold change and dispersion for RNA-seq data with DESeq2." *Genome Biol* 15 (12):550. doi: 10.1186/s13059-014-0550-8.

Luger, K., A. W. Mader, R. K. Richmond, D. F. Sargent, and T. J. Richmond. 1997. "Crystal structure of the nucleosome core particle at 2.8 A resolution." *Nature* 389 (6648):251-60. doi: 10.1038/38444.

Lumniczky, K., T. Szatmari, and G. Safrany. 2017. "Ionizing Radiation-Induced Immune and Inflammatory Reactions in the Brain." *Front Immunol* 8:517. doi: 10.3389/fimmu.2017.00517.

Luo, J., F. Su, D. Chen, A. Shiloh, and W. Gu. 2000. "Deacetylation of p53 modulates its effect on cell growth and apoptosis." *Nature* 408 (6810):377-81. doi: 10.1038/35042612.

Lytle, N. K., A. G. Barber, and T. Reya. 2018. "Stem cell fate in cancer growth, progression and therapy resistance." *Nat Rev Cancer* 18 (11):669-680. doi: 10.1038/s41568-018-0056-x.

Ma, J. B., J. Y. Bai, H. B. Zhang, J. Jia, Q. Shi, C. Yang, X. Wang, D. He, and P. Guo. 2020. "KLF5 inhibits STAT3 activity and tumor metastasis in prostate cancer by suppressing IGF1 transcription cooperatively with HDAC1." *Cell Death Dis* 11 (6):466. doi: 10.1038/s41419-020-2671-1.

MacDonald, J. L., and A. J. Roskams. 2008. "Histone deacetylases 1 and 2 are expressed at distinct stages of neuro-glial development." *Dev Dyn* 237 (8):2256-67. doi: 10.1002/dvdy.21626.

MacLeod, G., D. A. Bozek, N. Rajakulendran, V. Monteiro, M. Ahmadi, Z. Steinhart, M. M. Kushida, H. Yu, F. J. Coutinho, F. M. G. Cavalli, I. Restall, X. Hao, T. Hart, H. A. Luchman, S. Weiss, P. B. Dirks, and S. Angers. 2019. "Genome-Wide CRISPR-Cas9 Screens Expose Genetic Vulnerabilities and Mechanisms of

Temozolomide Sensitivity in Glioblastoma Stem Cells." *Cell Rep* 27 (3):971-986 e9. doi: 10.1016/j.celrep.2019.03.047.

Madhavan, S., J. C. Zenklusen, Y. Kotliarov, H. Sahni, H. A. Fine, and K. Buetow. 2009. "Rembrandt: helping personalized medicine become a reality through integrative translational research." *Mol Cancer Res* 7 (2):157-67. doi: 10.1158/1541-7786.MCR-08-0435.

Makale, M. T., C. R. McDonald, J. A. Hattangadi-Gluth, and S. Kesari. 2017. "Mechanisms of radiotherapy-associated cognitive disability in patients with brain tumours." *Nat Rev Neurol* 13 (1):52-64. doi: 10.1038/nrneurol.2016.185.

Mann, B. S., J. R. Johnson, M. H. Cohen, R. Justice, and R. Pazdur. 2007. "FDA approval summary: vorinostat for treatment of advanced primary cutaneous T-cell lymphoma." *Oncologist* 12 (10):1247-52. doi: 10.1634/theoncologist.12-10-1247.

Martinez, R., J. I. Martin-Subero, V. Rohde, M. Kirsch, M. Alaminos, A. F. Fernandez, S. Ropero, G. Schackert, and M. Esteller. 2009. "A microarray-based DNA methylation study of glioblastoma multiforme." *Epigenetics* 4 (4):255-64. doi: 10.4161/epi.9130.

Masliantsev, K., B. Pinel, A. Balbous, P. O. Guichet, G. Tachon, S. Milin, J. Godet, M. Duchesne, A. Berger, C. Petropoulos, M. Wager, and L. Karayan-Tapon. 2018. "Impact of STAT3 phosphorylation in glioblastoma stem cells radiosensitization and patient outcome." *Oncotarget* 9 (3):3968-3979. doi: 10.18632/oncotarget.23374.

Matthews, G. M., A. Newbold, and R. W. Johnstone. 2012. "Intrinsic and extrinsic apoptotic pathway signaling as determinants of histone deacetylase inhibitor antitumor activity." *Adv Cancer Res* 116:165-97. doi: 10.1016/B978-0-12-394387-3.00005-7.

McClure, J. J., X. Li, and C. J. Chou. 2018. "Advances and Challenges of HDAC Inhibitors in Cancer Therapeutics." *Adv Cancer Res* 138:183-211. doi: 10.1016/bs.acr.2018.02.006.

McDermott, J., and A. Jimeno. 2014. "Belinostat for the treatment of peripheral T-cell lymphomas." *Drugs Today (Barc)* 50 (5):337-45. doi: 10.1358/dot.2014.50.5.2138703.

McLendon, Roger, Allan Friedman, Darrell Bigner, Erwin G. Van Meir, Daniel J. Brat, Gena M. Mastrogianakis, Jeffrey J. Olson, Tom Mikkelsen, Norman Lehman, Ken Aldape, W. K. Alfred Yung, Oliver Bogler, Scott VandenBerg, Mitchel Berger, Michael Prados, Donna Muzny, Margaret Morgan, Steve Scherer, Aniko Sabo, Lynn Nazareth, Lora Lewis, Otis Hall, Yiming Zhu, Yanru Ren, Omar Alvi, Jiqiang Yao, Alicia Hawes, Shalini Jhangiani, Gerald Fowler, Anthony San Lucas, Christie Kovar, Andrew Cree, Huyen Dinh, Jireh Santibanez, Vandita

Joshi, Manuel L. Gonzalez-Garay, Christopher A. Miller, Aleksandar Milosavljevic, Larry Donehower, David A. Wheeler, Richard A. Gibbs, Kristian Cibulskis, Carrie Sougnez, Tim Fennell, Scott Mahan, Jane Wilkinson, Liuda Ziaugra, Robert Onofrio, Toby Bloom, Rob Nicol, Kristin Ardlie, Jennifer Baldwin, Stacey Gabriel, Eric S. Lander, Li Ding, Robert S. Fulton, Michael D. McLellan, John Wallis, David E. Larson, Xiaoqi Shi, Rachel Abbott, Lucinda Fulton, Ken Chen, Daniel C. Koboldt, Michael C. Wendl, Rick Meyer, Yuzhu Tang, Ling Lin, John R. Osborne, Brian H. Dunford-Shore, Tracie L. Miner, Kim Delehaunty, Chris Markovic, Gary Swift, William Courtney, Craig Pohl, Scott Abbott, Amy Hawkins, Shin Leong, Carrie Haipek, Heather Schmidt, Maddy Wiechert, Tammi Vickery, Sacha Scott, David J. Dooling, Asif Chinwalla, George M. Weinstock, Elaine R. Mardis, Richard K. Wilson, Gad Getz, Wendy Winckler, Roel G. W. Verhaak, Michael S. Lawrence, Michael O'Kelly, Jim Robinson, Gabriele Alexe, Rameen Beroukhim, Scott Carter, Derek Chiang, Josh Gould, Supriya Gupta, Josh Korn, Craig Mermel, Jill Mesirov, Stefano Monti, Huy Nguyen, Melissa Parkin, Michael Reich, Nicolas Stransky, Barbara A. Weir, Levi Garraway, Todd Golub, Matthew Meyerson, Lynda Chin, Alexei Protopopov, Jianhua Zhang, Ilana Perna, Sandy Aronson, Narayan Sathiamoorthy, Georgia Ren, Jun Yao, W. Ruprecht Wiedemeyer, Hyunsoo Kim, Sek Won Kong, Yonghong Xiao, Isaac S. Kohane, Jon Seidman, Peter J. Park, Raju Kucherlapati, Peter W. Laird, Leslie Cope, James G. Herman, Daniel J. Weisenberger, Fei Pan, David Van Den Berg, Leander Van Neste, Joo Mi Yi, Kornel E. Schuebel, Stephen B. Baylin, Devin M. Absher, Jun Z. Li, Audrey Southwick, Shannon Brady, Amita Aggarwal, Tisha Chung, Gavin Sherlock, James D. Brooks, Richard M. Myers, Paul T. Spellman, Elizabeth Purdom, Lakshmi R. Jakkula, Anna V. Lapuk, Henry Marr, Shannon Dorton, Yoon Gi Choi, Ju Han, Amrita Ray, Victoria Wang, Steffen Durinck, Mark Robinson, Nicholas J. Wang, Karen Vranizan, Vivian Peng, Eric Van Name, Gerald V. Fontenay, John Ngai, John G. Conboy, Bahram Parvin, Heidi S. Feiler, Terence P. Speed, Joe W. Gray, Cameron Brennan, Nicholas D. Socci, Adam Olshen, Barry S. Taylor, Alex Lash, Nikolaus Schultz, Boris Reva, Yevgeniy Antipin, Alexey Stukalov, Benjamin Gross, Ethan Cerami, Wei Qing Wang, Li-Xuan Qin, Venkatraman E. Seshan, Liliana Villafania, Magali Cavatore, Laetitia Borsu, Agnes Viale, William Gerald, Chris Sander, Marc Ladanyi, Charles M. Perou, D. Neil Hayes, Michael D. Topal, Katherine A. Hoadley, Yuan Qi, Sai Balu, Yan Shi, Junyuan Wu, Robert Penny, Michael Bittner, Troy Shelton, Elizabeth Lenkiewicz, Scott Morris, Debbie Beasley, Sheri Sanders, Ari Kahn, Robert Sfeir, Jessica Chen, David Nassau, Larry Feng, Erin Hickey, Jinghui Zhang, John N. Weinstein, Anna Barker, Daniela S. Gerhard, Joseph Vockley, Carolyn Compton, Jim Vaught, Peter Fielding, Martin L. Ferguson, Carl Schaefer, Subhashree Madhavan, Kenneth H. Buetow, Francis Collins, Peter Good, Mark Guyer, Brad Ozenberger, Jane Peterson, Elizabeth Thomson, Network The Cancer Genome Atlas Research, School Tissue source sites: Duke University Medical, University Emory, Hospital Henry Ford, M. D. Anderson Cancer Center, Francisco University of California San, Medicine Genome sequencing centres: Baylor

College of, M. I. T. Broad Institute of, Harvard, Louis Washington University in St, Institute Cancer genome characterization centres: Broad Institute/Dana-Farber Cancer, Institute Harvard Medical School/Dana-Farber Cancer, California Johns Hopkins/University of Southern, University HudsonAlpha Institute/Stanford, Laboratory Lawrence Berkeley National, Center Memorial Sloan-Kettering Cancer, Chapel Hill University of North Carolina, Resource Biospecimen Core, Center Data Coordinating, Institute Project teams: National Cancer, and Institute National Human Genome Research. 2008. "Comprehensive genomic characterization defines human glioblastoma genes and core pathways." *Nature* 455 (7216):1061-1068. doi: 10.1038/nature07385.

Mehta, M., P. Wen, R. Nishikawa, D. Reardon, and K. Peters. 2017. "Critical review of the addition of tumor treating fields (TTFields) to the existing standard of care for newly diagnosed glioblastoma patients." *Crit Rev Oncol Hematol* 111:60-65. doi: 10.1016/j.critrevonc.2017.01.005.

Mehta, S., E. Huillard, S. Kesari, C. L. Maire, D. Golebiowski, E. P. Harrington, J. A. Alberta, M. F. Kane, M. Theisen, K. L. Ligon, D. H. Rowitch, and C. D. Stiles. 2011. "The central nervous system-restricted transcription factor Olig2 opposes p53 responses to genotoxic damage in neural progenitors and malignant glioma." *Cancer Cell* 19 (3):359-71. doi: 10.1016/j.ccr.2011.01.035.

Meijer, D. H., Y. Sun, T. Liu, M. F. Kane, J. A. Alberta, G. Adelmant, R. Kupp, J. A. Marto, D. H. Rowitch, Y. Nakatani, C. D. Stiles, and S. Mehta. 2014. "An amino terminal phosphorylation motif regulates intranuclear compartmentalization of Olig2 in neural progenitor cells." *J Neurosci* 34 (25):8507-18. doi: 10.1523/JNEUROSCI.0309-14.2014.

Memon, S., A. G. Heriot, D. G. Murphy, M. Bressel, and A. C. Lynch. 2012. "Robotic versus laparoscopic proctectomy for rectal cancer: a meta-analysis." *Ann Surg Oncol* 19 (7):2095-101. doi: 10.1245/s10434-012-2270-1.

Menezes, A., G. H. Dos Reis, M. C. Oliveira-Nunes, F. Mariath, M. Cabanel, B. Pontes, N. Goncalves Castro, J. M. de Brito, and K. Carneiro. 2019. "Live Cell Imaging Supports a Key Role for Histone Deacetylase as a Molecular Target during Glioblastoma Malignancy Downgrade through Tumor Competence Modulation." *J Oncol* 2019:9043675. doi: 10.1155/2019/9043675.

Methot, J. L., P. K. Chakravarty, M. Chenard, J. Close, J. C. Cruz, W. K. Dahlberg, J. Fleming, C. L. Hamblett, J. E. Hamill, P. Harrington, A. Harsch, R. Heidebrecht, B. Hughes, J. Jung, C. M. Kenific, A. M. Kral, P. T. Meinke, R. E. Middleton, N. Ozerova, D. L. Sloman, M. G. Stanton, A. A. Szewczak, S. Tyagarajan, D. J. Witter, J. P. Secrist, and T. A. Miller. 2008. "Exploration of the internal cavity of histone deacetylase (HDAC) with selective HDAC1/HDAC2 inhibitors (SHI-1:2)." *Bioorg Med Chem Lett* 18 (3):973-8. doi: 10.1016/j.bmcl.2007.12.031.

Methot, J. L., D. M. Hoffman, D. J. Witter, M. G. Stanton, P. Harrington, C. Hamblett, P. Siliphaivanh, K. Wilson, J. Hubbs, R. Heidebrecht, A. M. Kral, N. Ozerova, J. C. Fleming, H. Wang, A. A. Szewczak, R. E. Middleton, B. Hughes, J. C. Cruz, B. B. Haines, M. Chenard, C. M. Kenific, A. Harsch, J. P. Secrist, and T. A. Miller. 2014. "Delayed and Prolonged Histone Hyperacetylation with a Selective HDAC1/HDAC2 Inhibitor." *ACS Med Chem Lett* 5 (4):340-5. doi: 10.1021/ml4004233.

Meyers, R. M., J. G. Bryan, J. M. McFarland, B. A. Weir, A. E. Sizemore, H. Xu, N. V. Dharia, P. G. Montgomery, G. S. Cowley, S. Pantel, A. Goodale, Y. Lee, L. D. Ali, G. Jiang, R. Lubonja, W. F. Harrington, M. Strickland, T. Wu, D. C. Hawes, V. A. Zhivich, M. R. Wyatt, Z. Kalani, J. J. Chang, M. Okamoto, K. Stegmaier, T. R. Golub, J. S. Boehm, F. Vazquez, D. E. Root, W. C. Hahn, and A. Tsherniak. 2017. "Computational correction of copy number effect improves specificity of CRISPR-Cas9 essentiality screens in cancer cells." *Nat Genet* 49 (12):1779-1784. doi: 10.1038/ng.3984.

Miller, K. M., J. V. Tjeertes, J. Coates, G. Legube, S. E. Polo, S. Britton, and S. P. Jackson. 2010. "Human HDAC1 and HDAC2 function in the DNA-damage response to promote DNA nonhomologous end-joining." *Nat Struct Mol Biol* 17 (9):1144-51. doi: 10.1038/nsmb.1899.

Mithraprabhu, S., A. Kalff, A. Chow, T. Khong, and A. Spencer. 2014. "Dysregulated Class I histone deacetylases are indicators of poor prognosis in multiple myeloma." *Epigenetics* 9 (11):1511-20. doi: 10.4161/15592294.2014.983367.

Mittal, S., N. V. Klinger, S. K. Michelhaugh, G. R. Barger, S. C. Pannullo, and C. Juhasz. 2018. "Alternating electric tumor treating fields for treatment of glioblastoma: rationale, preclinical, and clinical studies." *J Neurosurg* 128 (2):414-421. doi: 10.3171/2016.9.JNS16452.

Montgomery, R. L., J. Hsieh, A. C. Barbosa, J. A. Richardson, and E. N. Olson. 2009. "Histone deacetylases 1 and 2 control the progression of neural precursors to neurons during brain development." *Proc Natl Acad Sci U S A* 106 (19):7876-81. doi: 10.1073/pnas.0902750106.

Moscatello, D. K., R. B. Montgomery, P. Sundareshan, H. McDanel, M. Y. Wong, and A. J. Wong. 1996. "Transformational and altered signal transduction by a naturally occurring mutant EGF receptor." *Oncogene* 13 (1):85-96.

Mrakovcic, M., and L. F. Frohlich. 2018. "p53-Mediated Molecular Control of Autophagy in Tumor Cells." *Biomolecules* 8 (2). doi: 10.3390/biom8020014.

Mrakovcic, M., J. Kleinheinz, and L. F. Frohlich. 2019. "p53 at the Crossroads between Different Types of HDAC Inhibitor-Mediated Cancer Cell Death." *Int J Mol Sci* 20 (10). doi: 10.3390/ijms20102415.

Mrugala, M. M., and M. C. Chamberlain. 2008. "Mechanisms of disease: temozolomide and glioblastoma--look to the future." *Nat Clin Pract Oncol* 5 (8):476-86. doi: 10.1038/ncponc1155.

Mukthavaram, R., X. Ouyang, R. Saklecha, P. Jiang, N. Nomura, S. C. Pingle, F. Guo, M. Makale, and S. Kesari. 2015. "Effect of the JAK2/STAT3 inhibitor SAR317461 on human glioblastoma tumorspheres." *J Transl Med* 13:269. doi: 10.1186/s12967-015-0627-5.

Munshi, A., J. F. Kurland, T. Nishikawa, T. Tanaka, M. L. Hobbs, S. L. Tucker, S. Ismail, C. Stevens, and R. E. Meyn. 2005. "Histone deacetylase inhibitors radiosensitize human melanoma cells by suppressing DNA repair activity." *Clin Cancer Res* 11 (13):4912-22. doi: 10.1158/1078-0432.CCR-04-2088.

Munster, P. N., D. Marchion, S. Thomas, M. Egorin, S. Minton, G. Springett, J. H. Lee, G. Simon, A. Chiappori, D. Sullivan, and A. Daud. 2009. "Phase I trial of vorinostat and doxorubicin in solid tumours: histone deacetylase 2 expression as a predictive marker." *Br J Cancer* 101 (7):1044-50. doi: 10.1038/sj.bjc.6605293.

Musa, J., M. M. Aynaud, O. Mirabeau, O. Delattre, and T. G. Grunewald. 2017. "MYBL2 (B-Myb): a central regulator of cell proliferation, cell survival and differentiation involved in tumorigenesis." *Cell Death Dis* 8 (6):e2895. doi: 10.1038/cddis.2017.244.

Natsume, A., M. Ito, K. Katsushima, F. Ohka, A. Hatanaka, K. Shinjo, S. Sato, S. Takahashi, Y. Ishikawa, I. Takeuchi, H. Shimogawa, M. Uesugi, H. Okano, S. U. Kim, T. Wakabayashi, J. P. Issa, Y. Sekido, and Y. Kondo. 2013. "Chromatin regulator PRC2 is a key regulator of epigenetic plasticity in glioblastoma." *Cancer Res* 73 (14):4559-70. doi: 10.1158/0008-5472.CAN-13-0109.

Nava, F., I. Tramacere, A. Fittipaldo, M. G. Bruzzone, F. Dimeco, L. Fariselli, G. Finocchiaro, B. Pollo, A. Salmaggi, A. Silvani, M. Farinotti, and G. Filippini. 2014. "Survival effect of first- and second-line treatments for patients with primary glioblastoma: a cohort study from a prospective registry, 1997-2010." *Neuro Oncol* 16 (5):719-27. doi: 10.1093/neuonc/not316.

Neftel, C., J. Laffy, M. G. Filbin, T. Hara, M. E. Shore, G. J. Rahme, A. R. Richman, D. Silverbush, M. L. Shaw, C. M. Hebert, J. Dewitt, S. Gritsch, E. M. Perez, L. N. Gonzalez Castro, X. Lan, N. Druck, C. Rodman, D. Dionne, A. Kaplan, M. S. Bertalan, J. Small, K. Pelton, S. Becker, D. Bonal, Q. D. Nguyen, R. L. Servis, J. M. Fung, R. Mylvaganam, L. Mayr, J. Gojo, C. Haberler, R. Geyeregger, T. Czech, I. Slavc, B. V. Nahed, W. T. Curry, B. S. Carter, H. Wakimoto, P. K. Brastianos, T. T. Batchelor, A. Stemmer-Rachamimov, M. Martinez-Lage, M. P. Frosch, I. Stamenkovic, N. Riggi, E. Rheinbay, M. Monje, O. Rozenblatt-Rosen, D. P. Cahill, A. P. Patel, T. Hunter, I. M. Verma, K. L. Ligon, D. N. Louis, A. Regev, B. E. Bernstein, I. Tirosh, and M. L. Suva. 2019. "An Integrative Model of

Cellular States, Plasticity, and Genetics for Glioblastoma." *Cell* 178 (4):835-849 e21. doi: 10.1016/j.cell.2019.06.024.

Ni, J., Y. Wang, X. Cheng, F. Teng, C. Wang, S. Han, X. Chen, and W. Guo. 2020. "Pathogenic Heteroplasmic Somatic Mitochondrial DNA Mutation Confers Platinum-Resistance and Recurrence of High-Grade Serous Ovarian Cancer." *Cancer Manag Res* 12:11085-11093. doi: 10.2147/CMAR.S277724.

Noch, E. K., R. Ramakrishna, and R. Magge. 2018. "Challenges in the Treatment of Glioblastoma: Multisystem Mechanisms of Therapeutic Resistance." *World Neurosurg* 116:505-517. doi: 10.1016/j.wneu.2018.04.022.

Oberoi, J., L. Fairall, P. J. Watson, J. C. Yang, Z. Czimmerer, T. Kampmann, B. T. Goult, J. A. Greenwood, J. T. Gooch, B. C. Kallenberger, L. Nagy, D. Neuhaus, and J. W. Schwabe. 2011. "Structural basis for the assembly of the SMRT/NCoR core transcriptional repression machinery." *Nat Struct Mol Biol* 18 (2):177-84. doi: 10.1038/nsmb.1983.

Ochs, K., and B. Kaina. 2000. "Apoptosis induced by DNA damage O6-methylguanine is Bcl-2 and caspase-9/3 regulated and Fas/caspase-8 independent." *Cancer Res* 60 (20):5815-24.

Oehme, I., H. E. Deubzer, D. Wegener, D. Pickert, J. P. Linke, B. Hero, A. Kopp-Schneider, F. Westermann, S. M. Ulrich, A. von Deimling, M. Fischer, and O. Witt. 2009. "Histone deacetylase 8 in neuroblastoma tumorigenesis." *Clin Cancer Res* 15 (1):91-9. doi: 10.1158/1078-0432.CCR-08-0684.

Ohgaki, H., and P. Kleihues. 2013. "The definition of primary and secondary glioblastoma." *Clin Cancer Res* 19 (4):764-72. doi: 10.1158/1078-0432.CCR-12-3002.

Olins, D. E., and A. L. Olins. 2003. "Chromatin history: our view from the bridge." *Nat Rev Mol Cell Biol* 4 (10):809-14. doi: 10.1038/nrm1225.

Omuro, A., and L. M. DeAngelis. 2013. "Glioblastoma and other malignant gliomas: a clinical review." *JAMA* 310 (17):1842-50. doi: 10.1001/jama.2013.280319.

Oronsky, B., T. R. Reid, A. Oronsky, N. Sandhu, and S. J. Knox. 2020. "A Review of Newly Diagnosed Glioblastoma." *Front Oncol* 10:574012. doi: 10.3389/fonc.2020.574012.

Ostrom, Q. T., G. Cioffi, K. Waite, C. Kruchko, and J. S. Barnholtz-Sloan. 2021. "CBTRUS Statistical Report: Primary Brain and Other Central Nervous System Tumors Diagnosed in the United States in 2014-2018." *Neuro Oncol* 23 (12 Suppl 2):iii1-iii105. doi: 10.1093/neuonc/noab200.

Ostrom, Q. T., D. J. Cote, M. Ascha, C. Kruchko, and J. S. Barnholtz-Sloan. 2018. "Adult Glioma Incidence and Survival by Race or Ethnicity in the United States From 2000 to 2014." *JAMA Oncol* 4 (9):1254-1262. doi: 10.1001/jamaoncol.2018.1789.

Pak, E., E. L. MacKenzie, X. Zhao, M. F. Pazyra-Murphy, P. M. C. Park, L. Wu, D. L. Shaw, E. C. Addleson, S. S. Cayer, B. G. Lopez, N. Y. R. Agar, L. L. Rubin, J. Qi, D. J. Merk, and R. A. Segal. 2019. "A large-scale drug screen identifies selective inhibitors of class I HDACs as a potential therapeutic option for SHH medulloblastoma." *Neuro Oncol* 21 (9):1150-1163. doi: 10.1093/neuonc/noz089.

Park, S. Y., and J. S. Kim. 2020. "A short guide to histone deacetylases including recent progress on class II enzymes." *Exp Mol Med* 52 (2):204-212. doi: 10.1038/s12276-020-0382-4.

Parsons, D. W., S. Jones, X. Zhang, J. C. Lin, R. J. Leary, P. Angenendt, P. Mankoo, H. Carter, I. M. Siu, G. L. Gallia, A. Olivi, R. McLendon, B. A. Rasheed, S. Keir, T. Nikolskaya, Y. Nikolsky, D. A. Busam, H. Tekleab, L. A. Diaz, Jr., J. Hartigan, D. R. Smith, R. L. Strausberg, S. K. Marie, S. M. Shinjo, H. Yan, G. J. Riggins, D. D. Bigner, R. Karchin, N. Papadopoulos, G. Parmigiani, B. Vogelstein, V. E. Velculescu, and K. W. Kinzler. 2008. "An integrated genomic analysis of human glioblastoma multiforme." *Science* 321 (5897):1807-12. doi: 10.1126/science.1164382.

Pastori, C., M. Daniel, C. Penas, C. H. Volmar, A. L. Johnstone, S. P. Brothers, R. M. Graham, B. Allen, J. N. Sarkaria, R. J. Komotar, C. Wahlestedt, and N. G. Ayad. 2014. "BET bromodomain proteins are required for glioblastoma cell proliferation." *Epigenetics* 9 (4):611-20. doi: 10.4161/epi.27906.

Patel, A. P., I. Tirosh, J. J. Trombetta, A. K. Shalek, S. M. Gillespie, H. Wakimoto, D. P. Cahill, B. V. Nahed, W. T. Curry, R. L. Martuza, D. N. Louis, O. Rozenblatt-Rosen, M. L. Suva, A. Regev, and B. E. Bernstein. 2014. "Single-cell RNA-seq highlights intratumoral heterogeneity in primary glioblastoma." *Science* 344 (6190):1396-401. doi: 10.1126/science.1254257.

Peng, X., Z. Sun, P. Kuang, and J. Chen. 2020. "Recent progress on HDAC inhibitors with dual targeting capabilities for cancer treatment." *Eur J Med Chem* 208:112831. doi: 10.1016/j.ejmech.2020.112831.

Petruccelli, L. A., D. Dupere-Richer, F. Pettersson, H. Retrouvey, S. Skoulikas, and W. H. Miller, Jr. 2011. "Vorinostat induces reactive oxygen species and DNA damage in acute myeloid leukemia cells." *PLoS One* 6 (6):e20987. doi: 10.1371/journal.pone.0020987.

Petryniak, M. A., G. B. Potter, D. H. Rowitch, and J. L. Rubenstein. 2007. "Dlx1 and Dlx2 control neuronal versus oligodendroglial cell fate acquisition in the developing forebrain." *Neuron* 55 (3):417-33. doi: 10.1016/j.neuron.2007.06.036.

Pettazzoni, P., S. Pizzimenti, C. Toaldo, P. Sotomayor, L. Tagliavacca, S. Liu, D. Wang, R. Minelli, L. Ellis, P. Atadja, E. Ciamporcero, M. U. Dianzani, G. Barrera, and R. Pili. 2011. "Induction of cell cycle arrest and DNA damage by the HDAC inhibitor panobinostat (LBH589) and the lipid peroxidation end product 4-hydroxynonenal in prostate cancer cells." *Free Radic Biol Med* 50 (2):313-22. doi: 10.1016/j.freeradbiomed.2010.11.011.

Phillips, H. S., S. Kharbanda, R. Chen, W. F. Forrest, R. H. Soriano, T. D. Wu, A. Misra, J. M. Nigro, H. Colman, L. Soroceanu, P. M. Williams, Z. Modrusan, B. G. Feuerstein, and K. Aldape. 2006. "Molecular subclasses of high-grade glioma predict prognosis, delineate a pattern of disease progression, and resemble stages in neurogenesis." *Cancer Cell* 9 (3):157-73. doi: 10.1016/j.ccr.2006.02.019.

Plaisier, C. L., S. O'Brien, B. Bernard, S. Reynolds, Z. Simon, C. M. Toledo, Y. Ding, D. J. Reiss, P. J. Paddison, and N. S. Baliga. 2016. "Causal Mechanistic Regulatory Network for Glioblastoma Deciphered Using Systems Genetics Network Analysis." *Cell Syst* 3 (2):172-186. doi: 10.1016/j.cels.2016.06.006.

Plaisier, C. L., M. Pan, and N. S. Baliga. 2012. "A miRNA-regulatory network explains how dysregulated miRNAs perturb oncogenic processes across diverse cancers." *Genome Res* 22 (11):2302-14. doi: 10.1101/gr.133991.111.

Pont, L. M., K. Naipal, J. J. Kloezeman, S. Venkatesan, M. van den Bent, D. C. van Gent, C. M. Dirven, R. Kanaar, M. L. Lamfers, and S. Leenstra. 2015. "DNA damage response and anti-apoptotic proteins predict radiosensitization efficacy of HDAC inhibitors SAHA and LBH589 in patient-derived glioblastoma cells." *Cancer Lett* 356 (2 Pt B):525-35. doi: 10.1016/j.canlet.2014.09.049.

Prager, B. C., S. Bhargava, V. Mahadev, C. G. Hubert, and J. N. Rich. 2020. "Glioblastoma Stem Cells: Driving Resilience through Chaos." *Trends Cancer* 6 (3):223-235. doi: 10.1016/j.trecan.2020.01.009.

Price, G., and D. A. Patel. 2022. "Drug Bioavailability." In *StatPearls*. Treasure Island (FL).

Pugh, C. W., and P. J. Ratcliffe. 2003. "Regulation of angiogenesis by hypoxia: role of the HIF system." *Nat Med* 9 (6):677-84. doi: 10.1038/nm0603-677.

Rapp, M., J. Baernreuther, B. Turowski, H. J. Steiger, M. Sabel, and M. A. Kamp. 2017. "Recurrence Pattern Analysis of Primary Glioblastoma." *World Neurosurg* 103:733-740. doi: 10.1016/j.wneu.2017.04.053.

Ray, S., C. Lee, T. Hou, I. Boldogh, and A. R. Brasier. 2008. "Requirement of histone deacetylase1 (HDAC1) in signal transducer and activator of transcription 3 (STAT3) nucleocytoplasmic distribution." *Nucleic Acids Res* 36 (13):4510-20. doi: 10.1093/nar/gkn419.

Reed, S. M., and D. E. Quelle. 2014. "p53 Acetylation: Regulation and Consequences." *Cancers (Basel)* 7 (1):30-69. doi: 10.3390/cancers7010030.

Reinartz, R., S. Wang, S. Kebir, D. J. Silver, A. Wieland, T. Zheng, M. Kupper, L. Rauschenbach, R. Fimmers, T. M. Shepherd, D. Trageser, A. Till, N. Schafer, M. Glas, A. M. Hillmer, S. Cichon, A. A. Smith, T. Pietsch, Y. Liu, B. A. Reynolds, A. Yachnis, D. W. Pincus, M. Simon, O. Brustle, D. A. Steindler, and B. Scheffler. 2017. "Functional Subclone Profiling for Prediction of Treatment-Induced Intratumor Population Shifts and Discovery of Rational Drug Combinations in Human Glioblastoma." *Clin Cancer Res* 23 (2):562-574. doi: 10.1158/1078-0432.CCR-15-2089.

Rettig, I., E. Koeneke, F. Trippel, W. C. Mueller, J. Burhenne, A. Kopp-Schneider, J. Fabian, A. Schober, U. Fernekorn, A. von Deimling, H. E. Deubzer, T. Milde, O. Witt, and I. Oehme. 2015. "Selective inhibition of HDAC8 decreases neuroblastoma growth in vitro and in vivo and enhances retinoic acid-mediated differentiation." *Cell Death Dis* 6:e1657. doi: 10.1038/cddis.2015.24.

Richardson, P. G., R. D. Harvey, J. P. Laubach, P. Moreau, S. Lonial, and J. F. San-Miguel. 2016. "Panobinostat for the treatment of relapsed or relapsed/refractory multiple myeloma: pharmacology and clinical outcomes." *Expert Rev Clin Pharmacol* 9 (1):35-48. doi: 10.1586/17512433.2016.1096773.

Robert, C., and F. V. Rassool. 2012. "HDAC inhibitors: roles of DNA damage and repair." *Adv Cancer Res* 116:87-129. doi: 10.1016/B978-0-12-394387-3.00003-3.

Rogakou, E. P., D. R. Pilch, A. H. Orr, V. S. Ivanova, and W. M. Bonner. 1998. "DNA double-stranded breaks induce histone H2AX phosphorylation on serine 139." *J Biol Chem* 273 (10):5858-68. doi: 10.1074/jbc.273.10.5858.

Romoli, M., P. Mazzocchetti, R. D'Alonzo, S. Siliquini, V. E. Rinaldi, A. Verrotti, P. Calabresi, and C. Costa. 2019. "Valproic Acid and Epilepsy: From Molecular Mechanisms to Clinical Evidences." *Curr Neuropharmacol* 17 (10):926-946. doi: 10.2174/1570159X17666181227165722.

Ropero, S., and M. Esteller. 2007. "The role of histone deacetylases (HDACs) in human cancer." *Mol Oncol* 1 (1):19-25. doi: 10.1016/j.molonc.2007.01.001.

Rosato, R. R., J. A. Almenara, S. C. Maggio, S. Coe, P. Atadja, P. Dent, and S. Grant. 2008. "Role of histone deacetylase inhibitor-induced reactive oxygen species and DNA damage in LAQ-824/fludarabine antileukemic interactions." *Mol Cancer Ther* 7 (10):3285-97. doi: 10.1158/1535-7163.MCT-08-0385.

Ruefli, A. A., M. J. Ausserlechner, D. Bernhard, V. R. Sutton, K. M. Tainton, R. Kofler, M. J. Smyth, and R. W. Johnstone. 2001. "The histone deacetylase inhibitor and chemotherapeutic agent suberoylanilide hydroxamic acid (SAHA) induces a cell-death pathway characterized by cleavage of Bid and production of reactive

oxygen species." *Proc Natl Acad Sci U S A* 98 (19):10833-8. doi: 10.1073/pnas.191208598.

Ryan, Q. C., D. Headlee, M. Acharya, A. Sparreboom, J. B. Trepel, J. Ye, W. D. Figg, K. Hwang, E. J. Chung, A. Murgo, G. Melillo, Y. Elsayed, M. Monga, M. Kalnitskiy, J. Zwiebel, and E. A. Sausville. 2005. "Phase I and pharmacokinetic study of MS-275, a histone deacetylase inhibitor, in patients with advanced and refractory solid tumors or lymphoma." *J Clin Oncol* 23 (17):3912-22. doi: 10.1200/JCO.2005.02.188.

Sachamitr, P., J. C. Ho, F. E. Ciamponi, W. Ba-Alawi, F. J. Coutinho, P. Guilhamon, M. M. Kushida, F. M. G. Cavalli, L. Lee, N. Rastegar, V. Vu, M. Sanchez-Osuna, J. Coulombe-Huntington, E. Kanshin, H. Whetstone, M. Durand, P. Thibault, K. Hart, M. Mangos, J. Veyhl, W. Chen, N. Tran, B. C. Duong, A. M. Aman, X. Che, X. Lan, O. Whitley, O. Zaslaver, D. Barsyte-Lovejoy, L. M. Richards, I. Restall, A. Caudy, H. L. Rost, Z. Q. Bonday, M. Bernstein, S. Das, M. D. Cusimano, J. Spears, G. D. Bader, T. J. Pugh, M. Tyers, M. Lupien, B. Haibe-Kains, H. Artee Luchman, S. Weiss, K. B. Massirer, P. Prinos, C. H. Arrowsmith, and P. B. Dirks. 2021. "PRMT5 inhibition disrupts splicing and stemness in glioblastoma." *Nat Commun* 12 (1):979. doi: 10.1038/s41467-021-21204-5.

Sambri, A., E. Caldari, M. Fiore, R. Zucchini, C. Giannini, M. G. Pirini, P. Spinnato, A. Cappelli, D. M. Donati, and M. De Paolis. 2021. "Margin Assessment in Soft Tissue Sarcomas: Review of the Literature." *Cancers (Basel)* 13 (7). doi: 10.3390/cancers13071687.

Sanai, N. 2019. "Phase 0 Clinical Trial Strategies for the Neurosurgical Oncologist." *Neurosurgery* 85 (6):E967-E974. doi: 10.1093/neuros/nyz218.

Sanai, N., and M. S. Berger. 2008. "Glioma extent of resection and its impact on patient outcome." *Neurosurgery* 62 (4):753-64; discussion 264-6. doi: 10.1227/01.neu.0000318159.21731.cf.

Sawa, H., H. Murakami, M. Kumagai, M. Nakasato, S. Yamauchi, N. Matsuyama, Y. Tamura, A. Satone, W. Ide, I. Hashimoto, and H. Kamada. 2004. "Histone deacetylase inhibitor, FK228, induces apoptosis and suppresses cell proliferation of human glioblastoma cells in vitro and in vivo." *Acta Neuropathol* 107 (6):523-31. doi: 10.1007/s00401-004-0841-3.

Schaue, D., and W. H. McBride. 2015. "Opportunities and challenges of radiotherapy for treating cancer." *Nat Rev Clin Oncol* 12 (9):527-40. doi: 10.1038/nrclinonc.2015.120.

Schwartzentruber, J., A. Korshunov, X. Y. Liu, D. T. Jones, E. Pfaff, K. Jacob, D. Sturm, A. M. Fontebasso, D. A. Quang, M. Tonjes, V. Hovestadt, S. Albrecht, M. Kool, A. Nantel, C. Konermann, A. Lindroth, N. Jager, T. Rausch, M. Ryzhova, J. O. Korbel, T. Hielscher, P. Hauser, M. Garami, A. Klekner, L. Bognar, M. Ebinger,

M. U. Schuhmann, W. Scheurlen, A. Pekrun, M. C. Fruhwald, W. Roggendorf, C. Kramm, M. Durken, J. Atkinson, P. Lepage, A. Montpetit, M. Zakrzewska, K. Zakrzewski, P. P. Liberski, Z. Dong, P. Siegel, A. E. Kulozik, M. Zapatka, A. Guha, D. Malkin, J. Felsberg, G. Reifenberger, A. von Deimling, K. Ichimura, V. P. Collins, H. Witt, T. Milde, O. Witt, C. Zhang, P. Castelo-Branco, P. Lichter, D. Faury, U. Tabori, C. Plass, J. Majewski, S. M. Pfister, and N. Jabado. 2012. "Driver mutations in histone H3.3 and chromatin remodelling genes in paediatric glioblastoma." *Nature* 482 (7384):226-31. doi: 10.1038/nature10833.

Seo, H. W., E. J. Kim, H. Na, and M. O. Lee. 2009. "Transcriptional activation of hypoxia-inducible factor-1alpha by HDAC4 and HDAC5 involves differential recruitment of p300 and FIH-1." *FEBS Lett* 583 (1):55-60. doi: 10.1016/j.febslet.2008.11.044.

Seto, E., and M. Yoshida. 2014. "Erasers of histone acetylation: the histone deacetylase enzymes." *Cold Spring Harb Perspect Biol* 6 (4):a018713. doi: 10.1101/cshperspect.a018713.

Shah, R. R. 2019. "Safety and Tolerability of Histone Deacetylase (HDAC) Inhibitors in Oncology." *Drug Saf* 42 (2):235-245. doi: 10.1007/s40264-018-0773-9.

Shannon, P., A. Markiel, O. Ozier, N. S. Baliga, J. T. Wang, D. Ramage, N. Amin, B. Schwikowski, and T. Ideker. 2003. "Cytoscape: a software environment for integrated models of biomolecular interaction networks." *Genome Res* 13 (11):2498-504. doi: 10.1101/gr.1239303.

Shao, J. B., X. Q. Luo, Y. J. Wu, M. G. Li, J. Y. Hong, L. H. Mo, Z. G. Liu, H. B. Li, D. B. Liu, and P. C. Yang. 2018. "Histone deacetylase 11 inhibits interleukin 10 in B cells of subjects with allergic rhinitis." *Int Forum Allergy Rhinol* 8 (11):1274-1283. doi: 10.1002/alr.22171.

Shergalis, A., A. Bankhead, 3rd, U. Luesakul, N. Muangsin, and N. Neamati. 2018. "Current Challenges and Opportunities in Treating Glioblastoma." *Pharmacol Rev* 70 (3):412-445. doi: 10.1124/pr.117.014944.

Shogren-Knaak, M., H. Ishii, J. M. Sun, M. J. Pazin, J. R. Davie, and C. L. Peterson. 2006. "Histone H4-K16 acetylation controls chromatin structure and protein interactions." *Science* 311 (5762):844-7. doi: 10.1126/science.1124000.

Singh, S. K., I. D. Clarke, M. Terasaki, V. E. Bonn, C. Hawkins, J. Squire, and P. B. Dirks. 2003. "Identification of a cancer stem cell in human brain tumors." *Cancer Res* 63 (18):5821-8.

Singh, S. K., R. Fiorelli, R. Kupp, S. Rajan, E. Szeto, C. Lo Cascio, C. L. Maire, Y. Sun, J. A. Alberta, J. M. Eschbacher, K. L. Ligon, M. E. Berens, N. Sanai, and S. Mehta. 2017. "Post-translational Modifications of OLIG2 Regulate Glioma

Invasion through the TGF-beta Pathway." *Cell Rep* 19 (11):2410-2412. doi: 10.1016/j.celrep.2017.05.039.

Singh, S. K., C. Hawkins, I. D. Clarke, J. A. Squire, J. Bayani, T. Hide, R. M. Henkelman, M. D. Cusimano, and P. B. Dirks. 2004. "Identification of human brain tumour initiating cells." *Nature* 432 (7015):396-401. doi: 10.1038/nature03128.

Song, Y., Y. Jiang, D. Tao, Z. Wang, R. Wang, M. Wang, and S. Han. 2020. "NFAT2-HDAC1 signaling contributes to the malignant phenotype of glioblastoma." *Neuro Oncol* 22 (1):46-57. doi: 10.1093/neuonc/noz136.

Sottoriva, A., I. Spiteri, S. G. Piccirillo, A. Touloumis, V. P. Collins, J. C. Marioni, C. Curtis, C. Watts, and S. Tavare. 2013. "Intratumor heterogeneity in human glioblastoma reflects cancer evolutionary dynamics." *Proc Natl Acad Sci U S A* 110 (10):4009-14. doi: 10.1073/pnas.1219747110.

Stazi, G., L. Taglieri, A. Nicolai, A. Romanelli, R. Fioravanti, S. Morrone, M. Sabatino, R. Ragno, S. Taurone, M. Nebbioso, R. Carletti, M. Artico, S. Valente, S. Scarpa, and A. Mai. 2019. "Dissecting the role of novel EZH2 inhibitors in primary glioblastoma cell cultures: effects on proliferation, epithelial-mesenchymal transition, migration, and on the pro-inflammatory phenotype." *Clin Epigenetics* 11 (1):173. doi: 10.1186/s13148-019-0763-5.

Stechishin, O. D., H. A. Luchman, Y. Ruan, M. D. Blough, S. A. Nguyen, J. J. Kelly, J. G. Cairncross, and S. Weiss. 2013. "On-target JAK2/STAT3 inhibition slows disease progression in orthotopic xenografts of human glioblastoma brain tumor stem cells." *Neuro Oncol* 15 (2):198-207. doi: 10.1093/neuonc/nos302.

Strahl, B. D., and C. D. Allis. 2000. "The language of covalent histone modifications." *Nature* 403 (6765):41-5. doi: 10.1038/47412.

Stricker, S. H., A. Feber, P. G. Engstrom, H. Caren, K. M. Kurian, Y. Takashima, C. Watts, M. Way, P. Dirks, P. Bertone, A. Smith, S. Beck, and S. M. Pollard. 2013. "Widespread resetting of DNA methylation in glioblastoma-initiating cells suppresses malignant cellular behavior in a lineage-dependent manner." *Genes Dev* 27 (6):654-69. doi: 10.1101/gad.212662.112.

Stummer, W., U. Pichlmeier, T. Meinel, O. D. Wiestler, F. Zanella, H. J. Reulen, and A. LA-Glioma Study Group. 2006. "Fluorescence-guided surgery with 5-aminolevulinic acid for resection of malignant glioma: a randomised controlled multicentre phase III trial." *Lancet Oncol* 7 (5):392-401. doi: 10.1016/S1470-2045(06)70665-9.

Stupp, R., M. E. Hegi, W. P. Mason, M. J. van den Bent, M. J. Taphoorn, R. C. Janzer, S. K. Ludwin, A. Allgeier, B. Fisher, K. Belanger, P. Hau, A. A. Brandes, J. Gijtenbeek, C. Marosi, C. J. Vecht, K. Mokhtari, P. Wesseling, S. Villa, E.

Eisenhauer, T. Gorlia, M. Weller, D. Lacombe, J. G. Cairncross, R. O. Mirimanoff, Research European Organisation for, Tumour Treatment of Cancer Brain, Groups Radiation Oncology, and Group National Cancer Institute of Canada Clinical Trials. 2009. "Effects of radiotherapy with concomitant and adjuvant temozolomide versus radiotherapy alone on survival in glioblastoma in a randomised phase III study: 5-year analysis of the EORTC-NCIC trial." *Lancet Oncol* 10 (5):459-66. doi: 10.1016/S1470-2045(09)70025-7.

Stupp, R., W. P. Mason, M. J. van den Bent, M. Weller, B. Fisher, M. J. Taphoorn, K. Belanger, A. A. Brandes, C. Marosi, U. Bogdahn, J. Curschmann, R. C. Janzer, S. K. Ludwin, T. Gorlia, A. Allgeier, D. Lacombe, J. G. Cairncross, E. Eisenhauer, R. O. Mirimanoff, Research European Organisation for, Tumor Treatment of Cancer Brain, Groups Radiotherapy, and Group National Cancer Institute of Canada Clinical Trials. 2005. "Radiotherapy plus concomitant and adjuvant temozolomide for glioblastoma." *N Engl J Med* 352 (10):987-96. doi: 10.1056/NEJMoa043330.

Stupp, R., S. Taillibert, A. A. Kanner, S. Kesari, D. M. Steinberg, S. A. Toms, L. P. Taylor, F. Lieberman, A. Silvani, K. L. Fink, G. H. Barnett, J. J. Zhu, J. W. Henson, H. H. Engelhard, T. C. Chen, D. D. Tran, J. Sroubek, N. D. Tran, A. F. Hottinger, J. Landolfi, R. Desai, M. Caroli, Y. Kew, J. Honnorat, A. Idbaih, E. D. Kirson, U. Weinberg, Y. Palti, M. E. Hegi, and Z. Ram. 2015. "Maintenance Therapy With Tumor-Treating Fields Plus Temozolomide vs Temozolomide Alone for Glioblastoma: A Randomized Clinical Trial." *JAMA* 314 (23):2535-43. doi: 10.1001/jama.2015.16669.

Sturm, D., S. Bender, D. T. Jones, P. Lichter, J. Grill, O. Becher, C. Hawkins, J. Majewski, C. Jones, J. F. Costello, A. Iavarone, K. Aldape, C. W. Brennan, N. Jabado, and S. M. Pfister. 2014. "Paediatric and adult glioblastoma: multiform (epi)genomic culprits emerge." *Nat Rev Cancer* 14 (2):92-107. doi: 10.1038/nrc3655.

Su, M., X. Gong, and F. Liu. 2021. "An update on the emerging approaches for histone deacetylase (HDAC) inhibitor drug discovery and future perspectives." *Expert Opin Drug Discov* 16 (7):745-761. doi: 10.1080/17460441.2021.1877656.

Subramanian, S., S. E. Bates, J. J. Wright, I. Espinoza-Delgado, and R. L. Piekarz. 2010. "Clinical Toxicities of Histone Deacetylase Inhibitors." *Pharmaceuticals (Basel)* 3 (9):2751-2767. doi: 10.3390/ph3092751.

Sun, P., S. Xia, B. Lal, C. G. Eberhart, A. Quinones-Hinojosa, J. Maciaczyk, W. Matsui, F. Dimeco, S. M. Piccirillo, A. L. Vescovi, and J. Laterra. 2009. "DNER, an epigenetically modulated gene, regulates glioblastoma-derived neurosphere cell differentiation and tumor propagation." *Stem Cells* 27 (7):1473-86. doi: 10.1002/stem.89.

Suraweera, A., K. J. O'Byrne, and D. J. Richard. 2018. "Combination Therapy With Histone Deacetylase Inhibitors (HDACi) for the Treatment of Cancer: Achieving the Full Therapeutic Potential of HDACi." *Front Oncol* 8:92. doi: 10.3389/fonc.2018.00092.

Suva, M. L., E. Rheinbay, S. M. Gillespie, A. P. Patel, H. Wakimoto, S. D. Rabkin, N. Riggi, A. S. Chi, D. P. Cahill, B. V. Nahed, W. T. Curry, R. L. Martuza, M. N. Rivera, N. Rossetti, S. Kasif, S. Beik, S. Kadri, I. Tirosh, I. Wortman, A. K. Shalek, O. Rozenblatt-Rosen, A. Regev, D. N. Louis, and B. E. Bernstein. 2014. "Reconstructing and reprogramming the tumor-propagating potential of glioblastoma stem-like cells." *Cell* 157 (3):580-94. doi: 10.1016/j.cell.2014.02.030.

Suva, M. L., N. Riggi, M. Janiszewska, I. Radovanovic, P. Provero, J. C. Stehle, K. Baumer, M. A. Le Bitoux, D. Marino, L. Cironi, V. E. Marquez, V. Clement, and I. Stamenkovic. 2009. "EZH2 is essential for glioblastoma cancer stem cell maintenance." *Cancer Res* 69 (24):9211-8. doi: 10.1158/0008-5472.CAN-09-1622.

Suva, M. L., and I. Tirosh. 2019. "Single-Cell RNA Sequencing in Cancer: Lessons Learned and Emerging Challenges." *Mol Cell* 75 (1):7-12. doi: 10.1016/j.molcel.2019.05.003.

Svechnikova, I., P. M. Almqvist, and T. J. Ekstrom. 2008. "HDAC inhibitors effectively induce cell type-specific differentiation in human glioblastoma cell lines of different origin." *Int J Oncol* 32 (4):821-7.

Sweeney, M. D., Z. Zhao, A. Montagne, A. R. Nelson, and B. V. Zlokovic. 2019. "Blood-Brain Barrier: From Physiology to Disease and Back." *Physiol Rev* 99 (1):21-78. doi: 10.1152/physrev.00050.2017.

Tan, A. C., D. M. Ashley, G. Y. Lopez, M. Malinzak, H. S. Friedman, and M. Khasraw. 2020. "Management of glioblastoma: State of the art and future directions." *CA Cancer J Clin* 70 (4):299-312. doi: 10.3322/caac.21613.

Tang, Y., W. Zhao, Y. Chen, Y. Zhao, and W. Gu. 2008. "Acetylation is indispensable for p53 activation." *Cell* 133 (4):612-26. doi: 10.1016/j.cell.2008.03.025.

Taverna, S. D., H. Li, A. J. Ruthenburg, C. D. Allis, and D. J. Patel. 2007. "How chromatin-binding modules interpret histone modifications: lessons from professional pocket pickers." *Nat Struct Mol Biol* 14 (11):1025-1040. doi: 10.1038/nsmb1338.

Tessarz, P., and T. Kouzarides. 2014. "Histone core modifications regulating nucleosome structure and dynamics." *Nat Rev Mol Cell Biol* 15 (11):703-8. doi: 10.1038/nrm3890.

Thorsson, V., D. L. Gibbs, S. D. Brown, D. Wolf, D. S. Bortone, T. H. Ou Yang, E. Porta-Pardo, G. F. Gao, C. L. Plaisier, J. A. Eddy, E. Ziv, A. C. Culhane, E. O. Paull, I. K. A. Sivakumar, A. J. Gentles, R. Malhotra, F. Farshidfar, A. Colaprico, J. S. Parker, L. E. Mose, N. S. Vo, J. Liu, Y. Liu, J. Rader, V. Dhankani, S. M. Reynolds, R. Bowlby, A. Califano, A. D. Cherniack, D. Anastassiou, D. Bedognetti, Y. Mokrab, A. M. Newman, A. Rao, K. Chen, A. Krasnitz, H. Hu, T. M. Malta, H. Noushmehr, C. S. Pedamallu, S. Bullman, A. I. Ojesina, A. Lamb, W. Zhou, H. Shen, T. K. Choueiri, J. N. Weinstein, J. Guinney, J. Saltz, R. A. Holt, C. S. Rabkin, Network Cancer Genome Atlas Research, A. J. Lazar, J. S. Serody, E. G. Demicco, M. L. Disis, B. G. Vincent, and I. Shmulevich. 2018. "The Immune Landscape of Cancer." *Immunity* 48 (4):812-830 e14. doi: 10.1016/j.immuni.2018.03.023.

Thurn, K. T., S. Thomas, P. Raha, I. Qureshi, and P. N. Munster. 2013. "Histone deacetylase regulation of ATM-mediated DNA damage signaling." *Mol Cancer Ther* 12 (10):2078-87. doi: 10.1158/1535-7163.MCT-12-1242.

Tirosh, I., and M. L. Suva. 2020. "Tackling the Many Facets of Glioblastoma Heterogeneity." *Cell Stem Cell* 26 (3):303-304. doi: 10.1016/j.stem.2020.02.005.

Toledo, C. M., Y. Ding, P. Hoellerbauer, R. J. Davis, R. Basom, E. J. Girard, E. Lee, P. Corrin, T. Hart, H. Bolouri, J. Davison, Q. Zhang, J. Hardcastle, B. J. Aronow, C. L. Plaisier, N. S. Baliga, J. Moffat, Q. Lin, X. N. Li, D. H. Nam, J. Lee, S. M. Pollard, J. Zhu, J. J. Delrow, B. E. Clurman, J. M. Olson, and P. J. Paddison. 2015. "Genome-wide CRISPR-Cas9 Screens Reveal Loss of Redundancy between PKMYT1 and WEE1 in Glioblastoma Stem-like Cells." *Cell Rep* 13 (11):2425-2439. doi: 10.1016/j.celrep.2015.11.021.

Tong, Z. T., M. Y. Cai, X. G. Wang, L. L. Kong, S. J. Mai, Y. H. Liu, H. B. Zhang, Y. J. Liao, F. Zheng, W. Zhu, T. H. Liu, X. W. Bian, X. Y. Guan, M. C. Lin, M. S. Zeng, Y. X. Zeng, H. F. Kung, and D. Xie. 2012. "EZH2 supports nasopharyngeal carcinoma cell aggressiveness by forming a co-repressor complex with HDAC1/HDAC2 and Snail to inhibit E-cadherin." *Oncogene* 31 (5):583-94. doi: 10.1038/onc.2011.254.

Torres, C. M., A. Biran, M. J. Burney, H. Patel, T. Henser-Brownhill, A. S. Cohen, Y. Li, R. Ben-Hamo, E. Nye, B. Spencer-Dene, P. Chakravarty, S. Efroni, N. Matthews, T. Misteli, E. Meshorer, and P. Scaffidi. 2016. "The linker histone H1.0 generates epigenetic and functional intratumor heterogeneity." *Science* 353 (6307). doi: 10.1126/science.aaf1644.

Tosi, U., H. Kommidi, O. Adeuyan, H. Guo, U. B. Maachani, N. Chen, T. Su, G. Zhang, D. J. Pisapia, N. Dahmane, R. Ting, and M. M. Souweidane. 2020. "PET, image-guided HDAC inhibition of pediatric diffuse midline glioma improves survival in murine models." *Sci Adv* 6 (30):eabb4105. doi: 10.1126/sciadv.abb4105.

Ugur, H. C., N. Ramakrishna, L. Bello, L. G. Menon, S. K. Kim, P. M. Black, and R. S. Carroll. 2007. "Continuous intracranial administration of suberoylanilide hydroxamic acid (SAHA) inhibits tumor growth in an orthotopic glioma model." *J Neurooncol* 83 (3):267-75. doi: 10.1007/s11060-007-9337-z.

Uhlen, M., L. Fagerberg, B. M. Hallstrom, C. Lindskog, P. Oksvold, A. Mardinoglu, A. Sivertsson, C. Kampf, E. Sjostedt, A. Asplund, I. Olsson, K. Edlund, E. Lundberg, S. Navani, C. A. Szigyarto, J. Odeberg, D. Djureinovic, J. O. Takanen, S. Hober, T. Alm, P. H. Edqvist, H. Berling, H. Tegel, J. Mulder, J. Rockberg, P. Nilsson, J. M. Schwenk, M. Hamsten, K. von Feilitzen, M. Forsberg, L. Persson, F. Johansson, M. Zwahlen, G. von Heijne, J. Nielsen, and F. Ponten. 2015. "Proteomics. Tissue-based map of the human proteome." *Science* 347 (6220):1260419. doi: 10.1126/science.1260419.

Ungerstedt, J. S., Y. Sowa, W. S. Xu, Y. Shao, M. Dokmanovic, G. Perez, L. Ngo, A. Holmgren, X. Jiang, and P. A. Marks. 2005. "Role of thioredoxin in the response of normal and transformed cells to histone deacetylase inhibitors." *Proc Natl Acad Sci U S A* 102 (3):673-8. doi: 10.1073/pnas.0408732102.

Vallstedt, A., J. M. Klos, and J. Ericson. 2005. "Multiple dorsoventral origins of oligodendrocyte generation in the spinal cord and hindbrain." *Neuron* 45 (1):55-67. doi: 10.1016/j.neuron.2004.12.026.

Valor, L. M., and I. Hervas-Corpion. 2020. "The Epigenetics of Glioma Stem Cells: A Brief Overview." *Front Oncol* 10:602378. doi: 10.3389/fonc.2020.602378.

Van Nifterik, K. A., J. Van den Berg, B. J. Slotman, M. V. Lafleur, P. Sminia, and L. J. Stalpers. 2012. "Valproic acid sensitizes human glioma cells for temozolomide and gamma-radiation." *J Neurooncol* 107 (1):61-7. doi: 10.1007/s11060-011-0725-z.

Vanan, M. I., and D. D. Eisenstat. 2015. "DIPG in Children - What Can We Learn from the Past?" *Front Oncol* 5:237. doi: 10.3389/fonc.2015.00237.

Venugopal, B., R. Baird, R. S. Kristeleit, R. Plummer, R. Cowan, A. Stewart, N. Fourneau, P. Hellemans, Y. Elsayed, S. McClue, J. W. Smit, A. Forslund, C. Phelps, J. Camm, T. R. Evans, J. S. de Bono, and U. Banerji. 2013. "A phase I study of quisinostat (JNJ-26481585), an oral hydroxamate histone deacetylase inhibitor with evidence of target modulation and antitumor activity, in patients with advanced solid tumors." *Clin Cancer Res* 19 (15):4262-72. doi: 10.1158/1078-0432.CCR-13-0312.

Verhaak, R. G., K. A. Hoadley, E. Purdom, V. Wang, Y. Qi, M. D. Wilkerson, C. R. Miller, L. Ding, T. Golub, J. P. Mesirov, G. Alexe, M. Lawrence, M. O'Kelly, P. Tamayo, B. A. Weir, S. Gabriel, W. Winckler, S. Gupta, L. Jakkula, H. S. Feiler, J. G. Hodgson, C. D. James, J. N. Sarkaria, C. Brennan, A. Kahn, P. T. Spellman, R. K. Wilson, T. P. Speed, J. W. Gray, M. Meyerson, G. Getz, C. M. Perou, D. N.

Hayes, and Network Cancer Genome Atlas Research. 2010. "Integrated genomic analysis identifies clinically relevant subtypes of glioblastoma characterized by abnormalities in PDGFRA, IDH1, EGFR, and NF1." *Cancer Cell* 17 (1):98-110. doi: 10.1016/j.ccr.2009.12.020.

Verreault, M., C. Schmitt, L. Goldwirt, K. Pelton, S. Haidar, C. Levasseur, J. Guehennec, D. Knoff, M. Labussiere, Y. Marie, A. H. Ligon, K. Mokhtari, K. Hoang-Xuan, M. Sanson, B. M. Alexander, P. Y. Wen, J. Y. Delattre, K. L. Ligon, and A. Idbaih. 2016. "Preclinical Efficacy of the MDM2 Inhibitor RG7112 in MDM2-Amplified and TP53 Wild-type Glioblastomas." *Clin Cancer Res* 22 (5):1185-96. doi: 10.1158/1078-0432.CCR-15-1015.

Vitanza, N. A., M. C. Biery, C. Myers, E. Ferguson, Y. Zheng, E. J. Girard, J. M. Przystal, G. Park, A. Noll, F. Pakiam, C. A. Winter, S. M. Morris, J. Sarthy, B. L. Cole, S. E. S. Leary, C. Crane, N. A. P. Lieberman, S. Mueller, J. Nazarian, R. Gottardo, M. Y. Brusniak, A. J. Mhyre, and J. M. Olson. 2021. "Optimal therapeutic targeting by HDAC inhibition in biopsy-derived treatment-naive diffuse midline glioma models." *Neuro Oncol* 23 (3):376-386. doi: 10.1093/neuonc/noaa249.

Vitanza, N. A., and M. Monje. 2019. "Diffuse Intrinsic Pontine Glioma: From Diagnosis to Next-Generation Clinical Trials." *Curr Treat Options Neurol* 21 (8):37. doi: 10.1007/s11940-019-0577-y.

Vogelbaum, M. A., D. Krivosheya, H. Borghei-Razavi, N. Sanai, M. Weller, W. Wick, R. Soffietti, D. A. Reardon, M. K. Aghi, E. Galanis, P. Y. Wen, M. van den Bent, and S. Chang. 2020. "Phase 0 and window of opportunity clinical trial design in neuro-oncology: a RANO review." *Neuro Oncol* 22 (11):1568-1579. doi: 10.1093/neuonc/noaa149.

von Burstin, J., S. Eser, M. C. Paul, B. Seidler, M. Brandl, M. Messer, A. von Werder, A. Schmidt, J. Mages, P. Pagel, A. Schnieke, R. M. Schmid, G. Schneider, and D. Saur. 2009. "E-cadherin regulates metastasis of pancreatic cancer in vivo and is suppressed by a SNAIL/HDAC1/HDAC2 repressor complex." *Gastroenterology* 137 (1):361-71, 371 e1-5. doi: 10.1053/j.gastro.2009.04.004.

Walker, M. D., E. Alexander, Jr., W. E. Hunt, C. S. MacCarty, M. S. Mahaley, Jr., J. Mealey, Jr., H. A. Norrell, G. Owens, J. Ransohoff, C. B. Wilson, E. A. Gehan, and T. A. Strike. 1978. "Evaluation of BCNU and/or radiotherapy in the treatment of anaplastic gliomas. A cooperative clinical trial." *J Neurosurg* 49 (3):333-43. doi: 10.3171/jns.1978.49.3.0333.

Wang, D. F., O. Wiest, P. Helquist, H. Y. Lan-Hargest, and N. L. Wiech. 2004. "On the function of the 14 A long internal cavity of histone deacetylase-like protein: implications for the design of histone deacetylase inhibitors." *J Med Chem* 47 (13):3409-17. doi: 10.1021/jm0498497.

Wang, J., E. Cazzato, E. Ladewig, V. Frattini, D. I. Rosenbloom, S. Zairis, F. Abate, Z. Liu, O. Elliott, Y. J. Shin, J. K. Lee, I. H. Lee, W. Y. Park, M. Eoli, A. J. Blumberg, A. Lasorella, D. H. Nam, G. Finocchiaro, A. Iavarone, and R. Rabadan. 2016. "Clonal evolution of glioblastoma under therapy." *Nat Genet* 48 (7):768-76. doi: 10.1038/ng.3590.

Wang, Q., B. Hu, X. Hu, H. Kim, M. Squatrito, L. Scarpace, A. C. deCarvalho, S. Lyu, P. Li, Y. Li, F. Barthel, H. J. Cho, Y. H. Lin, N. Satani, E. Martinez-Ledesma, S. Zheng, E. Chang, C. G. Sauve, A. Olar, Z. D. Lan, G. Finocchiaro, J. J. Phillips, M. S. Berger, K. R. Gabrusiewicz, G. Wang, E. Eskilsson, J. Hu, T. Mikkelsen, R. A. DePinho, F. Muller, A. B. Heimberger, E. P. Sulman, D. H. Nam, and R. G. W. Verhaak. 2017. "Tumor Evolution of Glioma-Intrinsic Gene Expression Subtypes Associates with Immunological Changes in the Microenvironment." *Cancer Cell* 32 (1):42-56 e6. doi: 10.1016/j.ccell.2017.06.003.

Wang, X. Q., H. M. Bai, S. T. Li, H. Sun, L. Z. Min, B. B. Tao, J. Zhong, and B. Li. 2017. "Knockdown of HDAC1 expression suppresses invasion and induces apoptosis in glioma cells." *Oncotarget* 8 (29):48027-48040. doi: 10.18632/oncotarget.18227.

Wang, Y., C. A. Dye, V. Sohal, J. E. Long, R. C. Estrada, T. Roztocil, T. Lufkin, K. Deisseroth, S. C. Baraban, and J. L. Rubenstein. 2010. "Dlx5 and Dlx6 regulate the development of parvalbumin-expressing cortical interneurons." *J Neurosci* 30 (15):5334-45. doi: 10.1523/JNEUROSCI.5963-09.2010.

Wang, Z., C. Zang, K. Cui, D. E. Schones, A. Barski, W. Peng, and K. Zhao. 2009. "Genome-wide mapping of HATs and HDACs reveals distinct functions in active and inactive genes." *Cell* 138 (5):1019-31. doi: 10.1016/j.cell.2009.06.049.

Was, H., S. K. Krol, D. Rotili, A. Mai, B. Wojtas, B. Kaminska, and M. Maleszewska. 2019. "Histone deacetylase inhibitors exert anti-tumor effects on human adherent and stem-like glioma cells." *Clin Epigenetics* 11 (1):11. doi: 10.1186/s13148-018-0598-5.

Wasserberg, N., and H. Gutman. 2008. "Resection margins in modern rectal cancer surgery." *J Surg Oncol* 98 (8):611-5. doi: 10.1002/jso.21036.

Wawruszak, A., J. Kalafut, E. Okon, J. Czapinski, M. Halasa, A. Przybyszewska, P. Miziak, K. Okla, A. Rivero-Muller, and A. Stepulak. 2019. "Histone Deacetylase Inhibitors and Phenotypical Transformation of Cancer Cells." *Cancers (Basel)* 11 (2). doi: 10.3390/cancers11020148.

Weichert, W. 2009. "HDAC expression and clinical prognosis in human malignancies." *Cancer Lett* 280 (2):168-76. doi: 10.1016/j.canlet.2008.10.047.

Weichert, W., C. Denkert, A. Noske, S. Darb-Esfahani, M. Dietel, S. E. Kalloger, D. G. Huntsman, and M. Kobel. 2008. "Expression of class I histone deacetylases

indicates poor prognosis in endometrioid subtypes of ovarian and endometrial carcinomas." *Neoplasia* 10 (9):1021-7. doi: 10.1593/neo.08474.

Weichert, W., A. Roske, V. Gekeler, T. Beckers, M. P. Ebert, M. Pross, M. Dietel, C. Denkert, and C. Rocken. 2008. "Association of patterns of class I histone deacetylase expression with patient prognosis in gastric cancer: a retrospective analysis." *Lancet Oncol* 9 (2):139-48. doi: 10.1016/S1470-2045(08)70004-4.

Weller, M., M. van den Bent, M. Preusser, E. Le Rhun, J. C. Tonn, G. Minniti, M. Bendszus, C. Balana, O. Chinot, L. Dirven, P. French, M. E. Hegi, A. S. Jakola, M. Platten, P. Roth, R. Ruda, S. Short, M. Smits, M. J. B. Taphoorn, A. von Deimling, M. Westphal, R. Soffietti, G. Reifenberger, and W. Wick. 2021. "EANO guidelines on the diagnosis and treatment of diffuse gliomas of adulthood." *Nat Rev Clin Oncol* 18 (3):170-186. doi: 10.1038/s41571-020-00447-z.

Wen, Y. D., V. Perissi, L. M. Staszewski, W. M. Yang, A. Krones, C. K. Glass, M. G. Rosenfeld, and E. Seto. 2000. "The histone deacetylase-3 complex contains nuclear receptor corepressors." *Proc Natl Acad Sci U S A* 97 (13):7202-7. doi: 10.1073/pnas.97.13.7202.

Whitfield, B. T., and J. T. Huse. 2022. "Classification of adult-type diffuse gliomas: Impact of the World Health Organization 2021 update." *Brain Pathol*:e13062. doi: 10.1111/bpa.13062.

Wick, W., M. Platten, and M. Weller. 2001. "Glioma cell invasion: regulation of metalloproteinase activity by TGF-beta." *J Neurooncol* 53 (2):177-85. doi: 10.1023/a:1012209518843.

Wick, W., M. Weller, M. van den Bent, M. Sanson, M. Weiler, A. von Deimling, C. Plass, M. Hegi, M. Platten, and G. Reifenberger. 2014. "MGMT testing--the challenges for biomarker-based glioma treatment." *Nat Rev Neurol* 10 (7):372-85. doi: 10.1038/nrneurol.2014.100.

Wiegmans, A. P., A. E. Alsop, M. Bots, L. A. Cluse, S. P. Williams, K. M. Banks, R. Ralli, C. L. Scott, A. Frenzel, A. Villunger, and R. W. Johnstone. 2011. "Deciphering the molecular events necessary for synergistic tumor cell apoptosis mediated by the histone deacetylase inhibitor vorinostat and the BH3 mimetic ABT-737." *Cancer Res* 71 (10):3603-15. doi: 10.1158/0008-5472.CAN-10-3289.

Wilson, B. J., A. M. Tremblay, G. Deblois, G. Sylvain-Drolet, and V. Giguere. 2010. "An acetylation switch modulates the transcriptional activity of estrogen-related receptor alpha." *Mol Endocrinol* 24 (7):1349-58. doi: 10.1210/me.2009-0441.

Wilson, T. A., M. A. Karajannis, and D. H. Harter. 2014. "Glioblastoma multiforme: State of the art and future therapeutics." *Surg Neurol Int* 5:64. doi: 10.4103/2152-7806.132138.

Wolburg, H., K. Wolburg-Buchholz, J. Kraus, G. Rascher-Eggstein, S. Liebner, S. Hamm, F. Duffner, E. H. Grote, W. Risau, and B. Engelhardt. 2003. "Localization of claudin-3 in tight junctions of the blood-brain barrier is selectively lost during experimental autoimmune encephalomyelitis and human glioblastoma multiforme." *Acta Neuropathol* 105 (6):586-92. doi: 10.1007/s00401-003-0688-z.

Wood, P. J., R. Strong, G. A. McArthur, M. Michael, E. Algar, A. Muscat, L. Rigby, M. Ferguson, and D. M. Ashley. 2018. "A phase I study of panobinostat in pediatric patients with refractory solid tumors, including CNS tumors." *Cancer Chemother Pharmacol* 82 (3):493-503. doi: 10.1007/s00280-018-3634-4.

Wormann, S. M., L. Song, J. Ai, K. N. Diakopoulos, M. U. Kurkowski, K. Gorgulu, D. Ruess, A. Campbell, C. Doglioni, D. Jodrell, A. Neesse, I. E. Demir, A. P. Karpathaki, M. Barenboim, T. Hagemann, S. Rose-John, O. Sansom, R. M. Schmid, M. P. Protti, M. Lesina, and H. Algul. 2016. "Loss of P53 Function Activates JAK2-STAT3 Signaling to Promote Pancreatic Tumor Growth, Stroma Modification, and Gemcitabine Resistance in Mice and Is Associated With Patient Survival." *Gastroenterology* 151 (1):180-193 e12. doi: 10.1053/j.gastro.2016.03.010.

Wu, A., J. Wei, L. Y. Kong, Y. Wang, W. Priebe, W. Qiao, R. Sawaya, and A. B. Heimberger. 2010. "Glioma cancer stem cells induce immunosuppressive macrophages/microglia." *Neuro Oncol* 12 (11):1113-25. doi: 10.1093/neuonc/noq082.

Wu, G., A. Broniscer, T. A. McEachron, C. Lu, B. S. Paugh, J. Becksfort, C. Qu, L. Ding, R. Huether, M. Parker, J. Zhang, A. Gajjar, M. A. Dyer, C. G. Mullighan, R. J. Gilbertson, E. R. Mardis, R. K. Wilson, J. R. Downing, D. W. Ellison, J. Zhang, S. J. Baker, and Project St. Jude Children's Research Hospital-Washington University Pediatric Cancer Genome. 2012. "Somatic histone H3 alterations in pediatric diffuse intrinsic pontine gliomas and non-brainstem glioblastomas." *Nat Genet* 44 (3):251-3. doi: 10.1038/ng.1102.

Wu, Y., L. Dong, S. Bao, M. Wang, Y. Yun, and R. Zhu. 2016. "FK228 augmented temozolomide sensitivity in human glioma cells by blocking PI3K/AKT/mTOR signal pathways." *Biomed Pharmacother* 84:462-469. doi: 10.1016/j.biopha.2016.09.051.

Xia, P., R. Zhang, and G. Ge. 2015. "C/EBPbeta Mediates TNF-alpha-Induced Cancer Cell Migration by Inducing MMP Expression Dependent on p38 MAPK." *J Cell Biochem* 116 (12):2766-77. doi: 10.1002/jcb.25219.

Yamaguchi, T., F. Cubizolles, Y. Zhang, N. Reichert, H. Kohler, C. Seiser, and P. Matthias. 2010. "Histone deacetylases 1 and 2 act in concert to promote the G1-to-S progression." *Genes Dev* 24 (5):455-69. doi: 10.1101/gad.552310.

Yang, X. J., and S. Gregoire. 2005. "Class II histone deacetylases: from sequence to function, regulation, and clinical implication." *Mol Cell Biol* 25 (8):2873-84. doi: 10.1128/MCB.25.8.2873-2884.2005.

Yanginlar, C., and C. Logie. 2018. "HDAC11 is a regulator of diverse immune functions." *Biochim Biophys Acta Gene Regul Mech* 1861 (1):54-59. doi: 10.1016/j.bbagrm.2017.12.002.

Yelton, C. J., and S. K. Ray. 2018. "Histone deacetylase enzymes and selective histone deacetylase inhibitors for antitumor effects and enhancement of antitumor immunity in glioblastoma." *Neuroimmunol Neuroinflamm* 5. doi: 10.20517/2347-8659.2018.58.

Yoo, Y. G., G. Kong, and M. O. Lee. 2006. "Metastasis-associated protein 1 enhances stability of hypoxia-inducible factor-1alpha protein by recruiting histone deacetylase 1." *EMBO J* 25 (6):1231-41. doi: 10.1038/sj.emboj.7601025.

Yoshida, M., M. Kijima, M. Akita, and T. Beppu. 1990. "Potent and specific inhibition of mammalian histone deacetylase both in vivo and in vitro by trichostatin A." *J Biol Chem* 265 (28):17174-9.

Yoshida, M., N. Kudo, S. Kosono, and A. Ito. 2017. "Chemical and structural biology of protein lysine deacetylases." *Proc Jpn Acad Ser B Phys Biol Sci* 93 (5):297-321. doi: 10.2183/pjab.93.019.

You, A., J. K. Tong, C. M. Grozinger, and S. L. Schreiber. 2001. "CoREST is an integral component of the CoREST- human histone deacetylase complex." *Proc Natl Acad Sci U S A* 98 (4):1454-8. doi: 10.1073/pnas.98.4.1454.

Young, R. M., A. Jamshidi, G. Davis, and J. H. Sherman. 2015. "Current trends in the surgical management and treatment of adult glioblastoma." *Ann Transl Med* 3 (9):121. doi: 10.3978/j.issn.2305-5839.2015.05.10.

Zaja, F., F. Salvi, M. Rossi, E. Sabattini, A. Evangelista, G. Ciccone, E. Angelucci, G. Gaidano, M. Zanni, M. Ladetto, A. Chiappella, U. Vitolo, P. L. Zinzani, C. Califano, A. Tucci, C. Patti, S. A. Pileri, V. Lenti, P. P. Piccaluga, F. Cavallo, S. Volpetti, G. Perali, S. Assouline, K. K. Mann, R. Morin, M. Alcaide, K. Bushell, R. Fanin, and A. Levis. 2018. "Single-agent panobinostat for relapsed/refractory diffuse large B-cell lymphoma: clinical outcome and correlation with genomic data. A phase 2 study of the Fondazione Italiana Linfomi." *Leuk Lymphoma* 59 (12):2904-2910. doi: 10.1080/10428194.2018.1452208.

Zaware, N., and M. M. Zhou. 2019. "Bromodomain biology and drug discovery." *Nat Struct Mol Biol* 26 (10):870-879. doi: 10.1038/s41594-019-0309-8.

Zhang, F., T. Zhang, Z. H. Teng, R. Zhang, J. B. Wang, and Q. B. Mei. 2009. "Sensitization to gamma-irradiation-induced cell cycle arrest and apoptosis by the

histone deacetylase inhibitor trichostatin A in non-small cell lung cancer (NSCLC) cells." *Cancer Biol Ther* 8 (9):823-31. doi: 10.4161/cbt.8.9.8143.

Zhang, J., and Q. Zhong. 2014. "Histone deacetylase inhibitors and cell death." *Cell Mol Life Sci* 71 (20):3885-901. doi: 10.1007/s00018-014-1656-6.

Zhang, L. Y., Q. Guo, G. F. Guan, W. Cheng, P. Cheng, and A. H. Wu. 2019. "Integrin Beta 5 Is a Prognostic Biomarker and Potential Therapeutic Target in Glioblastoma." *Front Oncol* 9:904. doi: 10.3389/fonc.2019.00904.

Zhang, L., J. Zhang, Q. Jiang, L. Zhang, and W. Song. 2018. "Zinc binding groups for histone deacetylase inhibitors." *J Enzyme Inhib Med Chem* 33 (1):714-721. doi: 10.1080/14756366.2017.1417274.

Zhang, Y., M. Adachi, R. Kawamura, and K. Imai. 2006. "Bmf is a possible mediator in histone deacetylase inhibitors FK228 and CBHA-induced apoptosis." *Cell Death Differ* 13 (1):129-40. doi: 10.1038/sj.cdd.4401686.

Zhang, Y., T. Carr, A. Dimtchev, N. Zaer, A. Dritschilo, and M. Jung. 2007. "Attenuated DNA damage repair by trichostatin A through BRCA1 suppression." *Radiat Res* 168 (1):115-24. doi: 10.1667/RR0811.1.

Zhang, Y., N. Li, C. Caron, G. Matthias, D. Hess, S. Khochbin, and P. Matthias. 2003. "HDAC-6 interacts with and deacetylates tubulin and microtubules in vivo." *EMBO J* 22 (5):1168-79. doi: 10.1093/emboj/cdg115.

Zhang, Y., S. A. Sloan, L. E. Clarke, C. Caneda, C. A. Plaza, P. D. Blumenthal, H. Vogel, G. K. Steinberg, M. S. Edwards, G. Li, J. A. Duncan, 3rd, S. H. Cheshier, L. M. Shuer, E. F. Chang, G. A. Grant, M. G. Gephart, and B. A. Barres. 2016. "Purification and Characterization of Progenitor and Mature Human Astrocytes Reveals Transcriptional and Functional Differences with Mouse." *Neuron* 89 (1):37-53. doi: 10.1016/j.neuron.2015.11.013.

Zhang, Z., Y. Wang, J. Chen, Q. Tan, C. Xie, C. Li, W. Zhan, and M. Wang. 2016. "Silencing of histone deacetylase 2 suppresses malignancy for proliferation, migration, and invasion of glioblastoma cells and enhances temozolomide sensitivity." *Cancer Chemother Pharmacol* 78 (6):1289-1296. doi: 10.1007/s00280-016-3188-2.

Zhao, W. J., and M. Schachner. 2013. "Neuregulin 1 enhances cell adhesion molecule l1 expression in human glioma cells and promotes their migration as a function of malignancy." *J Neuropathol Exp Neurol* 72 (3):244-55. doi: 10.1097/NEN.0b013e3182863dc5.

Zhao, Z., K. N. Zhang, Q. Wang, G. Li, F. Zeng, Y. Zhang, F. Wu, R. Chai, Z. Wang, C. Zhang, W. Zhang, Z. Bao, and T. Jiang. 2021. "Chinese Glioma Genome Atlas (CGGA): A Comprehensive Resource with Functional Genomic Data from

Chinese Gliomas." *Genomics Proteomics Bioinformatics*. doi: 10.1016/j.gpb.2020.10.005.

Zheng, S., W. Wang, J. Aldahdooh, A. Malyutina, T. Shadbahr, Z. Tanoli, A. Pessia, and J. Tang. 2022. "SynergyFinder Plus: Toward Better Interpretation and Annotation of Drug Combination Screening Datasets." *Genomics Proteomics Bioinformatics*. doi: 10.1016/j.gpb.2022.01.004.

Zupkovitz, G., R. Grausenburger, R. Brunmeir, S. Senese, J. Tischler, J. Jurkin, M. Rembold, D. Meunier, G. Egger, S. Lagger, S. Chiocca, F. Propst, G. Weitzer, and C. Seiser. 2010. "The cyclin-dependent kinase inhibitor p21 is a crucial target for histone deacetylase 1 as a regulator of cellular proliferation." *Mol Cell Biol* 30 (5):1171-81. doi: 10.1128/MCB.01500-09.

Zupkovitz, G., J. Tischler, M. Posch, I. Sadzak, K. Ramsauer, G. Egger, R. Grausenburger, N. Schweifer, S. Chiocca, T. Decker, and C. Seiser. 2006. "Negative and positive regulation of gene expression by mouse histone deacetylase 1." *Mol Cell Biol* 26 (21):7913-28. doi: 10.1128/MCB.01220-06.